SYNTHESIS AND BIOLOGICAL ACTIVITY OF CINNAMIC ACIDS AMIDES

Tsenka Milkova[a,b *], Maya Spasova[c], Galya Ivanova[b], Stefan Philipov[b], Lubomira Nikolaeva-Glomb[d], Galina Radeva[c]

(Plenary report)

[a]*South-West University "Neofit Rilski" Blagoevgrad, Bulgaria*
[b] *Institute of Organic Chemistry with Centre of Phytochemistry, Bulgarian Academy of Sciences, Sofia, Bulgaria*
[c]*Institute of Molecular Biology, Bulgarian Academy of Sciences, Sofia, Bulgaria*
[d] *The Stephan Angeloff Institute of Microbiology, Bulgarian Academy of Sciences, Sofia, Bulgaria*

Abstract: *Seventeen cinnamoyl-, feruloyl- and sinapoyl- amino acids amides have been synthesized using the standard methods in peptide chemistry. The antioxidant activity of six feruloyl- and three sinapoyl- amino acid amides was studied on the oxidation stability of a lipid system. Some of the synthesized compounds have been tested for their antibacterial and antiviral activity. Twenty three N-alkylcinnamoyl amides have been prepared in solution and by sonochemical and microwave activated Wittig reaction. Some of the synthesized hydroxycinnamoyl amides were tested for their antiradical activity by DPPH* tests. All sinapoyl alkylamides were more active than the feruloyl amides. The results obtained demonstrated that the amides are twice less active than the free hydroxycinnamic acids*

The alkaloid glaucine has been modified and connected with cinnamoyl- and hydroxycinnamoyl residue. The compounds obtained have been tested for their antiradical activity by DPPH tests.*

Keywords: *cinnamoyl amides, sonochemical and microwave activated Wittig reaction, glaucine, antibacterial- and antiviral activity; DPPH* test*

1. INTRODUCTION

The biochemical properties of polyphenolic secondary plant metabolites such esters of cinnamic acids (caffeic, ferulic, p- and o-coumaric, sinapic) attract much attention in biology and medicine. These compounds show antiviral, antibacterial, vasoactive, antiflammatory and other properties. Cinnamic acid conjugates also are commonly isolated from plant sources as the corresponding N-substituted amides. While esters of cinnamic acids occur widely in higher plants, amides of cinnamic acids seem to be rare. In order to define precisely the scope of their biological activity we synthesized a series of amides of cinnamic acids. The growing interest during the last years to naturally and synthetic amides of phenyl propenoic acids is due to the more metabolically stability of the amide group in comparison to the ester group [6].

In this paper we discuss our results in:

- synthesis of cinnamoyl, feruloyl and sinapoyl- amino acids amides.
- synthesis of amides of substituted cinnamic acids with aliphatic monoamines.
- synthesis of cinnamoyl- and hydroxycinnamoyl amides of the alkaloid glaucine.
- biological activity of the synthesized amides.

2. RESULTS AND DISCUSSION

N-substituted amides of cinnamic acids are commonly isolated from plant sources in different forms [8]. In one of them phenylpropenoic acids (basic, water soluble) are linked with aromatic amino acids (tyrosine, phenylalanine, tryptophane) [1, 3, 9]. Little is known about the biological function of the last class of compounds in nature. The formation of these amides is regarded as a protective mechanism in plants after virus infection, wounding, heavy metal ions, high temperature etc [4]. Fifteen amides have been obtained by a standard method of coupling of phenylpropanoic acids with natural and unnatural *C*-protected amino acids (Tab. 1).

The synthesized amides 10, 12, 14 and 16 have been found in nature. The rest of cinnamoyl and hydroxycinnamoyl conjugates of amino acids are new.

The antioxidant activity of six feruloyl- (7-12) and three sinapoyl- (14-16) amino acid amides on the oxidation stability of a lipid system (kinetically pure triacylglicerols of sunflower oil) during oxidation at 80^{o}C in bulk phase was investigated. The highest antioxidant activity was found for the compounds 10 and 14, containing the same phenylalanine rest [7, 11].

Feruloyl- and sinapoyl amides of phenylalanine showed antibacterial activity against *E.coli* and *Bacillus subtilis*. The antiviral activity was assessed by the agar-diffusion plaque-inhibition test which revealed that sinapoyl phenylalanine amide possessed moderate effect against Coxsakivirus B1 and poliovirus type 1 (Lsc-2ab). Cinnamic acid amides of phenylalanine, 3-fluorophenylalanine and tyrosine were found to possess border effect against both viruses.

The second topic in this report is the synthesis of amides of substituted cinnamic acids with aliphatic monoamines. As our attempts to prepare amides of caffeic acid with aliphatic amines by the methods used in the peptide chemistry failed, we tried to find alternative ways for their synthesis. In order to obtain amides without protection of the phenolic hydroxyl groups a recently developed new method for the synthesis of esters of cinnamic acids (including caffeic acid) by sonochemical [2, 5] and microwave [10] activated Wittig reaction was applied.

Tab. 1. Synthesized N-cinnamoyl- and N-hydroxycinnamoyl amino acid amides.

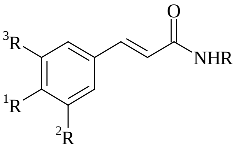

№	$-NR_1R_2$	R'	R''	R'''	Molecule Weight	$[a]^{20}_{D}$, MeOH	Yields, %
1	$-NH-CH(CH_3)-COOC(CH_3)_3$	H	H	H	275.35 $C_{16}H_{21}NO_3$	(-) 3.55, c=0.19	85. 0
2	$-NH-CH(CH(CH_3)_2)-COOCH_3$	H	H	H	261.32 $C_{15}H_{19}NO_3$	(+) 4.96, c=0.19	13. 0
3	$-NH-CH(CH_2-CH(CH_3)_2)-COOCH_3$	H	H	H	275.35 $C_{16}H_{21}NO_3$	(-) 16.35, c=0.38	14. 5
4	$-NH-CH(CH_2-C_6H_5)-COOC(CH_3)_3$	H	H	H	351.45 $C_{22}H_{25}NO_3$	(-) 22.00, c=0.25	71. 0
5	$-NH-CH(CH_2-C_6H_4$-F-m)$-COOCH_3$	H	H	H	327.35 $C_{19}H_{18}NO_3F$	(-) 44.27, c=0.13	77. 1
6	$-NH-CH(CH_2-C_6H_4$-OH-p)$-COOCH_3$	H	H	H	309.36 $C_{19}H_{19}NO_3$	(-) 28.19, c=0.19	40. 5
7	$-NH-CH(CH_3)-COOC(CH_3)_3$	OCH_3	OH	H	321.37 $C_{17}H_{23}NO_5$	(+) 41.86, c=0.43	55. 0
8	$-NH-CH(CH(CH_3)_2)-COOCH_3$	OCH_3	OH	H	307.35 $C_{16}H_{21}NO_5$	(+) 10.00, c=0.31	41. 0
9	$-NH-CH(CH_2-CH(CH_3)_2)-COOCH_3$	OCH_3	OH	H	321.37 $C_{17}H_{23}NO_5$	(-) 5.83, c=1.00	34. 0
10	$-NH-CH(CH_2-C_6H_5)-COOC(CH_3)_3$	OCH_3	OH	H	397.47 $C_{23}H_{27}NO_5$	(-) 20.83, c=0.36	45. 0
11	$-NH-CH(CH_2-C_6H_4$-F-m)$-COOCH_3$	OCH_3	OH	H	373.38 $C_{20}H_{20}NO_5F$	(-) 24.17, c=0.20	62. 6
12	$-NH-CH(CH_2-C_6H_4$-OH-p)$-COOCH_3$	OCH_3	OH	H	371.39 $C_{20}H_{21}NO_6$	(-) 28.74, c=3.25	62. 0
13	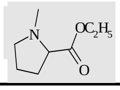	OCH_3	OH	H	319.35 $C_{17}H_{21}NO_5$	(-) 26.25, c=0.47	24.8
14	$-NH-CH(CH_2-C_6H_5)-COOC(CH_3)_3$	OCH_3	OH	OCH_3	427.50 $C_{24}H_{29}NO_6$	(-) 11.35, c=2.42	47. 1
15	$-NH-CH(CH_2-C_6H_4$-F-m)$-COOCH_3$	OCH_3	OH	OCH_3	403.41 $C_{21}H_{22}NO_6F$	(-) 91.76, c=0.17	28. 9
16	$-NH-CH(CH_2-C_6H_4$-OH-p)$-COOCH_3$	OCH_3	OH	OCH_3	400.41 $C_{21}H_{22}NO_7$	(-) 36.75, c=0.42	40. 5
17	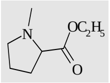	OCH_3	OH	OCH_3	348.37 $C_{18}H_{23}NO_6$	(-) 8.62, c=0.29	31. 0

The three step synthesis of N-alkylcinnamoyl amides are summarized in the Sch. 1.

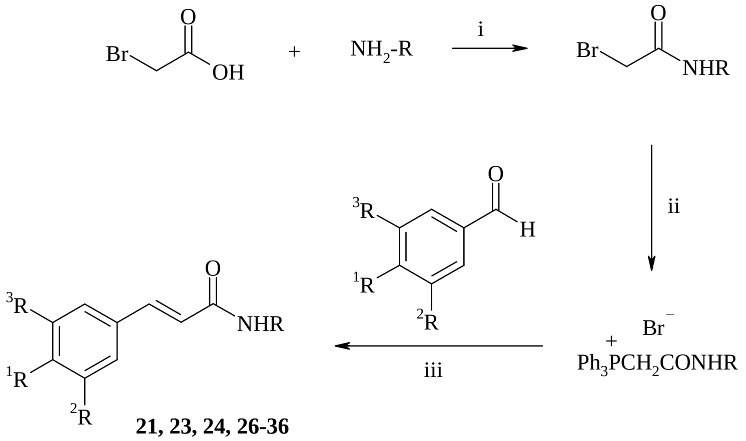

21, 23, 24, 26-36

Sch. 1.

As it is shown in Tab. 2 the advantage of the microwave accelerated Wittig reaction is a short time (10 min).

Some of the synthesized hydroxycinnamoyl amides were tested for their antiradical activity by DPPH* tests. All sinapoyl alkylamides are more active than the feruloyl amides. The results obtained demonstrated two times lower activity of the obtained amides than the free hydroxycinnamic acids.

From the literature it is known that the alkaloid glaucine possesses radical scavenging activity. We modified the glaucine by introduction of amino group and connection of this function with cinnamoyl residue as shown in Sch. 2. Interesting biological activity could be expected for this new molecules combining two different parts, everyone of which posseses antioxidant properties.

№	R	^{1}R	^{2}R	^{3}R	Reaction time			Yields, %				
					a (h)	b (h)	c (min)	a	b	c		
											^{1}H-NMR E:Z	GC-MS E:Z
18	$(CH_2)_3CH_3$	H	H	H	HBTU, (5)	–	–	58.1	–	–		
19	$(CH_2)_5CH_3$	H	H	H	HBTU, (5)	–	–	64.4	–	–		
20	$(CH_2)_6CH_3$	H	H	H	HBTU, (5)	–	–	24.5	–	–		
21	$(CH_2)_3CH_3$	OH	OCH_3	H	HBTU, (5)	13.00	10	52.6	50.0	30.1		
22	$(CH_2)_5CH_3$	OH	OCH_3	H	HBTU, (5)	–	–	61.0	–	–		
23	$(CH_2)_6CH_3$	OH	OCH_3	H	HBTU, (5)	13	10	33.7	42.9	25.9		
24	$(CH_2)_3CH_3$	OH	OCH_3	OCH_3	EDC/HOBt, (22)	55.30	10	35.7	49.3	36.4		
25	$(CH_2)_5CH_3$	OH	OCH_3	OCH_3	EDC/HOBt, (22)	–	–	18.3	–	–		
26	$(CH_2)_6CH_3$	OH	OCH_3	OCH_3	EDC/HOBt, (22)	13	10	38.6	69.9	23.4		
27	$(CH_2)_3CH_3$	OCH_3	OH	H	–	–	10	–	–	48.1	5:1	3:1
28	$(CH_2)_6CH_3$	OCH_3	OH	H	–	–	10	–	–	46.6	5:1	2:1
29	$(CH_2)_3CH_3$	OCH_3	OCH_3	H	–	55.30	10	–	37.3	68.2	7:1	4:1
30	$(CH_2)_6CH_3$	OCH_3	OCH_3	H	–	55.30	10	–	41.7	87.5	7:1	4:1
31	$(CH_2)_3CH_3$	OCH_3	OCH_3	OCH_3	–	55.30	10	–	87.5	63.6	2.5:1	1.5:1
32	$(CH_2)_6CH_3$	OCH_3	OCH_3	OCH_3	–	13	10	–	40.0	83.9	4:1	1.5:1
33	$(CH_2)_3CH_3$	H	OCH_2O		–	–	10	–	–	70.7	4:1	2:1
34	$(CH_2)_6CH_3$	H	OCH_2O		–	–	10	–	–	91.7	6:1	4:1
35	$(CH_2)_3CH_3$	H	OH	H	–	–	10	–	–	45.7	8:1	5:1
36	$(CH_2)_6CH_3$	H	OH	H	–	–	10	–	–	64.2	20:1	11:1

Tab. 2. Cinnamoyl amides obtained in solution and by sonochemical and microwave accelerated Wittig reaction.

^{a} In solution;^{b} Sonochemical activated Wittig reaction;^{c} Microwave activated Wittig reaction.

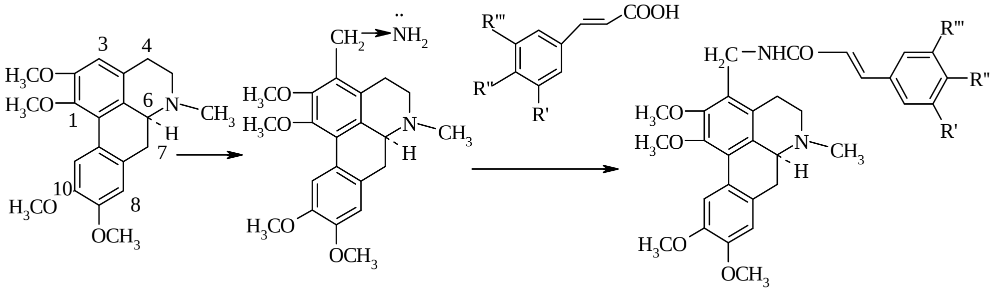

Sch. 2.

3. ACKNOWLEDGMENTS

We are grateful for the support of this work to the National Found for Sci Research of Bulgaria (VUH–07/05), to the South-West University “Neofit Rilski”.

4. REFERENCES

[1] Adam K.-P. (1995) Caffeic acid derivatives in fronds of the lady fern (Athyrium filix-femina) Phytochemistry 40, 1577-1578

[2] Bankova, V.S. (1990) Synthesis of natural esters of substituted cinnamic acids, J Nat Prod 53, 821–824.

[3] Clifford MN., Kellard B., Ah-Sing E. (1989) Caffeoyltyrosine from green Robusta coffee beans. Phytochemistry 28, 1989–1990.

[4] Clifford M. N., Knight S. (2004) The cinnamoyl–amino acid conjugates of green robusta coffee beans, Food Chemistry 87, 457-463.

[5] Elenkov I., Todorova D., Bankova V., Milkova Ts. (1995) . Synthesis of steryl esters of phenolic acids by heterogenic Wittig reaction, Journal of Natural Products, 58, 280 -283.

[6] Graefe, E.U., Veit, M. (1999) Urinary metabolites of flavonoids and hydroxycinnamic acids in humans after application of a crude extract from Equisetum arvense, Phytomedicine 6, 239-246

[7] Kortenska-Kancheva V., Spasova M., Totseva I., Milkova Ts.(2006) Study on the antioxidant activity of N-hydroxycinnamoyl-amino acid conjugates in bulk lipid autoxidation, Riv. Ital. Sost. Grasse 83, 162-169.

[8] Martin-Tanguy J., Deshayes A., Pedrizet E., Martin C. (1979) Hydroxycinnamic acid amides in Zea mays:distribution and change with cytoplasmic male sterile, FEBS Letters 108, 176-178.

[9] Morishita H., Takai Y., Yamada H., Fukuda F., Sawada M., Iwahashi H., Kido R. (1987) Caffeoyltryptophan from green robusta coffee beans, Phytochemistry 26, 1195-1196.

[10] Spasova M., Bankova V., Ivanova G., Pajpanova T., Milkova Ts. (2006) Synthesis of Esters of Substituted Phenolic Acids by Microwave Assisted Wittig Reaction, Oxid.Commun.29, 172-175.

[11] Spasova M., Kortenska-Kancheva V., Totseva I., Ivanova G., Georgiev L., Milkova Ts. (2006) Synthesis of cinnamoyl and hydroxycinnamoyl-amino acid conjugates and evaluation of their antioxidant activity, Journal of Peptide Science 12, 369-375.

MAGNETIC NANOCOMPOSITES BASED ON MFe_2O_4/SiO_2, THEIR PREPARATION AND PHYSICAL PROPERTIES

Jiří Plocek[(a)], Daniel Nižňanský[(a,b)]

(Plenary report)

[(a)] *Institute of Inorganic Chemistry,Academy of Sciences of the Czech Republic, 250 68 Rez, Czech Republic*
[(b)] *Department of Inorganic Chemistry, Faculty of Science, Charles University of Prague, Prague, Czech Republic*

Abstract: *The nanocomposites are the subject of many studies during last years due to the new properties they expected to show. One of the widely studied nanocomposite groups are metal oxide compounds in the silica matrix. We studied nanocomposites MFe2O4/SiO2 (M = Co, Ni, Zn, Cd, Cu, Mg). The samples were characterized by X-ray diffraction, Moessbauer spectroscopy, magnetic measurements, scanning microscopy and high resolution transmission microscopy. All the materials show interesting magnetic behavior and their properties could be finely tuned during preparation. Expected usage of these materials is data storage, magnetic cooling, imaging in medicine, targeted drugs carrying, magnetic separating of polluted soils etc.*

Keywords*: sol-gel, spinel ferrite, silica matrix, nanocomposite*

1. INTRODUCTION

The nanocomposites are the subject of many studies during last years due to the new properties they expected to show. One of the widely studied nanocomposite groups are the metal oxide compounds in the silica matrix. These materials have often interesting magnetic and magnetooptical properties and.

An easy way to prepare of nanocomposites with the required properties represents sol-gel method. For nanocomposites of metal oxide in silica matrix, the samples with an arbitrary cation/silica ratio can be prepared and the particle size and size distribution can be controlled by the parameters of the heat treatment.

We prepared several nanocomposite series: MFe_2O_4/SiO_2 (M = Ni[1], Co[1,2], Zn[3], Cd[3], Cu[4], Mg). These materials were heat treated at 800-1100℃ and then characterized using X-ray diffraction, HR-TEM, SEM, Moessbauer spectroscopy, and magnetic measurements.

2. SAMPLE PREPARATION

Conventional sol-gel method using tetraethoxysilane, HNO_3 as an acid catalyst, formamide as a modifier, and methanol as a solvent was applied for silica matrix preparation. $Fe(NO_3)_3$.9H2O and $M(NO_3)_x.yH_2O$ dissolved in methanol were used as active compound precursor. The Si/Fe molar ratio was 5/1.

The samples were subsequently gelated at 40°C for 24 hour, dried at 40°C for 3 days in flowing nitrogen-atmosphere, then they were slowly preheated to 300°C in vacuum, and then slowly heated to various temperatures (800, 900, 1000, or 1100°C) under atmospheric pressure. Holding time at final temperature was 2 hour.

3. RESULTS

3.1. X-ray diffraction

All samples were characterised by X-ray diffraction measurements. Ni sample heated to 800°C is rentgenographically amorphous, higher temperature heated Ni-samples show presence of nanocrystaline spinel phase. Co-samples are crystalline at all studied temperatures. Both, nickel- and cobalt- ferrites have inverse spinel structure. Silica matrix is amorphous by both the samples at all the temperatures.

Zinc ferite start to crystallize from 800°C, but diffraction peaks are very broad, because of particle size is very small – about 4 nm. Spinel structure in silica matrix is stable up to 1100°C. Silica matrix slightly crystallizes at 1100°C to quartz.

Cadmium spinel was detected only at samples heated to 800 and 900°C. At higher temperatures, the $CdFe_2O_4$ reacts with SiO_2 matrix to $CdSiO_3$ and α-Fe_2O_3. Both, cadmium- and zinc- ferrites have normal spinel structure.

Copper ferrite is crystalline and stable at all the studied temperatures [fig. 1]. Cubic spinel structure is slightly distorted to tetragonal due to Jahn-Teller effect. Amorphous silica matrix starts to crystalize to crystobalite at 1000°C. Copper ferrite in the silica matrix has not exactly the structure of inverse spinel. The tetrahedral and octahedral sites occupation is more likely statistic.

Magnesium ferrite crystalises from 900°C to inverse spinel structure. The silica matrix is amorphous at all the studied temperatures.

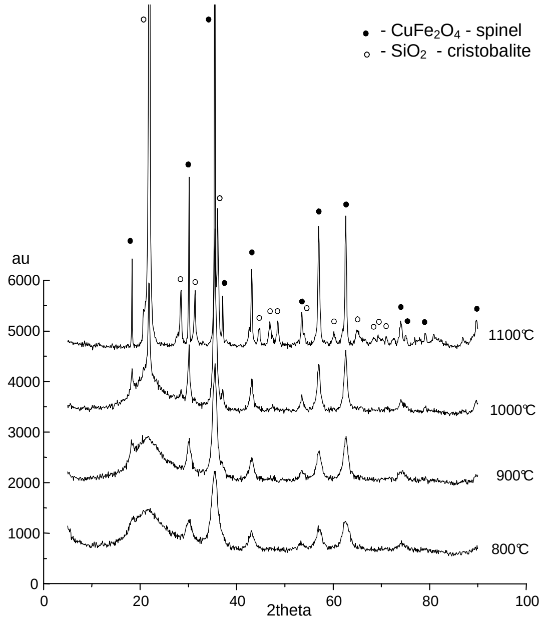

Fig. 1: X-ray diffraction pattern of $CuFe_2O_4/SiO_2$ prepared at different temperatures

3.2. HR-TEM

Nanoparticle size and morphology was observed using high resolution transmission electron microscopy [Fig. 2]. Mean particle size shows table 1

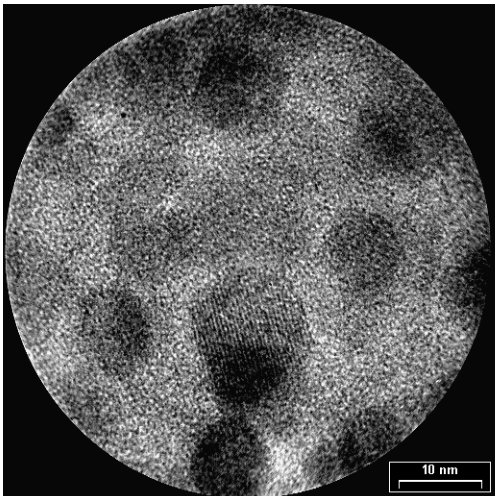

Fig. 2: HR-TEM of $ZnFe_2O_4/SiO_2$ treated 1000℃. Dark spots are ferrite nanoparticles, light places are silica matrix

Tab. 1: Mean particle size in nm

MFe_2O_4 / preparation temperature	800℃	900℃	1000℃	1100℃
Ni	2		25	
Co	2		25	
Zn	4	6		15
Cd	3	6		
Cu	7	9	15	127
Mg				30

3.3. Moessbauer spectroscopy

Moessbauer measurements were performed to get more information about structure, especially cation distribution and magnetic state.

All our ferrite materials heat treated at 800℃ are at room temperature in superparamagnetic state. With increasing particle size the transition temperature to superparamagnetic state decreases.

3.4. Magnetic measurements

Magnetic properties were measured at vibrating magnetometer and/or as ZFC-FC measurements at temperatures from 4 K to room temperature.

Magnetic measurement of the copper ferrite revealed us, that spinel structure has the mixed state character. The calculated saturation magnetic moment is consistent with the approximate distribution of the Cu and Fe in the tetrahedral and octahedral positions corresponding to the formula $(Fe_{0,87}Cu_{0,13})[Fe_{1,13}Cu_{0,87}]O_4$. Similar conditions are also by other ferrite nanomaterials: for example magnesium ferrite could be written as $(Fe_{0.37}Mg_{0.63})[Fe_{0.63}Mg_{1.37}]O_4$

4. CONCLUSION

Six series of MFe_2O_4/SiO_2 (M = Co, Ni, Zn, Cd, Cu, Mg) nanocomposites were prepared by the sol-gel method and studied using X-ray diffraction, HRTEM, SEM, Moessbauer spectroscopy and magnetic measurements. These materials have interesting magnetic properties, which could be finely tuned in wide area by preparation process. It is supposed, that these materials could be used in data storage, magnetic cooling, imaging in medicine, targeted drugs carrying, magnetic separating of polluted soils etc.

Thanks to: Petr Holec, Alzbeta Hutlova, and Jana Vejpravova

Acknowledgement: this work was supported by Czech Science Foundation, project No. 106/07/0949

5. REFERENCES

[1] Hutlova A, Niznansky D, Plocek J, et al. (2003) Nanocomposites $NiFe_2O_4/SiO_2$ and $CoFe_2O_4/SiO_2$-preparation by sol-gel method and physical properties; Journal of Sol-Gel Science and Technology 26 (1-3): 473-477

[2] Vejpravova J, Plocek J, Niznansky D, et al.(2005) Sol-gel fabricated $CoFe_2O_4/SiO_2$ nanocomposites: Synthesis and magnetic properties; IEEE Transactions on Magnetics 41 (10): 3469-3471

[3] Plocek J, Hutlova A, Niznansky D, et al. (2003) Preparation of $ZnFe_2O4/SiO_2$ and $CdFe_2O4/SiO_2$ nanocomposites by sol-gel Metod; Journal of Non-Crystalline Solids 315 (1-2): 70-76

[4] Plocek J, Hutlova A, Niznansky D, et al. (2005) Preparation of $CuFe_2O_4/SiO_2$ nanocomposite by the sol-gel Metod; Materials Science-Poland 23 (3): 697-705

DENSIFICATION OF TRANSITIONAL NANOSCALED ALUMINA

E.Fidancevska[1], J.Bossert[2], R.Adjiski[1], V.Vasilev[3], M.Milosevski[1]

[1] *Faculty of Technology and Metallurgy, Rudjer Boskovic 16, Skopje, Republic of Macedonia*
[2] *Universitat Friedrich Schiller,Materialwissenschaft und Technology, Lobdergraben 32, Jena, Germany*
[3] *University of Chemical Technology and Metallurgy, 8 Kl. Ohridski blvd., Sofia, Bulgaria*

***Abstract**: Transitional nanoscaled alumina contains γ, δ, θ and α-Al203. DTA investigations of this powder showed exopeak at 1304 oC corresponding to the α-Al203 transformation. Sintered samples of as received powder possesses vermicular structure and density of 0.73TD. Mechanically activated powder sintered in the interval RT-1500 oC without soaking time, possesses density of 0.95TD and grain size distribution from 0.5 to 3.0 μm.*

***Keywords:** nano alumina ceramics, sintering, mechanical activation*

1. INTRODUCTION

Al_2O_3 nano powder is a superfine ceramic powder which can be widely used in the field of electronics, fine ceramics, composite materials, biomaterials etc. A lot of different processes for production of ceramic nanoscaled powders have been developed such as thermal spraying, coprecipitation, heterogeneous azeotropic distilation, sol-gel, laser induced chemical vapour deposition etc.

Studies on producing nanocrystalline ceramics from nanoscaled powders have highlighted the problem of achieving high densities without excessive grain growth. This fact is particularly proved for transition alumina powders which are currently produced with very high specific surface area and ultra fine crystalline size. In some cases, a solid-state phase transformation has been exploited to aid sintering at these temperatures to produce high-density polycrystalline alumina with submicron grain size.

It is known that many transformations in ceramics proceed by a nucleation and growth process. To initiate the transformation sufficient energy must be supplied to the system to exceed the nucleation barrier. After nucleation the transformation occurs rapidly, by growth.

Kumagai et al [1,2] showed that the nucleation step may effectively be eliminated by supplying nuclei to the system. This process known as seeding, involves adding ceramic particles of the high-temperature phase to the ceramic matrix to be transformed. By eliminating the nucleation step less energy is required for the transformation and it can occur at a lower temperature. According to Legros [3] $2\cdot10^{14}$ seeds/cm^3 of α-Al_2O_3 with particle size of 0.15 μm are sufficient for elimination of the step of nucleation.

Wakao and Hibino [4] reported that the transformation of θ to α-Al_2O_3 was reduced with CuO and Fe_2O_3, lowering the transformation temperature to as low as 1050 ^oC. Bye and Simpkin [5] added chromium and iron via a solution technique to γ-Al_2O_3 powder. They showed that the transformation temperature was lowered to 1100 ^oC with 2 % Fe and to 995 ^oC with 5 % Fe.

The goal of this paper is the obtaining of α-Al_2O_3 dense ceramics starting from transition nanocrystalline alumina, which contains some amount γ-Al_2O_3. Using mechanical activation, the present inactive α-Al_2O_3 can be activated and together with created lattice defects to act as heterogeneous nucleation sites in the system, controlling the transformation to α-Al_2O_3 and enhance the densification.

2. EXPERIMENTAL PROCEDURE

The nano aluminium oxide powder (99.98%) used in this study was obtained from firm IBU-tech, Germany. The code of the powder was NA 226-2. This powder was obtained by aluminium tri-sec-butylat.

The powder morphology was observed via transmission electron microscopy (TEM). Specific surface area was measured using nitrogen gas adsorption (multipoint BET method), Gemini, Micromeritics USA.

DTA/TG investigations were performed by NETZSCH STA 409C in air atmosphere in the temperature interval 20-1500 ^oC using heating rate of 10 $^oC\ min^{-1}$.

Phase analysis of the transition nanoscaled alumina was carried out by X-ray difraction (XRD) with Ni-filtered CuK_α radiation.

Mechanical activation (wet milling) of the started powder was performed by attritor mill NETZSCH using alumina balls at pH 5 for 0.5, 1 and 1.5 h. The suspension with solid load of 30 wt. % was used. Viscosity of the slip was controlled using Viscotester 6l/R, Haake.

After milling, the suspension was sieved by the sieve of 11 μm, dried in porous plates at RT, milled by agate mortar and dried at 105 ^oC.

Pressing was carried out in two steps: First, by uniaxial at P=2 MPa (WEBER PRESSEN KIP 100) and by cold isostatic pressing (CIP) at 500 MPa (WEBER PRESSEN KIP 500 E).

The samples in the form of rod 30x4x4 mm^3 were produced. Sintering was carried out under a constant heating rate of 10 $^oC\ min^{-1}$ in the interval
RT-1500 ^oC without soaking time.

The green density of the compacts was determined by measuring the mass and volume with help of a micrometer to the nearest of 0.001 cm and final density was determined by Archimedes displacement method.

The shrinkage was followed by dilatometry (NETZSCH TMA 402E) in air atmosphere, using heating rate of 10 $^oC\ min^{-1}$ in the temperature interval 20-1500 ^oC.

Microstructure and grain sizes were observed by scanning electron microscopy (Leica IS 110) on fractured and polished surface. The polished samples were thermally etched at 100 ^oC below sintering temperature for 1 h to reveal the grain structure.

3. RESULTS AND DISCUSSION

The characteristics of as received powder are reported in Table1.

Tab. 1. Characteristics of a transitional alumina nano powder

Specific surface area (BET), m^2/g	XRD phases	Tap density, g/dm^3
89.0	δ, θ, γ, α	30.15

The TEM micrograph shows the spatial arrangement of the nano particles. The size of primary alumina particles was 5-50 nm. One part of these primary particles are aggregated in the as received powder and the aggregate sized ranged from around 100-800 nm, Fig.1.

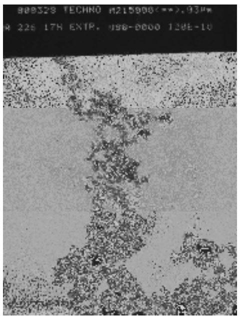

Fig.1 TEM photograph of the starting transitional alumina powder (bar 30 nm)

The dominant phases are δ- and γ-Al_2O_3. The θ-crystalline phase which is the last metastable transitional alumina with a cubic closed packing of oxygen ions and stable α-phases with hexagonal oxygen packing are approximately 6±1 %.

DTA investigation of the started powder showed one exopeak at 1304 ^{o}C what corresponding to the α-Al_2O_3 transformation. By using cold isostatic pressing of 500 MPa, the exopeak is shifted at 1146.7 ^{o}C .The transformation temperature is reduced for 157.3 ^{o}C. According to [7], the effect of pressing is to reduce the apparent incubation time and to increase the constants of the transformation kinetics. After mechanical activation by attriting the exopeak is shifted at 1126,4 ^{o}C. Mechanically activated and pressed powder of nanoscaled alumina shows exopeak of θ→α-Al_2O_3 transformation at 1079.3 ^{o}C.

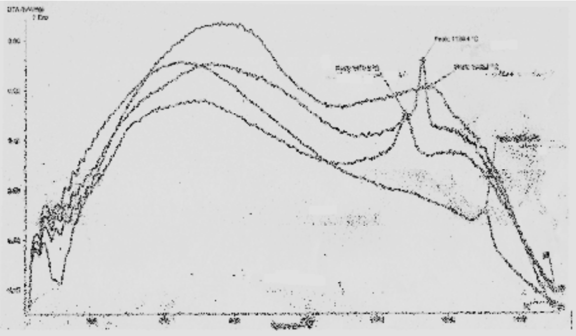

Fig 2. DTA of the started (1) pressed (2) mechanically activated (3) and mechanically activated and pressed (4) transitional nanoscaled alumina.

Mechanical activation causes changes in a materials structure, which has a direct influence on properties dependent on structure-transport as well as reactive properties [9-12].

During the wet milling chemical and physical interaction of the alumina particles surface exists with the surrounding medium. This interaction can be influenced by surface changes, the type and concentration of surface defects, unsaturated bonding states and the morphology of the particle surface. In wet grinding the reological and colloid chemical behaviour of the particles is crucial in respect of the process flow and resulting material properties. The fine particles become electrically charged when they are dispersed in aqueous system charged in the order of the state of the lattice, which are caused by formation of the lattice distortion, surface defects and decreasing crystallite size [9,10].

The green density of the compacts after CIP was 2.00 g/cm^3 what is 0.55TD.

The sinterability of the compacts formed from the started powder is shown in Fig.3, where $\Delta L/L_0$ is plotted as a function of the temperature ($\Delta L=L_0-L$), where L_o is the initial length of the sample and L is instantaneous sample length. The temperature of 985 ^{o}C at which measurable shrin-kage begins is comparable to that commonly observed for compacts of sub micrometer α-Al_2O_3 powders [8]. The densification of transitional alumina shows two regions of densification during the constant heating rate.

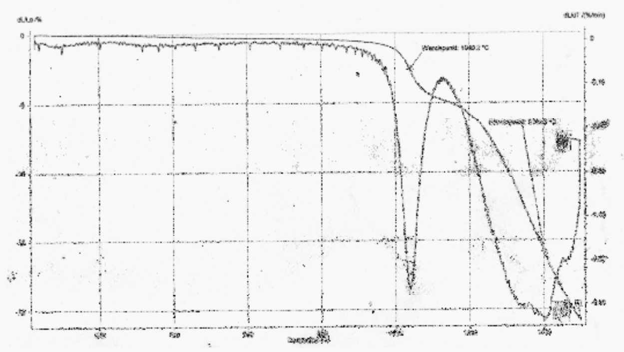

Fig. 3 Shrinkage ($\Delta L/L_o$) (1) and shrinkage rate (dL/dT) (2) of the compact formed of the as-received powder, during sintering at 10 ^{o}C min^{-1} to 1500 ^{o}C.

The first one is distinctive feature of sintering kinetics, with rapid shrinkage in the temperature region 985-1134 ^{o}C, with maximum shrinkage rate at 1040.2 ^{o}C. This densification is associated with the phase transformation of γ-Al_2O_3 via δ and θ to stabile α-phase. The second region of shrinkage above 1134 ^{o}C is densification of the α-Al_2O_3 at higher temperatures. At temperature of 1500 ^{o}C shrinkage got value of $\Delta L/L_o$=21.0 %, where density of 0.73 TD was achieved.

The vermicular microstructure of the sintered sample up to 1500 ^{o}C is shown in Fig.4. The elongated grains have size of 0.5-1.8 μm.

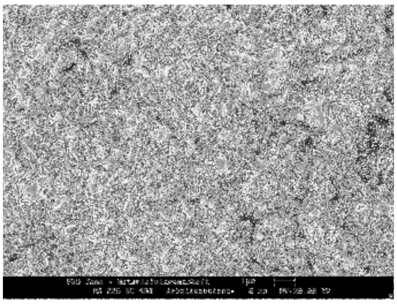

Fig.4 SEM micrograph of fractured surface of the sample, sintered at 1500 ^{o}C, ρr=0.73TD (bar 1 μm).

Sintering of the mechanically activated powder in the temperature interval RT-1500 ^{o}C without soaking time showed shrinkage of 18.8 %. The density of the sintered samples at 1500 ^{o}C was 3.79 g/cm^3 (0.95TD). The same value of the relative density was obtained by Karagerov and Lyakhov [13]. The microstructure of the sample is shown in Fig 5.

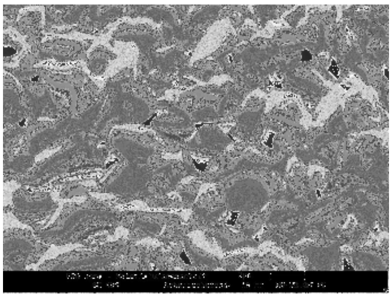

Fig.5 SEM micrograph of the sintered sample of the mechanically activated powder, up to 1500 ^{o}C, ρ=3.79 g/cm^3 (0.95TD), polished and thermally etched surface, (bar 2 μm).

The α-alumina microstructure exhibits grain size distribution from 0.5 to 3 μm.

This type of alumina ceramics due to its density and microstructure exhibits good bioinert properties and represents a biomaterial which can be used in medicine.

4. CONCLUSION

Transitional nano alumina powder obtained by pulse reactor tech-nique, among γ, δ, θ-Al_2O_3 contains also cca 6±1 wt. % α-Al_2O_3. This α-Al_2O_3 has no seeding effect.

The consolidation of the system was made by means of the isostatic pressure of 500MPa and non-isostatic sintering RT-1500 ^{0}C, obtaining compacts with vermicular structure and density of 0.73TD. The elongated α-Al_2O_3 grains have size of 0.5-1.8 μm. Using mechanical activation, realised by attrition for 0.5 h treatment, it was obtained an active nanoscaled powder, in which the transformation into α-Al_2O_3 is carried out at 1079 ^{0}C. The consolidate system obtained in temperature interval RT-1500 ^{0}C has a density of 0.95TD and a grain size 0.5-3 μm. This type of alumina ceramics due to its density and microstructure exhibits good bioinert properties and represents a biomaterial which can be used in medicine.

5. ACKNOWLEDGMENT

The authors acknowledge thankfully the financial support for this work from the Ministry of education and science of Republic of Macedonia (contract 071005).

6. REFERENCES

[1] Kumagai M., G. Messing, (1985), Controlled transformation and sintering of a boehmite sol-gel by α-alumina seeding J. Am. Ceram. Soc., **68** (9), 500-505

[2] Messing G. L., M. Kumagai, R. Shelleman, J. McArdle, (1986), Seeded Transformation for Microstructural Control in Ceramics, in Science of Ceramic Chemical Processing, Eds. L: L. Hench and D. R. Ulrich, J. Wiley &Sons, P25919.

[3] Legros C., C. Carry, P. Bowen, H. Hofmann, (1999), Sintering of a Transition Alumina: Effect of Phase Transformation, Powder Characteristics and Thermal Cycle, J. Eu. Ceram. Soc.,**19**,1967-1978

[4] Wakao Y., T. Hibino, (1962), Effect of Metallic Oxides on Alpha Transformation, Nagoya Koguo Gijytsy Skikensko Hokuku, **11**, 588-95, quoted after K. Kumagai, G. Nesing, J. Am. Ceram. Soc., **68** (9) 500-505 (1982)

[5] Bye G. C., G. T. Simpkin, (1974), *Influence of Cr and Fe on Formation of α-Al_2O_3 from γ-Al_2O_3,* J. Am. Ceram. Soc., **57** (8), 367-371

[6] Zou R. S., R. Snyder, (1991), Structure and transformation mechanisms of the η,γ and θ transition aluminas, Acta Crys. **B47,** 617-630

[7] Dynys W., J. W. Halloran, (1982), Alpha alumina formation in alumina derived gamma alumina, J. Am. Ceram., **65** (9), 442-448

[8] Wu S., L. De Jonghe, (1996), Sintering of nanophase γ-Al_2O_3 powder, J. Am. Ceram. Soc., **79** (8), 2207-2211

[9] Kirchuchi S., T. Ban, K. Okada, N. Otsuka, (1992), Mechanochemical effect for some Al_2O_3 powder by wet grinding, J. Mat. Sci. Lett., **11**, 471-474

[10] Bennet R. B., D. E. Niesz, (1972), Defects of surface-chemical reactions during wet milling of alumina., Tech. report No 3., Battelle, Columbus Lab., presented of 74 annual meeting of Am. Ceram. Soc.

[11] Nikolic M., N. Nikolic, S. Radic, (2000), Mechanical activation of a mixture of oxides of the MgO-Al_2O_3-SiO_2 system, Sci. Sintering, 32 (3), 149-152

[12] Brankovic A., V. Vidojkovic, S. Milosevic, (1998), Mechanochemical Activation of (SeO_2+Na_2CO_3) Mixture and Sodium Selenite Synthesys in Vibrational Mill, J. Solid State Chem., **135,** 256-259

[13] Karagedov G. R., N. Z. Lyakhov, (1999), Preparation and sintering nanosized Al_2O_3 powder, Nanostructured Materials, 11 (5), 559-562

DESIGN OF PYRIMIDINE AND PURINE NUCLEOSIDE WITH ANTIVIRAL ACTIVITY

Ivanka Stankova

Department of Chemistry, South-West University ''Neofit Rilski''

INTRODUCTION

A rational approach to the design of antiherpetic nucleoside analogues is based in part on the broad specificity of virus-coded thymidine kinases. Herpes virus thymidine kinase ‘activates’ many 5-substituted 2′-deoxyuridines, analogues ol thymidinc (*e.g.*, idoxuridine, trifluridine, edoxudine, brivudine), 5-substituted arabinofuranosyluracil derivatives (*e.g.*, 5-Et-Ara-U, BV-Ara-U, Cl-Ara-U), acyclonucleosides of guanine (*e.g.*, aciclovir, ganciclovir, penciclovir), and purine nucleosides with the pentafuranosyl ring replaced by a cyclobutane ring (*e.g.*, cyclobut-G, cyclobut-A). Activation involves selective, and frequently regiospecific, phosphorylation all these analogues to the 5′-monophosphales. These are further phosphorylated by cellular enzymes to the 5′-triphosphates, which are usually competitive inhibitors of the viral-coded DNA polymerases. Some analogues are also incorporated into viral, and to a lesser extent cellular, DNA.

Because of the nature of viruses as intracellular parasites, very few clinical useful agents that treat virus infections have been produced. Development of drugs that are active against viruses is one of the most challenging areas in antimicrobial chemotherapy.

New leads in drug discovery can be found by screening a large number of compounds. Once an active molecule is identified, it can be used as a model for chemical modification. The use of this strategy has proved successfully in the discovery of drugs active against HSV-1. A more rational approach is based on crystallographic methods and computer-assisted modelling.

I. Pyrimidine nucleosides

1. 1. 5-Substituted 2’-deoxyuridines as anti-HSV agents (Fig. 1.).

Boc 5-iodo-2’-deoxyuridine was the first antiviral nucleoside to be discovered [1]. In this series of 5-substituted 2’-deoxyuridine it was followed by the second generation antivirals: 5-trifluoromethyl-2’-deoxyuridine, 5-ethyl-2’deoxyuridine, 5-(E)-bromovinyl-2’-deoxyuridine [2-6].

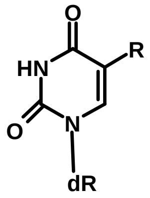

Fig. 1.

2’-Deoxynucleosides with a 5-substituted pyrimidine base moiety have been synthesized an evaluated for anti-HSV-1 activity: 2’-deoxynucleosides derivatives with saturated 5-substituent (Table. 1.), 2’-deoxynucleosides derivatives with an unsaturated 5-substituent (Table 2.) and 5-heteroaryl substituted 2’-deoxyuridines derivatives (Table 3.) [7].

Table 1. 2’-Deoxyuridine derivatives with saturated 5-substituent

SUBSTITUENT	*SUBSTITUENT*
$-CH_2-CH_3$(De Clercq, Shugar)	$-CH_3-N_3$ (De Clercq)
$-CH_2-CH_2-CH_3$(De Clercq)	$-CH_2-S-CH_3$ (Schmidt)
$-CH(CH_3)_2$(De Clercq)	$-CH_2SO_2-CH_3$ (De Clercq)
$-CH_2-CH_2-CH_2-CH_3$(Goodchild)	$-CH_2OH$ (De Clercq)
$-CH_2-CH_2-F$ (Griengl)	$-CH_2-O-CH_3$ (Gupta,)
$-CH_2-CH_2-Cl$ (Griengl)	$-CH(OCH_3)-CH_2-Br$ (Kumar)
CH_2-CH_2-Br (Griengl)	$-CH(OCH_3)-CH_2-I$ (Kumar)
CH_2-CH_2-I (Griengl)	$-CH(OH)-CH_2-Cl$ (Kumar)
$-CH_2-CH_2-CH_2-Cl$ (Griengl)	-CH(OH)-CH(I)-COOEt (Kumar)
	-CH(OH)-CH(Br)COOEt(Kumar)

The compounds identified in Table 1 which have a flexible 5-substituent provide less information than those in either Table 2 or Table 3. After synthesizing several 5-unsaturated derivatives *Goodchild et al.* concluded that, for anti-HSV-1 activity, the 5-substituent should be conjugated, not larger 4 carbon, hydrophobic, inductive and unbranched [8-14].

Table 2. *2'-Deoxyuridine derivatives with unsaturated 5-substituent*

SUBSTITUENT	*SUBSTITUENT*
$-CH=CH_2$ (De Clercq)	$-CH\equiv CH$ (De Clercq)
-CH=CH-Cl (Walker)	$-CH\equiv C-CH_3$ (De Clercq)
-CH=CH-Br(De Clercq)	$-CH\equiv C-CH_2-CH_3$ (De Clercq)
-CH=CH-I (De Clercq)	$-CH\equiv C-CH_2-O-CH_3$ (De Clercq)
$-CH=CH-CF_3$ (Bergstrom et al.)	$-CH\equiv C-C(CH_3)_3$ (De Clercq)
-CH=CH-F (Reefschläger et al.)	$-CH\equiv C-CH_2-CH_2-CH_3$ (De Clercq)
$-CH=CH-CH_3$ (Bergstrom et al.)	$-CH\equiv C-CH=CH_2$ (De Clercq)
$-CH=CF_2$(Bobek et al.)	-CH=O (Park et al.)
$-CF=CF_2$ (Herdewijn et al)	-CH=N-OH (Park et al.)
-CF=CFCl (Coe et al.)	$-CH=CBr_2$ (Goodchild et al)
$-CH=CH-COOCH_3$ (Griengl et al.)	$-CH=CH-S-CH_3$ (Goodchild et al)
$-CCl=CH_2$ (De Clercq)	$-C(CH_3)=CH-Br$ (Goodchild et al)
$-CH=CH-CH_2-CH_3$ (Goodchild et al)	$-CH=C(Br)-CH_3$ (Goodchild et al)
$-CH_2-CH=CH-CH_3$ (Goodchild et al)	

The 5-heteroaromatic substituted 2'-deoxyuridine can be divided into two groups (Table 3). The first group of very potent compounds involves 5-(thien-2-yl)-2'-deoxyuridine and 5-(furan-2-yl)-2'-deoxyuridine as lead structures. The antiviral activity of these compounds is retained when the heterocyclic rings is connected via its 3-position. When in thiophene ring has halogeno substituent, the activity against HSV-1 increases. However, this is not so pronounced when a halogen substituent is introduced in the furan ring. Clearly, there is a difference between both groups of compounds. The presence of a saturated or unsaturated alkyl group in the same position of the thiophene ring does not improve the anti-HSV-1 activity [15-17].

Table 3.
5-Heteroaryl substituted 2'-Deoxyuridines derivatives

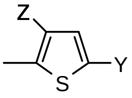 Z = H, Y = H (Vincent, 1984) (Wigerick, 1991) (Peters, 1991) (Hassan, 1991) Z = H, Y = Cl, Br (Wigerick, 1991) Z = H, Y = I, NO_2, CH_3, $CH=CH_2$, C Z = H, Y = C_6H_5 (Peters, 1991) Z = CH_3, C_6H_{13}, Y = H (Peters, 1991, Peters, 1992)	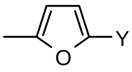 Y = H (Wigerick, 1991) (Hassan, 1991) Y = Cl, Br (Wigerick, 1991)
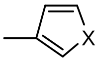 X = O (Wigerick, 1993) X = S (Vincent, 1984) (Wigerick, 1993)	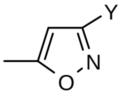 Y = H (Wigerick,1993) Y = C_6H_5, Br, CH_3,C_2H_5,C_6H_5(p)Cl (Wigerick,1991)

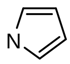 Widerinck, 1991	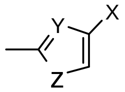 Y = N, Z = S, X = H (Wigerick, 1991) (Wigerick, 1991) (Peters, 1991) Y = N, Z = S, X = $CH_{3,}C_6H_5$ (Wigerick, 1991) Y = CH, Z = N-CH_3, X = H (Hassan, 1991)

1. 2. 2'-deoxy-(3'- and 3',5'-O- substituted) pyrimidine nucleosides

Azido and amino analogues of pyrimidine 2'-deoxynucleosides

3'-Azido-3'-deoxythymidine (AZT) was first synthesized by Horwitz at all. to be a potent inhibitor of the replication of human immunodeficiency virus (HIV) that is responsible for the acquired immunodeficiency syndrome [18]. AZT has been reported to be of marked benefit in the therapy of AIDS patients, but the usefulness of AZT is limited by its bone marrow toxicity. Various 3'-azido, 3'-amino, 2',3'-insaturated, 2',3'-dideoxy, and 5-substtituted analogues of pyrimidine deoxyribonucleosides have been synthesized and their antiviral activity was evaluated [19-21].

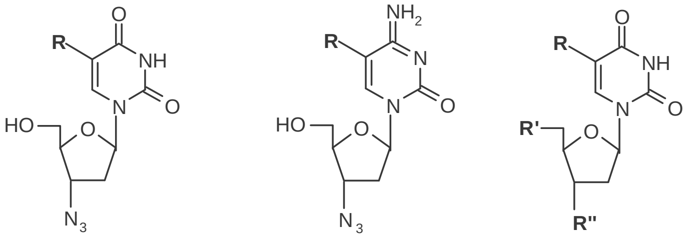

1: **R** = H
2: **R** = CH_3
3: **R** = CF_3
4: **R** = F
5: **R** = Br

6: **R** = I
7: **R =** H
8: **R** = F
9: **R** = CH_3
10: **R** = CH_3,**R'** = N_3, **R"** = OH

11: **R** = CH_3, **R'** = **R"** = N_3
12: **R** = CH_3, **R'** = OH, **R"** = NH_2
13: **R** = CF_3, **R'** = OH, **R"** = NH_2
14: **R** = CH_3, **R'** = NH_2, **R"** = OH
15: **R** = CH_3, **R'** = **R"** = NH_2

Fig. 2.

Among these 3'-azido and 3'-amino derivatives, 3'-azido-3'-deoxythymidine (**2**, AZT),(**Fig. 1-2),** was the most active against HIV. The 3'-azido analogues of 5-bromo- and 5-iodo-2'-deoxyuridine compound **5** and **6** also showed significant antiviral activity. The 3'-azido derivative of 2'-deoxyuridine (**1** AZDU) and the 3',5'-diazido and 3;-amino derivatives of thymidine **11, 12,** demonstrated moderate antiviral activity. Conversely, the 3'-azido analogue of 2'-deoxycytidine, compound **7**, only showed moderate inhibition against HIV-1.

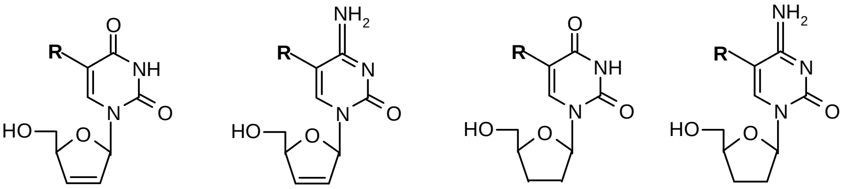

16: R **= H**　　18　　19: **R = H**　　24

17: R **= CH_3**　　20: **R = CH_3**

21: **R = Br**

22: **R = I**

23: **(E)-HC = CH(Br)**

Fig. 3.

The other 3'-azido and 3'-amino derivatives in this group were found to be practically inactive. Among the 2',3'-insaturated, 2',3'-dideoxy derivatives of pyrimidine deoxyribonucleosides, the 2',3'-unsaturated analogue of thymidine (**17** D4T) and 2'-deoxycitidine (**18** D4C) and the 3'-deoxy analogue of 2'-deoxycytidine (**24** DDC) produced significant antiviral activity. Replacement of uracil moiety of the 3'-azido nucleoside analogue **1** with the cytosine to form **7** did not affect its antiviral activity, however, when the substituent on carbon-5 of the cytosine moiety was either fluoro **8** or methyl **9**, the antiviral activity was markedly reduced. This could be explained if these 3'-azido-2',3'-dideoxycytidine analogues are not substrates. Other possibilities include differences in metabolic conversion to the di- and tri-phosphates analogues, as well, as the relative affinities of the triphosphate analogues for the reverse transcriptase.

The azido group in the 3'-position of the deoxyribose moiety of the thymidine (**2** AZT) is critical since transfer to the 5'-position, **10**, resulted in marked decrease in activity. However, retention of the 3'-azido group with addition of an azido group to the 5'-position (as in **11**) increased the antiviral activity relative to **10,** but decreased its activity relative to **2**. Thus a primary hydroxyl group in the 5'-position is beneficial. Although one may presume the 5'-hydroxyl moiety is required for substrate activity for thymidine kinase, this can not be a prerequisite for antiviral activity of the 3',5'-diazido analogue **11**, unless the 5'-azido moiety were hydrolytically cleaved, either chemically or enzymatically, to a hydroxyl group, a reaction which is most unlikely.

Reduction of the 3'-azido moiety of **2** to an amino group **12** markedly decreased activity: however, moderate antiviral activity was retained. Whether the activity of **12** is related to the bonafide antiviral activity of this compound or to the cytotoxic properties of **12** is not clear.

Replacement of 3'-azido moiety of **2** with hydrogen **20** resulted in loss of activity; however subsequent removal of a hydrogen atom from both the 2'- and 3'-carbon produced the active compound **17** (D4T); thus the azido moiety per se is not an absolute requirement for the antiviral activity of the thymidine analogues. However, replacement of the 5-methyl group of **17** with a hydrogen **16** yielded a loss of activity. The azido moiety conferred moderate antiviral activity to 2'-deoxycytidine **7**, but this moiety also is not an absolute requirement since its replacement with a hydrogen **24** resulted in a marked increase in activity. Subsequent removal of a hydrogen from the 2'- and 3'-carbon of **24** to produced **19** with a concomitant loss of antiviral activity, which could not be recovered by insertion of a variety of substituents on the carbon-5 of the uracil moiety (**20-23**).

We have modifited in the 5'-position with amino acid (glycine) and peptides (Gly-Gly, Gly-Gly-Gly) 3'-azido-3'-deoxythymidin (AZT) and have evaluated their anti-HIV activity. The results showed that the peptide derivatives of AZT had the same anti-HIV activity in comparison with AZT [22] .

The toxicity of the peptide derivatives of AZT and the AZT were measured on MT_4 uninfected cell line. It was clearly shown that one of the peptide analogues - Gly-Gly, is at least 5 times less toxic comparing to AZT (parent drug).

The chemical stability of the new analogues of AZT was studied in experimental conditions simulating some relevant biological medias (pH 1.0 and 7.4 and 37ºC). Compounds are considered as stable, although their slow conversion to 3'-azido-3'-deoxythymidin. The stability of the former group of esters outlines them as suitable candidates for prodrugs: higher lipopholicity stability per os absorption, satisfying chemical stability and a possibility to release the active moiety following enzymatic hydrolysis.

Various 3'-amino analogues of 5-substituted pyrimidine deoxuribonucleosides have been synthesized and their biological activity evaluated [23-24] . Among these compounds, 3'-amino-2',3'-dideoxy-5-fluorouridine **27**, 3'-amino-3'-deoxythymidine **28**, 3'-amino-2',3'-deoxycytidine **32,** and 3'-amino-2',3'-dideoxy-5-fluorocytidine **33** were found to have significant activity against HSV-1. The 3'-azido derivatives **25, 26,** demonstrated either less activity in comparison to their 3'-amino analogues. The 3'-azido-5'-fluoro and 3'-amino-5'-fluoro derivatives of thymidine **31** and **33,** and the 5'-amino and 3',5'-diamino derivatives of thymidine **30** and **35,** to be not active against HSV-1 in vitro.

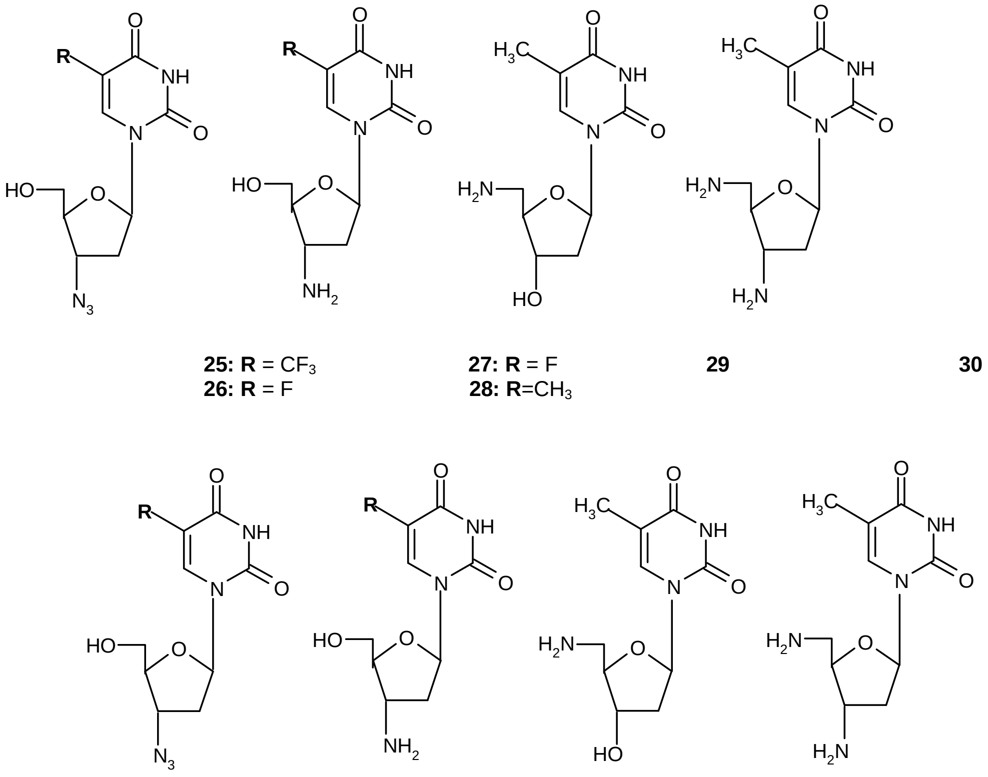

25: R = CF_3
26: R = F

27: R = F
28: R=CH_3

29

30

31

32: R = NH_2
33: R = F

34: R = H

35: R = F

Fig. 4

The modification of various biological active compounds with amino acids allows them to be hydrolyzed more quickly under the influence of plasma enzymes, thus leading to their transformation as prodrugs.

We have synthesized and have evaluated antiviral activity of several amino acid and peptide derivatives of 5-bromo-2'-deoxyuridine and thymidine [25-28]. We have also considered the role of chirality, aromatic, heterocyclic amino acid residues, the addition of the long peptide chains formed of glycine to 5-bromo-2'-deoxyuridine and thymidine, and the effect of these structural modifications on antiviral activity.

Initially the new analogues were evaluated for their antiviral activity towards influenza virus, (FPV) and pseudorabies virus, (PsRV).

The data clearly demonstrate the marked anti–herpes virus potential of these compounds, comparable with that of 5-bromo - 2' - deoxyuridine in the case of BUdR-Gly-Gly. It is important to stress that there is no difference in activity between the R and S isomers BUdR- phenylalanine and Thymidine-phenylalanine**.**

Analogue of phenylalanine with 5-bromo-2'-deoxyurdine do not show activity, and the same analogue of thymidine exhibited a borderline activity. Compound BUdR-Gly-Gly has a strong activity against the herpes virus PsRV. This activity was comparable with that of BUdR used as a reference antiherpes virus compound. Compounds BUdR-Gly**,** BudR-Gly-Gly-Gly, showed a marked but less pronounced effect compared to BUdR-Gly-Gly. The rest of the compounds were inactive, and neither analogue showed activity against the influenza virus model. The corresponding derivatives of the normal metabolite – thymidine - do not show any antivirus activity.

The three compounds BUdR-BUdR-Gly**,** BudR-Gly-Gly-Gly, BUdR-Gly-Gly proved antiherpes activities to HSV-1. However, they showed a decrease of the effect selectivity, especially strongly expressed in BudR-Gly-Gly-Gly.

These results demonstrated that among the testing compounds, the peptide analogues possessed a marked antiviral activity in comparison with these of the amino acids. In addition, elongation of the peptide chain enhanced the antiviral activity.

The chemical stability of thymidine, 5-bromo-2’-deoxyuridine was studied at pH 1 and pH 7.4 both at 37°C and at ambient temperature.

The compounds (Thymidine-Ala, BUdR-Gly, BudR-Gly-Gly-Gly) with simple aliphatic straight side chain (containing Ala-, Gly-Gly-Gly-, Gly-, residues) are relatively stable both at acidic and neutral media and a temperature of 37°C. More complex esters with branched side chain-methyl group substitution on the beta carbon of the amino acid T i , with phenyl residue as well as containing thiazol ring BUdR are rather unstable especially at acidic conditions. They undergo rapid hydrolysis resulting in the respective chemical precursor.

II. Purine nucleosides

The necessity of effective therapeutic agents for the cure of infections caused by herpes viruses of the type herpes-simplex virus (HSV-1, 2), varicella zoster virus (VZV), cytomegalovirus (CMV), Epstein-Barr virus (EBV)] stimulates the synthesis of various biologically active compounds [29-30]

A further reason for developing anti-HSV-1 agents is that HSV strains could develope resistance to the drug. Resistance to antiherpes drugs is a serious clinical problem in immunocompromised patients [31].

When an otherwise healthy person is infected with HSV-1, the infection normally can be left untreated. However, special treatment might be required in immunologically deficient people (for example transplantation, cancer, or AIDS patients). Also HSV encephalitis, which contributes to mortality in neonates, needs antiviral treatment.

The discovery of aciclovir, (9-[(2-hydroxyethoxy)methyl)]-9H-guanine, Zovirax® twenty years ago, directed the interest to the acyclic guanozine nucleosides as potential antiviral agents. Other drugs similarly to aciclovir, as e.g. ganciclovir, penciclovir, have been applied on patients and have shown different antiviral activity. Concurrently, however, such drugs have exhibited toxicity at systematic use. One of the problems with these drugs of antiviral activity is their poor bioavailability: 15% for aciclovir, 4.2-7.5% for ganciclovir and very low oral absorption for penciclovir . Most of these drugs are toxic (ganciclovir, for example, inflict neutropenia) and their harmful effect limits the dosage (Fig.6) [32-35].

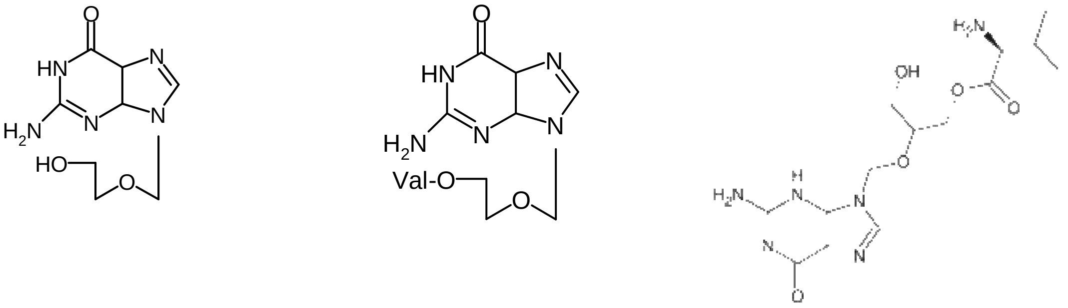

acyclovir **valacyclovir** **valgancyclovir**

Fig.6

In order to improve the acyclovir bioavailability the drug valacyclovir (L-Val-acyclovir ester), that is the famous and the most used in the practice today acyclovir prodrug. In living organisms it is rapidly transformed into acyclovir and valine. The advantage of this analogue is its higher bioavailability (nearly 60%) [36-38].

The similar effect is achieved by some other antiviral drug possessing purine structure –gancyclovir (9-(1,3-dihydroxy-2-propoxymethyl)guanin. Valgancyclovir (L-Val-gancyclovir ester), suppresses cytomegalovirus (CMV) replication and it is applied at medical treatment of (CMV) retinitis and AIDS suffering patients. It is observed absolute bioavailability at its per oral application.

Two amino acid ester prodrugs of acyclouir (ACV), glutamate-ACV (EACV) and L-tyrosine-ACV (YACV), was studied across rabbit cornea. The results demonstrated that YACV and EACV exhibited excellent antiviral activity against HSV-1 and 2 and VZV in comparison to ACV.

A series of dipeptide prodrugs (Gly-Val, Val-Val, Tyr-Val, Val-Tyr) of acyclovir were designed to target the oligopeptide transporter on the cornea with an improving of the ocular bioavailability and therapeutic activity of acyclovir. ACV prodrugs were found to be more stable at pH 5.6 in comparison to L-Val-ACV , an amino acid prodrug of ACV. The prodrugs exhibited higher solubility than ACV. Val-Val-ACV and Val-Gly-ACV were found to have excellent antiviral activity against HSV-1.

The stability, the solubility and the antiviral activity increase of the biological active compounds can be achieved by their covalent linking to polymer. Acyclovir and valaciclovir, were coupled with activated poly(ethylene glycol) [39].

PEG–valacyclovir is more suitable for therapeutic use since it is more stable in various buffer and releases more of the free, active drug over time (40% in 24 h). Thus, PEG–valacyclovir could be used orally, by intramuscolar injection, or topically. PEG–acyclovir, on the other hand, may be suitable for administration (in all ways except orally) in those cases in which a rapid therapeutic effect is desired [40-42].

It is well known that modified amino acids, containing five heterocycle ring, take part in a variety of compounds with antiviral, antibacterial and antitumour activity. That is the reason, the synthesis of amino acids with thiazole ring and their application in some antiviral drugs, to be of great interest.

We synthesized thiazole containing amino acids (Gly, Val, Ala, Leu) esters of acyclovir and to explore their activity on the HSV-1 [43].

The Val-thiazole-4-yl-acyclovir and 2-aminomethyl-thiazole-4-yl-acyclovir shown insignificant effects on the herpesvirus replication – 20 and 10% inhibition respectively. The Ala- thiazole-4-yl-ACV and Leu-thiazole-4-yl-ACV shown insignificant effects on the herpesvirus replication – 20 and 8 % inhibition respectively.

These results suggest that it should be of great interest if the antiviral activity of these compounds is tested on the resistance viral strain.

Design of amino acid esters of some purine nucleosides seems to be an attractive strategy to enhance the solubility of the otherwise poorly aqueous soluble compounds and also to afford a targeted and possibly enhanced delivery of the active drug. An implicit proof of this assumption is the fact that L-valyl ester of acyclovir (valacyclovir) shows bioavailability of 60%.

CONCLUSION

Pyrimidines and purines occupy a distinct and unique place in our life. These heterocyclic moieties have great biological and medicinal significance. A large array of pyrimidine and purine drugs possess a variety of medicinal properties. These properties include anticancer, antiviral activities.

REFERENCES

[1] Prusoff W. H. (1959), *Biochim. Biophys. Acta*, 1959, 32, 295-296. Herrmann E. E., , *Proc. Soc. Exp. Boil. Med.,* **1961,**107, 142-145.
[2] Kaufman H. E.,, *Proc. Soc. Exp. Boil. Med.,* **1962,** 109, 251-252.
[3] De Clercq E., Degreef H., Wildiers J., *Brit. Med. J.* 1980, *281, 1178*
[4] De Clercq E., Descamps J., De Somer P., Barr P. J., Jones A. S. and Walker R. T. in: Control of Virus Diseases, New York: Marsel Dekker., **1983.**
[5] De Clercq E., Degreef H., Wildiers J., *Brit. Med. J.*1982*, 371, 1228*
[6] Herdewijn P., *Antiviral Chem.,Chem.,* **1994,** 5,3, 131-146.
[7] Smith R., Kirpatrick. Ribavirin, a Broad Spectrum Antiviral Agent. New York, Academic Press, **1980.**
[8] Balzarini J., Bernaerts J., Verbruggen A., and De Clercq E., *Mol. Pharmacol*, **1990, 37,** 402-407.
[9] Kaufman H. E., Varnell E.D., Cheng Y., C., Bobek M., Dutschman G. E., *Antiviral Res.,* **1990,** 16, 227-232.
[10] Vincent P., Beaucourt J. P. and Picat L. (1984), *Tetrahedron Lett.,* **1984, 25**, 201-202.
[11] Wigerinck P., Pannecouque C., Snoeck R., Claes P., De Clercq E. and Herdewijn P, *J. Med. Chem.,* **1991, 34**, 2383-2389.
[12] Wigerinck P., Kerremans L., Claes P., Snoeck R., Maudgal P., De Clercq E. and Herdewijn P. , *J. Med. Chem.,* **1993, 36**, 538-543.
[13] Goodchild J., Porter R. A.., Raper R. H., Sim I.S., Upton R. M., Viney J. and Wasworth H. J., *J. Med. Chem.,* **1983, 26,** 1252-1257.
[14] Griengl H., Wanek E., Schwarz W., Streicher W., Rosenwirth B. and De Clercq E, *J. Med. Chem*., **1987, 30**, 1199-1204.
[15] Schmidt R. A., Chang C. T., De Clercq E., Descamps J. and Mertes M. P., *J. Med. Chem.,* **1980, 23**, 251-256.
[16] De Clercq E., Descamps J., Verhelst G., Walker R. T., Jones A. S., Torrence P. F., and Shugar D. , *J. Infect. Dis.,* **1990, 141**, 563-574.
[17] Horwitz P. J., Chua J., Da Rooge A. M., Noel M. and Klundt L. I. *J. Org. Chem.* **1966, 3**, 205-205.
[18] De Clercd E., *J.Med. Chem.,* **1995, 38**, (14), 2491-2517.

[19] Karpas A., Ash S., and Bainbrdge D.,, *Molec. Med. Today*, **1998, June**, 244-249.

[20] Bartlett J. and Moore R. , *Scient. Amer*., **1998, July**, 64-67.

[21] Stankova I. G., Beschkov D. A. and Evgeny V. Golovinsky , *Peptides,* **2000,** 745-746, Jean Martinez and Jean-Alain Fehrenz (eds.), EDC Paris, France, **2001**

[22] Mandelbrot L., Le Chenadec J., and Berrebi A.., *JAMA*, **1998, 280**, 55-60.

[23] King C., Rudin C., and Siegrist C. A. , *AIDS*, **1998***12*, 205-210.

[24] Stankova I. G., Videnov G. I., Golovinsky E.V., and Jung G., *J. Peptide Sci.*, **1999,** 5, 392-398,

[25] Stankova I. G., Videnov G. I., Tabakova Sv., Golovinsky E.V. and Jung G., *Peptides*, **1998,** 248 - 249, S. Bajusz and F. Hudecz (eds.), Akademiai Kiady, Budapest.

[26] Stankova I. G., Videnov G. I., Galabov A. S. and Golovinsky E. V.**,** *Peptides*, **1996,** 813 - 814, R. Ramage and R. Epton (eds.), MPG Books LTD, Bodmin, Kornwall, England, UK.

[27] Stankova I. G., Simeonov F. M., Maximova V., Galabov A. S. and Golovinsky E.V., *Zeitschrift fuer Naturforsch*., **1999,** 1-2, 75-83.

[28] Chatis, P. A. and Crumpacker, C. S.,*Antimicrob Agents Chemother*. **1992, 36**, 1589-1595.

[29] Coen, D. M.. *Antiviral Res*, **1991, 15**, 287-300.

[30] Alrabian F. A. and Sacks S. L. . *Drugs*, **1996, 52 (1)**, 17-32.

[31] Moss, N., Beaulieu, P., Duceppe, J., Ferland, J., Garneau, M., Gauthier, J., Ghiro, E., Goulet, S., Guse, I., Jaramillo, J., Llinas-Brunet, M., Malenfant, E., Plante, R., Poirier M., Soucy, F., Wernic, D., Yoakim, C. and Deziel R., *J. Med. Chem*., **39**, **1996,** 4173-4180.

[32] O'Brien, J. J, Campli-Richards, D. M., *Drugs,* **1989**, 37, 233-309**2.** Périgaud C., Gosselin G., Imbach J.L, *Nucleosides and nucleotides* **1992.**: 11(2-4).

[33] Anand BS and Mitra AK , *Pharm Res,* **2002**, 1194–1202

[34] Beauchamp LM, Orr GF, de Miranda P, Burnette TC and Krenitsky TA, *Antiviral Chem Chemother* ,**1992**, 3: 157-164

[35] Beauchamp LM and Krenitsky TA, *Drugs Future,* **1993**, 18: 619-628,

[36] Anand BS, Katragadda S and Mitra AK, *J. Pharmacol. Exp. Ther*., **2004**, 311(2): 659 – 667,

[37] Lacy CH,: Drug information. UpToDate, 8.1, **2000.**

[38] Sanna Tolle-Sander, Kimberley A. Lentz, Dean Y. Maeda, Andrew Coop, and J. E. Polli, *Molecular Pharmaceutics*, **2004**, 1, 1, 40-48,

[39] Zacchigna M., G. Di Luca, V. Maurich, E. Boccu, *Il Farmaco* 57 , **2002**, 207–214

[40] Mallal S, Nolan D, Witt C, *et al.*, *Lancet* 359**, 2002,** 727–32.

[41] Hetherington S, Hughes AR, Mosteller M.., *Lancet* 359 ,**2002**, 1121–2.

[42] Rauch A, Nolan D, Martin A,*. Clin Infect Dis* 43 (1), **2006**., 99–102.

[43] Stankova I. G., Tzambova T., Chichkov S., *Peptides*, **2006, 226-227,** Kr. Rolka, P. Rekowsi, J. Silberring (eds.), Kenes International, 2005.

SN(II)-ION-SELECTIVE ELECTRODE BASED ON CHALCOGENIDE GLASSES

V. S. Vassilev[1], T. K. Hristova-Vasileva[1],

L. N. Aljihmani[1], V. A. Vachkov[2]

[1] *University of Chemical Technology and Metallurgy, 8, Kl. Ohridski blvd. 1756 Sofia, Bulgaria, e-mail: venciv@uctm.edu*
[2] *South-West University "Neofit Rilski", 2700 Blagoevgrad, Bulgaria*

Abstract*: Based on new chalcogenide glasses from the As2Se3-As2Te3 -SnTe system, Sn(II)-ion-selective electrodes from the "layered wire" type were produced. The main analytical characteristics of the electrodes were investigated, such as: linearity and slope of the electrode function, working pH interval, limits of detection, results reproduction and response time. The influence of some bicharged interfering ions on the responce of the Sn(II)-electrode was investigated. A mechanism for explanation the type of the investigated relations is proposed.*

Keywords: *ion-selective electrode, chalcogenide glasses, electrode function.*

1. INTRODUCTION

One of the possible applications of the chalcogenide glasses (ChG) is their use as ion-selective membranes characterized with: high sensitivity of the electrode function, good selectivity, acid-resistance, short response time and others.

The first use of ChG as membranes for ion-selective electrodes (ISE) is performed by Trachtenberg et al. [1-5]. In the present time chalcogenide sensors sensitive to Ag^+ [6,7], Cu^{2+} [8,9], Pb^{2+}[10], Cd^{2+} [11,12], Fe^{3+} [13,14], Zn^{2+}[15,16] and other ions are produced and investigated. The ChG find more and more wide application as membrane material for ISE [17].

The Sn(II)-ions are often met in different analytical objects. Their determination by the classic methods is complicated and labor-consuming task. The potentiometric method is one of the most perspective ones for their determination. The first developments were on the basis of membranes from polycrystalline chalcogenides with different additives (AgJ, Ag_2S, CuS, CuSe, etc.), which increase the ionic electroconductivity [11,18].

Due to the strong instability of the electrode function owed to change of the properties of the sensor's membrane surface produced by polycrystalline materials, the scientific investigations are pointed on Sn-containing ChG.

The aim of the present work is producing of solid state Sn(II)-ISE based on ChG form the As_2Se_3-As_2Te_3-SnTe system and investigation of their main analytical characteristics.

2. EXPERIMENTAL PROCEDURES

ISE from the "layered wire" type are constructed. For this purpose the active component (ChG) is introduced into inert polymer matrix (epoxy resin) in concentration of 2 mass. %. The compositions of the used ChG are shown in Tab. 1 and the glass-forming region form the As_2Se_3-As_2Te_3-SnTe system – on Fig.1. The internal reference electrode is produced by the following way: Ag-wire (∅=1 mm) is cleaned with 10 % solution of HNO_3, after which is wrecked in 0,5 M solution of $FeCl_3$ for 24 hours (the surface covers with thick layer of AgCl). In the ISE from the "layered wire" type the composite (ChG + epoxy resin) is deposited as thick layer on the surface of the Ag/AgCl-electrode.

Tab. 1. Composition and condition of the investigated ChG from the As_2Se_3-As_2Te_3-SnTe system (m=y/(x+y))

№	mol %			condition
	As_2Se_3	As_2Te_3	SnTe	
14	42	28	30	glass
11	22,5	67,5	10	glass
8	85,5	4,5	10	glass
6	54	36	10	glass

The potentiometric studies are led with a cell from the following kind:

Hg/Hg_2Cl_2	KCl (concentr.)		Investigated solution		Ion-selective composite membrane	Ag/AgCl

The standard solutions for calibration are obtained from starting solution (1M $SnCl_2$) by the method of the consecutively dilution. The electrode potential is measured at continuous agitation of the solutions with speed 300 rev/min. The conditioning of the ISE is performed in 10^{-3} M solution of the potential-determining ion. The pH influence on the electrode function is investigated in solutions with constant concentration of the Sn(II)-ion (10^{-1}, 10^{-2} и 10^{-3} mol/l), as concentrated HCl or 25 % solution of NH_3 is added in them. The response time and the limits of detection are defined in solutions with concentration of the Sn(II)-ions from от 10^{-8} to 10^{-1} M.

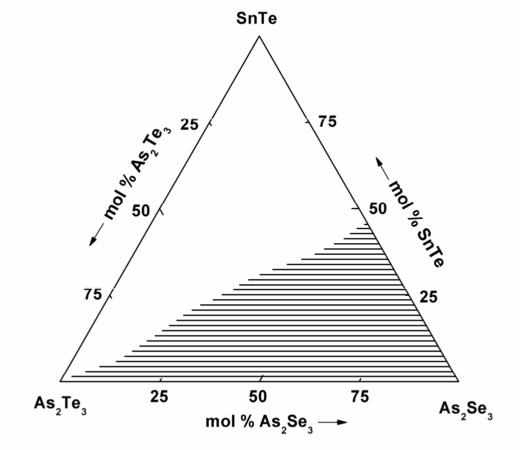

Fig.1. Glass-forming region in the As_2Se_3-As_2Te_3-SnTe system [19]

3. RESULTS AND DISCUSSION

3.1. Stability, linearity and slope of the electrode function. Limits of detection.

As criteria for valuation of the ISE work the following analytical characteristic are used: slope (S) and length (L) of the linear section of the calibration function, limits of detection (LD), response time (τ) and working pH-interval.

We have received a stable response to all investigated ISE with membranes from ChG. The electrode functions were built for non-conditioned and conditioned for 15 min ISE. The electrode function of the conditioned ISE possess slope near to the theoretic one and the time necessary for fixing of the equilibrium electrode potential is 10-15 s, while for the non-conditioned ISE is about 1 min. Conditioning for 15 min stabilizes and improves the electrode function of ISE.

The calibration function of the non-conditioned ISE-6 (Fig. 2) linear in the range L=10^{-4}÷10^{-1} mol/l Sn(**II**) and has a slope of S=41 mV/dec. The conditioned for 15 min ISE-6 (Fig. 2) is characterized by linearity of the function in the interval L=10^{-5}÷10^{-1} mol/l Sn(**II**) and a slope of the linear section S= 28,5 mV/dec (LD=5,62.10^{-6} mol/l). The conditioning of the electrode improves its work. After conditioning of ISE-6 for 30 min has not been detected considerable improvement of its characteristics, due to which the next investigations were led after 15 min conditioning in 10^{-3} M $SnCl_2$.

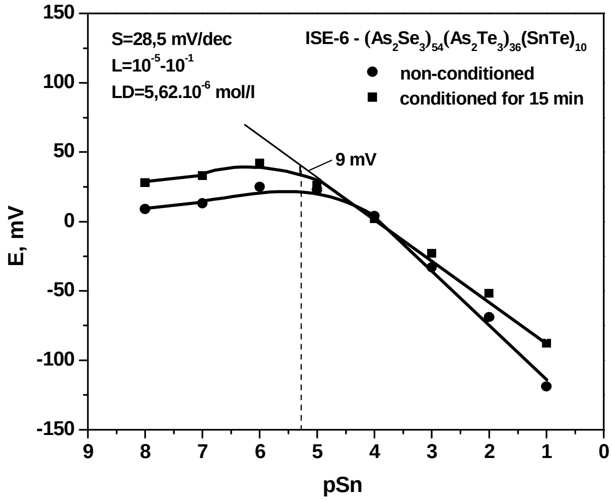

Fig.2. Calibration functions of ISE-6
1 – conditioned for 15 min; 2 – non-conditioned

The results from the measurement of S, L and LD after the primary measurements of the conditioned electrodes are generalized in Tab. 2.

Tab. 2. Analytical characteristics of the investigated Sn(II)-ISE.

	L,mol/l		S, mV/dec		LD, mol/l	
	1st day	30th day	1st day	30th day	1st day	30th day
ISE-14	10^{-5}÷10^{-1}	10^{-5}÷10^{-1}	42,5	32,5	1,25.10^{-6}	5,01.10^{-6}
ISE-11	10^{-5}÷10^{-1}	10^{-5}÷10^{-1}	45,5	45,0	5,62.10^{-6}	6,31.10^{-6}
ISE-8	10^{-5}÷10^{-1}	10^{-5}÷10^{-1}	28,5	37,75	2,51.10^{-6}	3,16.10^{-6}
ISE-6	10^{-5}÷10^{-1}	10^{-5}÷10^{-1}	28,5	37,0	5,62.10^{-6}	3,98.10^{-6}

The slope of the electrode function of the ISE-8 and ISE-6 is near to the theoretic value for bivalent ion according to the Nernst equation (S=29,58 mV/dec). S changes in the range from 28,5 to 45,5 mV/dec, which values are indication that the potential generating process is exchange of bivalent ions between the ion-selective membrane and the solution.

The higher values of S are indication for the presence of parallel passing potential generating processes (redoxy, exchange of other type ions, etc.), which lead to formation of mixed potential on the membrane//solution border and the registration of higher S values, i.e. supernernst slope.

Investigations on the same ISE were led 30 days after their producing (Tab. 2).

After 30 days the electrodes possess: $S>0{,}3.S_{theor.}$ and $L=10^{-5}\div10^{-1}$, which together with the absence of any ageing indications, makes the ChG from the As_2Se_3-As_2Te_3-SnTe system appropriate membrane material for Sn(II)-ISE.

3.2. Influence of pH on the electrode function.

The exact value of pH of the solutions is determined by measurement in electrochemical cell. A glass-electrode is used as indicating electrode. It is determined that the working pH interval for the investigated Sn(II)-ISE is up to pH<2,5. At pH=2,5 falls a sediment of $Sn(OH)_2$.

3.3. Response time (τ_{95}).

The response time τ_{95} is in the range 15-20 s, as it increases when the concentration of the investigated solution decreases. The composition of the ChG does not render crucial influence on this characteristic, i.e. the exchange reaction of Sn(II)-ions between the membrane and the analyzed solution passes equal rate.

These results are commensurate with these shown in the literature for electrodes with homogeneous membranes.

3.4. Selectivity ($K_{i,j}^{pot}$).

The interfering influence of the bicharged (Zn^{2+}, Cd^{2+}, Ba^{2+}и Pb^{2+}) ions on the response of the Sn(II)-ISE is investigated (Tab. 3).

Tab. 3. Values of the selectivity coefficient $K_{Sn,Me}^{Pot}$.

ISE	Concentration of the interfering ion, mol/l	$K_{Sn,Zn}^{Pot}$	$K_{Sn,Cd}^{Pot}$	$K_{Sn,Ba}^{Pot}$	$K_{Sn,Pb}^{Pot}$
14	10^{-3}	$4.\ 10^{-6}$	$7{,}5.\ 10^{-5}$	1	$2{,}5.\ 10^{-6}$
	10^{-2}	$9{,}5.\ 10^{-5}$	$4.\ 10^{-4}$	0,5	$7.\ 10^{-5}$
	10^{-1}	$4{,}5.\ 10^{-3}$	$2.\ 10^{-3}$	0,2	-
11	10^{-3}	$4.\ 10^{-6}$	$5{,}0.\ 10^{-5}$	1	$1.\ 10^{-7}$
	10^{-2}	$7{,}5.\ 10^{-5}$	$2.\ 10^{-4}$	0,75	$4.\ 10^{-5}$
	10^{-1}	$6.\ 10^{-3}$	$4{,}5.10^{-3}$	0,32	-
8	10^{-3}	$3{,}5.\ 10^{-6}$	$2{,}5.\ 10^{-5}$	8	$1.\ 10^{-7}$
	10^{-2}	$3.\ 10^{-4}$	$7{,}5.\ 10^{-4}$	5	$1.\ 10^{-5}$
	10^{-1}	$6.\ 10^{-3}$	$6.\ 10^{-3}$	0,53	-
6	10^{-3}	$1.\ 10^{-6}$	$6{,}5.\ 10^{-5}$	6,5	$5{,}510^{-7}$
	10^{-2}	$7.\ 10^{-5}$	$2.\ 10^{-4}$	3	$3.\ 10^{-5}$
	10^{-1}	$5{,}8.\ 10^{-3}$	$4{,}5.\ 10^{-3}$	$4{,}9.\ 10^{-3}$	-

From the electrode functions of the Sn(II)-ISE introducing of interfering ions in concentrations of 10^{-1}, 10^{-2} и 10^{-3} M the $K_{i,j}^{pot}$ is calculated and it is determined that $K_{i,j}^{pot}$ is smaller than 10^{-2}, which means that in this range of concentrations the investigated ions do not interfere the work of the Sn(II)-ISE. At concentrations of the interfering Pb(II)-ion ≥ 10^{-1} a sediment is liberated, which passivates the active surface and makes impossible the measurement. At increment of the interfering ion concentration the length of the linear section logically decreases, due to which the advisable concentration of interfering ions is ≤10^{-2} mol/l.

3.5. Mechanism of the potential formation for the investigated Sn (II)-ISE.

When breaking the bonds of the O, S, Se and Te atoms in the oxide and chalcogenide glasses the electronic couple stays in one of the fragments. As a result of a heterolytic reaction two (positively and negatively charged) defect centers appear – Fig. 3.

The positive and negative defect centers fix themselves in the process of the glass setting since it is not possible all broken bonds to be restored.

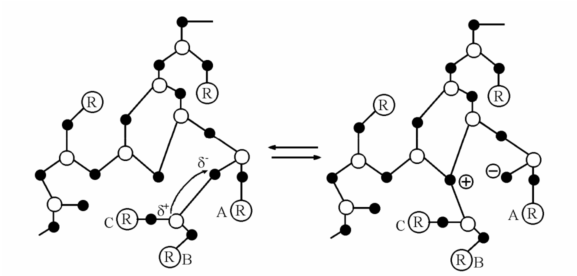

O = As; ● = Se или Te; R_1 = – Sn – Te –

$[(3R_1).2(AsTe_{3/2}).2(AsSe_{3/2}] \Longleftrightarrow [(2R_1).Se(AsTe_{2/2})_2.(AsSe_{2/2})]^+ + [R_1.AsSe_{2/2}Se]^-$

Fig. 3. Formation of positively and negatively charged defect centers in glesses from the As_2Se_3-As_2Te_3-SnTe system

At the beginning of the measurement in the exchange process $Sn(II)_{liquid} \Leftrightarrow Sn((II)_{glass}$ participate Sn-ions from the negatively charged defect centers $R_1AsSe_{2/2}Se^-$. The exchange is realized by the scheme:

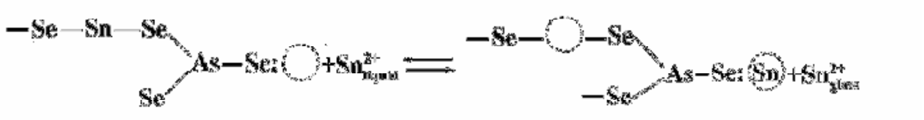

As a result of self-arbitrary processes (diffusion, crystallization, phase transitions and others) or external influences (electric or magnetic field, heating, irradiation, conditioning, etc.) the defects are torn from the basic matrix of the glass and penetrate in its volume interacting between themselves as a result of which new defect centers are formed.

The negatively charged defects $(R_1.AsSe_{2/2}Se)^-$ possess larger mobility from the positively charged $[(2R_1).Se(AsTe_{2/2})_2.(AsSe_{2/2})]^+$ and interact between themselves by the scheme:

$$2(R_1.AsSe_{3/2}Se)^- \rightarrow [(R_1)_2.(AsSe_{2/2})_2.Se_2]^{2-}$$

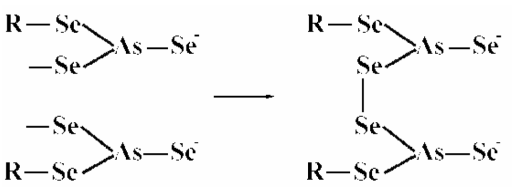

The structure of a defect center obtained after conditioning is shown in Fig. 4.

After conditioning of the Sn(II)-ISE and during the time of its work, the Sn^{2+}-ions from the solution take position 2 in the defect center (Fig. 4 a, b) provoking brake of the bond between the two bridge Se-atoms (Fig. 4 b), as a result of which two new uncombined bonds are formed. During the following functioning of the ISE the incoming in the solution Sn^{2+}-ions take position 1 and the Sn^{2+}-ions from position 2 go in the solution (Fig. 4 c). Again two new uncombined bonds are obtained and the filling and liberation process of the active positions 1 and 2 in the defect center is also repeated.

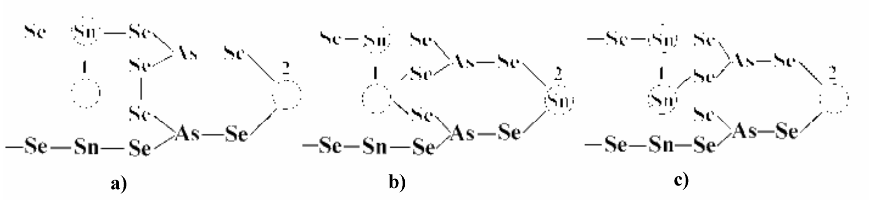

Fig.4. Structure of the negatively charged defect centers in different moments of the ISE work (a-before conditioning; b-after conditioning and during the work; c-next measurement).

The assuming for formation of double ionized defects by the above scheme explains the step-by-step stabilization of the electrode function slope after some time from the ISE work around a value characteristic for bivalent ion.

External influences (contamination, dissolution, precipitation, oxidation, etc.) could lead to blocking or exhaustion of the membrane surfaces, whose after polishing quickly regenerate and start to work according to the above-described mechanism.

4. CONCLUSIONS

On the basis of new ChG from the As_2Se_3-As_2Te_3-SnTe system ISE from the "layered wire" type are produced.

The proposed construction and technology of the Sn(II)-ISE guarantees high reproducibility of the analytical characteristics with a very good ionic selectivity in the case of Zn^{2+}, Cd^{2+}, Ba^{2+}и Pb^{2+}-ions.

The tin ion-selective membrane do not show any signs of ageing or destruction of the active layer connected with the passing of undesired processes (crystallization, destruction of the polymer, oxidation/reduction of the ChG, etc.).

5. ACKNOWLEDGEMENT

The authors acknowledge thankfully the Ministry of Education and Science ("Scientific investigations" fund) for the financial support of the present investigation through contract TN 1503/05 and to the Scientific Research Sector in the University of Chemical Technology and Metallurgy-Sofia (contract 10299).

6. REFERENCES

[1] Baker C. T., I. Trachtenberg, (1971), J. Electrochem. Soc., 118, 571-576

[2] Jasinski K., I. Trachtenberg, (1972), Anal. Chem., 44, 2373-2376

[3] Jasinski K., I. Trachtenberg, (1973), J. Electrochem Soc., 120, 1169-1174

[4] Jasinski K., I. Trachtenberg, (1973), Anal. Chem., 45, 1277-1279

[5] Jasinski K., I. Trachtenberg, G. Rice, (1974), J. Electrochem Soc., 121, 363-368

[6] Vlasov Yu. G., E. A. Bychkov, B. L. Seleznev, (1990), Sens. Actuators B, 2, 23-31

[7] Hadjinicolova St., L. Ilcheva, I. Stojaniva, V. Vassilev, A. Atanasova, (1995), Analyt.. Labor., 4 (2), 105-107

[8] Vlasov Yu. G., E. A. Bychkov, A. M. Medvedev, (1986), Anal. Chim., 185, 137-144

[9] Hadjinikolova S., S. Boycheva, V. Vassilev, L. Ilcheva, L. Nikolova, (1999), 13th Conf. “Glass and Ceramics”, 29.IX- 1.X.’99, Publ. House “Sci. Invest”, Proceedings, vol.1, 304-309

[10] Vlasov Yu.G., E.A. Bychkov, A.V. Legin, (1985), J. Anal. Chimii, 40 (10) 1839-1845 (in Russian)

[11] Jukov A.F., A.V. Vishniakov, Ya.L. Harif, Yu.I. Urusov, F.K. Bolinec, E.I. Ryjkov, A.V. Gordievskii, (1975), J. Anal. Chimii, 30 (9) 1761-1768 (in Russian)

[12] Vassilev V., V. Parvanova, L. Aljihmani, B. Pejova, St. Hadjinikolova, P. Petkov, (2004), XVIII Congress of Chemists and Technologists of Macedonia, September 23-25, 2004, Ohrid, R. Macedonia, Extended Abstracts, ICT-19, 58-60

[13] Koenig C. E., E. W. Grabner, (1995), Electroanalysis 7 (11) 1090-1997

[14] Hadjinikolova St., S. Boycheva, V. Vassilev, L. Ilcheva, (1999), God. Na HTMU-S., 34, 45-51 (in Bulgarian)

[15] Boycheva S. V., V. S. Vassilev, Z. G. Ivanova, (2002), J. Appl. Electrochem.,32, 281-285

[16] Vassilev V.S., S.H. Hadjinikolova, S.V. Boycheva, (2005), Sensors and Actuators B, 106, 401-406

[17] Vassilev V.S., S.V. Boycheva, (2005), Talanta, 67 (1), 20-27

[18] Hirata H., Higashiyama K., (1972), Talanta, 19, (4), 391-198

[19] Vassilev V., S. Parvanov, T. Hristova-Vasileva, L. Aljihmani, V. Vachkov, T. Vassileva-Evtimova, (2007), Mat. Lett., 61, 3676-3678

PHASE DIAGRAM AND SMALL PARTICLES APPROACHES IN INTERPRETATION OF BISMUTH AND TELLURIUM VAPORIZATION IN PRESENCE OF RODHIUM MODIFIER BY ELECTROTHERMAL ATOMIC ABSORPTION SPECTROMETRY

Nicolai Tsarevsky*, Savka Stoeva, Petar Stoimenov, ,

Vera Slaveykova, Stefan Manev**

**Department of Chemistry Carnegie Mellon University*
4400 Fifth Avenue Pittsburgh, PA 15213, USA
**South-West University, Faculty of Mathematics & Natural Sciences,
Blagoevgrad, Bulgaria

Abstract: *The phase diagram and small particles approaches were compared and applied in studying vaporization of Bi and Te from graphite substrate in the presence of Rh modifier. Differentiation of Bi and Te experimental vaporization curves facilitates the determination of distinct such as inflexion points, local extrema and permits to make conclusion about existence of possible Te-Rh and Bi-Rh species on the graphite substrate, producing stabilization of volatile Bi and Te species.*

Keywords: *ETAAS, vaporization of Bi and Te, Rh modifier, phase diagrams, thermal stabilization, atomic absorption spectrometer, graphite substrate, intermetallic compounds*

1. INTRODUCTION

The aim of the present study is to demonstrate applicability of phase diagram and small particles approaches in explanation of stabilizing effect of rhodium modifier during pyrolysis in electrothermal atomic absorption spectrometry (ETAAS) determination of Bi and Te.

Phase diagrams between the analyte and the modifier have been applied by several authors [1-4] in order to seek for a relationship between the existing phases with different thermodynamic properties and the thermal stabilization taking place in the graphite atomizer of ETAAS. It is generally believed that depression of the analyte volatility is due to formation of low-volatile species such chemical compounds, solid solutions, etc. and significant analyte losses occur when a liquid phase appears in the system.

Solutions analyzed by ETAAS are dilute which leads to formation of small particles on the substrate [5,6]. The law quantity of the Bi and Te analyte and the modifier is not sufficient to cover the graphite surface with monoatomic layer. Since the energy of interaction between identical atoms is greater than this between the same atoms and those of the graphite, cluster formations, but not layer structures, is usually the most stable configuration. The obtained small particles are well known to posses quite different properties compared to that of the corresponding bulk phase.

Recently attempts have been made [7] to study the difference of the phase equilibrium between a bulk alloy and the corresponding nm-sized alloy cluster. It is to be expected that the use of phase diagrams based on small particles is more correct than that of ‘bulk phase diagrams’.

2. EXPERIMENTAL

The experiments were carried out with a Perkin–Elmer Model 4100 ZL atomic absorption spectrometer equipped with a THGA atomizer, longitudinal Zeeman effect background corrector and an AS-71 autosampler.

Temperature program for study of vaporization losses of Bi and Te includes stepwise treatment as follows: 110 °C (5 + 15s) , 130 °C (5 + 10s), Varied (5 + 15s), 1800 °C (0 + 5s), 2200 °C (5 + 15s).

Ascorbic acid is used to reduce metal salts to nanosized metal particles.

3. RESULTS AND DISCUSSION

The analysis of the vaporization curve shape is the first step in the study of the processes occurring in the graphite atomizer. Experimental vaporization curves could be approximate with almost linear regions with different slopes characterizing the degree of vaporization of the analyte in the corresponding temperature interval [8]. The smaller the slope is, the least the analyte losses are due to low volatile species or absorbates in the graphite. Consequently the slope of the declining portion is a measure of the extent to which the analyte is modified. Since slope is well characterized by first derivative, differential vaporization curves (DVC) [9] representing the first partial derivative of the integrated absorbance with respect to pyrolysis temperature was used to estimate analyte losses.

Bi/Rh system

Fig. 1 represents vaporization and DVC curves of Bi at different Rh masses. In case of 0.05 ng Rh significant Bi losses occur in the region 200-400°C that could be related to vaporization of liquid Bi that does not strongly interact with the modifier or graphite substrate.

The formed Bi-containing particles with different sizes are fractionated which determines the observed shape. Interaction between Bi and Rh probably takes place in the region 400-1000°C. Spontaneous alloying between Bi and Rh becomes intensive enough to be formed intermetallic particles above 400°C. Statistically significant Bi losses begin at 1000°C, which is consistent with Bi/Rh phase diagram [10], showing existence of three incongruent melting intermetallic compounds between Bi and Rh with higher melting points than pure Bi. No chemical interaction between Bi and Rh occurs above 997°C, independently of the initial Bi/Rh ratio. When Rh is injected at larger quantity (0.2ng) the shape of the vaporization curve changes. The gradual Bi losses

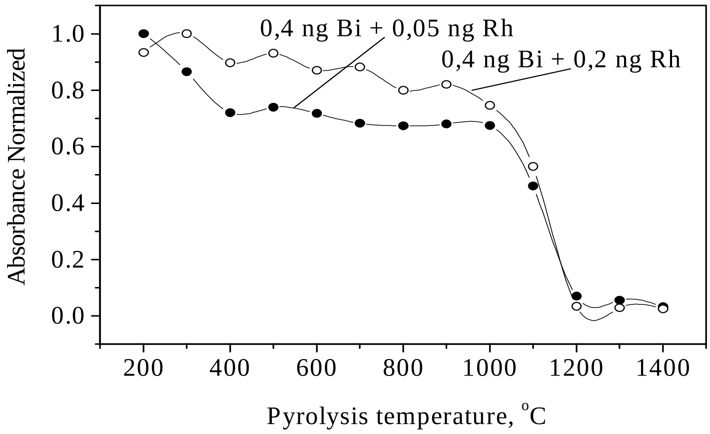

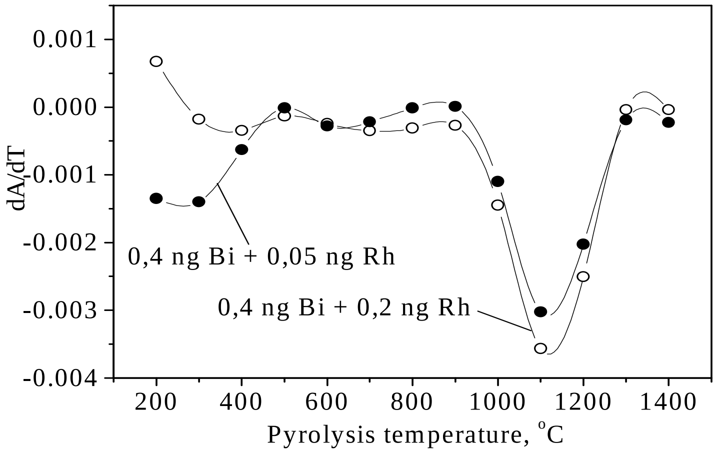

Figure1. a) Vaporization curves of 0.4 ng Bi in the presence
of (•) 0.05 ng and (o) 0.2 ng Rh.
b) Corresponding differential vaporization curves.

take place in the region 200-1000°C. This could be due to formation of small Bi-containing particles fractionated to different sizes and thus having different volatility. Significant Bi losses are observed again above 1000°C.

Te/Rh system

Vaporization curves for Te in the presence of 0.5 and 0.9 ng Rh are quite similar in the region 300-1000°C. Gradual Te losses occur which could be due to fractionation of Te-containing particles with different sizes. For both systems losses begin at 1000°C which is in consistence with Te/Rh phase diagram [11]. Seven intermediate compounds between Te and Rh with higher melting points than pure Te exist. The temperature of liquidification of the whole Te quantity

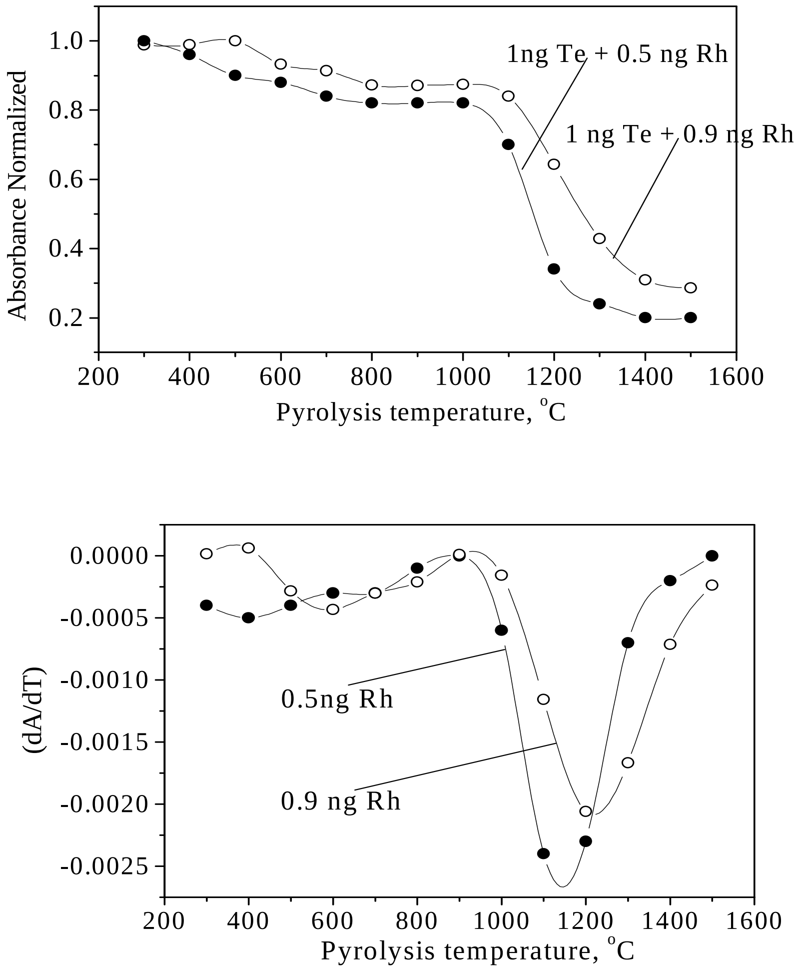

Figure2. a) Vaporization curves of 1.0 ng Te
in the presence of (•) 0.5 ng and (o) 0.9 ng Rh.
b) Corresponding differential vaporization curves.

depends on the initial Te/Rh ratio. In the concentration interval of almost pure Rh to approximately 40 at.% Rh liquid phase appears above 1000^{o}C, independently of the initial Te/Rh ratio. Above 1000^{o}C rapid analyte losses begin but when 0.9 ng Rh is applied the stabilizing effect is better. This is seen from DVC where the absolute derivative value for Te in the presence of 0.9 ng Rh is lower than that in the presence of 0.5 ng Rh.

Phase diagram v/s small particles approaches

Phase diagrams relate the initial analyte/modifier ratio to the physico-chemical properties of the system and could give an idea about the different types of analyte - modifier interaction.

It should be emphasized that phase diagrams are plotted when annealed mixtures are cooled down and at equilibrium conditions, while ETA processes are far from equilibrium, or assumed to be quasi-equilibrium (For review see [12]). Consequently, phase diagrams must be used very carefully in ETAAS.

Mori and Yasuda [13, 14] show by transmission electron microscopy that alloying in nm-sized particles takes place at an extremely high rate compared to the rate of interdiffusion in bulk materials. This process is intensified with the increase of temperature [7], because the diffusion coefficient is an exponential function of temperature. This makes possible the movement of relatively large clusters or islands over the surface at moderate temperature.

Thus, the relatively high losses of volatile analytes at pyrolysis temperatures lower than 300^{o}C could be explain with slow particles movement and little probability to alloy each other. The analyte usually has a measurable pressure at this temperature and significant losses occur. At higher temperatures considerably faster diffusion occur and alloying takes place, reducing the pressure over the alloy.

Hence, as size is getting smaller, the melting temperature decreases [15] according to the well-known Kelvin equation, the negative effect on stabilization could be expected. When alloy liquidifies, the partial pressure of analyte is increasing and the effect of stabilization is not enough. Furthermore, the temperature at which statistically significant analyte losses is always lower than the melting temperature of the pure modifier . The small particles formed in the graphite furnace are not uniform in size and therefore they have different volatility. Thus, a gradual decrease of the absorption with the increase of pyrolysis temperature could be due to 'fractionation' of particles with different volatility.

4. REFERENCES

[1] Hirokawa, K., Yasuda, K., Takada, K., GFAAS and phase diagrams of alloys, Anal. Sciences, 8, 411-417 (1992)

[2] Ouishi, K., Yasuda, K., Morishige, Y., Hirokawa, K., Role of metal matrix modifier in ashing and beginning of the atomization process in GFAAS, Fresenius J. Anal. Chem., 348, 195-200 (1994)

[3] Yasuda, K., Hirano, Y., Kamino, T., Hirokawa, K., Relationship between the formation of intermetallic compounds by matrix modifiers and atomization in GFAAS, and an observation of the vaporization of intermetallic compounds by means of electron microscopy, Anal. Sciences, 10, 623-631 (1994)

[4] Hirano, Y., Yasuda, K., Hirokawa, K., Lessening unexpected increases of atomic vapor temperature of arsenic in GFAAS, Anal. Sciences, 10, 481-484 (1994)

[5] Slaveykova V.I, Manev St., Lazarov D., Application of Kelvin equation to vaporization of silver and gold in ETAAS, Spectrochim. Acta B 50B, 1725-1732 (1995)

[6] Slaveykova, V. I., Stoimenov, P. K., Manev, S. G., Lazarov, D. L., Preatomization behaviour of palladium in ETAAS, Spectrochimica Acta, part B, 52, 1259-1267 (1997)

[7] Yasuda, H., Mori, H., Phase equilibrium in nanometer-sized Sb-Au alloy clusters, Materials Sci. Forum, 269-272, 333-338 (1998)

[8] S. Stoeva, N. Tsarevsky, V. Slaveykova, S. Manev, Role of some matrix modifiers during pyrolysis processes in electrothermal atomic absorption spectrometry, VIII Symposium of Instrumental and Analytical Spectrometry and Chromatography, 17–19.IX.1997, St st. Konstantin and Elena, Varna, Bulgaria, Poster AAS 13.

[9] Slaveykova V.I. , Lampugnani L., Tsalev D.L., Sabbatini L., E. De Giglio, Permanent iridium modifier deposited on tungsten and zirconium treated platforms in electrothermal atomic absorption spectrometry. Vaporization of bismuth, silver and tellurium, Spectrochim . Acta, 54B, 455-467 (1999).

[10] Hansen, M., Anderko, K., Strukturai dvoinih splavov, M., Metalurgizdat, 1962, Tom.1

[11] Ding, Zh., Kleykamp, H., Thummler, F., The constitution of the rhodium-tellurium system, J. Nucl. Materials, 171, 134-138 (1990)
[12] Tsalev D.L., Slaveykova V.I., Chemical modification in electrothermal atomic absorption spectrometry, in J. Sneddon (Ed.), Advances in Atomic Spectroscopy, Vol. IV, JAI Press, Greenwich, Connecticut, 1998, ch. 2, pp.27–150.
[13] Yasuda, H., Mori, H., Effect of cluster size on the chemical ordering in nanometer-sized Au-75%Cu alloy clusters, Z. Phys., D37, 181-186 (1996)
[14] Mori, H., Yasuda, H., Materials Sci. Forum, 269-272, 327-332 (1998)
[15] Skripov, V. P., Koverda, V. P., Skokov, V. N., Size effect on melting of small particles, Phys. Status Solidi, (a) 66, 109-118 (1981)

CONTROLLED TRANSFORMATION AND SINTERING OF TRANSITIONAL NANOSCALED AL_2O_3 BY α-AL_2O_3 SEEDING

E.Fidancevska[1], J.Bossert[2], R.Adjiski[1], V.Vasilev[3], M.Milosevski[1]

[1] *Faculty of Technology and Metallurgy, Rudjer Boskovic 16, Skopje,Republic of Macedonia*
[2] *Universitat Friedrich Schiller,Materialwissenschaft und Technology,Lobdergraben 32,Jena,Germany*
[3] *University of Chemical Technology and Metallurgy,8 Kl.Ohridski blvd.,Sofia,Bulgaria*

***Abstract**: Transitional nanoscaled alumina contains γ, δ, and θ-Al203. The size of the primary particles was 5-30 nm. DTA investigations of the cold pressed powder showed exopeak at 1125 oC what corresponds to the α-Al203 transformation. Sintered samples of the as received powder possess vermicular structure and density of 0.75TD. Seeds of α-Al203 in content of 1.5 wt% were used to avoid nucleation process during phase transformation. DTA investigation of the seeded and mechanically activated powder showed exopeak at 1078 oC. Compacts with a relative density of 0.935TD and grain size distribution from 100 to 800 nm were obtained by sintering in the interval RT-1400 oC/0.5h.*

***Keywords:** nano alumina ceramics, sintering, seeding effect, mechanical activation*

1. INTRODUCTION

One of the more important challenges in the fabrication of nanostructured alumina is how to achieve full densification of the powder while simultaneously retaining a nanoscale microstructure. At present, relatively high density (>98%TD) can be achieved with 10-20 nm particles, but high density is accompanied by significant grain growth (grain size >100 nm). To reduce grain growth during sintering, where most of the densification process occurs, a high density homogeneous green body with minimum pore size is desired. For transitional alumina powders which possess high specific surface area and ultra fine size, the transformation into the stabile α-Al_2O_3 phase is characterized by rapid grain growth, generally accompanied by vermicular microstructure consisting of a network of large pores. To achieve high densities very high temperature is required.

It is known that transformation of alumina proceed by nucleation and growth process. To initiate the transformation sufficient energy must be supplied to the system to exceed the nuclear barrier. After nucleation the transformation occurs rapidly, by growth.

In [1-5] is shown that the nucleation step may effectively be eliminated by supplying nuclei of the system. High pressure compaction of nanosized particles has been used in an attempt to achieve the desired nanoscale microstructure and high density of the body. Typical compaction pressure usually exceed 1.0 GPa [6].

The goal of this paper is the obtaining of dense α-Al_2O_3 nanoceramics, starting from transitional nanocrystalline alumina, which contains δ, γ, and θ-alumina. To avoid nucleation process 1.5% α-Al_20_3 was used. After homogenization and mechanical activation, the green compacts were produced. The present active α-Al_2O_3 and structural defects formed by mechanical activation act as nucleation sites in the system which enhance the densification.

2. EXPERIMENTAL PROCEDURE

The nano aluminium oxide powder used in this study was obtained from firm IBU-tech, Germany. The code of the powder was NA 226-IV-1. This powder was obtained by aluminium tri-sec-butylat at 850°C by pulse reactor technique.

The powder morphology was observed via transmission electron microscopy (TEM).

The specific surface area was determined by 5-point-BET measurement (Micromeritics Gemini 2370). DTA investigations were performed in air atmosphere in the temperature interval 20-1500°C using heating rate of $10^{o}min^{-1}$ (Netzsch STA 409C). The phase analysis of transitional alumina was carried out by X-ray diffraction method operating at CuKα radiation. (Philips PV 1051-difractometer).

The α-Al_20_3 particles with particle size of 50 nm (Degussa) used for seeding were added to the transition alumina in quantity of 1.5 % wt.

Homogenization and mechanical activation (wet milling) of the powder with seeding particles, was performed by attritor mill using alumina balls (Netzsch). The milling was performed at pH 5 for 0.5 h, using solid load of 30%w.

The activated nano powder consisted of δ, γ, θ and α-Al_20_3 was compacted by means of axial pressing at 30 MPa and cold isostatic redensification (CIP) at 550 MPa. The green specimens were sintered in the temperature interval RT -1400°C/0.5h and RT-1500 °C/8h in air atmosphere and heating rate of 5 °C min^{-1} in electrically heated chamber furnace.

The final density of the samples was determined by Archimedes displacement method.

The shrinkage during sintering, was followed by dilatometry in air atmosphere, using heating rate of 10 °C min^{-1} in temperature interval RT- 1500 °C (Netzsch TMA 402)

The ceramographic investigations were made with a scanning electron microscope on the polished and thermally etched surface treated at 100 °C below sintering temperature for 1h to reveal the grain structure (Leica S 440i).

3. RESULTS AND DISCUSSION

3.1. Characterization and consolidation of as received nano alumina

TEM observation of the as received transition nano alumina, Fig. 1 shows typically ultrafine high surface area powder. The size of primary alumina particles was 5-30 nm. These nanosized primary particles are aggregated in the as received powder and the aggregate size ranged from 50 - 100 nm - Fig. 1.

XRD shows that the powder is consisted of δ, θ, γ phases or using their common name “Greek-letter-alumina” [5]. The dominant phases are δ and γ-Al_2O_3. Specific surface area was 83 m^2/g. The tap density of the powder was 37.55 g/dm^3.

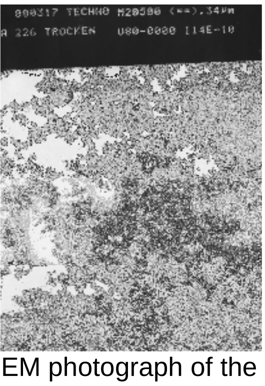

Fig.1. TEM photograph of the starting

transition alumina powder (bar 0.34 μm)

DTA investigation of the cold isostatic pressed at 550 MPa nano powder showed one exopeak at 1125 ^{o}C, what corresponds to the α-Al_2O_3 transformation, Fig. 2.

The green density of the compacts of the started powder was 2.01 g cm^{-1} what is 0.50 TD. After sintering in the interval RT-1500 ^{o}C, density was 2.99 g/cm^{3} what is 0.75 TD. Open porosity was 24%. The sinterability of the compacts is shown in Fig.3, where $\Delta L/L_o$ is plotted as a function of the temperature ($\Delta L=L_o-L$), where L_o is the initial length of the sample and L is instantaneous sample length. $d(\Delta L/L_o)/dT$ is plotted as a function of temperature and represents the shrinkage rate. The temperature of 970 ^{o}C at which the measurable shrinkage begins is comparable to that commonly observed for compacts of submicrometer α-Al_2O_3 powders [7]. The densification of transition alumina shows two regions of densification during the constant heating rate.

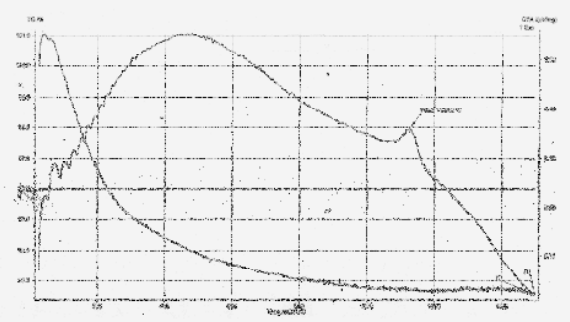

Fig.2. DTA of the starting (as received) transition alumina cold isostatic pressed at 550 MPa

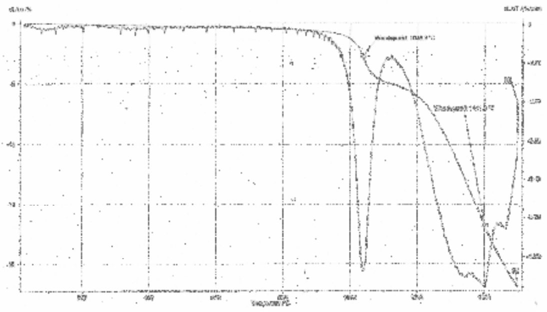

Fig.3. Shrinkage ($\Delta L/L_o$) (1) and $d(\Delta L/L_o)$ /dT (2) of the compact formed of as-received powder sintered in temperature interval RT-1500 ^{o}C

The first one is distinctive feature of sintering kinetics, with rapid shrinkage in the temperature region 970-1140 ^{0}C, with maximum shrinkage rate at 1038.7 ^{o}C. This densification is associated with the phase transformation of γ-Al_2O_3 via δ and θ to stabile α-phase. The second region of shrinkage above 1140^{o}C is densification of the α-Al_2O_3 at higher temperatures. At temperature of 1500 ^{o}C shrinkage got value of $\Delta L/L_o$ = 21 %, where density of 0.75TD was achieved.

A vermicular microstructure of the sintered sample can be seen in Fig.4.

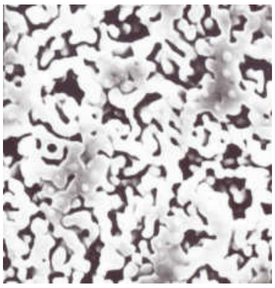

Fig.4. Microstructure of sintered sample at 1500 ^oC, ρ_f=2.99 gcm^{-3} (0.75 TD), polished and thermally etched surface (bar 2 μm)

The elongated pores with size of 0.5-3.5 μm can be seen. The grain size is in the range of 0.5-3.4 μm. The mechanism of pore coarsening and growth of vermicular particles has been discussed by Dynys and Halloran [8].

After sintering at 1500 ^oC/8h at the same heating rate, the density of the sample was 3.71 g cm^{-3} (0.93TD). The obtained microstructure was inhomogeneous Fig. 5.

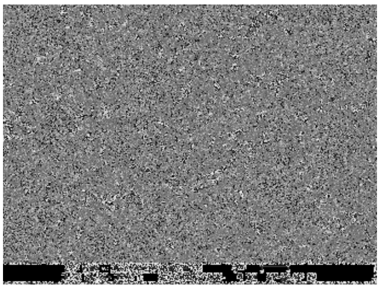

Fig.5. Microstructure of sintered sample at 1500 ^oC/8h, ρ_f=3.71 g cm^{-3} (0.93 TD), polished and thermally etched surface (bar 2 μm)

The grain size was in the range 1-6 μm. Among the grains, pores with size of 0.5 to 1 μm. are located It is clear that for transition alumina powders which possess high specific surface area and ultra fine size, the transformation into the stabile α-Al_2O_3 phase is characterized by rapid grain growth. To achieve higher densities a very high temperature of >1600 ^oC is required.

3.2. Consolidation of transition nanoscaled alumina using α-Al_2O_3 seeds

The transformation of alumina proceed by nucleation and growth process. To initiate the transformation, sufficient energy must be supplied to the system to exceed the nuclear barrier. After nucleation the transformation occurs rapidly by growth.

To avoid nucleation process 1.5% α-Al_20_3 was used. The homogenization and mechanical activation was realized by attriting.

The mechanical activation involves the creation of large contact stresses, which cause an increase in the internal energy of the material. The created lattice defects together with α-Al_2O_3 act as heterogeneous nucleation sites for the transformation.

Mechanical activation causes changes in a materials structure, which has a direct influence on properties dependent on structure-transport and reactive properties [9,10].

The specific surface area of the mechanically activated powder for 30 min. at pH 5, after drying and mortared was 98 m^2 g^{-1}. Larger time of attriting is not recommended, because powder with smaller surface area was produced. The accumulated mechanical energy is among other things used for increasing the specific surface energy of a disperse material. This is one of the reasons for agglomeration of the particles and reduction of the specific surface area. Using attriting time of 50 min, the specific surface area was reduced to 90 $m^2 g^{-1}$.

During the mechanical activation, changes in the lattice properties of the powder could be expected. These changes can be regarded as changes in the order state of the lattice, which are caused by formation of lattice distortions and defects and decreasing crystallite size [11].

DTA investigation of the seeded and mechanically activated powder showed one exopeak at 1078 °C, what corresponds to the α-Al_2O_3 transformation, Fig. 6.

According to DTA the $\theta \rightarrow \alpha$-$Al_20_3$ transformation was realized in the temperature interval from 1047 to 1113 °C. If we compare Fig. 2. and Fig.6. it is evident that seeding and mechanical activation reflect to the reduction of the temperature of $\theta \rightarrow \alpha$-$Al_20_3$ transformation for 47 °C.

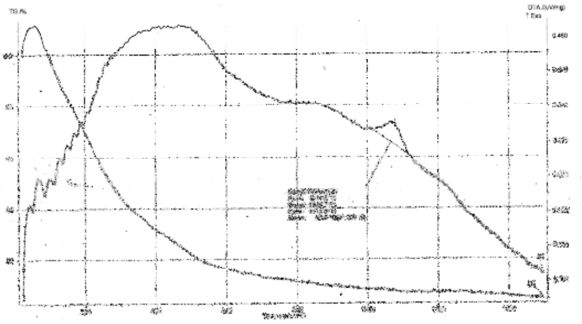

Fig. 6. DTA seeded and mechanically activated transition alumina powder cold isostatic pressed at 550 MPa

The green density of the compacts of the seeded and mechanically activated powder after pressing at 550 MPa was 2.31 g cm^{-1} what is 0.58TD.

The sinter ability of the compacts of seeded and mechanically activated nanoalumina is shown in Fig.7. The temperature at which measurable shrinkage begins is 940°C .This temperature is comparable to that commonly observed for compacts of sub micrometer α-Al_2O_3 powders.

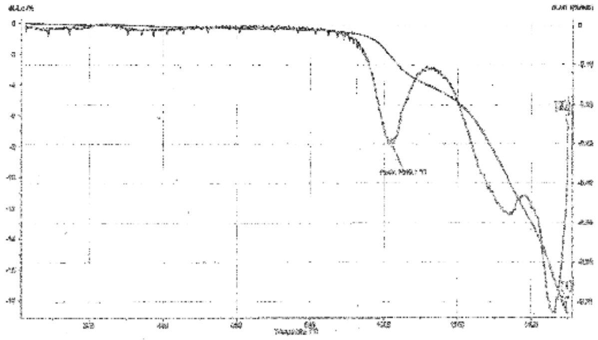

Fig.7. Shrinkage ($\Delta L/L_o$) (1) and $d(\Delta L/L_o)/dT$ (2) of the compact of seeded and mechanically activated powder during sintering in the temperature interval RT- 1500°C

The shrinkage in the temperature interval RT-1500°C is 18.9%. The first region of densification associated with the phase transformation to α-Al_2O_3 has maximum shrinkage rate at 1019.1 °C, what is 19.2°C lower of those of the started powder.

The green samples of the seeded and mechanically activated powder were sintered at 1400 °C/0.5h. The density of the sintered samples was 3.73±0.02 g cm^{-3} (0.935 TD). The microstructure of the sintered samples is shown in Fig. 8.

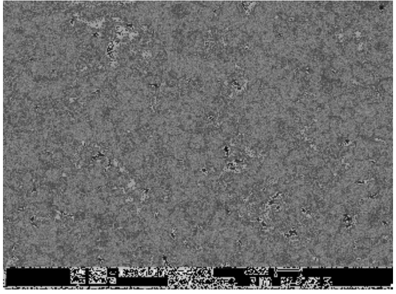

Fig.8. SEM micrograph of polished and thermally etched surfaces of the sintered sample at 1400°C/0.5h, density 3.73 g cm^{-3} (0.935 TD)

The grain size is ranged in the interval of 100-800 nm. The size of the pores is 100-250 nm. At Fig. 9. is given the microstructure of the sintered sample at 1500 °C/1.5h

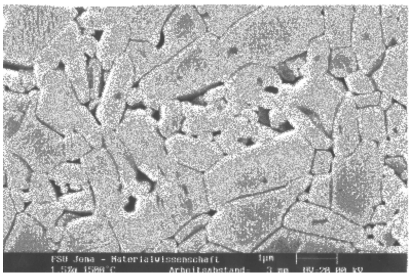

Fig.9. SEM micrograph of polished and thermally etched surfaces of the sintered sample at 1500°C/1.5h, density 3.75 g cm^{-3} (0.94 TD)

The density of compacts was 3.75±0.01 g cm^{-3} (0.94TD), grain size is ranged in the interval of 0.3-3.0 μm. The size of the inter-grains pores is 0.3-0.7μm, indicating that these pores are probably formed during α-Al_2O_3 discontinuous grain growth. The size of the intra-grains pores is 200-300 nm. The presence of intra-granular pores indicates that the densification rate may have been slower than grain growth rate at the processing temperature (1500 °C) [12].

Nano alumina ceramics from Fig 8. because of its nano structure has good bioinert and biofunctional properties and can be potentially used in medicine.

4. CONCLUSION

Transition nanoalumina consisted of γ, δ, and θ-Al_20_3 posses specific surface area of 83 m^2/g ,tap density of 37.55 g/dm^3 and primary particle size of 5-30 nm. After pressing at 550 MPa and sintering at 1500 °C/2h, the compacts possesses vermicular structure, density of 0.75 TD and grain size of 0.5-3.4 μm. After sintering at 1500°C/8h at the same heating rate, the density of the sample was 0.93 TD**,** the grain size was in the range 1-6 μm and pores size of 0.5 to 1 μm. In order to reduce sintering temperature and avoid the nucleation process, 1.5 wt% of α-Al_20_3 was added to the transition alumina. The transformation θ→α-Al_20_3 was realized at 1078 °C what is a temperature reduction of 47°C. The mechanically activated transition alumina with content of 1.5% α-Al_20_3 sintered at 1400 °C/0.5h possess density 0.935 TD. This type of nanoalumina ceramics because of its nanostructure has good bioinert and biofunctional properties and can be potentially used in medicine.

5. ACKNOWLEDGMENT

The authors acknowledge thankfully the financial support for this work from the Ministry of education and science of Republic of Macedonia (contract 071005).

6. REFERENCES

[1] Kumagai M., G. Messing, (1985), J.Am. Ceram. Soc., 68 (9), 500-505
[2] Messing G.L., M. Kumagai, R. Shelleman, J. Mc Ardie, (1986), in Science of Ceramic Chemical Processing, Eds. L.L.Hench and D.R.Ulrich, J.Wiley & Sons, p. 259
[3] Wakao Y., T. Hibino, Nagoya Koguo Gijytsy Skikensko Hokuku, (1962), 11, 588-95, quoted after K. Kumagai, G. Messing, J. Am. Ceram. Soc.68 (9) 500 (1985)
[4] Bye G. C., G. T. Simpkin, (1971), J. Am. Ceram. Soc., 57 (8), 367-71
[5] Lecros C., C. Carry, P. Bowen, H. Hofmann, (1999), J. Eu. Ceram. Soc., 19,1967
[6] Handbook of Nanostructured Materials and Nanotechnology, edited by H. S. Nalwa, Vol. 1, p. 237
[7] Kichuchi S., T. Ban, K. Okada, N. Otsuka, *(1992),* J. Mat. Sci. Lett., 11, 471
[8] Dynys W., J. Halloran, (1982), J. Am. Ceram. Soc., 65 (9), 442
[9] Nicolic M., N. Nicolic, S. Radic., (2000), Sci. Sintering, 32 (3), 149
[10] Brankovic A., V. Vidojkovic, S. Milosevic, (1998), J. Solid State Chem. 135, 256
[11] Wu S., L. De Jonghe, (1996), J. Am. Ceram., *79 (8), 2207*
[12] Chiang Y.-M., D. P. Birnie, W. D. W. Kingery, (1997), Physical Ceramics, John Wiley &Sons New York

SECONDARY METABOLITE PRODUCTION IN *HYPERICUM PERFORATUM* L. *IN VITRO* REGENERATED PLANTLETS

Sonja Gadzovska[1,2], Stéphane Maury[2], Valentina Pavlova[3], Mirko Spasenoski[1], Claude Joseph[2], Daniel Hagège[2]

[1]*Institute of Biology, Faculty of Natural Sciences and Mathematics, "Ss. Cyril and Methodius" University, P.O.Box 162, 1000 Skopje, Macedonia, e-mail:* sonjag@iunona.pmf.ukim.edu.mk
[2]*Laboratoire de Biologie des Ligneux et des Grandes Cultures, Faculté des Sciences, Université d'Orléans, BP 6759, 45067 Orléans, Cedex 2, France*
[3]*Institute of Chemistry, Faculty of Natural Sciences and Mathematics, "Ss. Cyril and Methodius" University, P.O.Box 162, 1000 Skopje, Macedonia*

Abstract: *Over the past decade, medicinal plants have received considerable interest for their phytomedicinal chemical compounds. Among them Hypericum perforatum L. has been considered according to its biochemical characteristics and secondary metabolite production. The main goal of the research was to summarize the influence of plant growth regulators on secondary metabolite production including hypericin and pseudohypericin in Hypericum in vitro regenerated plantlets. A reversed-phase high performance liquid chromatography (HPLC) method was developed for analyzing of secondary metabolites. The specific accumulation of secondary metabolites in in vitro cultures was influenced by phytohormonal supplementation of the medium. Combination of auxin and cytokinin concentrations improved the production of secondary metabolites.*

Keywords: *auxins, cytokinins, High-performance liquid chromatography, Hypericum perforatum L., hypericin, pseudohypericin, secondary metabolites.*

1. INTRODUCTION

The importance of H. perforatum as a medicinal plant is mainly due to the presence of naphtodianthrones such as hypericin and pseudohypericin, and their precursors: protohypericin, protopseudohypericin and cyclopseudohypericin [2]. In the presence of light, hypericins act as photosensitizers and are thereby capable of destroying surface structures of viruses**.** Hypericin show antiviral effect against Human immunodeficiency virus type 1 (HIV-1) by reduction of its spread and might be an agent for the photodynamic therapy of AIDS an immunodeficiency syndrome [14]. The flavonoid glycosides (rutin, hyperosid, isoquercitrine, quercitrine) and aglycones (quercetin, kaempferol and luteolin) found in Hypericum are also considered to be potentially therapeutic compounds due to their antiinflammatory and spasmolytic effects [1].

Since hypericin and pseudohypericin are important as therapeutic agents, the production of these constituents by plant in vitro cultures has been examined. Consequently, many investigations have been directed at understanding and enhancing hypericin production by studying leaf structure [7], field cultivation [3] and in vitro tissue culture establishment [4]. Hypericin was detected in regenerated plantlets of H. perforatum cv. Topas [4]. Dias et al., [5] identified 22 compounds including flavonoids, hypericin, pseudohypericin, phloroglucinols and phenolic acids present in in vivo and in vitro biomass of H. perforatum**.** These results showed clearly evidenced distinguish phenolic composition between in vivo plants and in vitro cultures. Therefore, the objective of our research was to develop an efficient protocol for micropropagation to improve secondary metabolite productions in H. perforatum in vitro regenerated plantlets. The consequences of growth regulator concentrations according to the developmental stages of plantlets have been examined.

2. MATERIAL AND METHODS

Micropropagation of *H. perforatum* L.

The protocol for micropropagation of *Hypericum* in *in vitro* conditions was described by Gadzovska et al., [8]. First pair of leaves were excised from two week old *in vitro* grown plants and used as explants to establish shoot cultures in the presence of the cytokinin N^6-benzyladenine (0.1-2.0 $mg \cdot L^{-1}$ BA). *Hypericum* shoots were successfully regenerated after subculturing in the presence of auxin (0.05-1.0 $mg \cdot L^{-1}$) indol-3-acetic acid (IAA).

High performance liquid chromatography (HPLC) analyses

HPLC analysis of phenolic compounds and naphtodianthrones in metanolic extracts were performed on an apparatus Hewlett Packard Series HP 1100 consisting G1311A pump equipped with G1315A photodiode-array detector [8]. Methanolic extracts were filtered through Sep-pack C_{18} cartridges before HPLC analysis. Separation of the compounds were performed on a Hypersil reversed-phase C_{18} column (150 x 4.6 mm, 5 μm, Interchim, France) at a flow-rate 1 $mL \cdot min^{-1}$ with 20 μL injected volume. The column was used at ambient temperature. Composition of the extracts was separated by linear gradient program with following solvents: A, water:acetic acid (99.5:0.5, v/v) and B, methanol:acetonitrile (1:1, v/v). The detection wavelength was in the of range 200-700 nm and chromatograms were acquired at 270 for flavonoids, 280 nm for phloroglucinols, 350 nm for flavonols, 530 nm for anthocyanins and 592 nm for hypericin and pseudohypericin.

Statistical analyses

The statistical analyses were performed with the SPSS statistical software program (SPSS version 11.0.1 PC, USA, IL). Means were expressed with their standard error and compared by one-way ANOVA (GML procedure). All statistical tests were considered significant at $p \leq 0.05$.

3. RESULTS

Hypericum shoots were successfully regenerated after subculturing in the presence of auxin IAA (0.05-1.0 $mg \cdot L^{-1}$). Rooting was observed with or without phytohormones. Roots developed in the presence of IAA were thin, long and green coloured, with compact tissues [8].

Experiments were carried out to reveal the effect of auxin IAA on secondary metabolite contents: phenolic compounds (Fig. 1A), flavonoids (Fig. 1B), flavonols (Fig. 1C), anthocyanins (Fig. 1D), hypericin (Fig. 1E) and pseudohypericin (Fig. 1F) in regenerated plantlets. Secondary metabolite contents were lower compared with control levels. Linear negative correlations between IAA levels and contents of phenolic compounds ($r = -0.684$, $p<0.01$) and flavonols ($r = -0.615$, $p<0.01$) were found. Hypericin and pseudohypericin productions were in positive correlations with contents of phenolic compounds, flavonols and anthocyanins.

HPLC analyses revealed that pseudohypericin and hypericin were the only naphtodianthrones present in regenerated plantlets [8]. Content of both hypericins in plantlets was examined according auxin supplementation in the medium. Differences in the hypericin or pseudohypericin content were not noticed between control plantlets and those treated with 0.05-0.5 mg·L^{-1} IAA. However, a significant lower hypericin ($p<0.05$) and pseudohypericin ($p<0.001$) production was confirmed in plantlets rooted with 1.0 mg·L^{-1} IAA. Statistical analyses showed significant negative correlation between IAA concentration and hypericin ($r = -0.625$, $p<0.005$) or pseudohypericin ($r = -0.706$, $p<0.001$) contents (Fig. 1 E,F). In plantlets, correlation between hypericin and pseudohypericin content was significantly positive ($r = 0.652$, $p<0.005$).

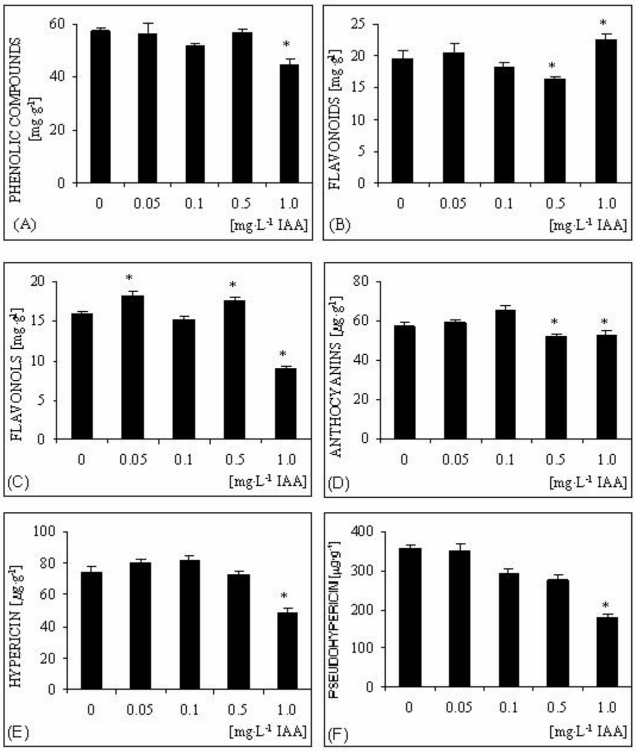

Fig. 1: Secondary metabolite productions in H. perforatum *L.* in vitro *plantlets.*

4. DISCUSSION

Many aspects of cell growth, cell differentiation, and organogenesis in tissue and organ cultures have been found to be controlled by an interaction between cytokinins and auxins. The auxin-controlled rooting assay and the cytokinin-induced morphogenetic assay are based upon the ability of auxins to induce adventitious root formation and cytokinins to induce adventitious shoots [6]. The type and concentration of auxin or cytokinin or the auxin/cytokinin ratio could alter growth and secondary metabolite production in cultured plant cells. A large number of in vitro cultures cultivated on medium with phytohormones produced specific medicinal compounds at a rate similar or superior to that of intact plants [15]. The response of in vitro cultures to exogenously applied phytohormones can vary with cultural conditions, the type of explant, and the genotype. Therefore, it is necessary to find an optimal concentration of phytohormones for growth and secondary metabolite production of different in vitro cultures.

H. perforatum has a high regenerative potential. Rooting of multiplied shoots *in vitro* was successfully obtained on medium with 0.05-1.0 mg·L^{-1} IAA and the influence of auxin on naphtodianthrone production in regenerated plantlets has been examined [8]. Accordingly, micropropagation of *Hypericum* has been reported through shoot regeneration from leaves [11], hypocotyls [10], shoot cuttings [4], stamens [9] and roots [15]. In our previous work [8], regenerated plantlets accumulated hypericin and pseudohypericin corresponding to values for total hypericins in *H. perforatum* L. cv. Topas regenerated plantlets [4].

Hypericum regenerated plantlets showed negative correlation between the level of IAA and secondary metabolite productions. High levels of auxin which favored root formation and elongation were deleterious to secondary metabolite productions. An increase of auxin levels stimulated cell dedifferentiation and consequently diminished the level of secondary metabolites. According to these results, some alterations in the activity and expression of several enzymes from phenylpropanoid pathway, like phenylalanine ammonium lyase (PAL) or tyrosine ammonium lyase (TAL) due to the influence of auxins and cytokinins have been reported [12]. The negative effect of auxins on secondary metabolite production is probably linked to the role of phytohormones in faciliting or hampering the expression and activity of specific enzymes, including naphtodianthrone biosynthesis. The negative correlation between auxin level and secondary metabolite production allowed to conclude that auxins have to be used in low concentrations or to be removed from the medium [8]. Consequently, the specificity of *in vitro* conditions used has an important impact on the secondary metabolism in regenerated plantlets.

5. CONCLUSIONS

The limited area of occurance of H. perforatum, seasonal harvesting, loss of biodiversity, variability in quality, and contamination issues, trigger to search alternative methods for secondary metabolite production. In pharmaceutical industry, one solution could be the production of in vitro micropropagated plantlets. In vitro derived plantlets may be useful not only as a source of uniform plantlets for mass propagation, but also as a simple experimental system in studies on secondary metabolite biosynthesis.

6. REFERENCES

[1] Berghöfer, R., Hölzl, J. (1987) Biflavonoids in Hypericum perforatum. Part I. Isolation of I3, II8-biapigenin, Planta Med., 53, 216-217.

[2] Briskin, D. (2000) Medicinal plants and phytomedicines. Linking plant biochemistry and physiology to human health, Plant Physiol., 124, 507-514.

[3] Büter, B., Orlacchio, C., Soldati, A., Berger, K. (1998) Significance of genetic and environmental aspects in the field cultivation of Hypericum perforatum, Planta Med., 64, 431-437.

[4] Čellárová, E., Kimáková, K., Daxnerová, Z., Martonfi, P. (1995) XIV Hypericum perforatum (St. John's Wort): In vitro culture and the production of hypericin and other secondary metabolites. Medicinal and Aromatic Plants VIII. Biotech. Agric. Forestry, 33, 261-275.

[5] Dias, A.C.P., Seabra, R. M., Andrade, P. B., Fernandes-Ferreira, M. (1999) The development and evaluation of an HPLC-DAD method for the analysis of the phenolic fractions from in vivo and in vitro biomass of Hypericum species, J. Liq. Chrom. Rel. Technol., 22, 215-227.

[6] DiCosmo, F., Misawa, M. (1995) Plant cell and tissue culture alternatives for metabolite production, Biotech. Adv., 13, 425-453.

[7] Fornasiero, R.B., Bianchi, A., Pinetti, A. (1998) Anatomical and ultrastructural observations in Hypericum perforatum L. leaves, J. Herbes Species Med. Plants 5, 21-33.

[8] Gadzovska S., Maury S., Ounnar S., Righezza M., Kascakova S., Refregiers M., Spasenoski M., Joseph C., Hagège D. (2005) Identification and quantification of hypericin and pseudohypericin in different Hypericum perforatum L. in vitro cultures, Plant Physiol. Biochem., 43, 591–601.

[9] Kirakosyan, A., Hayashi, H., Inoue, K., Charchoglyan, A., Vardapetyan, H. (2000) Stimulation of the production of hypericins by mannan in Hypericum perforatum shoot cultures, Phytochem., 53, 345-348.

[10] Murch, S.J., Choffe, K.L., Victor, J.M.R., Slimmon, T.Y., KrishnaRaj, R., Saxena, P.K. (2000) Thidiazuron-induced plant regeneration from hypocotyl cultures of St. John's wort (Hypericum perforatum. cv. Anthos), Plant Cell Rep., 19, 576-581.

[11] Pretto, F.R., Santarém, E.R. (2000) Callus formation and plant regeneration from Hypericum perforatum leaves, Plant Cell Tiss. Org. Culture, 62, 107-113.

[12] Stibon, F., Perrot-Rechenmann, C. (1997) Expression of auxin-regulated genes, Physiol. Plant., 100, 443-455.

[13] Vanisree, M., Lee, C., Lo, S., Nalawade, S., Lin, C., Tsay, H. (2004) Studies on the production of some important secondary metabolites from medicinal plants by plant tissue cultures, Bot. Bull. Acad. Sin., 45, 1-22.

[14] Vlietinck, A.J., De Bruyne, T., Apers, S., Pieters, L. A. (1998) Plant derived leading compounds chemotherapy of human immunodeficiency virus (HIV-1) infection, Planta Med., 64, 97-109.

[15] Zobayed, S.A., Saxena, P.K. (2003) In vitro–grown roots, a superior explant for profilic shoot regeneration of Hypericum perforatum L. in a temporary immersion bioreactor, Plant Sci., 165, 463-470.

DEVELOPMENT AND OPTIMIZATION OF HPLC METHOD FOR DETERMINATION OF TERBUTHYLAZINE AND TERBUMETON

Vera Trajkovska, Valentina Pavlova, Simka Petrovska-Jovanović

Institute of Chemistry, Facilty of Science, "St. Cyril and Methodius University", POB 162, 1000 Skopje, Macedonia

Abstract: *One of the most used herbicides onto farming lend – vineyard, apple and pear tree, is the herbicide by commercial name "Karagard kombi A-50 VP" produced by AD "OHIS" Skopje. The substance terbuthylazine and terbumeton are the active compounds in this pesticide formulation.The aim of this work is to optimize the experimental conditions for simultaneous HPLC determination of these two compounds. This method can be applied for further determination of their residue in different matrix. The best results for terbuthylazine and terbumeton are obtained with: analytical column Lichrosorb RP 18, 200 x 4.6 mm, 5 μm, flow rate 1.3 ml/min, isocratic elution by mobile phase CH3OH-H2O/80-20 (v/v).*

Keywords: *terbuthylazine, terbumeton, HPLC, determination*

1. INTRODUCTION

Triazines are still widely used as herbicides in agriculture. During and after the herbicide application onto farming land, triazines may be transported to the environmental waters [2,3], and to the soil [7]. Therefore, their determination is of great importance in environmental studies. Clearly there is a need for analytical methods that allow simultaneous determination of pesticides and their metabolites.

The methods actually used for the determination of trace amounts of triazines include gas chromatography (GC) [1,4,6] and high performance liquid chromatography (HPLC) [5,8].

A disadvantage of gas chromatography is that it is limited to volatile chlorotriazines. The hydroxy derivatives cannot be analyzed without derivatization. High performance liquid chromatography is directly applicable to triazines and their degradation products.

In this paper, we introduce optimization of HPLC conditions for simultaneous determination of terbuthylazine and terbumeton, at relatively low levels, less than 5 ppb.

2. EXPERIMENTAL

Materials

The compounds analyzed are shown in Fig.1. Acetonitrile (HPLC grade) was from Sigma – Aldrich (Germany). Methanol (for liquid chromatography) and water (for chromatography) were from Merck (Germany).

a) b)

Figure 1. Moleculare structures of: terbuthylazine a) and terbumeton b)

Standard solutions

Stock solutions of 1000 ppm terbuthylazine and terbumeton were prepared by dissolving 10 mg of the respective triazine in 10 ml of methanol. Stock solutions were used to prepare standard mixtures with different triazine concentrations in methanol / water (50/50, v/v). These mixtures were used for external calibration as well as for the preparation of artificial samples. All solutions were stored at 4^{o}C.

HPLC analysis

A HPLC system (Varian) equipped with a ternary gradient pump (9012), 20 μl loop (Rheodyne) and polychrom diode array detector (Varian-9065) was used for the HPLC analysis. Separation was performed using analytical column Lichrosorb RP18, 200 x 4.6 mm, 5 μm (Hewlett – Packard).

3. RESULTS AND DISCUSSION

The best composition of mobile phase, the flow rate as well as the detection limit were determined. For best separation and symmetrical peak shape, several isocratic and gradient programs for the mobile phase were evaluated. It is found out that the best mobile phase is methanol-water / 80-20 isocratic, so that mobile phase was used for further investigations. For best separation, several flow rates of mobile phase (0.5 – 1.5 ml/min.) are evaluated. It was found out that the best flow rate is 1.3 ml/min. Retention times of terbuthylazine and terbumeton are 3.28 and 4.83 min, respectively. The flow rates down to 1.3 ml/min give no symmetrical peak shape, and those up to 1.3 ml/min give peaks that are very close (low resolution).

Separation under above mentioned HPLC conditions is shown in Fig.2.

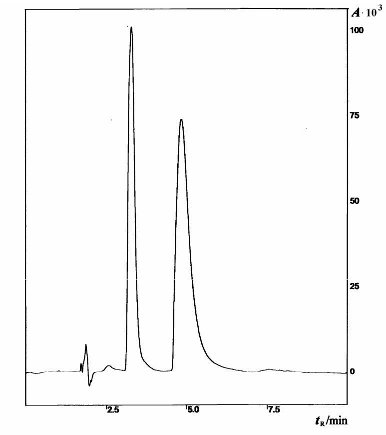

Figure 2. HPLC separation of terbuthylazine (3.28 min) and terbumeton (4.83 min)

Absorbance was measured continuously in the range 190-350 nm by diode array detection following solute separation on the HPLC column. The peaks were measured at a wavelength of 220 nm, where the compounds of interest have an absorption maximum (Fig.3).

Figure 3. Absorption spectra of terbuthylazine (____) and terbumeton

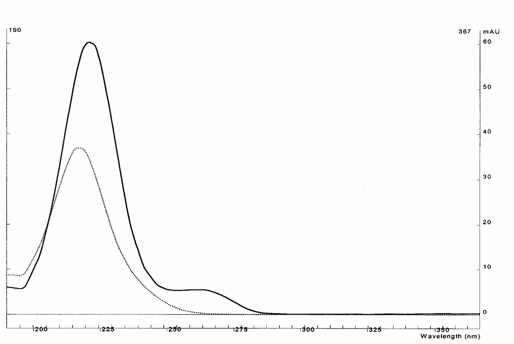

(..........)

The values calculated for the retention factors, separations factors and resolutions for investigated pesticides are given in Table 1.

Table 1. Retention Factors (*k*), Separations factors (*α*) and Resolution for ivestigated pesticides

Compound	t_R /min	*k*	*α*	*R*
Terbuthylazine	3,28	0,76	2,10	2,34
Terbumeton	4,83	1,58	-	-

The calibration was carried out by injecting standard solutions onto the HPLC column (external calibration). The calibration curves had a correlation coefficient r^2>0.997 for both measured triazines (Table 2).

Table 2. Statistical Data of Calibration Curves for investigated pesticide

Compound	Regression equation	RSD (%)	R^2
Terbuthylazine	$y = 795{,}95\,x$	4,48	0,9983
Terbumeton	$y = 645{,}48\,x$	6,37	0,9976

The sensitivity of the method was also determined and the results are given in Table 3.

Table 3. Limit of Detection (LOD) and Limit of Quantification (LOQ) for invesigated pesticides

Compound	Regression equation	SD	LOD/ng	LOQ/ng
Terbuthylazine	$y = 1023{,}47\,x + 155{,}71$	507,45	1,6	4,9
Terbumeton	$y = 984{,}77\,x + 20{,}06$	321,15	1,1	3,3

4. CONCLUSION

The developed HPLC procedure is suitable for detection and determination of terbuthylazine and terbumeton. The optimal HPLC conditions are: mobile phase methanol-water / 80-20 isocratic, flow rate 1.3 ml/min, detection at wavelength of 220 nm, analytical column Lichrosorb RP18, 200x4.6 mm, 5 μm.

5. REFERENCES

[1] Aguilar, C., Borrull, F., Marce, R. M. (1997) Determination pf pesticides in environmental waters by solid-phase extraction and gas chromatography with electron-capture and mass spectrometry detection, J. Chromatogr. A 771, 221-231.

[2] Berg, M., Muller. S. R., Schwarzenbach, R. P. (1995) Simultaneous determination of triazines including atrazine and their mmetabolites hidroxyatrazine, desethylatrazine, and deisopropylatrazine in natural waters, Anal. Chem. 67, 1860-1865.

[3] Chiron, S., Dupas, S., Scribe, P., Barcelo, D. (1994) Application of on-line solid-phase extraction followed by liquid chromatography-thermospray mass spectrometry to the determination of pesticides in environmental waters, J. Chromatogr. A 665, 295-305.

[4] Crespo, C., Marce, R. M., Borrull, F. (1994) Determination of various pesticides using membrane extraction discs and gas chromatography-mass spectrometry , J. Chromatogr. A 670,135-144.

[5] Pichon, V., Hennion, M. C. (1994) Determination of pesticides in environmental waters by automated on-line trace-enrichment and liquid chromatography, J. Chromatogr. A 665, 269-281.

[6] Psattthaki, M., Manoussaridou, E., Stephanou, E., G. (1994) Determination of organophosphorus and triazine pesticides in ground and drinking water by solid-phase extraction an gas chromatography with nitrogen-phosphorous or mass sspectrometric detection, J. Chromatogr. A 667, 241-248.

[7] Schewes, R., Maidl, F.X., Frichbeck, G. (1993) Trace determination of weathered atrazine and terbuthylazine and their degradation products in soil by high-performance liquid chromatography diode-array detection, J. Chromatogr. A 641,89-93.

[8] Vitali, P., Venturini, E., Bonora, C., Calori, R., Raffaelli, R. (1994) Determination of triazines and dinitroanilines in waters by high-performance liquid chromatography after solid-phase extraction, J. Chromatogr. A 660, 219-222.

OPTIMIZATION OF THE DERIVATIZATION PROCEDURE FOR DETERMINATION OF SOME PHENETHYLAMINES USING 3,5-DINITROBENZOYLCHLORIDE

Valentina Pavlova, Vera Trajkovska, Simka Petrovska-Jovanović

Institute of Chemistry, Faculty of Natural Sciences and Mathematics, The "Ss. Cyril and Methodius" University, Gazi Baba b.b. P.O.Box 162, 1000 Skopje, Macedonia, e-mail: vpavlova@iunona.pmf.ukim.edu.mk

***Abstract**: Most liquid chromatography methods incorporate a chemical reaction to convert the analytes into highly detectable products. Derivatization, when performed in the pre-column mode, also facilitates the chromatographic separation. In this work, we evaluated different alternatives for the rapid and sensitive determination of some phenethylamines, by High-performance liquid chromatography with UV detection. The reliability of the derivatization procedure and the optimization with 3,5-dinitrobenzoylchloride is done.*

***Keywords:** optimization, determination, derivatization procedure, phenetilamines, 3,5-dinitrobenzoylchloride*

1. INTRODUCTION

Liquid phase chromatography (HPLC) is a method of choice for the determination of inorganic and organic substances in various matrices. Unfortunately, many substances of interest cannot be detected in HPLC because they do not contain the necessary chromophoric, fluophoric or redox groups. However, this problem can be overcome by inducing derivatization reactions that add one of the above groups to the molecule investigated [1]. A derivatization reaction is very often required in order to increase sensitivity or selectivity and can be achieved by a specific detection, such as fluorescence or absorption in the visible light, at a high wavelength. Derivatization is particularly important for trace analyses of complex biological samples.

There are many derivatization methods, according to the achievable literature references. Herráez-Hernández et all [2] developed sensitive determination of methylendioxylated amphetamines using 9-fluorenylmethyl chloroformate in combination with HPLC/fluorimetric detection. The same authors demonstrate derivatization techniques for automated chromatographic analysis of amphetamine using *o*-phthaldialdehyde [3].

The aim of our work to optimise the derivatization procedure of 1-(1,3-benzodioxol-5-yl) propan-2-amine; *N*-[2-(1,3-benzodioxol-5-yl)-1-methylethyl]-*N*-methylamine; *N*-[2-(1,3-benzodioxol-5-yl)-1-methylethyl]-*N*-ethylamine; *N*-[1-(1,3-benzodioxol-5ylmethyl)propyl]-*N*-methylamine, using 3,5-dinitrobenzoylchloride.

2. EXPERIMENTAL

The chromatographic system used consisted of a ternary pump (Model 9012, Varian), with a UV-Diode Array detector (Model 9065, Varian) with a sample loop injector of 20 μL. The UV detector operated at 200 nm for the detection of DNB derivatives. All chromatograms recorded at ambient temperature.

All the reagents were of analytical-reagent grade. Acetonitrile and methanol (HPLC grade) purchased from Merck, Germany. 3,5- dinitrobenzoylchloride were obtained from Aldrich, Germany. Phosphoric acid, borax, and sodium hydroxide Alkaloid, Macedonia, also used.

Stock solutions of 1-(1,3-benzodioxol-5-yl) propan-2-amine, *N*-[2-(1,3-benzodioxol-5-yl)-1-methylethyl]-*N*-methylamine, *N*-[2-(1,3-benzodioxol-5-yl)-1-methylethyl]-*N*-ethylamine, *N*-[1-(1,3 benzodio-xol-5-ylmethyl)propyl]-*N*-methylamine, were prepared by dissolving each standard substance in methanol with concentrations of 1.00 mg/mL. The mixture of the four components by mixing the appropriate quantities of each stock solution was prepared and diluting with methanol to the working concentration of 0.025 mg/mL. The 3,5- dinitrobenzoylchloride solutions were prepared daily by dissolving the pure compound in acetonitrile.

3. RESULTS AND DISCUSSION

The effect of the experimental conditions affecting the derivatization with 3,5-dinitrobenzoylchloride (DNB) was investigated using methanol solutions of the analytes at a concentration of 25.0 μg/mL. The main parameters affecting the reaction yields being the concentration of reagent and the time of reaction, and the other experimental parameter such as, pH in the reaction medium optimized.

Derivatization with 3,5-dinitrobenzoylchloride

The effect of the reaction time was examined by allowing the derivatization to proceed for times ranging from 1 to 20 min (for a concentration of reagent of 0.010 mol/L). Maximum analyte conversions were obtained for a reaction time of 5 min. The effect of the concentration of 3,5-dinitrobenzoylchloride on analyte conversation was examined within the range 0.001-0.015 mol/L, using a reaction time of 5 min. The results obtained demonstrated that the responses for analysed compounds reached a maximum when using concentration of 3,5-dinitrobenzoylchloride with 0.005 mol/L. Consequently, a reaction time of 5 min and a concentration of reagent of 0.005 mol/L were selected as the best conditions for derivatization of the analytes.

Derivatization were carried out as follows: 0.100 mL of the samples and 0.100 mL of a borate buffer (pH 10.0) were placed in a 2 mL glass vials, then 0.050 mL of reagent were added and the resulting mixture was left to react for a defined period of time. Finally, aliquots of 20 μL of the mixtures were injected into the chromatograph.

It is interesting that for the given concentration of reagent, the reaction time required to achieve maximum conversation of the examined phenethylamines was higher than that required for amphetamines.

Chromatographic conditions

Separations of 1-(1,3-benzodioxol-5-yl) propan-2-amine, *N*-[2-(1,3-benzodioxol-5-yl)-1-methylethyl]-*N*-methylamine, *N*-[2-(1,3-benzodioxol-5-yl)-1-methylethyl]-*N*-ethylamine, *N*-[1-(1,3 benzodio-xol-5-ylmethyl)propyl]-*N*-methylamine, were performed on column LiChrospher® 60 RP-select B (250 mm x 4.6 mm, 5 μm), Merck, protected by a appropriate guard column. A mixture of phosphate buffer (pH 2.1) and acetonitrile selected as an optimal mobile phase. An isocratic elution phosphate buffer 87 % (2.1): 13 % CH_3CN (15 minutes) was performed at ambient temperature, and flow rate of 1.5 mL/min. Samples were injected through injector valve Rheodyne Model 7125 with a 20 μL sample loop.

After chromatographic separation we obtained this retention times for DNB phenetilamines: 3.8 min, 4.5 min, 5.7 min, 6.8 min, and 12.8 min, for 3,5-dinitrobenzoylchloride (Fig. 1).

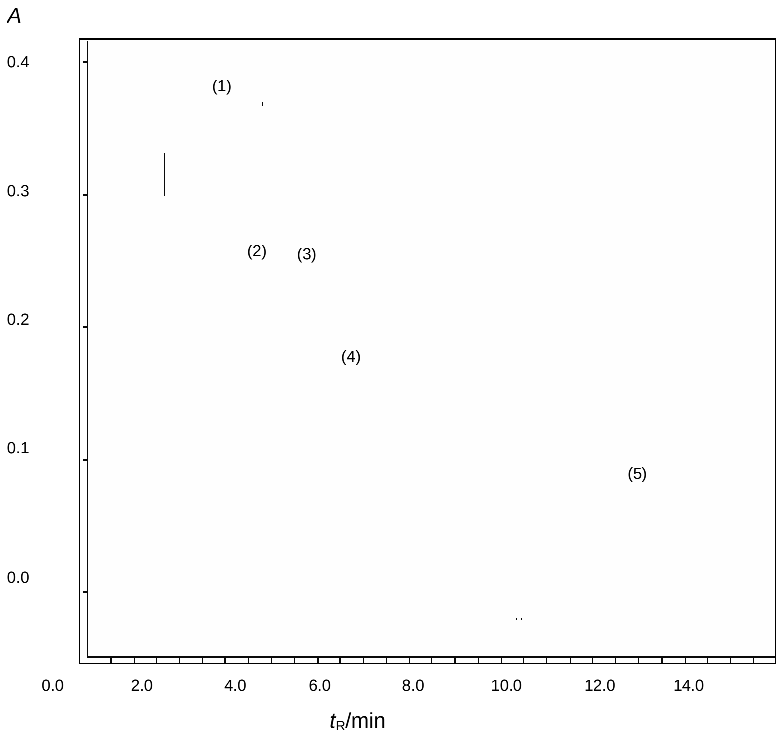

Fig.1. Chromatogram obtained of DNB derivatives: **(1)** [1-(1,3-benzodioxol-5-yl) propan-2-amine, **(2)** *N*-[2-(1,3-benzodioxol-5-yl)-1-methylethyl]-*N*-methylamine, **(3)** *N*-[2-(1,3-benzodioxol-5-yl)-1-methylethyl]-*N*-ethylamine, **(4)** *N*-[1-(1,3 benzodio-xol-5-ylmethyl)propyl]-*N*-methylamine), **(5)** 3,5-dinitrobenzoylchloride. Concentration of each analyte, 25.0 μg/mL. For other experimental details, see text.

4. CONCLUSIONS

A HPLC method for determination of some phenethylamines using UV detection at 200 nm has been reported. The derivatization procedure with 3,5-dinitrobenzoylchloride is done. After optimization, the best results are obtained using a reaction time of 5 min and a concentration of derivatization reagent of 0.005 mol/L. This procedure can be applied for determination of analyzed compounds in different samples, such as biological matrices, urine, blood, plasma, hair, etc.

5. REFERENCES

[1] Coppex, L. (2000) *Derivatives for HPLC analysis-diploma thesis*, Faculty of Chemistry and Pharmacy, University of Genf, 4.

[2] Herráez-Hernández, R., Campíns-Falkó P., Verdú-Andrés, J. (2001) Sensitive determination of methylenedioxylated amphetamines by liquid chromatography, *The Analyst,* 126, 581-586.

[3] Herráez-Hernández, R., Campíns-Falkó, P., (2000) Derivatization techniques for automated chromatographic analysis of amphetamine using *o*-phthaldialdehyde: a comparative study, *Chromatographia*, 52, 169-174.

REACTIONS OF (BENZAMIDOMETHYL)TRIETHYLAMMONIUM CHLORIDE WITH SOME 1,3-DIKETONES IN AQUEOUS MEDIA

Ana Mateska[1], Jane Bogdanov[1], Frosa Anastasova[1], Evamarie Hey-Hawkins[2] and Emil Popovski[1]

[1]Institute of Chemistry, Faculty of Natural Sciences & Mathematics, Sts. Cyril and Methodius University, PO Box 162, 1000 Skopje, Macedonia; e-mail:
emilp@iunona.pmf.ukim.edu.mk*;*
[2]Institute of Inorganic Chemistry, Faculty of Chemistry and Mineralogy, Leipzig University, Johannisallee 29, 04103 Leipzig, Germany

Abstract: *(Benzamidomethyl)triethylammonium chloride (1) smoothly reacts with several 1,3-diketones, in aqueous media, under alkaline conditions (pH ≥ 9), at ambient temperature. From reaction of 1 with dibenzoylmethane (2a) and benzoylacetone (2b) only mono-C-benzamidomethylation products (3a, 3b) were isolated, respectively. Reaction of 1,3-indandione (2c) with 1, gave di-C-benzamidomethylation product (3c).*

O-benzamidomethyl alkylation products have not been detected or isolated. The reactions occurred under mild conditions to give products in moderate yields.

Keywords: *C–C bond formation, aqueous medium, benzamidomethylation, 1,3-Diketones.*

1. INTRODUCTION

In the past a large number of benzamidomethyl compounds have been synthesized, compounds which have different properties. Many of them are used as radiolabels [1], functional derivates of α-amino acids and peptides [2], antibiotics [3, 4], antiviral drugs [5, 6], emulators [7], as intermediers for synthetic resin [8], etc. Preparation of different benzamidomethyl compounds was an object of interest in our previous research work, which showed that (benzamidomethyl)triethylammonium chloride (**1**) is an excellent agent for nucleophilic substitution in aqueous media, in reactions with different nucleophiles that occur under mild conditions, with high yields and simple isolation of the products [9-11]. The emphasis of this paper is based on the possibility quternarum ammonium salt **1** to build C-C bonds in aqueous media, with different 1,3-Diketones. C-C bond formation is the essence of organic synthesis and provides the foundation for generating more complicated organic compounds from the simpler ones. Many C-C bond forming processes involve reaction between a nucleophilic carbon atom and an electrophilic one [12]. Water as a medium can promote various reactions of this type that can be carried out as diverse as those in nonaqueous conditions. Organic synthesis in water can significantly shorten the synthetic route, increase product selectivity and reduce volatile organic consumption [13].

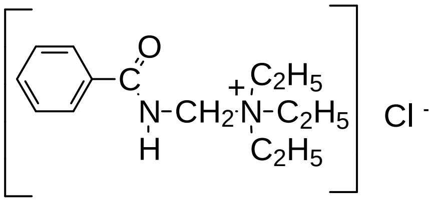

1

2. RESULTS AND DISCUSSION

Reactions of **1** with the enolate-anions (derived from 1,3-diketones) were preformed in stirred aqueous conditions, in the presence of small quantities of triethylamine (TEA) pH ≥ 9, at ambient temperature. A very general means of generating C-nucleophiles involves removal of a proton from a carbon atom (between two C=O groups, in the molecule of the diketone), by a Bronstead base [12]. The C=O group bonded directly to the anionic carbon can delocalize the negative charge by resonance (Scheme I). Actually the presence of two electron-withdrawing substituents favours formation of the enolate-anion [12].

Scheme I

We were interested in the alkylation reactions of different enolate-anions (Scheme II).

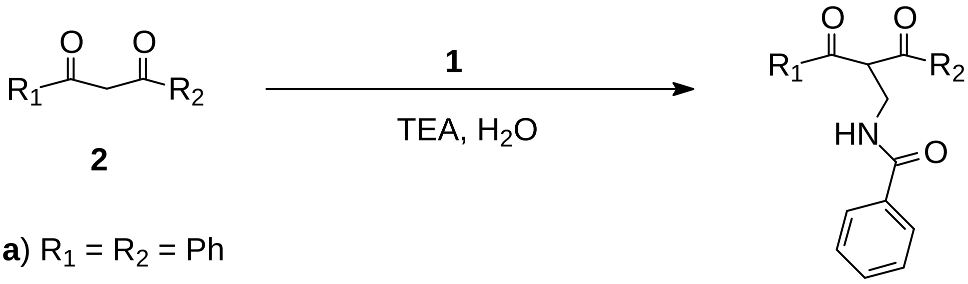

a) $R_1 = R_2 = Ph$

b) $R_1 = CH_3;\ R_2 = Ph$

3

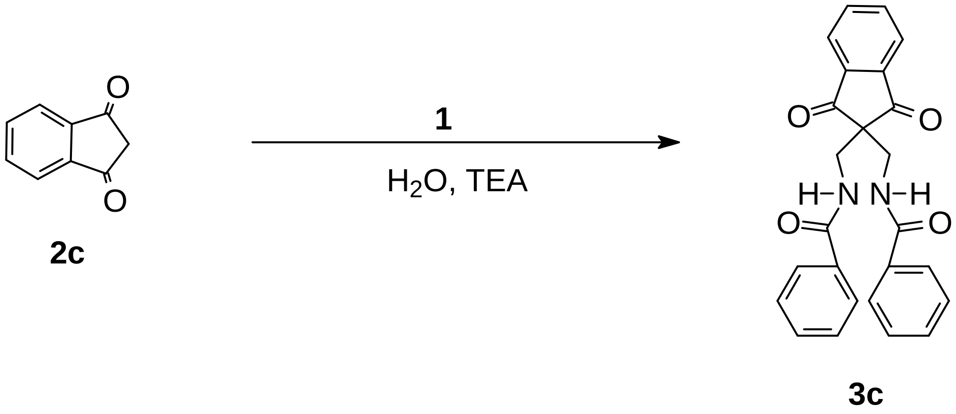

Scheme II

The reaction of the symmetrical **2a** and unsymmetrical **2b** diketone with **1** gave mono-C-alkylation products, **3a** and **3b**, respectively, while the reaction of the symmetrical **2c** with **1** gave di-C-alkylation product **3c**. The reasons for these different reaction products are due to the differences in acidity of the enolate-anions, which means that the protons from the carbon atom situated between two-withdrawing groups (C=O) in **2c** are more acidic than the ones in **2a** and **2b**. Because of the acidity of the previously named protons in the molecule of **2c**, the kinetics of the reaction of **2c** with **1** is significantly higher than the one with **2a** and **2b**, which resulted in attachment of two benzamidomethyl groups to the molecule of the **2c** enolate-anion, instead of one in the **2a** and the **2b** enolate-anions. In these reactions the process of alkylation of enolat-anions occurs at the carbon atom (instead of the oxygen atom), which is affected by using water as a solvent (process of solvation at the oxigen atom, which directs the process of nucleophilic addition to take place primarily on the C atom [14]). In the case of **3a** and **3b**, the mass spectra indicate that in the reactions between **1** and **2a-b** a mono alkylation process occurs. The IR spectra gave peaks from Amide I and Amide II groups in both cases. In the IR spectrum of **3a** one peak from the carbonyl group (split in two from C-COPh) at 1696 cm^{-1} can be observed, while in the spectrum of **3b**, there are two peaks from two carbonyl groups (C-COPh and C-COCH$_3$) at 1723 cm^{-1} and 1661 cm^{-1} present. ^{1}H-NMR spectra are the final evidence for the molecule structures. In ^{1}H-NMR spectra of **3a**, a triplet from protons of CH$_2$ (NHCH$_2$-CH) group can be noticed, while in the spectra of **3b** two quadruplets from the protons of the same group can be noticed. These differences are due to the attachement of CH$_2$ group to a chiral center in the molecule of **3b**, which makes the two protons unequal in their properties. In the case of **3c**, the mass spectrum indicates that in the reaction between **1** and **2c** a dialkylation process occurs. The IR spectrum similarly as above gave peaks from Amide I and Amide II groups and one peak from both carbonyl groups (C-CO). ^{1}H-NMR gives a dublet from the protons of the CH$_2$ (NHCH$_2$) group which confirms the absence of a proton at the C atom between the two carbonyl groups.

3. CONCLUSIONS

This paper is evidence that C-C bond forming processes can occur in aqueous media in reaction between quaternary ammonium salt **1** and different 1,3-diketones. The reactions gave mono and di-C-alkylation products respectively, under mild reaction conditions with moderate yield. The products are easily isolated from the reaction mixture by simple filtration.

4. EXPERIMENTAL

Melting points were determined with Reichert heating plate and were uncorrected. Nitrogen elemental analysis was carried out by the Dümas method. ^{1}H-NMR and ^{13}C-NMR spectra were recorded on a Bruker 400 MHz and 100 MHz, respectively using DMSO-d_6 and $CDCl_3$ as solvents. Infrared spectra were measured on a Perkin-Elmer System 2000 FT IR, by the method of KBr pellets. All the reagents and solvents were obtained from commercial sources and were used without further purification.

(Benzamidomethyl)triethylammonium chloride (**1**) was obtained in manner described in previous work [9].

N-(2-benzoyl-3-oxo-3-phenylpropyl)benzamide (**3a**).

A solution of **1** (0.85 g, 3.14 mmol) in water (10 ml) was added to acetone solution of **2a** (0.47 g, 2.10 mmol) and TEA (pH ≥ 9). The mixture was stirred for 1 h at ambient temperature and the product **3a** was collected by filtration. Yellow crystals, recrystalized from acetone; Yield 54.6 %; mp = 157-158 °C (lit. 1 58-160 °C [15]); (Calc. 77.29 C, 5.36 H, 3.92 N, Found 77.11 C, 5.59 H, 3.76 N); IR(KBr)/cm^{-1}: 3400 (νNH), 1696 (CO), 1685 (CO), 1648 (Amide I), 1529 (Amide II); ^{1}H-NMR (400 MHz, DMSO-d_6): 8.03 (t, 1H, CONH), 7.71-7.40 (m, 15H, Ar), 6.085 (t,1H, CH), 3.89 (t, 2H, $NHCH_2$); ^{13}C-NMR (100 MHz, DMSO-d_6): 195.44 (C=O), 166.98 (CONH), 68.39 (CH), 54.76 (CH_2), Aromatics: 135.64, 133.97, 133.89, 131.23, 129.04, 128.39, 128.16, 127.10.

N-(2-benzoyl-3-oxobutyl)benzamide (**3b**).

A solution of **1** (1.5 g, 0.006 mmol) in water (10 ml) was added to wather solution of **2b** (0.45 g, 0.003 mmol) and TEA (pH ≥ 9). The mixture was stirred for 1 h at ambient temperature and the product **3b** was collected by filtration. White crystals, recrystalized from acetone; Yield 57.3 %; mp = 105-107 °C (lit. 1 12-113 °C [15]); (Calc. 73.20 C, 5.80 H, 4.74 N, Found 72.93 C, 6.08 H, 4.55 N); IR(KBr)/cm^{-1}: 3323 (νNH), 1723 (CO), 1637 (Amide I), 1534 (Amide II); ^{1}H-NMR (400 MHz, $CDCl_3$): 8.13 (t, 1H, CONH), 5.06 (t, 1H, CH), 4.10 (q, 1H, $NHCH_2$), 3.90 (q, 1H, $NHCH_2$), 2.25 (d, 3H, $COCH_3$); ^{13}C-NMR (100 MHz, $CDCl_3$): 204.20 (C=O), 196.72 (Ph-CO), 168.53 (CONH), 61.64 (CH), 39.52 (CH_2), 30.51 (CH_3), Aromatics: 136.47, 134.91, 134.52, 132.44, 129.78, 129.60, 129.30, 127.62.

N-[(1,3-dioxo-2,3-dihidro-1H-inden-2-yl)methyl]benzamide (**3c**).

3c was synthesized in a similar manner as **3b**. Purple crystals, recrystalized from acetone; Yield 49.8 %; mp = 200-203 °C; (Calc. 72.8 C, 4.89 H, 6.79 N, Found 72.6 C, 5.09 H, 6.89 N); IR(KBr)/ cm^{-1}: 3313 (νNH), 1698 (CO), 1657 (Amide I), 1541 (Amide II); ^{1}H-NMR (400 MHz, DMSO-d_6): 8.62 (t, 2H, CONH), 7.90-7.35 (m, 14H, Ar), 3.73 (d, 4H, $NHCH_2$); ^{13}C-NMR (100 MHz, DMSO-d_6): 199.26 (C=O), 166.90 (CONH), 58.40 (CH_2), 40.12 (C), Aromatics: 141.51, 135.80, 133.94, 131.25, 128.17, 127.10, 122.90.

5. REFERENCES

[1] Okarivi, S. M., Adriaens, P., Verbruggen, A., (1997) Synthesis, radiolabelling characteristics and biological evaluation of the derivatives of mercaptoacetyltriglucine. J. Labelled Comp. Radiopharm. 39 (10), 853-874.

[2] Zlotin, G. S., Sharova, V. I., Luk`yanov, A. O., (1996) Chemical properties of N-(amidomethyl) and N-(imidomethyl)glucine derivatives. 2.Reactions of alkoxycarbonyl and carboxyl groups. Russian Chemical Bulletin 45 (7), 1680-1687.

[3] Clayton, J. P., Kenneth, D., Guest, A. W. C., (1973) Aminomethylesters of penicilins and cephalosporins. Ger. Offen. 2,326,795 (Cl. C 07d), 43.

[4] Franceschi, G., Foglio, M., Arcamone, F., (1974) Rapidly absorbable (benz and primalamido)methyl penicilanates and cephalosporanates. Ger. Offen. 2,406,817 (Cl. C 07d), 30.

[5] Pandey, V. K., Misra, R. P., (1986) 1-(Amido/thioamido)-3-methyl-4-methylphthalimido/benzamido/nicotinamido-5-oxopyrazoles as potencial antiviral agents. Indian drugs, 23 (8), 462-465.

[6] Pandey, V. K., Garu, P., Chomdhuru, B. L., (1987) Synthesis and antiviral activity of 1-(oxoalkyl/aryl)-3-methyl-4-arylamidoalkyl-5-oxopyrazoles. Biol. Mem. 13 (1), 83-87.

[7] Graenacher, C., Sallmann, R., (1946) Condensation products of thiourea compounds. U. S. 2,411,655.

[8] Mowry, T., (1950) Unsaturated amides. U. S. 2,529,455.

[9] Popovski, E., Klisarova, L., Vikic-Topic, D., (1999) Simple Method for Benzamidomethylation of Phenoles in Water Solution. Synth. Commun. 29, 3451-3458.

[10] Popovski, E., Klisarova, L., Vikic-Topic, D., (2000) Benzamidomethylation with (Benzamidomethyl)triethylammonium chloride. 2. A Simple Method for Benzamidomethylation of Thioles, Amines and Carboxylic acids. Molecules 5, 927-936.

[11] Popovski, E., Bogdanov, J., Najdoski, M., Hey-Hawkins, E., (2006) Reactions of (Benzamidomethyl)triethylammonium Chloride with Some Inorganic Nucleophiles in Aqueous Medium. Molecules. 11, 299-285.

[12] Carey, F. A., Sundberg, R. J., (1990) Advanced Organic Chemistry, 3-th edition. New York, Plenum Press.

[13] Chao-Jun, L., (2005) Organic Reactions in Aqueous Media with a Focus on Carbon-Carbon Bond Formations: A Decade Update. Chem. Rev. 105, 3095-3165.

[14] Pine, S. H., (1987) Organic Chemistry, Fifth edition, New York, McGraw-Hill, Inc.

[15] Monti, (1930) Some condensation products of methylolbenzamide. Gazz. Chim. Ital. 60, 39-42.

[16] Silverstein, R. M., Bassler, G. C., Morrill, T. C., (1991) Spectrometric Idemntification of Organic Compounds, Fifth edition, New York, Wiley.

SPECTROPHOTOMETRIC STUDY OF 3, 4- SUBSTITUTED 1-PHENYL-PYRAZOL-5-ONES IN DIFFERENT SOLVENTS

Atanas G. Chapkanov[1], Bojidarka B. Koleva[2]

[1]South-West University "Neofit Rilski", Department of Chemistry, 66 "I. Mihailov" str., 2700 Blagoevgrad, Bulgaria
[2]University of Sofia "St. Kl. Ohridski", Faculty of Chemistry, 1 "J. Boucher" blvd., 1164 Sofia, Bulgaria

Abstract: *A comparative UV-spectral analysis of samples derivatives of pyrazolones as 3-methyl-1-phenyl pyrazol-5-one (MPhP), 1,3 – diphenyl pyrazol-5-one (DPhP) and 4-benzyl-3-methyl-1-phenyl pyrazol-5-ones (4-BMPhP) were carried out. The experimental UV-spectra of the compounds in different solvents have been compared with previous our data. The obtained results showed the presence of the different tautomeric forms of the compounds depending on polarity effects of solvents, type of substituents at 3-and 4-position and other interactions. The spectral behavior of the investigated compounds illustrated the specific influence of the point out above factors on the stabilization of the tautomeric forms.*

Keywords: *3,4-substituted 1-phenyl pyrazol-5-ones, UV-spectral analysis, tautomeric forms,*

1. INTRODUCTION

The tautomerism of 1-phenyl-substituted-pyrazol-5-one derivatives have been extensively studied for many years. Their important chemical reactivity and practical application is a subject of large numbers of reviews [1-5]. The some substituted pyrazol-5-ones exhibit three basic tautomeric forms (CH-, OH- and NH-) (Scheme 1 and 2), whose stabilization depends on the influence of the substituents, temperature, medium effects, inter- and intramolecular interactions [4, 5]. The theoretical and stereo structural characterization of the CH-tautomer of two derivatives - 3-methyl-1-phenyl pyrazol-5-one (MPhP) and 1,3–diphenyl pyrazol-5-one (DPhP), have been carried out by IR-spectroscopic study including linear-dichroic (IR-LD) analysis [6, 7].

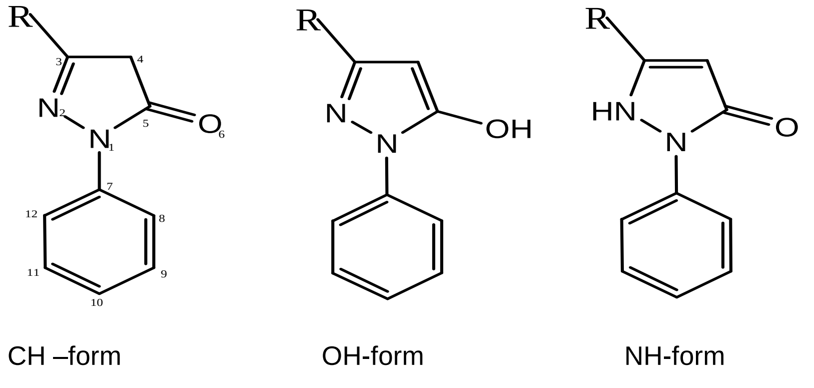

Scheme 1: Tautomeric forms of 1-phenyl-3-substituted pyrazol-5-ones;
R = -CH_3 (**MPhP**); R = -C_6H_5 (**DPhP**)

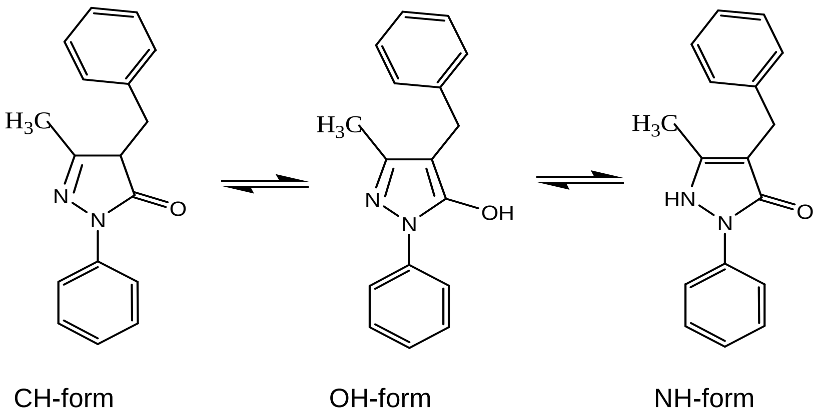

Scheme 2: Tautomeric forms of 4-benzyl-3-methyl-1-phenyl pyrazol-5-one (**4BMPhP**)

The NH-tautomeric form of the DPhP was obtained after irradiation in polymer film and have been characterized by redussing-difference IR-spectral analysis [8]. Similar kind of transformation was obtained for DPhP in ethanol solution by UV-spectroscopy [9].

2. EXPERIMENTAL PART

The synthesis of the investigated compounds are described in [10]. Solvents used were Uvasol (Merk) products.

The UV-absorption spectra of the compounds studied were carry out at a following condition: as 1.10^{-4} mol/l solutions, path length 1cm, room temperature. The UV-spectra in used solvents isooctane, n-hexane, tetrahydrofuran (THF), methanol, ethanol, H_2O were recorded on a SPECORD UV-VIS spectrophotometer.

3. RESULTS AND DISCUSSION

This work continued our investigation on the tautomerism and photoisomerization of the substituted 1-phenyl-pyrazol-5-ones. Nevertheless the application of the UV-spectroscopy is complicated as a result of the overlapping of the absorption maxima [2-4], this work considers the experimental UV-spectral data of the compounds characterized their tautomeric forms (Scheme 1 and 2) in different solvents. The main purpose was to carry out a comparative UV-spectral analysis with some previous obtained results [9] and establishment of dependency if it is possible about medium effects and structure of the compounds.

The UV-spectral data of the investigated compounds in different solvent with dielectric constants increase are presented in Table 1.

4. UV-SPECTRAL ANALYSIS

The spectral data in Table 1 can be interpreted as a following manner. According to our results in nonpolar solvent as a cyclohexane, chloroform and 1,2-dichloroethane DPhP and MPhP stabilezed CH-form with corresponding bands [12]. The spectral data for DPhP in other nonpolar solvent as n-hexane, isooctane and tetrahydrofuran (THF) showed main absorption maximum at 265-270 nm and second one at 325 nm (see Table 1). The last one is typical for CH-tautomer showing its stabilization in this solvents and confirmed our results [7,9]. For MPhP in solution of n-hexane the main band at 246 nm and the sholder at 270-330 nm confirmed the presence and stabilization of the CH-form too. However, in isooctane and THF solutions the absorption maximum is only at 248 nm like a absorption maximum of MPhP in cyclohexane and 1,2 -dichloroethane, but second maximum at 300-330 nm absent [12]. In this case means, that a polarity effects of the solvents play a significant and important role on the spectral behaviuor of the compounds [4]. At the concentration conditions necessary for UV-spectral analysis especially for MPhP (< 10^{-4} mol/l) the possibilities of self-associations between guest-molecules are eliminated and equilibrium is shifted to OH-tautomeric form. This is contrary to the results obtained for other nonpolar solvents till now and showed the specific influence of solvent kind on the stabilization of corresponding tautomeric forms. On the other hand the obtained results showed too a specific influence and the phenyl substituent at 3-position in comparison with 3-methyl group on the UV-absorption bands of the two compounds using the same solvents.

Tab.1. UV-spectral data in different solvent for studied compounds

Com-pound	Solvent **λ [nm]**					
	n-Hexane	Iso-octane	THF	EtOH	MeOH	H_2O
MPhP	246, 270-330sh	248	248	244	246	240, 275sh
DPhP	234, 264, 322	265, 325	270, 320	268	270	264
4BMPhP	245	248	246	250, 278sh	248, 270sh	248, 270

The compound 4-benzyl-3-methyl-1-phenyl- pyrazol-5-ones (4BMPhP) can be considered as a derivatives of MPhP, where at 4-position there is additionally substituent as a benzyl group (-$CH_2C_6H_5$). Nevertheless the UV-spectral data in nonpolar solvent pointed above (see Table 1) showed absorption maxima at 245-248 nm respectively which are almost the same with these of MPhP and no influence of the substituent on spectral data.

In solution of polar solvents as ethanol and methanol DPhP and MPhP stabilized OH-tautomeric form with absorption maximum at 244-246 nm and 268-270 nm respectively [7, 9]. In these solvents 4BMPhP showed absorption maximum at 248 – 250 nm and sholder at 270-280 nm is appeared (see Table 1)

Increasing the dielectric constant of the solvents (from EtOH to water), a absorption maxima for DPhP is at 264 nm which is close to bands in ethanol and methanol solutions. However, for MPhP in order the main maximum at 240 nm, a sholder at 275 nm is appeared. The same is situation for 4BMPhP, where two maxima at 248 nm and 270 nm are at hand. The formed two maxima should be characterized third NH–tautomeric form in water solution. Similar absorption bands can be seen in the UV-spectra of 2,3-dimethyl-1-phenyl pyrazol-5-one (antipyrine) in different solvents which is typical fixed NH-tautomer [12]. As in solution in THF, MPhP showed different behaviour and water solution too, where polarity of solvent is basic reason for these differences in the UV-spectra.

5. CONCLUSION

The comparative UV-spectral analysis of the substituted 1-phenyl-pyrazol-5-ones were carry out. The different UV-spectral behavior of the investigated compounds in series of nonpolar and polar solvents can be explain with the specific influence of several factors: polarity effects of the solvents in connection with their dielectric constants, structure of the compounds and especially structure of the substituents at 3-and 4-position as and specific condition of spectral analysis. The obtained results showed, that no strong relation between spectral characteristics of the compounds and their tautomeric forms according to used solvents and their structure confirming some data in other solvents in the literature [13, 14].

6. REFERENCES

[1] Katritzky, A.R., Maine, F.M., (1964), “The tautomerism of heteroaromatic compounds with five-membered rings – IV: 1-substituted pyrazolin-5-ones”, Tetrahedron, 20, 299-314.

[2] Krohs, W., in: G. de Stevens (Ed.), (1965) “Analgetics”, Chap. 7, Academic Press, New York, .

[3] Elguero, J., Marzin, C., Katritzky, A.R. and Linda, P., (1976), Advances in Heterocyclic Chemistry, Suppl. 1; Katritzky, A.R., Boulton, A. J. Eds, Academic Press, New York,

[4] J. Elguero, J., (1984), Comprehensive Heterocyclic Chemistry, Pergamon Press, Oxford, 5, 167-314

[5] A.R. Katritzky, A., (1992), Chemistry of Heterocyclic compounds, 291

[6] Ivanova, B.B., Chapkanov,A.G., Arnaudov, M.G., Petkov, I. K., (2005), “IR-LD spectral study and ab initio calculations of 1-phenyl 3–substituted pyrazol –5-ones”, Struc. Chem., 16 (1), 47-53.

[7] Ivanova, B.B., Chapkanov, A.G., Arnaudov, M. G., Petkov, I. K., (2006), “Tautomerism in 1-phenyl- 3-substituted pyrazol-5-ones – FT-infrared spectral analysis and ab initio calculations”, Spectr. Lett., 39, 1-13.

[8] Ivanova, B. B., Chapkavov, A. G., Arnaudov, M. G., Petkov, I. K., (2003), “IR-study of photoinduced tautomerization in 1,3-diphenyl-pyrazol-5-one”, Centrl. Europ. J. Chem., 4, 356-365.

[9] Chapkanov, A. G., Koleva, B. B., Arnaudov, M. G., Petkov, I. K., (2007), “On the tautomerism of 1-phenyl-3-substituted-pyrazol-5-ones and their photoinduced products–experimental and theoretical UV- spectral analysis, Colect. of Czech. Chem. Comm., (in submission).

[10] Marchetti, F., Pettinari, Cingolani, A., Pettinari, R., Rossi, M., Caruso, F., (2002), “Organotin (IV) derivatives of novel β-diketones: Part V. Synthesis and characterization of di- and triorganotin (IV) derivatives of 4-acyl-5-pyrazolones modified in position 3 of the pyrazole. Crystal structure of 1,3-diphenyl-4-benzoyl-pyrazolon-5-ato) triphenyltin(IV)”, J. Organomet. Chem., 645, 134-145;

[11] Chapkanov A. G., Petkov, I. K., (1998), “Spectral and photochemical behaviour of some pyrazolones in solutions, micelles and polymer films”, Analitycal Labolatory, 7 (3), 143-147.

[12] Chapkanov A. G., (2005), “IR-and UV-spectral analysis of 1-phenyl-3-substitued pyrazol-5-ones and their photoinduced products”, Theses of PhD, SWU”N. Rilski”, Blagoevgrad

[13] Katritzky, A. R., (1984), Comprehensive Heterocyclic Chemistry, Katritzky, A. R., W. Rees, C. W., Eds., 5, chap.1, Pergamon Press, Oxford

[14] Minkin V. Garnovski A., Elguero J., Katrytzky A., Denisko O., (2001) “Advaces in Heterocyclic chemistry”, 76, 157-191. Academic Press, San Diego, San Francisco, London, Tokyo.

SIMULTANEOUS DETERMINATION OF METHYLENEDIOXYLATED AMPHETAMINES IN ECSTASY TABLETS BY HIGH-PERFORMANCE LIQUID CHROMATOGRAPHY

Valentina Pavlova[1], Sonja Gadzovska[2],

Simka Petrovska-Jovanović[1]

[1]Institute of Chemistry, Faculty of Natural Sciences and Mathematics, The "Ss. Cyril and Methodius" University, Gazi Baba b.b. P.O.Box 162, 1000 Skopje, Macedonia, e-mail: vpavlova@iunona.pmf.ukim.edu.mk
[2]Institute of Biology, Faculty of Natural Sciences and Mathematics, The "Ss. Cyril and Methodius" University, Gazi Baba b.b. P.O.Box 162, 1000 Skopje, Macedonia, e-mail: sonjag@iunona.pmf.ukim.edu.mk

***Abstract**: Amphetamine derivatives have become trendy drugs of abuse because they are powerful stimulants of the central nervous system. In particular, a dramatic increase in the abuse and recreational use of methylenedioxylated amphetamine derivatives, detected in many countries, especially among young people. In the current paper, we developed a simple, reverse-phase HPLC method for analyzing of some drugs: MDA, MDMA, MDEA, and MBDB. The new method was fast, reproducible, and used for simultaneous determination of four methylenedioxylated amphetamines in 145 tablets, seized by Macedonian police in the period from 2005 to 2006, mainly in the area of Skopje, Macedonia.*

***Keywords:** High-performance liquid chromatography, determination, MDA, MDMA, MDEA, MBDB, ecstasy*

1. INTRODUCTION

The most representative substances in the group of methylenedioxy substituted amphetamines are: 3,4-methylenedioxyamphetamine (MDA), 3,4-methylenedioxymethamphetamine (MDMA), 3,4-methylenedioxyethyl-amphetamine (MDEA), N-methyl-1-(3,4-methylenedioxyphenyl)-2-butan-amine (MBDB), which are classified as illicit substances in most countries (Fig.1). The active constituent present in ecstasy tablets is MDMA. Analogue derivatives may also be present and these include MDA, MDEA, MBDB, amphetamine and methamphetamine. Because of dramatic increase in the abuse and recreational use of methylenedioxylated amphetamine derivatives detected in many countries, especially among young people, there is growing interest in the development of rapid, selective and sensitive methods for the identification and quantification of these compounds, in seized tablets.

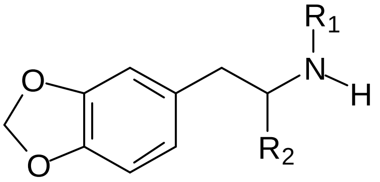

R_1-H, R_2-CH_3: MDA

R_1-CH_3, R_2-CH_3: MDMA

R_1-C_2H_5, R_2-CH_3: MDEA

R_1-CH_3, R_2-C_2H_5: MBDB

Fig.1: Chemical structure of methylenedioxy substituted amphetamines

Methylenedioxylated amphetamine determinations have been performed using high-performance liquid chromatography [4], capillary electrophoresis [2, 3, 6], gas chromatography coupled with different detection systems as MS [1, 7, 9], ECD [8], NPD [5] and FID [3, 6, 10] etc. Without doubt, GC coupled on-line to a MS detection system is the most powerful technique for identification and confirmation of amphetamines. Nevertheless, there are laboratories around the world, especially in developing countries, which cannot afford such an expensive instrument.

The aim of our study was to develop a new, simple, reverse-phase HPLC/DAD method for simultaneous determination of MDA, MDMA, MDEA, and MBDB without ion-pair reagents; because the evidence shows that, the use of ion pair reagents alters the chemistry of columns, rendering it useless for anything but a specific ion-pair analysis.

2. EXPERIMENTAL

The chromatographic system consisted of a Varian ternary pump Model 9012, with a UV-Diode Array detector Model 9065 and Varian Star 4.50 software for data handling is used. To obtain reproducible results, the column was thermostat with column heater (CH-30) and Eppendorf controller of temperature (TC-45). Methanol and acetonitrile used in this method were HPLC grade, *ortho*-phosphoric acid (> 99.95 percentage purity). Authentic samples of MDA, MDMA, MDEA, and MBDB supplied from the United Nations Drug Control Program (Vienna, Austria). Samples injected through the Rheodyne injector valve Model 7125 with a 20 μL sample loop. Separations were performed on the reverse phase column LiChrospher® 60 RP Select B (250 mm x 4.6 mm, 5 μm), protected by a guard column LiChrospher® 60 RP Select B (4 mm x 4.6 mm, 5 μm) (Merck).

Macedonian police seized all 145 samples analyzed (tablets, powders) in the period from 2005 to 2006, mainly in the area of Skopje, Macedonia.

3. RESULTS

The mechanism of retention in the reverse-phase packing is due to the partitioning of the molecule into the lipophylic stationary phase, which is primarly depends upon the lipophylicity of the compound. The other factor that influences the degree of retention is the nature of the mobile phase. The reverse-phase chromatography allows efficient separation of substances with different polarities by altering the composition/polarity of the mobile phase.

The determination of basic compounds requires special RP chromatographic sorbents. Retention, selectivity and peak symmetry of basic compounds are strongly influenced by the silica matrix. Strongly distorted peaks of the basic compounds often observed when unsuitable RP sorbents used, due to the interaction of the basic compounds with unreacted SiOH groups on the silica matrix. LiChrospher® 60 RP-select B is a spherical porous silica carrier, in which the starting silica material is optimized in order to prevent any secondary interactions with basic compounds. The usage of this type of column allows separation of basic compounds without the need of ion pair reagents.

Method development for LiChrospher® 60 RP-select B column involved investigation of mobile phases (organic solvent type and strength), pH (2.1, 2.5, 3, 3.5, 4), flow rates (0.5-3 mL min^{-1} in 0.5 mL min^{-1} increments), and column temperature (30-60 ^{o}C in 5 ^{o}C increments). The mobile phase consisted of phosphate buffer/acidified water with H_3PO_4 and methanol/acetonitrile in varying ratios. The test mixture containing four methylenedioxylated amphetamines: MDA, MDMA, MDEA and MBDB used to examine method selectivity and resolution.

4. DISCUSSION

After optimizing the separation, the best results obtained under these chromatographic conditions:

- column LiChrospher® 60 RP Select B (250 mm x 4.6 mm, 5 μm), protected by a suitable guard column;
- isocratic elution of mobile phase: mixture of acidified water with H_3PO_4 (pH = 2.1) and acetonitrile 90:10 (*v*/*v*);
- flow rate of 1.5 mL/min;
- the column temperature of 40 ^{o}C;
- UV detection performed at 282 nm.

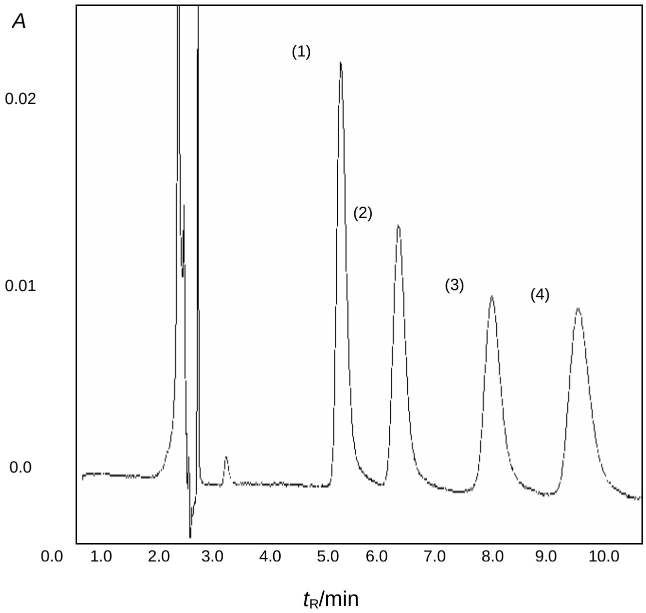

Fig. 2: Chromatogram of: (1) MDA, (2) MDMA, (3) MDEA, (4) MBDB, obtained under optimal chromatographic conditions

Under the proposed chromatographic conditions, MDA, MDMA, MDEA and MBDB is completely separated from each other, which indicates that the method is selective and can be used for their identification and quantification simultaneously. The method uses a simple procedure for sample preparation and allows separation of analysed compounds on LiChrospher® 60 RP Select B column in about 10 min.

A number of seized tablets, powders (145 samples) analyzed to demonstrate that the column Lichrospher® 60 RP Select B could be use in everyday analysis in the laboratory.

5. CONCLUSIONS

A new, reverse-phase HPLC method, for simultaneous determination of basic compounds, such as, 3,4-methylenedioxyamphetamine (MDA), 3,4-methylenedioxymethamphetamine (MDMA), 3,4-methylenedioxyethyl-amphetamine (MDEA), *N*-methyl-1-(3,4-methylenedioxyphenyl)-2-butan-amine (MBDB) have been developed. The method uses a simple procedure for sample preparation and allows separation of analysed compounds on LiChrospher® 60 RP Select B column in about 10 min. The proposed method could be use in the analysis of seized tablets containing some of methylenedioxy-substituted amphetamines these.

6. REFERENCES

[1] El-Haj, B.M., Al-Amri, A.M., Hassan, M.H., Ali, H.S., Bin Khadem, R.K. (2003) The use of cyclohexanone as a ‘‘derivatizing’’ reagent for the GC–MS detection of amphetamines and ephedrines in seizures and the urine, Forensic Sci. Int. 135, 16–26.

[2] Fang, C., Chung, Y., Liu, J., Lin, C. (2002) Rapid analysis of 3,4-methylenedioxymethamphetamine: a comparison of nonaqueous capillary electrophoresis/fluorescence detection with GC/MS, Forensic Sci. Int. 125, 142–148.

[3] Furnari, C., Ottaviano, V., Rosati, F., Tondi, V. (1998) Identification of 3,4-methylenedioxyamphetamine analogs encountered in clandestine tablets, Forensic Sci. Int. 92, 49–58.

[4] Hernandez, R.H., Falco, P.C., Andres, J.V. (2001) Sensitive determination of methylenedioxylated amphetamines by liquid chromatography, Analyst 126, 581–586.

[5] Jacob III, P., Tisdale, E.C., Panganiban, K., Cannon, D., Zabel, K., Mendelson, J.E., Jones, R.T. (1995) Gas chromatographic determination of methamphetamine and its metabolite amphetamine in human plasma and urine following conversion to N-propyl derivatives, J. Chromatogr. B 664, 449–457.

[6] Mc Avoy, Y., Cole, M.D., Gueniat, O. (1999) Analysis of amphetamines by supercritical fluid chromatography, high-performance liquid chromatography, gas chromatography and capillary zone electrophoresis; a preliminary comparison, Forensic Sci. Int. 102, 13–22.

[7] Okajima, K., Namera, A., Yashiki, M., Tsukue, I., Kojima, T. (2001) Highly sensitive analysis of amphetamine in human whole blood using headspace solid-phase microextraction and gas chromatography–mass spectrometry, Forensic Sci. Int. 116, 15–22.

[8] Paetsch, P.R., Baker, G.B., Caffaro, L.E., Greenshaw, A.J., Rauw, G.A., Coutts, R.T. (1992) Electron-capture gas chromatographic procedure for simultaneous determination of amphetamine and N-methylamphetamine, J. Chromatogr. 573, 313–317.

[9] Pelegrini, M., Rosati, F., Pacifici, R., Zuccaro, P., Romalo, F.S., Lopez, A. (2002) Rapid screening method for determination of ecstasy and amphetamines in urine samples using gas chromatography–chemical ionization mass spectrometry, J. Chromatogr. B 769, 243–251.
[10] Raikos, N., Christopoulou, K., Theodoridis, G., Tsoukali, H., Psaroulis, D. (2003) Determination of amphetamines in human urine by headspace solid-phase microextraction and gas chromatography, J. Chromatogr. B 789, 59–63.

RESENT GROUNDBASED METHODS FOR INVESTIGATION OF AEROSPACE AND ENVIRONMENT

J.N.Stamenov

Institute for Nuclear Research and Nuclear Energy
Bulgarian Academy of Sciences
72 Tzarigradsko chaussee Blvd., 1784 Sofia

(Plenary report)

1. INTRODUCTION

The High Mountain observatories (HMO) are the optimal sites for aerospace and environment studies because there are: no light and anthropogenic pollutions, the intensities of Ultra-violet and cosmic ray fluxes are high, the conditions for human life are extreme and the high mountain ecosystems are very sensitive and with very long recovery time. Usually the HMOs are placed at heights more than 2000 m a.s.l. Depending on aim of studies there are two basic types. The first one is using the low level of anthropogenic influences such as: Hydro-meteorological observatories (HMOs), Global atmospheric watch (GAW) and Biological observatories (BIO) and as expected Astronomical and Astrophysical (AA) observatories. The last type (AA) together with cosmic ray (CR) stations and Ultra high energy (UHE) observatories are using the phenomenon of the cascade development of the cosmic rays in the atmosphere.

The HMO covered scientific fields are: space weather forecast, cosmic ray physics, all wave lengths astronomy, physics and chemistry of the atmosphere, climatology, glaciology and seismology, mountain medicine and biology, telecommunication, remote sensing and satellite data calibration. Taking into account the main aims of the discussed investigations: space weather and terrestrial environment on can seen, that there are necessary complex measurements of the meteorological parameters, the physical and chemical characteristics of the atmosphere, the aerosol nature and dynamic and the cosmic ray behavior.

2. COSMIC RAYS

The primary cosmic rays are stable charged particles with energies in the range 10^9 – 10^{21} eV. The energy spectrum of the primary cosmic radiation (Nikolsky et al., 1984) (Fig. 1) is described with a power low function $F(>E_0) \sim E_0^{-\text{æ}}$, where æ is changing in dependence of described energy interval: $10^9 < E_0 < 10^{15}$ eV $\text{æ}_1 \approx 1,6 \div 1,7$; $3.10^{15} < E_0 < 10^{17}$eV $\text{æ}_2 = 2,0 \div 2,1$; and $E_0 > 10^{17}$ eV – $\text{æ}_3 = 1,6 \div 1,7$. The high energy cosmic rays are generated in active astrophysical objects as super nova explosions and additional accelerated in the magnetic fields of our Galaxy and Metagalaxy. The low energetic cosmic rays are mainly originated from the Sun. The magnetic fields of the Galaxy, Sun and the Earth each strongly affect the particles paths. The Sun has a strong magnetic field carried out well beyond Pluto by the solar wind and well known as Heliosphere. This field shows and tends to exclude lower-energy particles $E_0 < 1$GeV and varies on an 11 year cycle.

Reaching the upper part of the earth atmosphere the primary cosmic particles initiate nuclear and electron-proton cascades generating the secondary cosmic radiation. By low energies of the initiating particles the secondary muon and neutron fluxes and their time variations are the main information areas about the possible influence of cosmic rays on terrestrial atmosphere.

The variations of secondary cosmic rays may be responsible for the changes in the large-scale atmospheric circulation associated with solar activity phenomena (Haigh, 1996) and long term cosmic ray intensity variations (Dormann, 2006). At the same time the possibility that galactic cosmic rays (GCR) influence the Earth cloud cover (Christl et al., 2004, Usoskin et al., 2006) and then fore have an important role on inducting the Earth radioactive climate changes, has become a leading candidate for explaning the observed sun-climate connection (Jager, Usoskin, 2006).

The secondary cosmic ray neutrons are produced inside the initiated nuclear cascades in the atmosphere. Obviously the neutron production rate and energy distribution are strongly depending on the physical characteristics of the earth atmosphere mainly such as humidity and cloud density. In this connection those has to be taken into account that the space weather refers to conditions on the Sun, solar wind and the magnetosphere and ionosphere (Baker, 1998) on the Earth.

By energies of the initiating primary cosmic particle higher than 10^{13}–10^{14}eV extensive air showers (EAS) are generated in the atmosphere, which become the main information carrier for this energy range. Analyzing the behaviour of the characteristics of the main EAS components such as: electron-photon, hadron, muon and cherenkov light component and solving quite complicated inverse problems on can obtain unique information about the mass composition and energy spectrum of the primary cosmic radiation at high and ultra-high energies. Moreover, those could be studied the problems, connected with the origin of cosmic rays, as well with the processes occurring in our Universe (Nikolsky et al., 1984).

3. HYDRO-METEOROLOGICAL STATIONS (HMS)

HMS are the main supplier of the basic meteorological parameters. The resent measurements are performed with automatic devices (AWS –Automatic Weather Station f. e. VAISALA^{TM} – Finland). The time distribution of the main meteorological parameters as: air temperature, pressure, wind velocity and wind direction, humidity, precipitations, solar radiation and other are obtained and transmitted in real time (Fig.2).

The cloud formation and time development are fixed usually visual or automatically with help of video-cameras directed in four main directions: N, S, E, W and fixing the cloud shaped in 1 sec. intervals. The lightning effects are automatically registered and fixed in real time too.

Such an automation of meteorological parameter measurements gives the real possibility to study their correlations with different other atmospheric, aerosol transport and cosmic radiation parameters and process characteristics.

4. GLOBAL ATMOSPHERE WATCH (GAW) STATIONS

4.1 The GAW stations perform measurements connected with the physics and chemistry of the atmosphere. The gas concentrations measurements are usually performed with automatic gas analysers like. “Environment” f-e. The software gives usually possibilities for full remote control on each of the analyses. Normally are measured in real time the gas concentrations of: CO, CO_2, SO_2, O_3, NO, NO_2 and NO_x (fig.3).

4.2 The aerosol studies are performed with new devices of type TSI for measurements of scattering and back scattering coefficients of aerosols. The data of such high sensitivity Nephelometer with 3wave-lengths are collected in real time too.

The aerosol sampling devices with capacities 900 – 1500m^3/h combined with organic air filters with high (> 95%) efficiency are used for aerosol collection. The gamma spectrum of the filter samples is measuring with an H.P.G spectrometer towards to obtain the mass composition of the radionuclides in aerosols. The most important is the study of the ^{7}Be content in aerosols (fig. 4), what gives information about the stratospheric intrusions and contributes for better understanding of the ozone behavior in high altitudes (I. Penev et al., 2007).

The same filter samples are analyzed after the correspondent with help of AAS (Atomic Absorption Spectroscopy) towards to obtain the concentrations for heavy metals and toxic elements in aerosols having in main their important environmental and human health impact (I. Penev et al., 2007).

4.3 Radiation background measurements

The gamma radiation background measurements are carried out with active and passive detectors.

The Bulgarian National System is equipped with IGS 421 devices based on Geiger-Mueller tubes with a sensitivity range 10n – 10 Gy/h with an accuracy about 15%.

Additional measurements of the gamma-radiation background could be performed with Lulin LET spectrometer (Dachev et al., 1999). The LET spectrometer is based on a Si – semiconductor diode and the signals are digitalized and sampled as a 256 channel spectrum. On figure 5 is shown the comparison between IGS 421 device and Lulin LET spectrometer for December 2006 on peak Moussala. On one hand the differences are due essentially of different detector types and on other hand sensitivity surfaces of the calibration. The gamma radiation background could be measured with passive thermoluminiscent dosimeter of the TLE-4 type, based on $CaSO_4$: Dy detectors (Guelev et al., 1994). The dosimeter TLE-4 consists of two groups of detectors – one placed in a 2mm tin sphere and second placed in a 0.5mm polyethylene holder.

5. COSMIC RAY MEASUREMENTS

5.1. Muon telescopes

The muon telescopes are used for continuous measurements of the intensity of the muon components of the cosmic rays and its variations. Usually the detectors are placed in two parallel planes (fig. 6). The angular intervals have been determined using combinations of pairs of detectors connected to coincidence circuits. The outputs of the coincidence circuits are connected to counters, which count the number of coincidences from each detector pair.

The most famous correlation of the muon flux intensity with the atmospheric parameters is the so called barometric effect (Dorman 1975, Malamova 2001). The value measured for peak Moussala is – 0.318% / hPa with an uncertaincy ± 0.0041 / hPa using a muon telescope based on 8 water cerenkov detectors installed at BEO Moussala (Angelov et al., 2007) (fig. 7).

The muon telescopes provide the real possibility to study the interaction processes connected with Sun-Earth influences. On figure 8 is shown (Angelov et al. 2007) the Forbush decrease registrated with help of the same cerenkov muon telescope.

The telescopes with high angular precision (~1°) such as TEMP (Borog et al,2005) give the basis for estimation of continuous change of direction and velocity of the wind in the stratosphere, as well the study of dynamics of interval gravitational waves at height 10 – 30 km in the atmosphere and the temperature field there.

5.2 Neutron monitors and neutron flux meters

Because of the falling energy spectrum of the primary cosmic rays, the neutron monitors are most sensitive to the low energy (1÷20)GeV interval. As already printed out the secondary neutron production rate strongly depends on the chemical composition and humidity of the atmosphere and cloud density. Taking into account that the secondary neutron intensity is proportional to the primary cosmic ray intensity on can study their variations depending on 11 Year Sun cycle (fig.9) (Fluckiger et al., 2006). The sensitivity of the neutron flux to the atmospheric pressure so called barometric effect is well studied and similar as by muon component.

Last years are devoted to studies of the correlations between cosmic ray flux intensity and cloud cover (N. Marsh, H. Swensmark, 2000). On figure 10 are shown the changes in Earth total clouds cover for 4 cloud data sets obtained from satellite observation and cosmic ray flux intensity (solid curve).

At present time is this problem not definitively solved and serious additional investigations are needed.

Much more defined is the correlation between cosmic rays and the lightening in the atmosphere. Stozhkov Y. et al., 2000, studied the behavior of the yearly number of lightening (fig.11 – black points) and ion production rate (circles) in the air column. Quite good correlation between lightening activity end cosmic ray flux intensity on can see.

5.3 Cherenkov light telescopes

The cherenkov light in the atmosphere is generated by the fast electrons and muons in the cascades initiated by the primary cosmic ray particles.

The most of the cherenkov light telescopes are multimirror devices having quite good angular resolution about 0,1º. They permit to perform in clear cloudless and moonless nights systematical search of active astrophysical objects, which are local sources of primary gamma-quanta of ultra high energies.

One other type of cherenkov light telescopes are using the cherenkov light, reflected by the snow surface (Fig.12). Such devices give the possibility to study the enrgy spectrum of the primary cosmic radiation at energies bigger than 10^{14}eV and moreover to perform measurements of the total transparency of the atmosphere.

5.4 Astrophysical complex installations

The astrophysical complex installations are performing continuous registration of extensive air showers, initiated by primary cosmic ray particles with ultra high energies (Fig.13). They consist of big number of scintillator detectors displaced in big registration areas with surfaces of 1-100km^2 in average. The registrated events are directly connected with primary cosmic particles with ultra high energies. Nowadays the energy spectrum of such particles (Fig. 14) is the most interesting characteristic. The shape of this spectrum is directly connected with processes in our Galaxy (Rebel, 2006) and the maximal possible energy ~ 10^{20}-10^{21}eV, registrated now is an important reflection of the processes, occurring in our early Universe.

6. CONCLUSIONS

The resent groundbased methods for investigation of aerospace and terrestrial environment are connected with careful experimental studies of meteorological parameters, physical and chemical characteristics of the atmosphere and the cosmic ray flux in a very big energy interval. The biggest part of these measurements are performed in real time using automatic devices, quite elaborated computer and telecommunication techniques. Moreover continuous application of elaborated methods for data treatment is in process.

All these investigations have to clarify the existing Sun-Earth interactions and to increase our understanding of the processes in our Universe.

7. ACKNOWLEDGEMENTS

This work is partially supported by BEOBAL FP6 project (INCO-CT-2005-016663)

8. REFERENCES

[1] Angelov, I, Malamova E, Stamenov J., Muon Telescope at BEO – Moussala, 2007, http://arxiv.org/ftp/physics/papers/0702/0702242.pdf

[2] Baker D, What is space weather?, Advances in Space Research 1998; 22(1); 7-16.

[3] Borog V.V et al. Proc. 29 Int Conf Cosmic Rays, Pune, 2005.

[4] Christl M, Mangini A, Holzkämper S and Spötl C, Evidence for a link between the flux of galactic cosmic rays and Earth's climate during the past 200,000 years, Journal of Atmospheric and Solar-Terrestrial Physics 2004; 66 (3-4): 313-322.

[5] Dachev Ts, Tomov B, Matviichuk Yu,.Koleva R, Semkova J, Petrov V, Benghin V, Ivanov Yu, Shurshakov V and Lemaire J, Radiation Measurements 1999; 30; 269-274.

[6] Dimov Y., Guelev M., Hristov L., Ivanov P., Mishev A., Nishev A., Stamenov J. and Vachev B., Gamma background and neutron flux measurements at Basic Ecological Observatory Moussala, arXiv : physics/0409063, 2004.

[7] Dorman, L.I., Variations of Galactic Cosmic Rays, Moscow University Publishing House, 1975.

[8] Dorman L, Long-term cosmic ray intensity variation and part of global climate change, controlled by solar activity through cosmic rays, Advances in Space Research 2006; 37(8): 1621-1628.

[9] Flückiger E, Buetikofer R, Moser M, Desorgher L., The Extreme Solar Cosmic Ray Particle Event on January 20, 2005, Research at Jungfraujoch “Top of Science”, 75th anniversary High Altitude Research Station Jungfraujoch International conference, Interlaken, Switzerland, September 11-13, 2006.

[10] Haigh J, The impact of solar variability on climate, Science1996; 272: 981.

de Jager C and Usoskin I, On possible drivers of Sun-induced climate changes, Journal of Atmospheric and Solar-Terrestrial Physics 2006; 68(18): 2053-2060.

[11] Malamova E, Angelov I, Kalapov I, Davidkov K. and Stamenov J, Muon cerenkov telescope, 2001

[12] hppt://www.copernicus.org/icrc/papers/ici6585_p.pdf

[13]Marsh N, Svensmark H, Cosmic Rays, Clouds and Climate, Space Sci Rev 2000; 00: 1 – 16.

[14] Nikolski S.I., J. Stamenov, S. Ushev J Experimental Theoretical Physics 1984; 87: 1/7/18.

[15] Penev I, Drenska M, Damyanov B, Valova Tsc., Monitoring of aerosols radioactivity at BEO Moussala, In: Stamenov J, Vachev B., editors, Observatoire de montagne de Moussala OM2, INRNE, Sofia, 2007; vol. 12, in press.

[16] Rebel H Overview talk. Very High Energy Cosmic Rays, In: Proc of 25th Int. School of nuclear theory, Gulechitza, Bulgaria, INRNE, 2006.

[17] Stozhkov Y. et al, Space Science Reviews, 2000

[18] Usoskin I, Voiculescu M, Kovaltsov G.A and Mursula K, Correlation between clouds at different altitudes and solar activity: Fact or Artifact?, Journal of Atmospheric and Solar-Terrestrial Physics 2006, 68(18): 2164-2172.

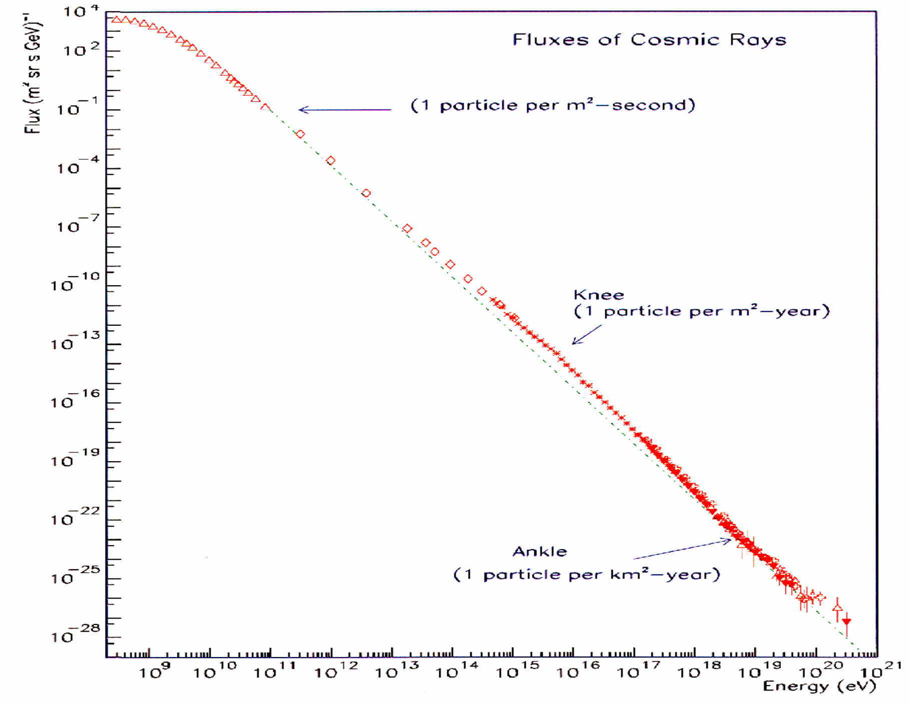

fig.1 Energy spectrum of the primary cosmic radiation

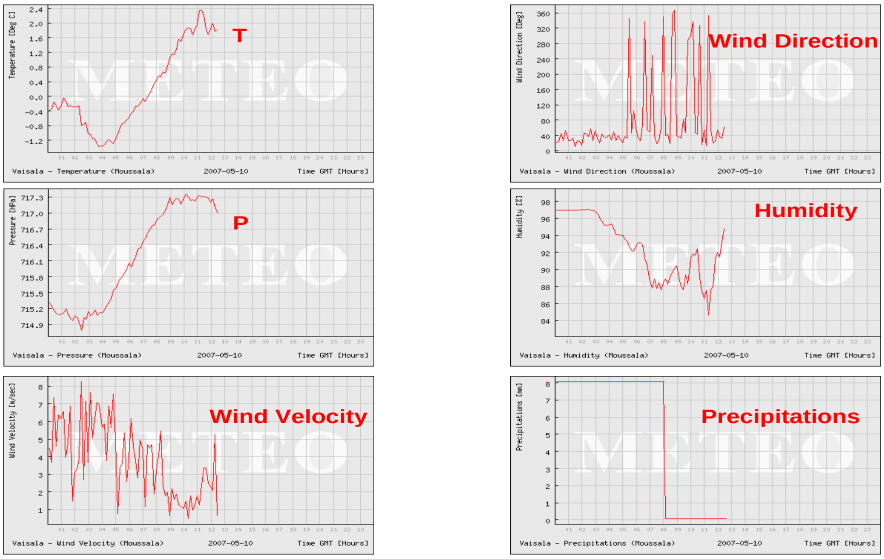

Fig.2 Climatic data

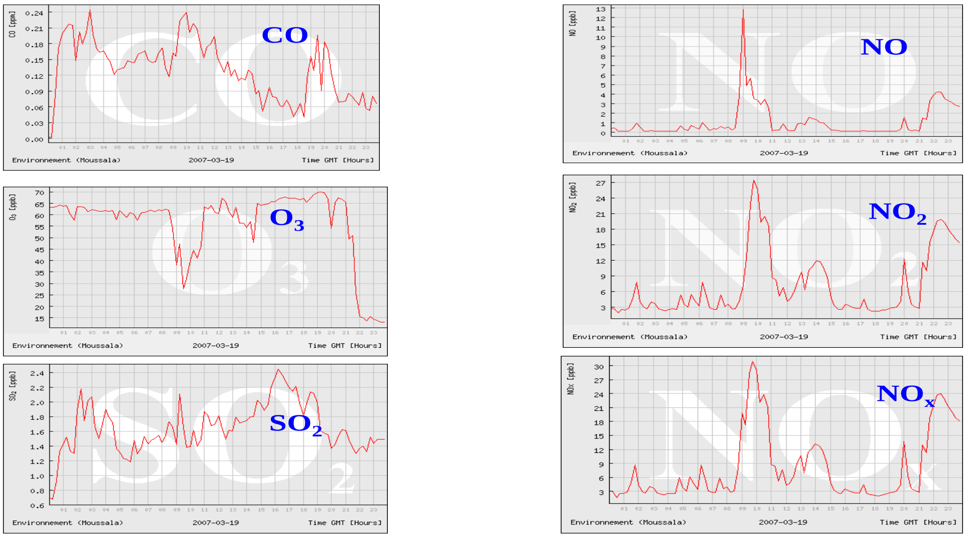

fig.3 Gas concentrations

7Be activity on the Moussala, mBq/m³

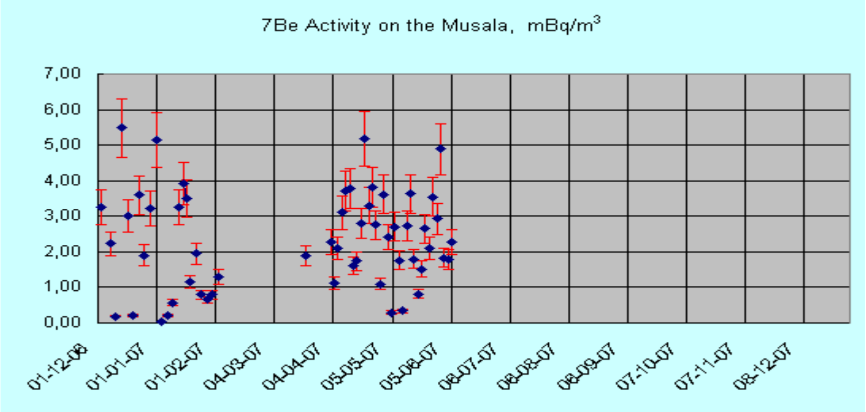

fig.4 7Be activity on the Moussala

A comparison between the measured daily average of gamma background for December 2006 with IGS 421 gamma probe and Liulin - 6MB

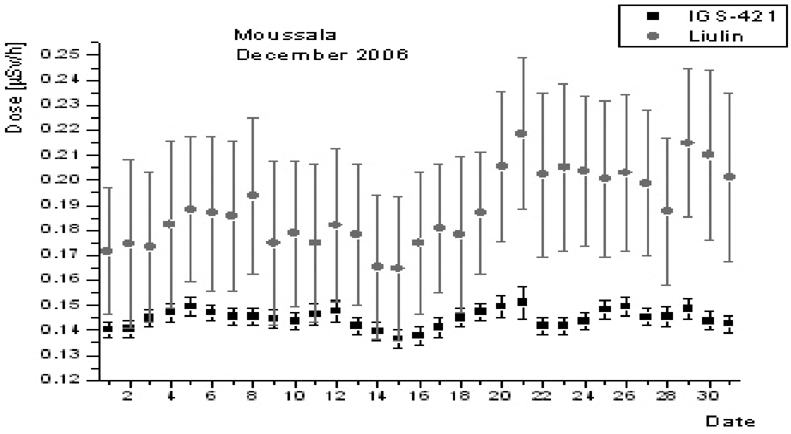

Fig. 5

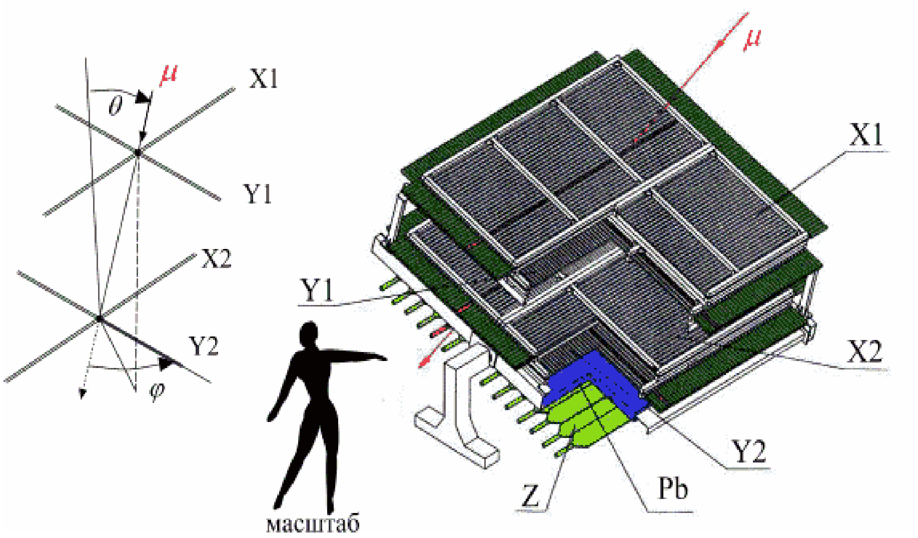

fig.6 Detectors location

Muon barometric effect

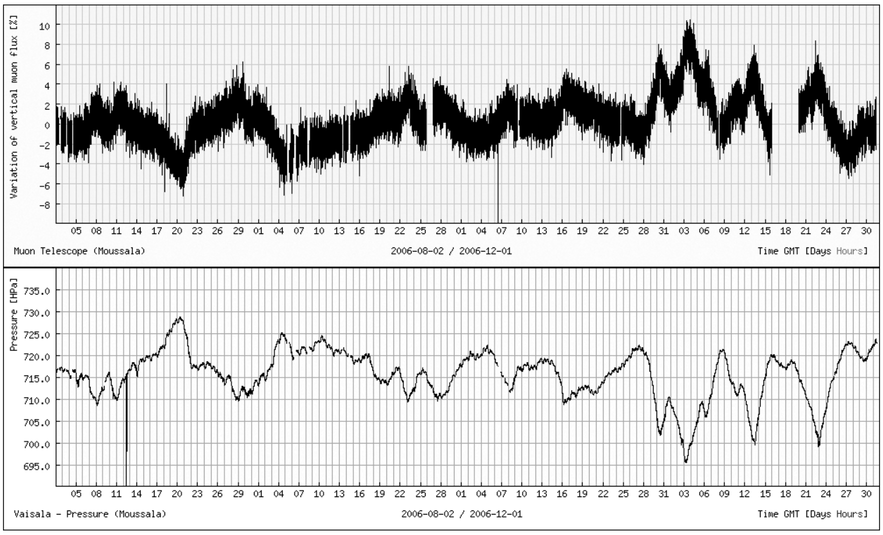

Fig. 7 Muon barometric effect

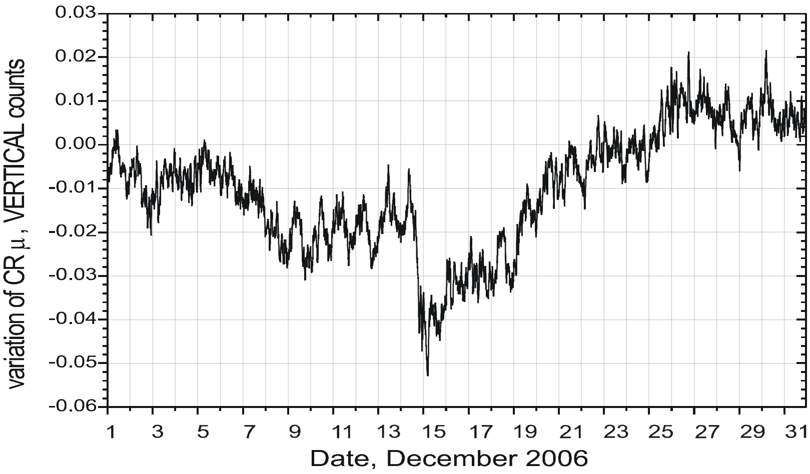

fig.8 Forbush decrease

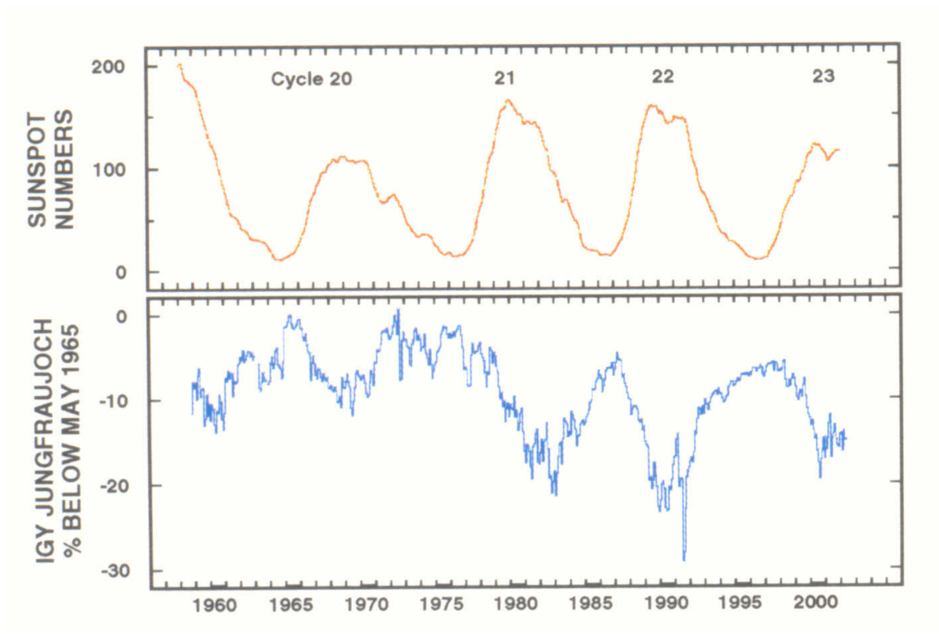

fig.9 11 Year Sun cycle

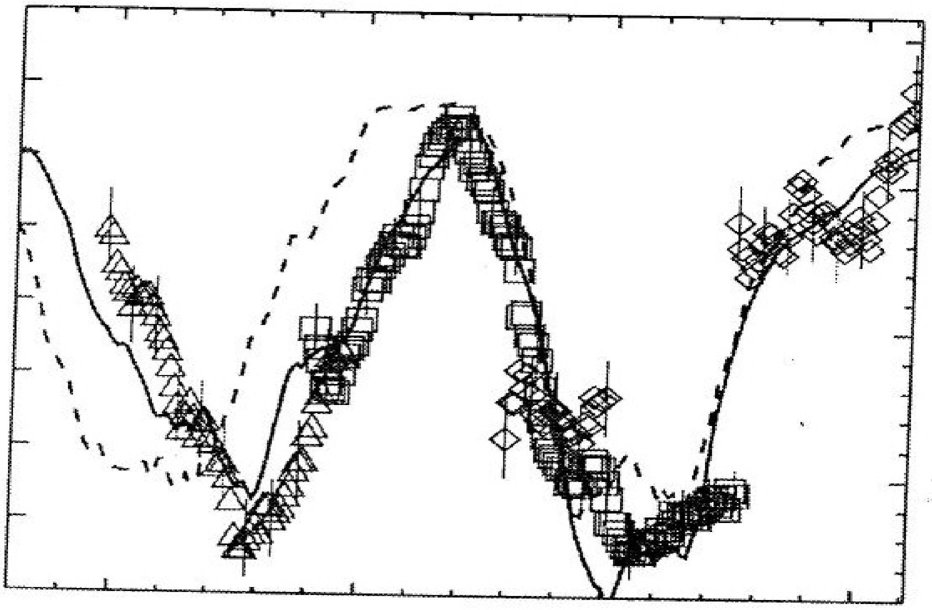

fig.10 Earth total clouds cover

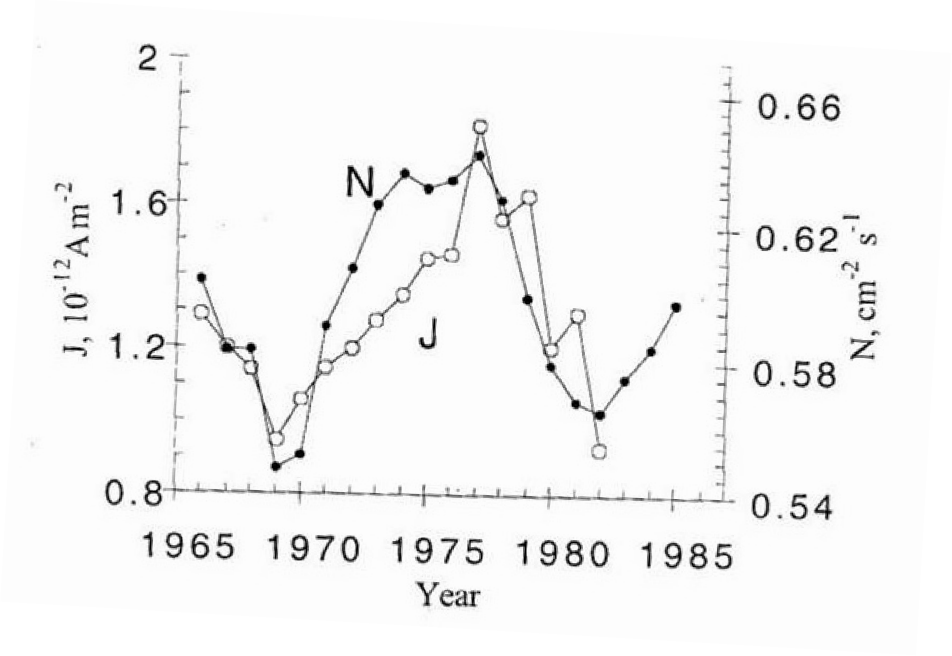

fig.11 Lightening in the atmosphere

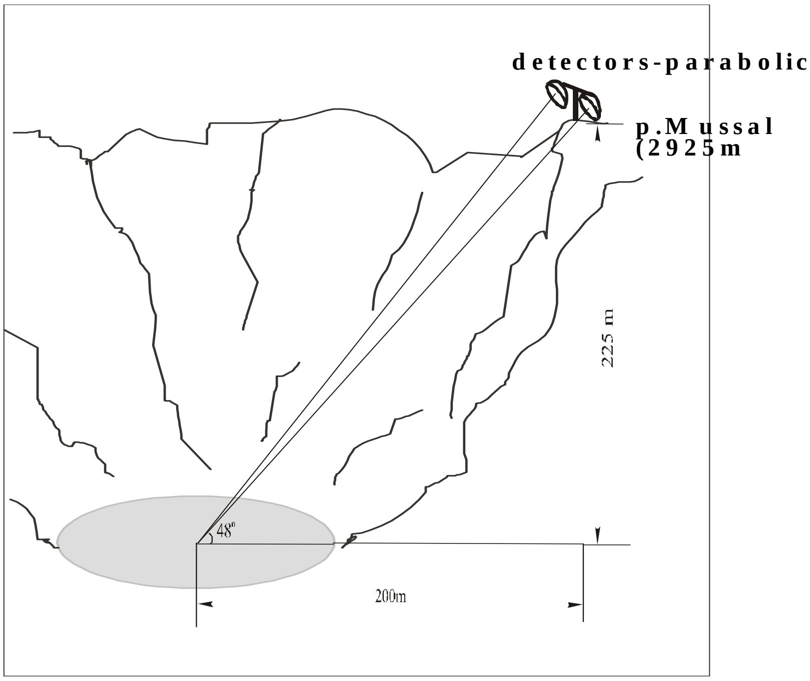

fig.12 Cherenkov light, reflected by the snow surface

fig.13 Astrophysical complex installations

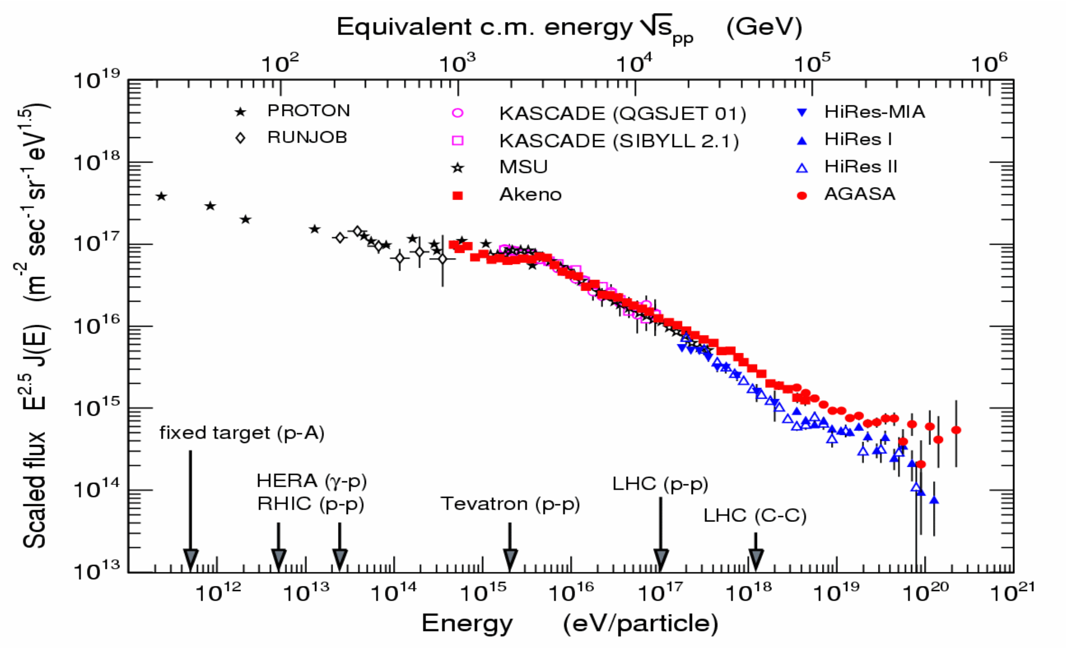

fig.14 Cosmic particles with ultra high energies - energy spectrum

NON-WAVE FEATURES OF RELATIVISTIC MAGNETOACTIVE PLASMA

Ilia Giudjenov, Marek Tassev

South-West University ‘Neofit Rilski’, Blagoevgrad, Bulgaria

Sergey Kirpichev, Peter Polyakov, Alexander Rusakov, Natalia Rusakova

Moscow State University, Moscow, Russia

Abstract: *An initial Landau problem for propagation of an electromagnetic disturbance in relativistic magnetoactive plasma is investigated. A non-wave behavior is shown to arise at high temperatures. The influence of the non-wave contribution in a plasma response is estimated. The results indicate that the non-wave properties can play a significant part at sufficiently high temperatures, especially ultrarelativistic, and may even exceed a classical wave contribution.*

Keywords: *Initial problem, Relativistic plasma, Landau contour, Non-wave contribution, Vlasov equation.*

1. INTRODUCTION

It is well known that zeros of the dispersion equations for eigenwaves completely determine an electromagnetic response of a non-relativistic plasma medium; i. e. the structure of an electromagnetic field disturbance is an eigenwave composition [1]. However, an eigenwave spectrum is not sufficient to describe an electromagnetic plasma response in a relativistically correct statement of the Landau problem on an evolution of an initial disturbance. An additional non-wave contribution appears that exceeds the traditional wave disturbance at certain conditions [2].

Here, a non-wave response in magnetoactive plasma is analyzed. Unlike [2], the contribution of essentially singular points $\omega = \pm\omega_H$ (instead of $\omega = \pm kc$) determines the value of the non-wave disturbance in presence of an external magnetic field.

2. PROBLEM STATEMENT

Let us consider an infinite spatially homogeneous plasma in a sufficiently strong external magnetic field H_0. In this case, the electron velocity distribution function is anisotropic: the thermal straggling of particle velocities across the field becomes much less than the thermal straggling along the field [4]. Thus we describe an evolution of the plasma medium across the field on the basis of cold hydrodynamics, and along the field on the basis of the kinetic Vlasov theory [5, 6]. We will analyze its vibration properties of a such plasma medium starting from the relativistic kinetic Vlasov equation:

$$\frac{u^i}{u_0}\frac{\partial f_a}{\partial x^i} + \frac{1}{m_a c^2}\frac{\partial}{\partial u^\alpha}\left(\frac{e_a}{c}F^{\alpha i}u_i\frac{f_a}{u_0}\right) = 0\,, \tag{1}$$

where $F^{\alpha i}$ is an electromagnetic field tensor with components $\vec{E}$ and $\vec{H}$ which are determined by Maxwell's equations:

(2) $$\operatorname{rot}\vec{E} = -\frac{1}{c}\frac{\partial \vec{H}}{\partial t}, \ \operatorname{div}\vec{H} = 0,$$

(3) $$\operatorname{rot}\vec{H} = -\frac{1}{c}\frac{\partial \vec{E}}{\partial t} + \frac{4\pi}{c}\vec{J}, \ \operatorname{div}\vec{E} = 4\pi\rho,$$

(4) $$\rho = \sum_a e_a n_a \int f_a \frac{d^3u}{u_0}, \ \vec{J} = \sum_a e_a n_a \int \vec{u} f_a \frac{d^3u}{u_0}.$$

Below we consider movement of electrons only since the ion component plays little part in relativistic plasma evolution, thus the "a" index will be omitted.

3. CALCULATION OF THE NON-WAVE CONTRIBUTION

After standard procedures of linearization, Fourier transformation of coordinates and Laplace transformation of time for the system of equations (1)–(4), we obtain the following system of linear equations for Fourier-Laplace images of the electric field strength:

(5) $$\left(k^2\delta_{ij} - k_i k_j - k_0^2\varepsilon_{ij}\right)E_j(k,\omega) = i\omega D_i\left(t=0,\vec{k}\right) + i\left[\vec{k}\times\vec{B}\left(t=0,\vec{k}\right)\right]_i .$$

where $D_i\left(t=0,\vec{k}\right)$ and $\vec{B}\left(t=0,\vec{k}\right)$ are the initial disturbances of electric and magnetic fields.

For simplicity, we assume $D_i\left(t=0,\vec{k}\right)=0$ below and let $A_i = i\left[\vec{k}\times\vec{B}\left(t=0,\vec{k}\right)\right]_i$. Solving the system with Cramer formulas and conducting a reverse Laplace transformation yields

(6) $$E_i = \frac{1}{2\pi}\int_{i\sigma-\infty}^{i\sigma+\infty}\Lambda_{ij}^{-1}A_j e^{-i\omega t}\,d\omega,$$

where $\Lambda_{ij} = k^2\delta_{ij} - k_i k_j - k_0{}^2\varepsilon_{ij}$.

In this paper, we limit us considering disturbances, which propagate perpendicularly to the external magnetic field, that corresponds to $\vec{k} = \{k,0,0\}$. In this case, E_x and E_y depend on the following components of the permittivity tensor:

(7) $$\varepsilon_{xx} = 1 - \frac{1}{K_1(\alpha)\beta^2x^2}\left(K_0(\alpha) - \frac{J_\alpha(x) - J_\alpha(-x)}{2x}\right),$$

(8) $$\varepsilon_{xy} = -\frac{i}{K_1(\alpha)\beta^2x^2}\frac{J_\alpha(x) + J_\alpha(-x)}{2x},$$

$$J_\alpha(x) = \int_1^\infty \frac{e^{-\alpha t}}{\left(t + x^{-1}\right)\sqrt{t^2-1}}\,dt\,, \tag{9}$$

$$\alpha = m/\Theta\,,\ x = \omega/\omega_H\,,\ \beta = \omega_H/\omega_p\,. \tag{10}$$

At relativistic temperatures, the region of hybrid resonance narrows and the hybrid frequency tends to the cyclotron one [4]. Since tensor components $\varepsilon_{\alpha\beta}$ contain function $J_\alpha(x)$ that has an essentially singular point $x = -1$, considering the vicinity of cyclotron and hybrid frequencies is of interest.

A short-wave limit corresponds to the hybrid resonance region where the component $E_x(\omega) = -\frac{A_x}{\omega^2\varepsilon_{xx}}$ dominates. After shifting the integration contour in (6) below, we isolate two parts: the wave one that is determined by the polar singularities at the relativistic hybrid frequency $\pm\omega_*$:

$$E_W = -\frac{2}{\omega_*^2}\sin\omega_* t \bigg/ \left(\frac{\partial\varepsilon_{xx}(\omega_*)}{\partial\omega}\right), \tag{11}$$

and the non-wave one that is an integral along the contour C (fig. 1).

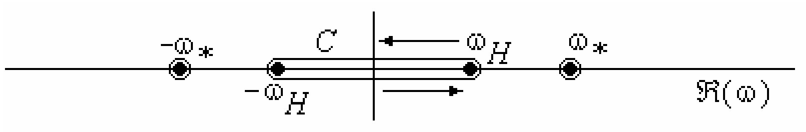

Fig. 1: The integration contour around the branch-cut between the essentially singular points.

We present the $J_\alpha(x)$ function on the cut banks in the following form by applying Sokhotsky’s formula:

$$J_\alpha(-x \pm i0) = V.p.\int_1^\infty \frac{e^{-\alpha t}}{\left(t - x^{-1}\right)\sqrt{t^2-1}}\,dt \pm \frac{i\pi x e^{-\alpha/x}}{\sqrt{1-x^2}}\,, \tag{12}$$

In an ultrarelativistic limit, the contour integral can be approximated with the saddle-point technique that yields at $\alpha << 1/\left(20\beta^2\right)$ the following expression for the non-wave contribution:

$$E_C = \frac{\sin\left(\omega_H x_0 t\right)}{\sqrt{\pi\omega_H x_0}}\exp\left(-\frac{t^2}{\sigma^2}\right), \tag{13}$$

$$x_0(\alpha,\beta) = \sqrt{-\frac{\alpha W\left(-1,-2\alpha\beta^2\exp(2\gamma)\right)}{2\beta^2}} \sim \frac{\sqrt{\alpha\ln\left(\alpha\beta^2\right)}}{\beta}\,, \tag{14}$$

(15)
$$\sigma = \frac{8\beta^2 x_0}{\pi\alpha\omega_H},$$

where $W(n,x)$ is an n-th branch of Lambert function (the solution of equation $We^W = x$) and γ is the Euler-Mascheroni constant. The wave part in the vicinity of the hybrid resonance equals to

(16)
$$E_W = -\frac{\pi^2\alpha^2 \sin(\omega_H t)}{2\beta^4\omega_H}.$$

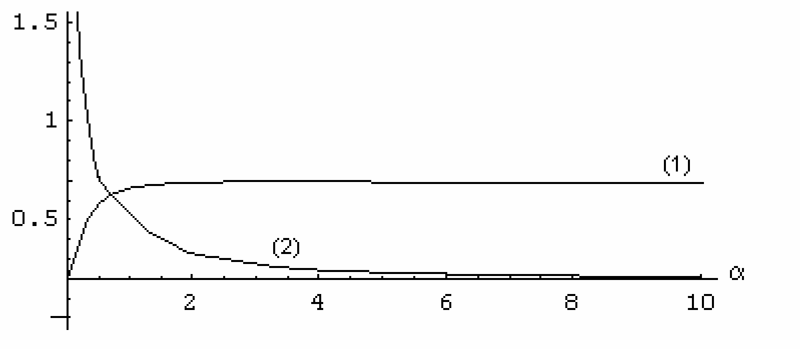

Fig. 2: Amplitudes of the wave (1) and the non-wave (2) parts depending on the temperature factor $\alpha = m/\Theta$.

Numerical calculations show (fig. 2) that the non-wave disturbance is comparable to E_W at $\alpha \sim 1$ and significantly exceeds it in an ultrarelativistic limit.

The non-wave disturbance damps with time also, like the wave one, but the damping law is different (see (14)) and $\sigma \propto \sqrt{\ln(\alpha)/\alpha} \to \infty$ at small α.

4. CONCLUSIONS

The provided investigations show that an analysis of a resonant response of magnetoactive plasma is incorrect at high temperatures without taking into account the non-wave contribution, which dominates in an ultrarelativistic limit. Thus a linear response of a relativistic plasma medium significantly differs from the one of non-relativistic plasma.

5. REFERENCES

[1] Krall, N., Trivelpiece, A. W. (1973) *Principles of Plasma Physics*, New York, McGraw-Hill.

[2] Silin, V. P., Ursov V. N. (1982) Ob okonchanii spectra lengmurovskikh voln ultrarelativistskoi plasmy, *Kratkiye soobscheniya po fizike FIAN (Bulletin of the Lebedev Physics Institute)*, No. 12, 53–59 [in Russian].

[3] Polyakov, P. A. and Tassev, M. A. (1986) Relativistichna kinetichna teoriya na klassicheskite zaredeni chatitsy, Blagoevgrad, NRB [in Bulgarian].

[4] Boltasova, Yu. V., Polyakov, P. A., and Rusakov, A. E. (2001) Relativistskoye vyrozhdeniye gibridnogo resonansa magnitoaktivnoi plasmy, *Izvestiya RAN. Ser. fizicheskaya (Bulletin of the Russian Academy of Sciences (Physics))*, 65(12), 1723-1725 [in Russian].

[5] Kim, N. E., Polyakov, P. A., Tassev, M. A. (2005) Some Features of Wave Propagation in Relativistic Plasma, *Mathematics and Natural Sciences (Proc. of the Int. Sci. Conf. 8-11.06.2005)*, Blagoevgrad, SWU “Neofit Rilsky”.

[6] Polyakov, P. A. (1983) Novyi vid kolebanii v relativistskoi plasme, *ZhETF (Journal of Experimental and Theoretical Physics)*, 85, 5 (11), 1585-1589 [in Russian].

STUDIES OF RELATIVISTIC ^{8}B NUCLEI IN PERIPHERAL INTERACTIONS WITH PHOTOEMULSION NUCLEI.

R. Zh. Stanoeva[1,2], J. N. Stamenov[1], P. I. Zarubin[2]

[1]*Institute for Nuclear Research and Nuclear Energy, Sofia, Bulgaria*
[2]*Joint Institute for Nuclear Research, Dubna, Russia*

The results of investigations dealing with the charge topology of the fragments produced in peripheral dissociation of relativistic 8B nuclei in emulsion are presented. 52 events of peripheral dissociation of the 8B nucleus were selected from the events which do not involve the production of the target-nucleus fragments and produced mesons (“white” stars). A leading contribution of the 8B→7Be+p decay mode having the lowest energy threshold was revealed on the basis of those events. Information on the relative probability of dissociation modes with a larger multiplicity was obtained. The dissociation of a 7Be core in 8B indicates an analogy with that of the free 7Be nucleus.

1. INTRODUCTION

This article reports on an investigation of ^{8}B interactions with photo-emulsion nuclei. In the investigation of the multifragmentation at relativistic energies, the possibilities of observing the final states consisting of charged fragments are defined by the accuracy of angular measurements. Owing to the best spatial resolution (0.5 μm), the nuclear emulsion ensures the angular resolution of the tracks of relativistic fragments of about 10^{-4} rad. This enables one to observe completely all the possible decays of nuclear excited states to fragments. That all charged secondaries can be recorded and identified permits studying the isotopic composition of fragments and projectile-fragmentation channels. Events in which the sum of the fragment mass numbers is equal to the projectile mass number form a special class. In these events, we record all secondaries and can determine both the transverse-momentum transfer to the nucleus and the fragment transverse momenta in the reference frame commoving with the nucleus undergoing fragmentation. If, in this case, the projectile charge is conserved, the dissociation channels are recorded, but, if the total fragment charge changes in relation to the initial value of the nuclear charge, we can single out charge-exchange transitions experienced by the projectile nucleus.

2. EXPERIMENT

A stack of layers of BR emulsion of a relativistic sensitivity was exposed to a beam of ^{8}B nuclei accelerated to a momentum of 2.0 A GeV/c at the Nuclotron of the Laboratory of High Energy Physics (JINR). The layer thickness and dimensions were 550 μm and 10x20 cm^2, respectively. The exposed beam was pointed parallel to the emulsion plane along its long side. Events were sought by viewing over the track length which provided the accumulation of statistics without selection. This made it possible to determine the mean free path of ^{8}B interactions in emulsion. In the events being investigated, we measured the polar and azimuthal emission angles for all charged particles.The standard BR-2 emulsion was used in which singly and doubly charged relativistic particles were well identified by sight, because a single ionization of relativistic single-charged particles is reliably discriminated from a four-fold ionization of particles with charge 2. Fragments with Z=3,...,6 were separated by counting δ electrons.

The results of the determination of the charges $Z_{primary}$=3-6 by this method are given in figure 1, which illustrates its high reliability.

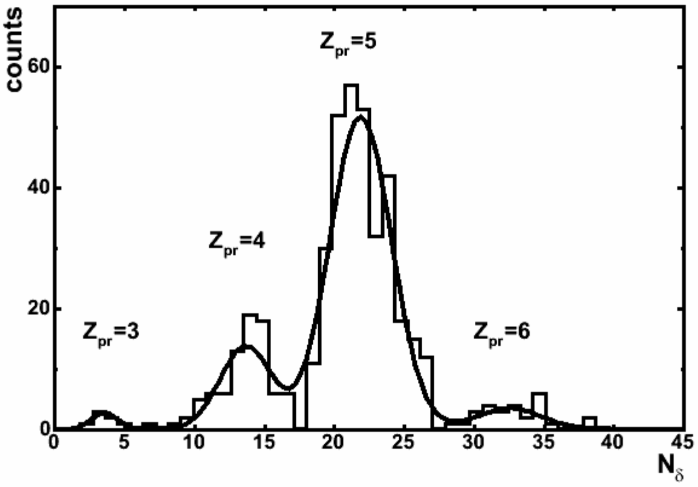

Fig. 1: Distribution of number of δ electrons per 1 mm length on the tracks of relativistic primaries with charges Z_{pr}=3, 4, 5, and 6 (about 440 events). The continuous line is the sum of four Gauss distributions.

The emission angles for $Z_{fr}>2$ are restricted in interval $\theta<3^\circ$, and the ones for doubly charged fragments to an interval $<8^\circ$. The angles for singly charged particles were measured in an interval $<15^\circ$. Basing on the momentum measurements, the angular distribution shape and the estimation of the projectile fragmentation angle by the equation

(1) $$\sin \theta_{fr} = 0.2/p_0 = 0.1 \rightarrow \theta_{fr} = 5.7^\circ$$

a limiting angle for singly charged fragments was chosen to be $\theta=8^\circ$.

3. THE MEAN FREE PATH FOR INELASTIC ^{8}B INTERACTIONS IN EMULSION

On the viewed track length of 143,7 m we found 1102 events. Thus the mean free path of interactions in emulsion is λ =(13.0 ± 0.4) cm. Table 1 gives the result obtained for the ^{8}B nucleus and the values of the mean free path of inelastic interactions of ^{6}Li, ^{7}Li, ^{7}Be, ^{10}B and ^{11}B in emulsion. The measured values for all these nuclei are within the errors nearly identical. The table gives also the values calculated by the Bradt-Peters equation [6].

Tab. 1: Mean free paths of ^{6}Li, ^{7}Li, ^{7}Be, ^{8}B, ^{10}B and ^{11}B nuclei for inelastic interactions in emulsion.

Nucleus	λ_{exp}, cm	λ_{calc}, cm	P_0, A GeV/c	Paper
^{6}Li	14.1±0.4	16.5	4.5	[1]
^{7}Li	14.3±0.4	15.9	3.0	[2]
^{7}Be	14.0±0.8	-	2.0	[5]
^{8}B	13.0±0.4	15.5-15.7	2.0	present paper
^{10}B	14.4±0.5	-	1.9	[4]
^{11}B	13.2±0.6	-	2.75	[3]

The fact that the experimental values of the mean free path for all these nuclei are smaller than the calculated ones is accounted for by an additional contribution from peripheral inelastic interactions of nuclei having a loosely bound cluster structure.

4. RESULTS

Of 1102 interactions found, we selected events in which the total fragment charge was equal to the Z_0=5 fragment charge and there were no produced particles. The selected events are divided in two classes. The events of the type of “white”star (52 events) and the interactions involving the production of one or a few target-nucleus fragments (124 events) belong to the first class. The name “white” is a conventional one that refers to the interactions in which there are neither target fragments nor produced particles. They are produced in case when the energy transferred to a fragmenting nucleus is minimal which leads to a distraction of inter-cluster bounds but, as a rule, the bounds inside the clusters remain unaffected. This is the reason for which they are of special interest for the study of the cluster structure of nuclei. The other class of events, we are interested in, reveals a simultaneous breakup of both interacting nuclei which results in the production of target-nucleus fragments.

Table 2 shows the charge multifragmentation topology which was studied for the events satisfying the above-mentioned conditions. The upper line is the Z>2 fragment charge, the second line is the number of single-charged fragments , the third one the number of twocharged fragments, and the fourth and fifth lines are the number of the detected events with a given topology for “white”stars and events with target-nucleus excitation for each channel, respectively. The last line present the total number of interactions calculated in absolute values.

Tab. 2: The charge topology distribution of the “white”stars and the interactions involving the target-nucleus fragment production in the ^{8}B dissociation at 2.0 A GeV/c momentum.

$Z_{fr.}$	5	4	3	3	—	—	—
$N_{z=1}$	—	1	—	2	5	3	1
$N_{z=2}$	—	—	1	—	—	1	2
$N_{w.s.}$	1	25	—	—	—	12	14
$N_{t.f.}$	13	16	2	5	2	42	44
N_{Σ}	14	41	2	5	2	54	58

The data of table 2 points to the predominance of the channel with the 4+1 charge configuration which has been studied in more detail. The mean free path for this channel $\lambda_{7Be+H}(^8B)$=3.5±0.55 m. Its fraction sharply increases when selecting ”white" stars: from 13% for the case of the presence of target fragments up to 48% for “white" stars. The threshold of this mode is the lowest one which is seen from the fact that it dominates the most peripheral events.

The presence of the “white” stars with more than two $N_Z>2$ fragments may be explained by the ^{7}Be core dissociation. In order to verify this suggestion, table 3 gives the relativistic fragment charge distribution in the “white” stars for ^{7}Be [5] and ^{8}B nuclei. The ^{8}B events are presented without one single-charged relativistic fragment, that is a supposed proton halo. The identical fraction of the two main 2He and He+2H dissociation channels is observed for ^{7}Be and ^{8}B nuclei which points out that the ^{7}Be core excitation is independent of the presence of an additional loosely bound proton in the ^{8}B nucleus.

Tab. 3: The charged dissociation mode distribution of the “white” stars produced by the ^{7}Be and ^{8}B nuclei.

Z	^{7}Be	%	^{8}B (+H)	%
2He	41	49.4	14	54
He+2H	42	50.6	12	46

The “white” stars of $^8B \to {}^7Be+p$ give a pair of observed tracks with a small angular deviation with respect to the primary nucleus track. Measurements gave the mean values of the polar emission angles $<\theta_p>\approx 2.0^\circ$ for protons and $<\theta_{Be}>\approx 0.4^\circ$ for ^{7}Be nuclei.

The angular measurements permit one to reconstruct with a good accuracy the spectra of transverse momenta P_T by the equation $P_T=AP_0\sin\theta$, where A is the mass number of a fragment, θ its emission angle and P_0 the momentum per ^{8}B nucleon (P_0=2.0 A GeV/c). The mean values of the transverse momenta in lab.s. $<P_T>$=65.5 MeV/c for protons and $<P_T>$=96.8 MeV/c for ^{7}Be nuclei. Figure 2 gives the distribution along the total transverse momentum $P_T(^8B)$ which was acquired by the ^{8}B nuclei in the formation of stars ^{7}Be+p; its mean value is about 100 MeV/c. The distribution peak is located at the $P_T(^8B)$ value of about 50 MeV/c. This asymmetry of the $P_T(^8B)$ distribution may be associated both with the emission of neutrons by the target-nuclei and the contribution from the core excitation process $^8B \to {}^7Be^*+p \to {}^7Be+\gamma+p$ [8].

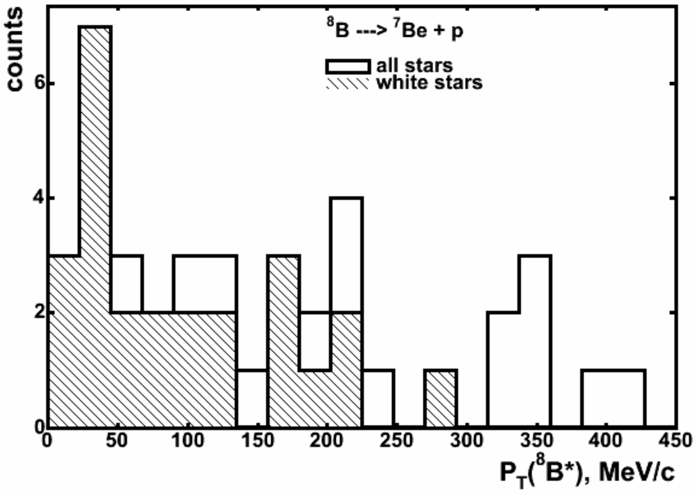

Fig. 2: The P_T (^{8}B) total transverse momentum distribution of ^{7}Be+p pairs produced in peripheral interactions $^8B \to {}^7Be+p$.

It is possible to estimate the role of the correlations by the azimuthal angle ε_{pBe} between ^{7}Be and p ($\varepsilon_{pBe} = \arccos(\mathbf{P_{Tp}P_{TBe}} / P_{Tp}P_{TBe})$). The azimuthal asymmetry A defined as

(2) $$A = (N_{\varepsilon ij \geq \pi/2} - N_{\varepsilon ij \leq \pi/2})/N_{0 \leq \varepsilon ij \leq \pi}.$$

This distribution has an asymmetry with respect to the angle π/2 A=0.52, which points to a noticeable contribution of pairing dissociations.

5. CONCLUSIONS

In conclusion we summarize the main results of the present paper. We give the results of the study of the dissociation of ^{8}B nuclei of a primary momentum of 2.0 GeV/c per nucleon in their interactions with the emulsion nuclei. The mean free path for inelastic ^{8}B interactions in emulsion $\lambda(^{8}\mathrm{B})=13.0\pm0.4$ coincides within the errors with those for inelastic ^{6}Li, ^{7}Li, ^{7}Be, ^{10}B and ^{11}B interactions. The charge topology distribution indicates the leading role of the 4+1 charge configuration channel. Its fraction sharply increases when selecting ”white" stars: from 13% for the case of the presence of target fragments up to 48% for “white" stars. We have obtained a strong azimuthal angle correlation between ^{7}Be and p.

6. REFERENCES

[1] Adamovich, M., et al. (1999), Phys. At. Nucl., 62, 1378-1387.
[2] Adamovich, M., et al. (2004), J. Phys. G: Nucl. Part. Phys., 30, 1479-1485.
[3] Artemenkov, D., et al. (2006), nucl-ex/0610023
[4] Adamovich, M.,et al. (2004), Phys. At. Nucl. 67, 514-517.
[5] Peresadko, N., et al. (2007), Phys. Atom. Nucl. in print, nucl-ex/0605014
[6] Bradt, H., Peters, B. (1950), Phys.Rev., 77, 54-70.
[7] Stanoeva, R., et al. (2007), Phys. Atom. Nucl. in print; nucl-ex/0605013.
[8] Meister, M., et al. (2003), Nucl. Phys. A718, 431-433.

GROWTH, OPTICAL AND DIELECTRIC PROPERTIES OF COMPLEX PEROVSKITE-TYPE $Pb_{0.92}Ba_{0.08}Sc_{0.053}Nb_{0.47}O_3$ SINGLE CRYSTALS

Dimitrina Petrova, Darina Kaisheva

South West University "Neophyt Rilsky", Blagoevgrad, Bulgaria

Vera Marinova

Central Laboratory of Optical Storage and Processing of Information, Bulgarian Academy of Sciences, Sofia, Bulgaria

***Abstract**: Pb0.92Ba0.08Sc0.53Nb0.47O3 (PBSN) single crystals were grown by the High Temperature Solution Growth (HTSG) method using a flux solution with composition of PbO: PbF2: B2O3 = 0.78: 0.20: 0.2. The growing process was performed in platinum crucibles in the temperature range 1475 -1193 K with cooling velocity of 1 deg/h. The addition of Ba shifts the optical absorption edge to lower energies in comparison with non-doped PSN and gives rise to extra absorption peaks at 457 nm and 710 nm. The frequency dependence of the dielectric constant was measured in temperature range from 220 K to 380 K. The dielectric permittivity maximum is shifted to lower temperatures and the dielectric constant values are reduced by Ba-addition in comparison with non-doped PSN.*

***Keywords:** relaxor ferroelectrics, optical properties, dielectric properties, crystal doping.*

1. INTRODUCTION

Relaxors are special class of ferroelectric materials with interesting properties: high dielectric permittivity; broad, diffuse phase transition; strong frequency dependence of dielectric constant as function of temperature; weak remnant (zero-field) polarization; large electrostrictive coefficient; large electrooptic coefficient. In view of these characteristics this materials are attractive for capacitors [1], important for actuators [2] and useful for information storage [3] and optical modulators [4].

Pb-based perovskites with general formula $PbB'_{1/2}B''_{1/2}O_3$ (B'-Sc, B''-Nb) attract special attention due to the possibility to control the degree of B-site chemical order and thus to modify the properties as well as to study the nature of relaxors. Stable relaxor state is able to reach in several ways - varying the degree of the B-site cation ordering by annealing or during the crystal growth; additional Pb vacancies in disordered PSN crystal lattice; partially substitution of Pb^{2+} ions with Ba^{2+} ions. Advantage of the last method is easier control of Ba distribution [5].

2. EXPERIMENT

$Pb_{0.92}Ba_{0.08}Sc_{0.053}Nb_{0.47}O_3$ (PSN:Ba) single crystals were grown by the High Temperature Solution Growth (HTSG) method using a flux solution with composition PbO : PbF_2: B_2O_3 = 0.78 : 0.20 : 0.2. The growing process is performed in platinum crucibles in temperature range 1475 -1193 K with cooling velocity of 1 deg/h. The obtained crystals are cubic-shaped with approximately 1 cm^3 of size.

Optical transmittance is measured with spectrophotometer in wave range of 300 nm to 2550 nm.

Dielectric measurements were made with flat-parallel plates with deposited silver electrodes on their opposite sides. Platinum fibers were attached to the electrodes. The thickness of the sample was 1 mm. Hewlett-Packard 4275A RLC bridge was using for dielectric measurements, over temperature range from 220 to 380 K at 10 kHz, 100 kHz and 1 MHz frequencies.

3. RESULS AND DISCUSSIONS

Fig.1 presents the optical transmittance of PSN:Ba and PSN crystals. The transmittance in range of 550-1200 nm wavelength of Ba-doped PSN crystals decrease about two times in comparison with non-doped PSN crystals. Transmittance value is 10% for 800 nm. After 1200 nm the transmittance of Ba-doped PSN crystals is bigger then non-doped PSN as in the end of investigated wave range it reaches to 60%.

The temperature dependence of the dielectric constant of PSN:Ba crystals at investigated frequencies (Fig. 2) shows removing of phase transition to higher temperatures at higher waves – 260 K, 270 K and 278 K at frequencies of 10 kHz, 100 kHz and 1 MHz respectively. The maximal value of the dielectric constant decreases with the increasing of the frequency and it is 800, 775 and 750 at frequencies of 10 kHz, 100 kHz and 1 MHz respectively. The maximum of dielectric constant is removed to lower temperatures and it is decreases about five times in comparison with non-doped PSN crystals.

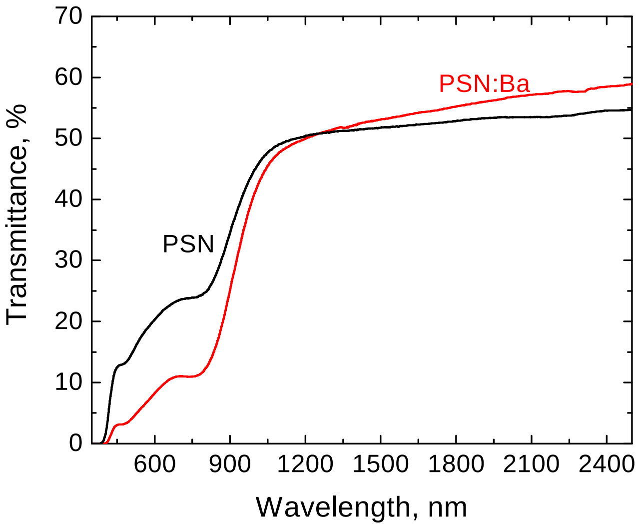

Fig. 1: Optical transmittance spectra of PSN:Ba and non-doped PSN crystals.

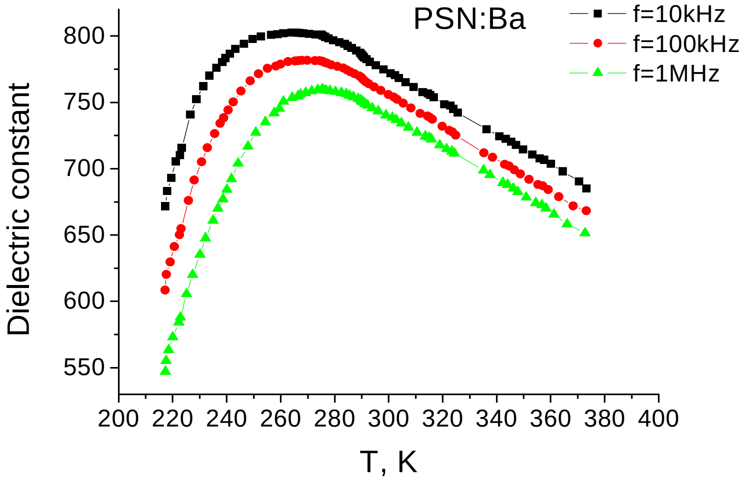

Fig. 2: Temperature dependence of the dielectric constant of PST:Ba crystals at frequencies of 10 kHz, 100 kHz and 1 MHz.

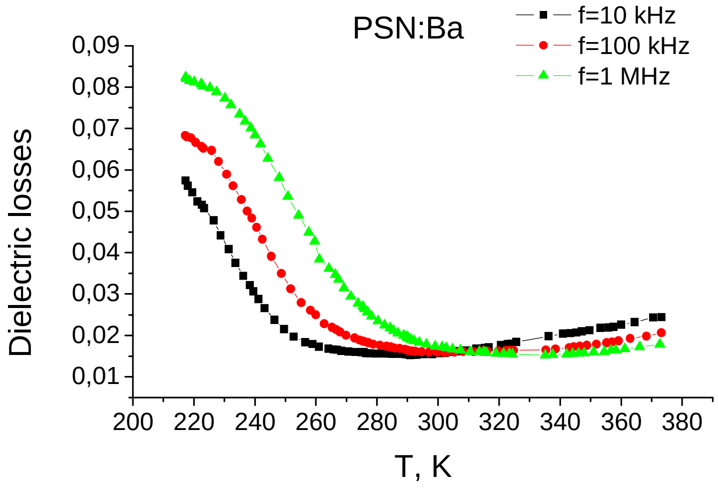

Fig. 3: Temperature dependence of the dielectric losses of PST:Ba crystals at frequencies of 10 kHz, 100 kHz and 1 MHz.

The temperature dependence of the dielectric losses of PST:Ba crystals at frequencies of 10 kHz, 100 kHz and 1 MHz are presented on fig. 3. Until room temperature the dielectric losses decrease with temperature increasing as at higher frequencies losses values are bigger then ones at lower frequencies. At temperatures after room temperature is not observed substantial temperature dependence of the dielectric losses. To the end of the investigated temperature range the losses stay in the borders of 0.015-0.03. As far as the tendency of temperature dependence Re $\sigma = f(10^3/T)$ follows temperature dependence tg $\delta = f(T)$ can be done a conclusion that PSN:Ba inductivity decreases to temperatures nearly room temperature as at higher frequencies it stays bigger and the actuation energy keeps equal for the three frequencies.

4. CONCLUSIONS

Lead scandium niobate single crystals with Ba have been prepared using HTSG method. The addition of Ba shifts the optical absorption edge to lower energies in comparison with non-doped PSN and gives rise to extra absorption peaks at 457 nm and 710 nm. Ba-doping removes the temperature of phase transition to lower temperatures in comparison with non-doped PSN and the maximal values of the dielectric constant are 800, 775 and 750 at frequencies of 10 kHz, 100 kHz and 1 MHz respectively.

5. REFERENCES

[1] Shrout T. R., Halliyal A. (1987) Preparation of Lead-Based Ferroelectric Relaxors for Capacitors, *Am. Ceram. Soc. Bulletin,* Volume 66, №4, pp.704-711.

[2] Uchino K. (1986) Electrostrictive Actuators: Materials and Applications, *Cer. Bull.,* Volume 65, №8, pp.647-652

[3] Scott J. F. (2005) [3D] Nano-Scale Ferroelectric Devices for Memory Applications, *Ferroelectrics,* Volume 314, pp.207-222.

[4] McHenry D. A., Giniewicz J. (1989) Optical Properties of Hot Pressed Relaxor Ferroelectrics, *Ferroelectrics,* Volume 93, pp.1137-1143.

[5] Камзина Л. С., Раевский И. П., Еремкин В. В., Смотраков В. Г. (2002) Особенности сегнетеэлектрических фазовых переходов в монокристаллах твердых растворов $Pb_{0.96}Ba_{0.04}Sc_{0.5}Nb_{0.5}O_3$ и $Pb_{0.94}Ba_{0.06}Sc_{0.5}Nb_{0.5}O_3$, *Физика твердого тела,* Том 44, Вып. 9, стр. 1676-1680.

NONLINEAR DYNAMICS OF FEMTOSECOND PULSES WITH ONE OR FEW OPTICAL CYCLES IN MEDIA WITH NON STATIONARY OPTICAL AND MAGNETIC RESPONSE

Kamen Kovachev[1], Luben Ivanov[1,2], Vladimir Serkin[3],

Ivaylo Tunchev[1], and Lubomir Kovachev[1]

[1] Institute of Electronics, Bulgarian Academy of Sciences,
72 Tzarigradsko shossee, 1784 Sofia, Bulgaria
[2] South-West University, Blagoevgrad, Bulgaria and
Institute of Electronics, Bulgarian Academy of Sciences
[3] Instituto de Ciencias, Benemerita Universidad Autonoma de Puebla,
AP 502, 72001 Puebla, Mexico

Abstract: *We investigate the propagation dynamics of optical pulses in media with no stationary optical and magnetic response. A new amplitude integro-differential equation is derived, governing the evolution of wave packets with only one or few harmonics under the envelopes.*

Keywords: *Femtosecond pulses, optical pulses with few cycles, nonlinear integro-differential amplitude equation.*

1. INTRODUCTION

One of the latest important trends in contemporary laser physics is the generation and investigation of the dynamics of ultra short femtosecond (fs) laser pulses. Recently were published results on generation also of autosecond pulses [1] and pulses with time duration of order of the optical period of the carrying frequency. The slowly varying envelope approximation describes the evolution of an optical envelope function, which vary slowly over an optical cycle. The time cycle of one wave in the optical region is of order of 2 fs. The pulse duration in the recent experiments varied from few fs to 15-20 fs, a regime where pulse envelopes can no longer be assumed to always vary slowly in space and time. Other important difference for these short optical pulses is that their time duration is approximately equal to relaxation time of electronic resonances of the media. The necessity of investigation more precisely the regime of no stationary optical linear and nonlinear response becomes obvious. The fs pulses give new possibility also for experiments on magneto-optical effects with ultra–fast magnetic response. The first experimental observations revealed demagnetization times of 260 fs [2-3], while the theoretical studies based on spin-orbit relaxation mechanisms gives relaxation times up to 10 fs [4]. These significant decreasing of the time scales lead to relatively appearing of new linear and nonlinear processes and methods for investigation.

In this paper we will investigate propagation of optical pulses in media with no stationary optical $\varepsilon(t-\tau)$ and magnet $\mu(t-\xi)$ response with pulse time durations of order of the optical period (large spectral bandwidth). The magnetization of the media was calculated by the standard Bloch equations, as the Ferro magnets are transformed to standard paramagnetic structures, when their temperature is up to Curie's point.

2. MAXWELL'S EQUATIONS FOR MEDIUM WITH NON-STATIONARY OPTICAL AND MAGNETIC RESPONSE.

In cases of ultra short fs optical pulses propagation with duration more or of the order the optical and the magnetic relaxation times in an isotropic medium, the linear electric polarization $\vec{P}_{lin}$ and non linear polarization $\vec{P}_{nl}$ can be represented as follows [5]:

$$\vec{P}_{lin} = \int_{-\infty}^{t}\left[\delta(t-\tau)+4\pi\chi^{(1)}(t-\tau)\right]\vec{E}(\tau,r))d\tau = \int_{-\infty}^{t}\varepsilon(t-\tau)\vec{E}(\tau,r)d\tau\,, \tag{2.1}$$

$$\vec{P}_{nl} = 3\pi\int_{-\infty}^{t}\int_{-\infty}^{t}\int_{-\infty}^{t}\chi^{(3)}(t-\tau_1,t-\tau_2,t-\tau_3)(\vec{E}(\tau_1,r)\vec{E}^{*}(\tau_2,r))\vec{E}(\tau_3,r)d\tau_1 d\tau_2 d\tau_3\,, \tag{2.2}$$

$$\vec{P} = \vec{P}_{lin} + P_{nl}\,, \tag{2.3}$$

and the magnetic induction in respect of the magnetic field $\vec{H}$ is:

$$\vec{B}_{lin} = \int_{-\infty}^{t}\left[\delta(t-\zeta)+4\pi\mu^{(1)}(t-\zeta)\right]\vec{H}(\zeta,r)d\zeta = \int_{-\infty}^{t}\mu(t-\zeta)\vec{H}(\zeta,r)d\zeta\,, \tag{2.4}$$

where $\vec{B}_{lin}$ is the magnetic induction and with $r = (x, y, z)$ are denoted the 3D spatial dimensions. The susceptibilities of different orders $\chi^{(n)}$ are related with the optical dipole transitions of the atoms and molecules, whereas the magnetic permeability μ is related with the magneto-dipole and the magneto-resonance transitions. In the present article we use this expression of the nonlinear polarization, as we investigate only linear or only circular polarized light and in addition we neglect the third harmonics term. In the equations (2.1) and (2.2) are used different relaxation times τ and ζ, because the optic-dipole and magneto-dipole transitions are different physical processes. The formers are related with the variation of the spatial distribution of the charges density and the seconds are related with the spatial distribution of the current’s density for quantum transitions in atoms and molecules. In this case the Maxwell’s equations obtain the form:

$$\nabla \times \vec{E}(r,t) = -\frac{1}{c}\frac{\partial}{\partial t}\int_{-\infty}^{t}\mu(t-\zeta)\vec{H}(r,\zeta)d\zeta, \tag{2.5}$$

$$\nabla \times \vec{H}(r,t) = \frac{1}{c}\frac{\partial}{\partial t}\begin{pmatrix} \int_{-\infty}^{t}\varepsilon(t-\tau)\vec{E}(\tau,r)d\tau + \\ 3\pi\int_{-\infty}^{t}\int_{-\infty}^{t}\int_{-\infty}^{t}\chi^{(3)}(t-\tau_1,t-\tau_2,t-\tau_3)(\vec{E}(\tau_1,r)\vec{E}^{*}(\tau_2,r))\vec{E}(\tau_3,r)d\tau_1 d\tau_2 d\tau_3 \end{pmatrix}, \tag{2.6}$$

$$\nabla \cdot \vec{H} = \nabla \cdot \vec{B} = 0, \tag{2.7}$$

$$\nabla \cdot \left(\vec{P}_{lin} + \vec{P}_{nl}\right) = 0. \tag{2.8}$$

The structures of the linear and the nonlinear polarization are conformed to the causality principle: the induction in any fixed point in the time-space, depend only on the previous moments in the time.

3. DERIVATION OF THE AMPLITUDE EQUATION

In the equation (2.5) the magnetic field $\vec{H}$ depend on the time variable ζ and for synchronization of the times variables we should to write the magnetic field in equation (2.6) to be depended on the same time variable:

$$\nabla \times \vec{H}(r,\zeta) = \frac{1}{c}\frac{\partial}{\partial \zeta}\begin{pmatrix} \int_{-\infty}^{\zeta}\varepsilon(\zeta-\tau)\vec{E}(\tau,r)d\tau + \\ 3\pi\int_{-\infty}^{\zeta}\int_{-\infty}^{\zeta}\int_{-\infty}^{\zeta}\chi^{(3)}(\zeta-\tau_1,\zeta-\tau_2,\zeta-\tau_3)\vec{E}(\tau_1,r)\vec{E}^{*}(\tau_2,r)\vec{E}(\tau_3,r)d\tau_1 d\tau_2 d\tau_3 \end{pmatrix}. \tag{3.1}$$

Taking the curl of equation (2.5) and using (4.1), we obtain:

$$\nabla\times\nabla\times\vec{E}(r,t)=-\frac{1}{c^2}\frac{\partial}{\partial t}\int_{-\infty}^{\zeta}\mu(t-\zeta)\times$$

$$\frac{\partial}{\partial\zeta}\left(\begin{array}{l}\int_{-\infty}^{\zeta}\varepsilon(\zeta-\tau)\vec{E}(\tau,r)d\tau+\\ 3\pi\int_{-\infty}^{\zeta}\int_{-\infty}^{\zeta}\int_{-\infty}^{\zeta}\chi^{(3)}(\zeta-\tau_1,\zeta-\tau_2,\zeta-\tau_3)\vec{E}(\tau_1,r)\vec{E}^{*}(\tau_2,r)\vec{E}(\tau_3,r)d\tau_1d\tau_2d\tau_3\end{array}\right)d\zeta . \tag{3.2}$$

In the left part of this equation we represent the electric field with its Fourier integral:

$$\vec{E}(r,\tau)=\int_{-\infty}^{\infty}\vec{E}(r,\omega)e^{-i\omega\tau}d\omega \quad \text{and} \quad \vec{E}(r,\tau_i)=\int_{-\infty}^{\infty}\vec{E}(r,\omega)e^{-i\omega\tau_i}d\omega , \tag{3.3}$$

and as result we obtain:

$$\nabla\times\nabla\times\vec{E}(r,t)=-\frac{1}{c^2}\frac{\partial}{\partial t}\int_{-\infty}^{\zeta}\mu(t-\zeta)\times$$

$$\frac{\partial}{\partial\zeta}\left(\begin{array}{l}\int_{-\infty}^{\zeta}\varepsilon(\zeta-\tau)\int_{-\infty}^{\infty}\vec{E}(r,\omega)e^{-\omega\tau}d\omega d\tau+\\ 3\pi\int_{-\infty}^{\zeta}\int_{-\infty}^{\zeta}\int_{-\infty}^{\zeta}\chi^{(3)}(\zeta-\tau_1,\zeta-\tau_2,\zeta-\tau_3)\int_{-\infty}^{\infty}\left|\vec{E}(r,\omega)\right|^2\vec{E}(r,\omega)e^{-i(\omega\tau_1-\omega\tau_2+\omega\tau_3)}d\omega d\tau_1d\tau_2d\tau_3\end{array}\right)d\zeta ,$$

or

$$\nabla\times\nabla\times\vec{E}(r,t)=-\frac{1}{c^2}\frac{\partial}{\partial t}\int_{-\infty}^{\zeta}\mu(t-\zeta)\times$$

$$\frac{\partial}{\partial\zeta}\left(\begin{array}{l}\int_{-\infty}^{\zeta}\vec{E}(r,\omega)\int_{-\infty}^{\infty}\varepsilon(\zeta-\tau)e^{-\omega\tau}d\tau d\omega+\\ 3\pi\int_{-\infty}^{\zeta}\int_{-\infty}^{\zeta}\int_{-\infty}^{\zeta}\left|\vec{E}(r,\omega)\right|^2\vec{E}(r,\omega)\int_{-\infty}^{\infty}\chi^{(3)}(\zeta-\tau_1,\zeta-\tau_2,\zeta-\tau_3)e^{-i(\omega\tau_1-\omega\tau_2+\omega\tau_3)}d\tau_1d\tau_2d\tau_3d\omega\end{array}\right)d\zeta . \tag{3.4}$$

The causality principle requires the follow conditions for the response functions: $\varepsilon(\zeta-\tau_i)=0$ when $\zeta<\tau_i$, and $\mu(t-\zeta)=0$, when $t<\zeta$.

These conditions give us the possibility to extend the upper limit of integration to infinity and to obtain the next expressions for the linear response functions:

$$\int_{-\infty}^{\zeta}\varepsilon(\zeta-\tau)e^{-i\omega\tau}d\tau=\int_{-\infty}^{\infty}\varepsilon(\zeta-\tau)e^{-i\omega\tau}d\tau=-\varepsilon(\omega)e^{-i\omega\zeta} ,$$

$$\int_{-\infty}^{t}\mu(t-\zeta)e^{-i\omega\zeta}d\zeta=\int_{-\infty}^{\infty}\mu(t-\zeta)e^{-i\omega\zeta}d\zeta=-\mu(\omega)e^{-i\omega t} ,$$

and nonlinear response functions:

$$\int_{-\infty}^{\zeta}\int_{-\infty}^{\zeta}\int_{-\infty}^{\zeta}\chi^{(3)}(\zeta-\tau_1,\zeta-\tau_2,\zeta-\tau_3)e^{-i(\omega\tau_1-\omega\tau_2+\omega\tau_3)}d\tau_1 d\tau_2 d\tau_3=-\chi^{(3)}(\omega)e^{-i\omega\zeta}.$$

Thus, after brief calculations equation (3.4) can be represented as:

$$(3.5)\quad \nabla\times\nabla\times\vec{E}(r,t)=\int_{-\infty}^{\infty}\left(\frac{\omega^2\varepsilon(\omega)\mu(\omega)}{c^2}\vec{E}(r,\omega)+\frac{3\pi\omega^2\chi^{(3)}(\omega)\mu(\omega)}{c^2}\left|\vec{E}(r,\omega)\right|^2\vec{E}(r,\omega)\right)e^{-i\omega t}d\omega\ .$$

We denote the square of the linear k^2 and nonlinear $\hat{k}_{nl}^2$ wave-vectors with the expression:

$$(3.6)\qquad k^2(\omega)=\omega^2\varepsilon(\omega)\mu(\omega)/c^2\,;\ \ \hat{k}_{nl}^2(\omega)=\frac{3\pi\omega^2\mu(\omega)\chi^{(3)}(\omega)}{c^2}.$$

Thereby we get:

$$(3.7)\quad \nabla\left(\nabla\cdot\vec{E}(r,t)\right)-\Delta\vec{E}(r,t)=\int_{-\infty}^{\infty}\left(k^2(\omega)+\hat{k}_{nl}^2(\omega)\left|\vec{E}(r,\omega)\right|^2\right)\vec{E}(r,\omega)e^{-i\omega t}d\omega\,.$$

Let us introduce here the one directional amplitude function $\vec{A}(r,t)$ for the electrical field $\vec{E}(r,t)$

$$(3.8)\qquad \vec{E}(r,t)=\vec{A}(r,t)e^{i(k_0z-\omega_0t)}\ ,$$

where ω_0 and k_0 are the carrier frequency and the carrier wave number of the wave packet. Here we also write the Fourier transform of the amplitude function $\vec{A}(r,\omega-\omega_0)$:

$$(3.9)\qquad \vec{A}(r,\omega-\omega_0)=\int_{-\infty}^{\infty}\vec{A}(r,t)e^{-i(\omega-\omega_0)t}dt\,.$$

The writing of the amplitude function in this form means that we consider propagation only in + z-direction and the neglecting the opposite one. After substitution of (3.8) and (3.9) in (3.7) and using the fact that $\nabla\left(\nabla\cdot\vec{E}\right)\approx 0$, we obtain the following integro-differential amplitude equation:

$$(3.10)\quad \Delta\vec{A}(r,t)+2ik_0\frac{\partial\vec{A}(r,t)}{\partial z}-k_0^2\vec{A}(r,t)=-\int_{-\infty}^{\infty}\left(k^2(\omega)+\hat{k}_{nl}^2(\omega)\left|\vec{A}(r,\omega-\omega_0)\right|^2\right)\vec{A}(r,\omega-\omega_0)e^{-i(\omega-\omega_0)t}d\omega\,.$$

In equation (3.10) the amplitude function is obtained with only one restriction: to be limited in space, time and frequency domains. The analytical functions $k^2(\omega)$ and $\hat{k}_{nl}^2(\omega)$ in the transparency region of a media are finite and since the Fourier transform of a localized function (pulse) of the electric field is localized function in frequency domain, the integral in the right part of the equation (3.10) is bounded and we can investigate optical pulses with duration of the order of the optical oscillation. Generally, with the integral-differential equation (3.10) we can describe wave-packets with duration of the order of the optical oscillation as well as wave-packets with high numbers of harmonics under the pulse in media with polarization and magnetization. In this way we obtain the nonlinear equation (3.10) which governed the evolution of pulses with duration of the order of the optical oscillation in medium with non stationary linear and nonlinear electrical response and non stationary linear magnetic response.

4. CONCLUSION

In this presentation we discuss the propagation of pulses with only few cycles within the context of a new nonlinear integro-differential equation (3.10). The equation is derived from first principles to the general case of non-stationary optical and magnetic response. The equation (3.10) can be reduced to equations for standard dielectric media without dispersion of the magnetic permeability with the substituting $\mu = const$. We hope our finding will stimulate future study of nonlinear wave dynamics of pulses with few fs and autosecond time duration. This work is partially supported by Bulgarian Science Foundation under grant F 1515/2005.

5. REFERENCES:

[1] Christov, I. P., Murname, M. M., and Kapteyn, H. C. (1998) Generation of single-cycle attosecond pulses in the vacuum ultraviolet, Opt. Commun. 148 , 75 -78.

[2] Beaurepaire, E., Merle, J.-C., Daunois, A., and Bigot, J.-Y. (1996) Ultrafast Spin Dynamics in Ferromagnetic Nickel, Phys. Rev. Lett. 76, 4250 - 4252.

[3] Hohlfeld, J., Matthias, E., Knorren, R., and Bennemann, K.H. (1997) Nonequilibrium Magnetization Dynamics of Nickel, Phys.Rev.Lett. 78, 4861 – 4865, (E)79, 960 (1997).

[4] Zhang, G. P. and Hubner, W. (2000) Laser Induced Ultrafast Demagnetization in Ferromagnetic Metals, Phys. Rev. Lett. 85, 3025- 3-29.

[5] K.L. Kovachev, Evolution of ultra-short optical pulses in media with non stationary optical and magnetic response, Batchelor thesis, Sofia University, 2003.

SLOWLY-VARYING EQUATION OF AMPLITUDES IN MEDIA WITH NON STATIONARY OPTICAL AND MAGNETIC RESPONSE. NEGATIVE GROUP VELOCITY

Lubomir Kovachev[1], Luben Ivanov[1,2], Vladimir Serkin[3],

Ivaylo Tunchev[1] , and Kamen Kovachev[1]

[1] Institute of Electronics, Bulgarian Academy of Sciences,
72 Tzarigradsko shossee, 1784 Sofia, Bulgaria
[2] South-West University, Blagoevgrad, Bulgaria and
Institute of Electronics, Bulgarian Academy of Sciences
[3] Instituto de Ciencias, Benemerita Universidad Autonoma de Puebla,
AP 502, 72001 Puebla, Mexico

Abstract: *We reduce the amplitude integro-differential equation and to nonlinear Slowly Varying Equation of Amplitudes (SVEA) in second approximation of linear dispersion and in first approximation to the nonlinear dispersion. The SVEA describes the evolution of an envelope function, which is assumed to vary slowly over an optical cycle. It is important to point, that the obtained SVEA in media with no stationary optical and magnetic response is similar to the SVEA equation with stationary magnetic response. The only different is the expressions for group velocity and dispersion parameters. Partially, in paramagnetic media near to magnetic resonances it is possible to reach negative group velocity and group velocity higher than velocity of light in vacuum.*

Keywords: *non-paraxial evolution equation, negative group velocity*

1. INTRODUCTION.

The pulse durations of typical femtosecond (fs) lasers varied now from 50 to 200 fs, a regime where pulse envelopes can be approximated as slowly varying in space/time in respect to one optical period (~ 2 fs). Typical feature of the magnetic permeability for the paramagnetic materials is that the static part μ_{st} is small magnitude - of the order $10^{-5}\div10^{-6}$. On the other hand we know that the typical spin lattice relaxation times are of order of $\Delta t \cong 100\,ps$. That is the reason the magnetic permeability dispersion μ(ω) to be 4-5 orders less than the electric susceptibility dispersion ε(ω) and to be neglected in the dynamics of the electromagnetic pulses propagation. The situation was significant changed in the last few years after observation the longitudinal relaxation time of magneto-optical transitions of the order of $T1\approx$50-100 fsec [1, 2]. The experiments were provided with ultra short femtosecond optical pulses on the base of the Kerr’s magneto-optical effect. The change of the polarization angle is significant for pulses with energies exceed the energies of the Curie’s point in case of ferromagnetic and over the Fermi’s level in case of semiconductor metal base structures. We should notice that for such kind of structures the static magnetic permeability μ_{st} obeys the Curie-Weiss law in respect of the temperature:

$$\mu_{st}(T) = C/(T-\theta), \qquad (1.1)$$

where C is the Curie constant and θ is the Curie's paramagnetic temperature. In these cases the static linear magnetic susceptibility can increase up to μ_{st} ~10^{-1}, with relaxation times $T_1 \approx$ 50-100 fs, and the magnetic permeability dispersion μ(ω) can be performed only one order less than the electric susceptibility dispersion ε(ω).

In this paper we will investigate propagation of optical pulses in media with no stationary optical $\varepsilon(t-\tau)$ and magnet $\mu(t-\xi)$ response, for pulses with many harmonics under the envelopes (SVEA approximation). The magnetization was calculated by the standard Bloch equations, as the Ferro magnets are transformed to standard paramagnetic structures, when their temperature is up to Curie's point.

2. SLOWLY-VARYING EQUATION OF AMPLITUDES (SVEA) IN MEDIA WITH MAGNETIZATION

In [3] the following integro - differential amplitude equation describing the evolution of optical pulses in media with linear and nonlinear polarization and magnetization is obtained:

(2.1) $$\Delta\vec{A}(r,t)+2ik_0\frac{\partial\vec{A}(r,t)}{\partial z}-k_0^2\vec{A}(r,t)=-\int_{-\infty}^{\infty}\left(k^2(\omega)+\hat{k}_{nl}^2(\omega)\left|\vec{A}(r,\omega-\omega_0)\right|^2\right)\vec{A}(r,\omega-\omega_0)e^{-i(\omega-\omega_0)t}d\omega\ ,$$

where we denote the square of the linear k^2 and nonlinear $\hat{k}_{nl}^2$ wave-vectors with the expression:

(2.2) $$k^2(\omega)=\omega^2\varepsilon(\omega)\mu(\omega)/c^2\ ;\ \ \hat{k}_{nl}^2(\omega)=\frac{3\pi\omega^2\mu(\omega)\chi^{(3)}(\omega)}{c^2}.$$

To obtain SVEA in second approximation to linear dispersion and to first approximation to nonlinear dispersion we develop k^2 in Taylor series around the wave-packets carrying frequency ω_0 :

(2.3) $$k^2=\frac{\omega^2\varepsilon(\omega)\mu(\omega)}{c^2}=k_0^2(\omega_0)+\frac{\partial\left(k^2(\omega)\right)}{\partial\omega_{\omega=\omega_0}}(\omega-\omega_0)+\frac{1}{2}\frac{\partial^2\left(k^2(\omega)\right)}{\partial\omega^2{}_{\omega=\omega_0}}(\omega-\omega_0)^2+.....\ ,$$

and also for the nonlinear wave vector:

(2.4)
$$k_{nl}^2=\frac{\omega^2\mu(\omega)\chi^{(3)}(\omega)}{c^2}=k_{0nl}^2(\omega_0)+\left.\frac{\partial\left(k_{nl}^2(\omega)\right)}{\partial\omega}\right|_{\omega=\omega_0}(\omega-\omega_0)+......$$

The substitution of these series into the right part of (2.1) leads to approximation for slowly varying amplitudes. The first term of the Taylor's series of linear wave vector cancels with the last term in the left part of the equation (2.1). The second and the third terms in the Taylor's development of the linear wave vector (2.2) (dispersion of first and second order) give main contribution in the Fourier's integral on the right part of equation (2.1). The convergence of the series (2.3) for gases and dielectrics materials depends on the harmonics under the wave-packet envelopes. For wave-packets with more than 10-15 harmonics under the envelope on the level “half-max” of the pulse the Taylor’s series (2.3) is strongly convergence and the third term is 3-4 times less than the second term. Therefore we can interrupt the Taylor’s series and to examine the dynamics of the wave-packets in the approximation up to second order of the dispersion. In the cases with 2-3 to 10 harmonics in the pulse the series (2.3) is slowly convergent and we can take into account also the higher order of dispersion as small parameter. In case of wave-packets with only two, one or less periods of the optical oscillations under the envelope curve the series (2.3) is non convergent. Therefore the equations for the slowly varying amplitudes which will be worked-out below, cannot describe the propagation dynamics of the wave-packets with duration in the order of the optic oscillation. After substituting of the series (2.3) and (2.4) into equation (2.1), and after brief calculation we obtained the next SVEA up to second approximation of linear dispersion and first approximation of the nonlinear optical dispersion:

(2.5) $$\Delta\vec{A} + 2ik_0\frac{\partial\vec{A}}{\partial z} = -2ik_0k'\frac{\partial\vec{A}}{\partial t} + \left(k_0k'' + k'^2\right)\frac{\partial^2\vec{A}}{\partial t^2} - k_{0nl}^2\left|\vec{A}\right|^2\vec{A} - 2ik_{0nl}k_{0nl}'\frac{\partial\left(\left|\vec{A}\right|^2\vec{A}\right)}{\partial t} + .. \ .$$

The equation (2.5) seems equal to SVEA equations of media with stationary magnetic response $\mu = const$. The important result here is that the including also of dispersion of magnetic response $\mu(\omega)$ in equation (2.5) gives us significant new dynamics of the localized optical waves. We now define the next important constants of the wave packets: linear wave number $k_0(\omega_0)$, nonlinear wave number $k_{0nl}(\omega_0)$, linear refractive index $n(\omega_0)$, nonlinear refractive index $n_2(\omega_0)$, group velocity v, nonlinear addition to the group velocity $1/k'_{nl}$, and dispersion of the group velocity $k''(\omega_0)$:

(2.6) $$k_0 \equiv k(\omega_0) = \frac{\omega_0}{c}\sqrt{\varepsilon(\omega_0)\mu(\omega_0)} \ ,$$

(2.7) $$k_{0nl}^2 \equiv k_{nl}^{\ 2}(\omega_0) = \frac{\omega_0^{\ 2}\varepsilon(\omega_0)\mu(\omega_0)}{c^2}\frac{3\pi\chi^{(3)}(\omega_0)}{\varepsilon(\omega_0)} = k^2(\omega_0)n_2(\omega_0) \ ,$$

(2.8) $$n(\omega_0) = \sqrt{\varepsilon(\omega_0)\mu(\omega_0)} \ ,$$

(2.9) $$n_2(\omega_0) = \frac{3\pi\chi^{(3)}(\omega_0)}{\varepsilon(\omega_0)} \ ,$$

(2.10) $$v = \frac{1}{k'}\bigg|_{\omega=\omega_0} = c/\left(\sqrt{\varepsilon(\omega_0)\mu(\omega_0)} + \frac{\omega_0}{2}\left(\sqrt{\frac{\mu}{\varepsilon}}\frac{\partial\varepsilon}{\partial\omega}\bigg|_{\omega=\omega_0} + \sqrt{\frac{\varepsilon}{\mu}}\frac{\partial\mu}{\partial\omega}\bigg|_{\omega=\omega_0}\right)\right),$$

(2.11) $$(k_{0nl}^2)' = \frac{2k_0n_2}{v} + k_0^2\frac{\partial n_2}{\partial\omega}\bigg|_{\omega=\omega_0} \ ,$$

(2.12) $$k''(\omega_0) = \left.\frac{\partial^2 k}{\partial \omega^2}\right|_{\omega=\omega_0} .$$

All these quantities allow a direct physical interpretation and we will rewrite equation (5.3) in a form consistence with these constants:

(2.13) $$-i\left[\frac{\partial \vec{A}}{\partial t} + v\frac{\partial \vec{A}}{\partial z} + \left(n_2 + \frac{k_0 v}{2}\frac{\partial n_2}{\partial \omega}\right)\frac{\partial\left(\left|\vec{A}\right|^2 \vec{A}\right)}{\partial t}\right] = \frac{v}{2k_0}\Delta\vec{A} - \frac{v}{2}\left(k'' + \frac{1}{k_0 v^2}\right)\frac{\partial^2 \vec{A}}{\partial t^2} + \frac{k_0 v n_2}{2}\left|\vec{A}\right|^2 \vec{A}.$$

The equation (2.13) can be considered to be SVEA of second approximation in respect to linear dispersion and first approximation in respect to nonlinear dispersion in media with no stationary linear and nonlinear optical and no stationary linear magnet response. It includes the effects of transition in z direction with group velocity v, self-steepening, diffraction, dispersion of second order and self-action. Similar expressions for group velocity and dispersion of the group velocity are obtained recently in one dimensional SVEA approximation [4] and in spatial-temporal approximation [5]. We use only the linear magnetic response, that why, as it can be seen from expression the linear effects as linear refractive index, group velocity and the dispersion of the group velocity are significantly different, than the expressions for these constants, when $\mu = const$ (standard dielectric media).

3. ULTRA-FAST MAGNETIC RELAXATION PROCESSES IN FERROMAGNETIC AND SEMICONDUCTOR STRUCTURES. CONDITIONS FOR NEGATIVE GROUP VELOCITY OR GROUP VELOCITY HIGHER THAN THE VELOCITY OF LIGHT IN VACUUM.

The physical mechanisms, which leads to such a fast response is spin-orbit interaction or *magnetic-dipole transitions* on optical frequencies. These transitions are between different orbit levels and spins. The well known magnetic resonance transition on one orbital level between states with opposite spins give resonances in microwave and radio region. Both processes *magnetic dipole transition* and *magnetic resonance transitions* are no stationary processes and are obtained from the oscillation between different orbital levels or between sublevels correspondingly with nonzero quantum current. One classical description of such processes can be described by solving the Bloch equation. Let we write the Bloch equation for an alternating longitudinal magnetic field (the magnetic part of the electromagnetic pulse) $\vec{H} = \vec{z}H_1\cos\omega t$. In consideration of the magnetization μ_z relaxes to the momentary value of the magnetic field $\mu_z^0 = \mu_{st}H\cos\omega t$ we can write:

(3.1) $$\frac{d\mu_z}{dt} = \gamma(\vec{M}\times\vec{H})_z + \frac{\mu_{st}H_1\cos\omega t - \mu_z}{T_1},$$

where ω is the carrying optical frequency of the localized electromagnetic wave. Because the vectors $\overrightarrow{M}$ and $\vec{H}$ are collinear the cross product in the equation (3.1) is zero. The solution for the real and the imaginary part is [10]:

$$\mu_z'(\omega)=\frac{\mu_{st}}{1+\omega^2T_1^2}\,,\qquad \mu_z''(\omega)=\frac{\mu_{st}\omega T_1}{1+\omega^2T_1^2}\,. \tag{3.2}$$

The real part of the longitudinal component of the magnetic susceptibility $\mu_z'(\omega)$ is an even function in respect to the frequency in distinction of the electric susceptibility, which is an odd function. It appears new possibilities for spreading of wave packets in media with no stationary optical and magnetic response. Particularly, when $\mu'(\omega)$ is even function (for paramagnetic this is the usual case) near to magnetic resonance, we can obtain the magnetic susceptibility to be of order of optical one ($\varepsilon(\omega)\propto\mu(\omega)$), and with opposite sign of their derivatives of frequencies:

$$\left.\frac{\partial\varepsilon}{\partial\omega}\right|_{\omega=\omega_0}>0\,;\qquad \left.\frac{\partial\mu}{\partial\omega}\right|_{\omega=\omega_0}<0\,. \tag{3.3}$$

This gives the unique possibilities to obtain group velocity higher than the phase velocity and velocity of light in vacuum, if the denominator in the expression of the group velocity (2.10) is small that one:

$$\sqrt{\varepsilon(\omega_0)\mu(\omega_0)}+\frac{\omega_0}{2}\left(\sqrt{\frac{\mu}{\varepsilon}}\left.\frac{\partial\varepsilon}{\partial\omega}\right|_{\omega=\omega_0}+\sqrt{\frac{\varepsilon}{\mu}}\left.\frac{\partial\mu}{\partial\omega}\right|_{\omega=\omega_0}\right)<1, \tag{3.4}$$

or negative group velocity, when the denominator in (5.8) is negative:

$$\sqrt{\varepsilon(\omega_0)\mu(\omega_0)}+\frac{\omega_0}{2}\left(\sqrt{\frac{\mu}{\varepsilon}}\left.\frac{\partial\varepsilon}{\partial\omega}\right|_{\omega=\omega_0}+\sqrt{\frac{\varepsilon}{\mu}}\left.\frac{\partial\mu}{\partial\omega}\right|_{\omega=\omega_0}\right)<0\ . \tag{3.5}$$

As the static and correspondingly no stationary magnetic susceptibility is with two or three order smaller than optical-dielectric one, the conditions (3.4) and (3.5) are practically unfulfilled for usual paramagnetic structures. In spite of this, for discussed above ferromagnetic with temperature slightly higher then Curie’s paramagnetic temperature near paramagnetic resonances, and also in some semiconductors, the conditions (3.4) or (3.5) can be satisfied.

We therefore make the following conclusion: The derived nonlinear SVEA (2.13) for media with dispersion of the optical susceptibility and magnet permeability, practically admit equal structures and terms as the equation with stationary magnetic and no stationary optical response. From other hand, the dynamics of the localized waves is quite different from the dynamics in media with $\mu=const$, as the expressions for linear refractive index (2.8), the group velocity (2.10) and the dispersion of the group velocity (2.12) are different from these of standard dielectrics.

4. CONCLUSION

In the last few years there have been made several experiments, demonstrated ultra short relaxation times of the linear magnetic response of order of 50-100 fsec [1-2]. It is important to point here also the significant increasing of the static magnetic response in such materials as nickel for temperatures up to Curie's paramagnetic temperature and also in some semiconductors.

The higher value of the static susceptibility and ultra-short relaxation times of the magnetic response request: to be taken into account also the no stationary magnetic response together with optical one in Maxwell's equations for such media. In this paper are investigated these no-stationary processes. For pulses with many optical harmonics under the envelopes, the Taylor series of the square of the linear and nonlinear wave vectors are strongly convergent. This is the reason the nonlinear integro-differential equation (2.1) to be reduced to the nonlinear differential SVEA (2.13). We mentioned agein, that derived here SVEA equation (2.13) for media with dispersion of the optical and magnet susceptibility, practically admit equal structures and terms as the equation with stationary magnetic and no stationary optical response, while the dynamics of the localized waves determinate from expression for group velocity (2.10), and the dispersion of the group velocity (2.12), is quite different than the corresponding dynamics for media with $\mu = const$. Particularly, there are spectral zones, near to paramagnetic resonances, where it is possible to obtain negative group velocity and group velocity higher than phase velocity and velocity of light in vacuum. This work is partially supported by Bulgarian Science Foundation under grant F 1515/2005.

5. REFERENCES:

[1] Beaurepaire, E., Merle, J.-C., Daunois, A., and Bigot, J.-Y. (1996) Ultrafast Spin Dynamics in Ferromagnetic Nickel, Phys. Rev. Lett. 76, 4250 - 4252.

[2] Hohlfeld, J., Matthias, E., Knorren, R., and Bennemann, K.H. (1997) Nonequilibrium Magnetization Dynamics of Nickel, Phys.Rev.Lett. 78, 4861 – 4865, (E)79, 960 (1997).

[3] K.L. Kovachev, Evolution of ultra-short optical pulses in media with non stationary optical and magnetic response, Batchelor thesis, Sofia University, 2003.

[4] Scalora, M., Syrchin, M.S., Akozbek, N., Poliakov, E. Y., D'Aguanno, G., Mattiucci, N., Blomer, M. J., and Zheltikov, A. M. (2005) Generalized Nonlinear Schredinger Equation for Dispersive Susceptybility and Permeability: Application to Negative Index Materials, Phys. Rev. Lett. 95, 013902.

[5] Makarov, V.P., Rukhadze, A.A., Samokhin, A.A.(2005) Waves with Negative Group Velocity. Conditions of their Existence in a Isotropic Medium, Ukr. Phys. Journal, 50, N 8A, 159-169.

SOLAR ENERGY DATA FOR THE TYPICAL TECHNICAL AND ECONOMICAL CALCULATION FOR SOLAR INSTALLATIONS

Stanko Vl. Shtrakov

South - West University “Neofit Rilski”,
66 Ivan Mihailov Str., 2700 - Blagoevgrad, BULGARIA,

Abstract*: In this article are analysed the available climatic data for typical technical and economical calculations for different type of solar application. Such type of calculation is based on statistical performed data for long time period of observation. Due to the big range of slope and orientation of absorbed elements surfaces of solar equipment there is need to perform solar data geometrically to the needed slope and orientation. Different models of geometrical conversion of solar radiation is analysed in this work. A computer program is created t delivery solar radiation for different applications.*

Keywords: *Solar energy, climatic data, technical and economical assessment.*

1. INTRODUCTION

The performance of solar systems depends upon local climatic conditions. From this point of view they are very different from conventional domestic heating system and system for hot water. Two sets of climatic data are needed to conduct analysis of the thermal solar systems. The first is the ‘normals’ of daily air temperature distributions for a typical day in each month of the year. These are required to calculate heat loses of solar elements during the working period. The heat loses should not be taken from tables of heating degree day figures, as they will vary according to the solar gains, wind speed, effective temperature of the sky, internal gains of the building etc.

The second set of climatic data is required to assess gains of the houses or the solar collectors due to absorption of solar radiation. They are affected by such climatic and geographical factors as the amount of cloudiness, the atmospheric clarity, local altitude and latitude, reflective characteristic of the environment and other. Because of these factors it is difficult to make accurate assessment of the solar radiation. Additional problem is the requirements of geometrical calculations for solar radiation, because the solar energy depends on the angle of incidence upon absorption surface. This angle veer during the day and year and it is necessary to use simulation calculations to assess the technical efficiency of solar equipment.

The assessment of the efficiency of thermal solar installations is in relation with observing potentiality of the available solar radiation for the region which is being explored. The main difficulty in observing this quantity is determined by the great number of variable factors that influence on the regime of entering solar energy upon the earth surface. That is the reason why it is necessary to observe solar radiation in statistic aspect on the base of long-term meteorological researches.

Determination of the area of the absorbed surface is a basic task in projecting of solar applications. One of the possible approaches for solving this task is to use long-term simulating calculations with the help of mathematical models for different type of solar installations. With such simulations it can be defined the annual or seasonal efficiency of installations when there is a certain collector field (absorptive surface). As we simulate variants with different in size collector field, we can define the optimal size of solar installation in reference to the surface of solar collectors. The main problem here is to find the accurate typical data for climatic parameters (solar radiation, ambient temperature, wind speed and other).

2. AVAILABLE METEOROLOGICAL DATA

In Bulgaria, the average annual period of sunshine is about 2100 hours. In some of its regions it may reach 2500 hours, which corresponds to 1400 ÷ 1600 kWh/m^2 annually on the horizontal surface. The assessment of long-term observations from more than 40 meteorological stations in Bulgaria has shown that the country can be divided into three "solar zones" [1].

For design purposes it is best to use a full year's data or full seasonal data if the process is seasonal one, and if data are available for many years it is necessary to select the best set. Klain [4] suggests the concept of a design year, which using many years data, selects for every month the radiation closest to the all year average for this month. Monthly average temperatures are used as a secondary criterion where necessary. The set of month's daily distribution of solar radiation and ambient temperature constitutes the design year data. These quantities are often estimated in hour-by-hour time period.

Radiation data are the best source of information for estimating the incident solar gain. However, the network collecting solar radiation in Bulgaria is still very scarce; complete radiation data are available only from Sofia and partially from any other places. The main concern is therefore, to use empirical relationship to estimate radiation from hours of sunshine or cloudiness. Data on average hours of sunshine are available from over 40 stations in Bulgaria. Many papers have been written on the sunshine based models to estimate solar radiation on horizontal surface [4,5]. Well-known Kimbal-Angstrom-Page model was used to calculate total radiation on horizontal surface through the day. Design year data for solar radiation we have received for the stations with available sunshine hours data. Temperature distribution data are available for many places in Bulgaria

As a basic source of information in defining solar radiation there are long-term measurements of summary solar radiation, related most frequently to horizontal surface. Such data about our country exist only about Sofia region (2,3). About other regions of the country actinometrical observations for a longer period of time do not exist yet.

Another source of information for assessment of the potentiality of solar radiation is data about the duration of sun-shining. These data with accuracy could be used for indirect determination of the course and distribution of solar radiation. The most common and accurately checked correlations for determination of the summary solar radiation on horizontal surface together with using data about duration of sun-shining are the equation of Masson, Angstrom, Sivkov and others [4].

Very often it is necessary to define solar radiation on inclined and differently orientated surfaces. It is known that the quantitative determination of direct solar radiation on inclined surface is a question of geometric dependencies. The question about diffuse radiation is more complicated since this radiation enters from different parts of the sky, but not from the sun disc. The unevenness in the atmosphere state determines significant anisotropy in the intensity of the diffuse solar radiation which appears especially in differently inclined and orientated surfaces.

For engineer calculations the hypothesis about isotropy of the diffuse radiation with observing variable character of the solar radiation, brings satisfying results. What is more, the maximal deal of diffuse radiation from the summary solar course does not increase 30%, which significantly reduces the influence of incorrectness from supposing isotropy.

Using the hypothesis for isotropy brings the influence of the incline and the orientation of the accepting surface to establishing different correlations between the two components of the diffuse radiation – radiation from the sky vault and reflected from the ground surface radiation. These correlations also are brought to certain geometric dependencies, but they are different from the dependencies related to the direct radiation. Therefore, when it is known only summary solar radiation, it is necessary to be divided in direct and diffuse. This could be accomplished, for example, using the equations of Lui and Jordan [2] and Page [3].

When the solar radiation is calculated with the data about duration of sun-shining, it is preferable to be used empirical dependencies about the direct and the diffuse radiation, in which we should admit the geographic place of the region and the atmosphere state. For example, the direct solar radiation intensity on a surface perpendicular to the sun rays could be defined from the expression:

(1) $$I = I_{sc} C \cdot A \cdot \exp(-B/\sin(h))$$

Where I_{sc} is a “solar constant” – 1380 W/m2,

C –corrective coefficient of the distance earth – sun,

A, B – coefficients, admitting the influence of the atmosphere pollution on the passing sun rays,

h – height angle of the sun.

The direct solar radiation on the inclined surface therefore is:

(2) $$Q_D = I \cdot \cos(\theta)$$

where θ is the angle of falling sun rays. [1].

The diffuse radiation on horizontal surface could be defined from the equation [1]:

(3) $$Q_d = I_{sc} C \cdot \sin(h) \cdot T_d$$

where for the coefficient of passing scattered radiation through the atmosphere T_d in an experimental way it is established the correlation:

(4) $$T_d = 0.271 - 0.2939 A \exp(-B/\sin(h))$$

On a surface inclined under an angle S, the total diffuse radiation could be defined from the equation:

(5) $$Q_{ds} = \frac{1+\cos(S)}{2} Q_d + \rho \frac{1-\cos(S)}{2} (I \cdot \sin(h) + Q_d)$$

where ρ is a coefficient of reflection of solar radiation from the soil.

On the base of the dependencies (1), (3) and (4) and on the existing data about solar radiation (for the region of city of Sofia) and the data about the duration of sun-shining for 35 meteorological stations in this work it is achieved an assessment of the potentiality of the solar radiation on the territory of Republic of Bulgaria. The data about the solar radiation are referred to the period 1970 – 1985 [2,3] and the data about the duration of sun-shining – to the period 1960 – 1985 [2].

When we constitute the algorithm for calculating the solar radiation there have been used the following suppositions:

- because of the insignificant difference in the day duration in southern and northern parts of the country, we can reckon that the special distribution of sun-shining about the total territory is determined only by the distribution of cloudiness;
- as far as the geographic length about the territory of the country varies in narrow limits (41 - 43 deg), solar radiation distribution is determined mostly by the duration of sun-shining. This means, for example, that the summary solar radiation in an absolutely sunny day, as well as diffuse radiation in a cloudy day is the same for the whole country (excluding regions with more polluted atmosphere). Apart from that, instead of calculated on equations /1-3/ data about the direct and the diffuse radiation for different regions, it can be used relevant data from calculations about the region of the city of Sofia.

Taking into account the previous suppositions, the distribution of solar radiation is determined by the relative duration of sun-shining for the certain day interval:

$$f_h = \frac{sum \cdot of \cdot monthly \cdot sunshine \cdot duration \cdot for \cdot apropriate \cdot hour \cdot in \cdot dasy}{number \cdot of \cdot days \cdot in \cdot month}$$

Average monthly solar radiation for appropriate hour interval can be expressed by:

(6) $$q_s = f_h \cdot q_t + (1 - f_h) \cdot q_d$$

where $\boldsymbol{q_t}$ is the summary solar radiation for the certain hour interval in conditions of a cloudless day; $\boldsymbol{q_d}$ – diffuse radiation for the certain hour interval in conditions of a cloudy day.

The question about defining solar radiation on differently inclined and orientated surfaces can be observed as defining $\boldsymbol{q_t}$ and $\boldsymbol{q_d}$ for the certain incline and orientation. As it was previously pointed it can be observed as geometric transformations of the data about direct and diffuse radiation determined in advance.

To accomplish the necessary calculations of the summary solar radiation for differently inclined and orientated surfaces, there have been used computer program SOLAR. With their help it can be determined the daily course of the summary solar radiation as well as the daily, monthly and annual sums of the solar radiation. Such calculations have been performed for the 35 meteorological stations on the territory of Bulgaria, for which there exist data about the duration of sun-shining. The results about the city of Sofia were compared with the existing data from the measurements of solar radiation as well as the results achieved through using the equation of Lui and Jordan [4]. It has been achieved a good correlation between the different data and the results.

The analysis of the achieved results reveals that it is useful to divide hypothetically the territory of Bulgaria into three "solar" zones[1].

The assessment of the radiation balance for the territory of Bulgaria reveals that for the summer season (31.03 – 31.10), the optimal incline angle of the absorbing surfaces is about 30^o , and the incident solar radiation on $1m^2$ is from 900 to 1200 kWh/m^2 season. For the winter season (31.10 – 31.03) the optimal angle is about 55^o, and the incident solar radiation is from 300 to 390 kWh/m^2 season. The annual summary solar radiation with an angle of incline 30 is from 1200 to 1500 kWh/m^2 year.

3. PROGRAM SOLAR

It is developed a software system SOLAR for modeling and simulation calculations of installations for thermal transformation of solar energy. The algorithm and the organization of the interface of the program provides a universal approach for adding new devices for exploring, including an opportunity for variation of parameters for the elements in the system.

The organization of the programming system contains three basic functional parts [2] (Fig. 1). As a basic infrastructural part of the system it appears the module of controlling simulation cycles in time and providing necessary climatic parameters in relation to discretion of the processes in time. In this time it is included the deliverance of data about the solar radiation and the air temperature for different geographical regions. In this functional part it is included special solar radiation' processor, which recalculate solar radiation for given slope and orientation of the received surface, and optical parameters for solar radiation penetration through the transparent covers.

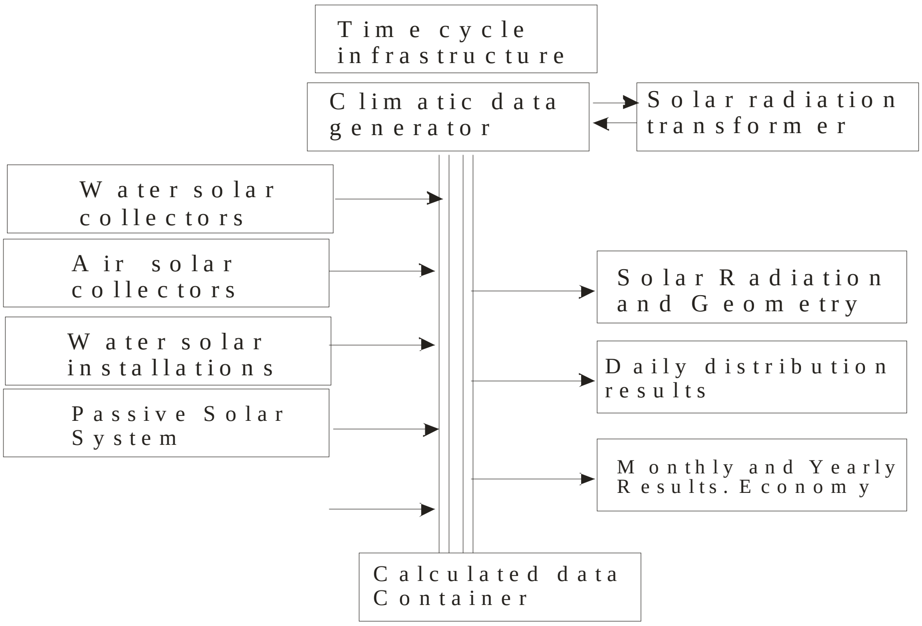

Fig. 1. Scheme of the program algorithm

The second functional part of the programming system is a set of programming modules for simulating heat and mass exchanging processes in different thermo-technical devices for utilizing solar energy. They are organized as separate programming structures according to the common infrastructural part of the programming system.

The third part of the programming system organizes the preservation of results from the calculations and a preparation of the necessary data. It is worked out a universal system for showing results for different periods of the simulation interval. Technical and economical estimations for solar systems can be generated on the base of received results from simulation calculations.

4. CONCLUSIONS

On the base of the existing data about solar radiation (for the region of city of Sofia) and the data about the duration of sun-shining it is achieved an assessment of the potentiality of the solar radiation on the territory of Republic of Bulgaria. A software product has been performed for simulation analyses of devices for thermal transformation of solar energy. It has modular structure for completing different installation schemes and it gives the opportunity to generate long-term assessments of thermal efficiency of devices. Program system can be successfully used not only for projecting purposes, but also for solving exploring tasks.

5. REFERENCES

[1] Shtrakov St, M. Batova (2002), Solar energy and thermal building analysis, *EuroSun 2002*, Bologna , June, 2002.
[2] Lui B.Y., R.C. Jordan (1960), The Interrelationship and Characteteristic Distribution of Direct, Diffuse and Total Solar Radiation, Solar Energy.
[3] Page J.K. (1978), Methods for the Estimation of Solar Energy on Vertical and Inclined Surfaces, Solar Energy Conversation.

[4] Duffie, J.,Beckman, W. (1980) Solar engineering of thermal processes, New York, Wiley Interscience.

[5] Halouani N., C.T.Nguyen (1993), Calculation of monthly average global solar radiation on horizontal surface using daily hours of bright sunshine, Solar Energy, 50, 247-258

INVESTIGATION OF AEROSOL SYSTEM EVOLUTION IN LIMITED VOLUME VIA LASER LIGHT SCATTERING

K.S. Damov* , A.S. Antonov**

**Mathematics and Natural Sciences Department, South-West University “Neofit Rilsky”, 66 Ivan Mihailov Str.,*
BG-2700, Blagoevgrad, Bulgaria
E-mail: damov@aix.swu.bg
***Institute of Nuclear Research and Nuclear Energy Bulgarian Academy of Sciences,*
BG-1784, 72, Tsarigradsko chausee blvd., Sofia, Bulgaria
E-mail: asantonov@abv.bg

Abstract: *This paper discusses some possibilities of researching the evolution of concentrated aerosol systems in a limited volume via laser light scattering. Changes of their density in the course of time are followed. Density measurements are carried out according to the method of free outflow. Experimental results concerning the smoke from different cigarette trademarks are presented. A new characteristic of the aerosol system – “state spectrum“, is introduced. The aerosol systems under investigation are characterized with its help.*

1. INTRODUCTION

An aerosol system with a volume of its own is a special state of the aerodispersion systems. This state can be witnessed in natural phenomena (fog, clouds, smoke from forest fires) as well as in laboratory conditions /1-5/. Because of the similarity of this state to a liquid state, i.e. the availability of a horizontal boundary when the system is formed in a closed vessel and of hydrostatic pressure, in /3, 4/ it was defined as “quasi-liquid” state. In essence this state is non-equilibrium since the system is open, i.e. the latter loses the substance held in it as a result of diffusion, evaporation via the upper boundary, sedimentation, deposition on the vessel walls, etc.

In some of our previous works /5-8/ we offered a method for measuring kinematics viscosity based on the aerosol outflow through a horizontal tube over the bottom of the vessel due to the action of the eigen aerosol hydrostatic pressure. In our papers /9,10/ we modified the method to measure the mass density of an aerosol system with eigen volume. The following expression for mass density was obtained

$$\rho_i = \frac{\eta_i}{\nu_i} = \frac{1}{b} . \frac{\Delta H_i}{\bar{H}_i} . \frac{\eta_0}{\Delta t_i} , \qquad (1)$$

where $b = \pi . r^4 . g \,/\, 8.l.S$, r is the radius of the horizontal tube, l - its length, g - earth acceleration, S – the cross-section of the vessel with aerosol, η_i - the dynamic viscosity, ρ_i - the density of the aerosol phase as referred to the interval ΔH_i , which is crossed by the diminishing upper boundary for time interval Δt_i , $\bar{H}_i$ is its average height with reference to the outlet tube.

Formula (1) makes it possible to define the density of the aerosol phase ρ_i , after measuring Δt_i and $\bar{H}_i$.

The present paper applies the modified method for determining the mass density to research of the evolution of the aerosol system after its formation. For this purpose before conducting the experiment to determine the mass density, the aerosol is left for some time t_z to stay in the chamber; we define that time as **"detention time"**. Then the tube at the lower end of the measurement chamber is opened and the aerosol is left to flow out through it. Seven values of mass density are determined (eight photodetectors being used). A series of experiments were conducted every other minute with detention times from zero to ten minutes.

2. EXPERIMENTAL RESULTS

2.1 Measuring the aerosol phase density in the course of time

Fig.1 illustrates the change in the mean density of the aerosol phase of the smoke of Arda cigarettes as a function of the detention time t_z . The mean density is defined by all the experiments with aerosol outflow. The same figure also presents approximation with an exponent (the thick line) and approximation with a straight line (the dotted line). The coefficient of linear regression - R^2, is pointed out. It can be seen that the two approximations practically overlap. This fact gives us ground to consider the dependence as a linear one. The lowest line is that of the mean quadratic error.

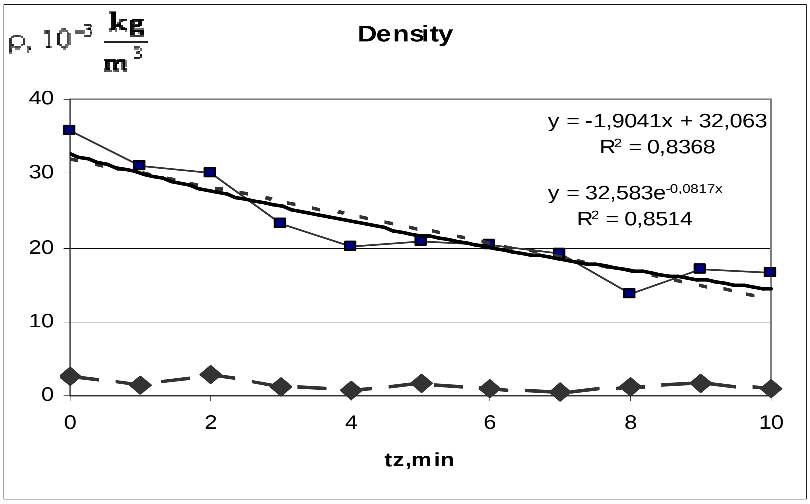

Fig.1 Change in the mean density of the aerosol phase of smoke from Arda cigarettes as function of the detention time t_z . The approximations are presented with a straight line (dotted) and with an exponential (thick) and the corresponding regression coefficients. The mean quadratic error for each detention time is also graphically illustrated – the lowest line.

Fig.2 presents the results obtained from Stuyvesant cigarette smoke. It can be seen that the initial density is twice as little as the density in the previous experiment. In either experiment the mean density for a particular detention time is determined on the basis of 21 values. The dependences to follow, curves, illustrate the mean quadratic errors for the respective experiments. Obviously, during detention time the density suffers fluctuations which are beyond the error limits. Analogous results were obtained in our papers (5-8) when determining the values of the aerosol system kinematics viscosity. Detention time t_z were analogous – from zero to ten minutes. That should be expected since $\nu_i = \frac{\eta_i}{\rho_i}$ and η_i is practically equal to the dynamic viscosity of air η_0 /1,81 . 10^{-5} ,Ns/m^2/.

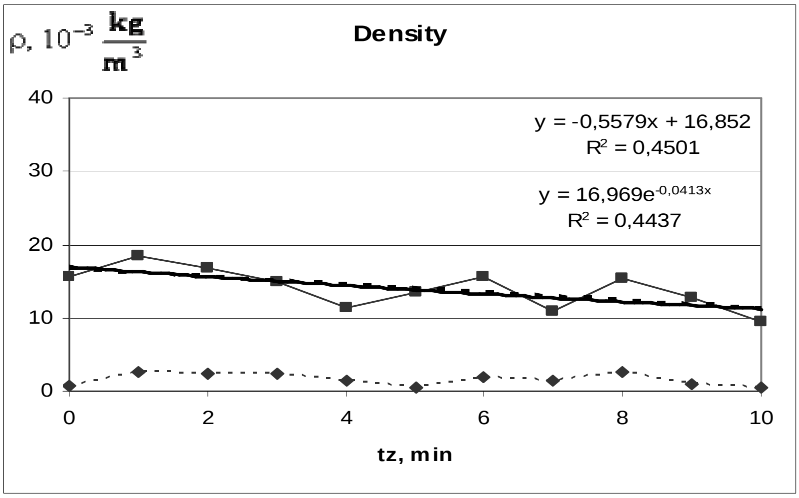

Fig.2 Change in the mean density of the aerosol phase of smoke from Stuyvesant cigarettes as a function of the detention time t_z. Approximations are presented with a straight line (dotted) and with an exponential (thick) and the corresponding regression coefficients. The mean quadratic error is also graphically illustrated – the lowest line.

Fig.3 illustrates time dependences of the aerosol system density (smoke from Arda cigarettes) at different heights of the upper limit. The curves come closest to each other within the 3rd - 6th minute time slot. This is a feature of the volume homogeneity of the system. The declension of the curve describing the change in system density at an upper limit of 0,285 m is the smallest. This is a proof that the system is the most stable in full volume, i.e. it evolves most slowly. Then the relative loss of substance, too, is the smallest due to sedimentation, deposition on walls, coagulation, etc.

Fig. 4 depicts the density (Ro) of the aerosol system (smoke from Arda cigarettes) in case of different volumes, i.e. at different heights of the upper aerosol limit. The data of the entire array is used. The straight line approximation (Linear Ro), the linear regression coefficient (R2) and the mean quadratic errors (S-Ro) are presented. The graphic shown (approximating a straight line) is a proof of the general volume homogeneity of the system.

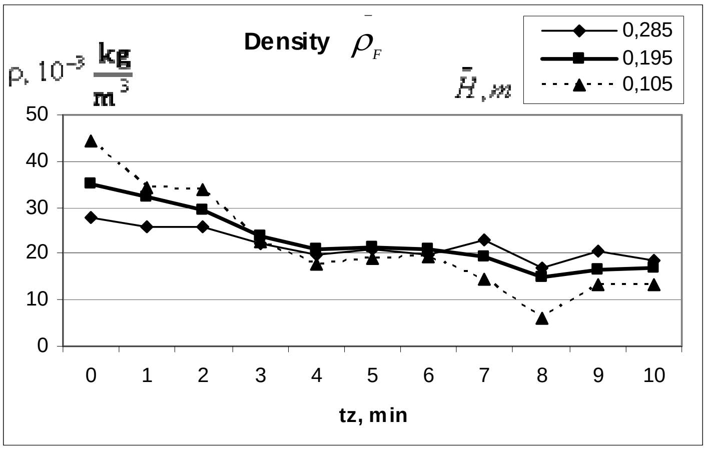

Fig.3 Change in the mean aerosol phase density of smoke from Arda cigarettes in case of three different volumes (the upper heights of the aerosol limit are indicated) and detention time from 0,min. to 10,min.

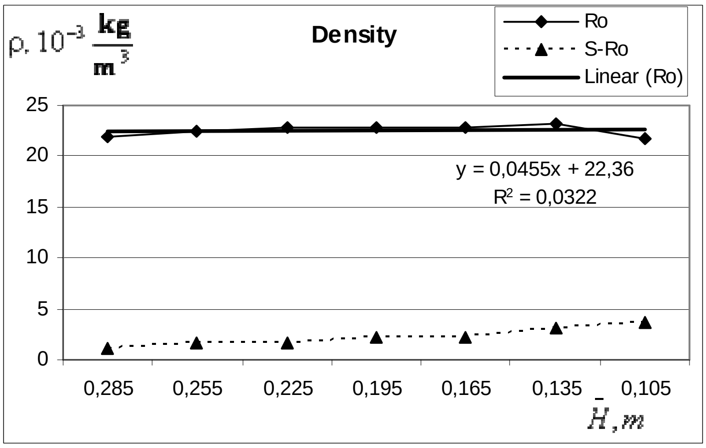

Fig.4 Mean aerosol phase density of the smoke from Arda cigarettes in different volumes (the upper heights of the aerosol limit are indicated along the OX axis). The data is summarized for the entire array of detention times, tz (from 0,min. to 10,min.). The straight line approximation and the mean quadratic errors are represented.

2.2 SPECTRUM OF THE STATE OF AEROSOL SYSTEM WITH EIGEN VOLUME

Change in aerosol system density depending on detention time t_z , in case of different heights from the vessel bottom can be characterized by means of the function of density distribution obtained via the following formula :

$$f_i = \frac{W_i}{\Delta\rho_i} = \frac{N_i}{\sum N_i} \frac{1}{\Delta\rho_i} \quad , \qquad (2)$$

where N_i is the number of ρ values in the interval $\Delta\rho_i$, $\sum N_i$ is the sum total of the values. $\Delta\rho_i = \Delta\rho = const$ are the steps in the change of the density, which is constant in our experiment and is equal to .10^{-3} kg/m^3. We called this function **“spectrum**

of the state of an aerosol system”. It is a general characteristic of the aerosol system and includes the array of all density values. The latter are obtained in the course of its time evolution at different heights of the upper level with respect to the vessel bottom.

Fig. 5 illustrates the spectrum of Arda cigarette smoke. The smoke of one cigarette can fill up the measurement chamber three times. Therefore we divided the cigarette relatively in three parts. A1 is the smoke released from the beginning of the cigarette, and A3 from the end respectively (the part nearest the butt). The shift of the spectra of the separate thirds is inconsiderable. This is a proof of the poor filtering quality of the tobacco in the cigarette.

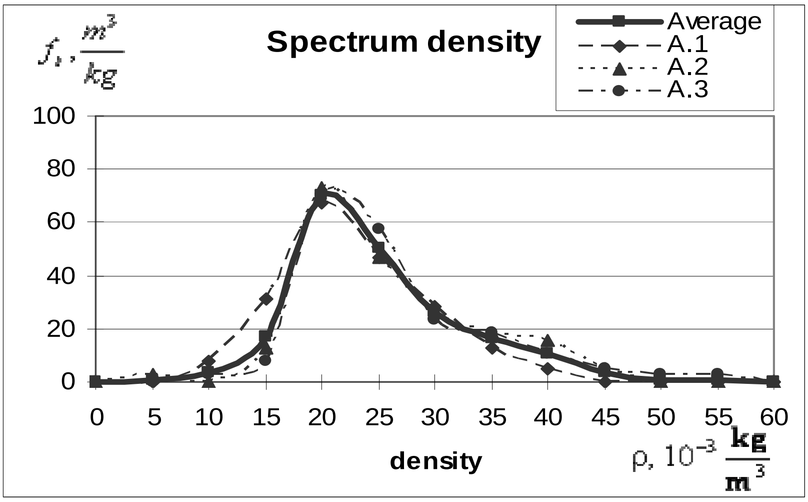

Fig.5 Spectrum of the state of Arda cigarette smoke – thick line. A1 through A3 are spectra of the state of the separate thirds.

Fig.6 illustrates the same dependence but for Stuyvesant cigarettes – a thick curve. Shift of the spectra of the separate thirds is obvious. This is a proof of the good filtering quality of the well-stamped tobacco in these cigarettes.

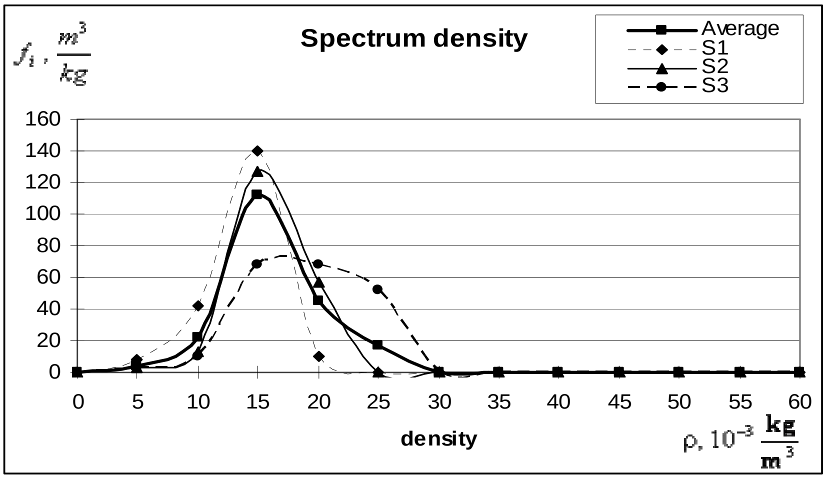

Fig.6 Spectrum of the state Stuyvesant cigarette smoke – a thick line , and of the separate thirds (S1 – S3).

The mean arithmetic density values (Average), the corresponding mean quadratic errors (SKG), the minimum (min) and maximum (max) values in the arrays for smoke from different cigarette trademarks are quoted in Table 1. The last two lines illustrate the semi-width (Semi-Width) and the fi function maximum from the corresponding spectra.

Table 1. Density of smoke obtained from different cigarette trademarks. The table illustrates the mean value, the mean quadratic error, the minimum and the maximum value in the array.

	DensIty Cigarette Smoke					
		Arda	Stuyvesant	Gauloises	Gitanes	Vega
Average	$\bar{\rho}, 10^{-3}\frac{kg}{m^3}$	22,54	14,06	24,15	19,31	24
SD	$\sigma_{\rho}, 10^{-3}\frac{kg}{m^3}$	0,498	0,261	0,422	0,336	0,47
Density-min	$\rho_{\min}, 10^{-3}\frac{kg}{m^3}$	4,28	2,79	12,36	7,09	6,05
Density-max	$\rho_{\max}, 10^{-3}\frac{kg}{m^3}$	50,57	24,72	44,5	38,37	57,69
fi-max	m^3/kg	80	130	66	118	64
Semi-Width	$\Delta\rho/\frac{1}{2}/, 10^{-3}\frac{kg}{m^3}$	11	6	18	8	17

3. CONCLUSIONS AND DISCUSSIONS

It is evident that the aerosol systems differ in density beyond the limit of the experimental (mean quadratic) error. This means that the state spectrum can be utilized as one new characteristic of the aerosol systems, in particular – for comparison and qualification of cigarette products.

What impresses is that the functions of density distribution for the different aerosol systems have a characteristic peak with a definite amplitude and semi-width. This shows that aerosol systems with eigen volume have a preferable density coinciding with the peak position. Probably, this is a basic regularity of these aerosol systems.

The range between the minimum ($\rho_{\min}$) and the maximum ($\rho_{\max}$) mass densities measured by us for the investigated aerosol systems (cf. Table-1) is too narrow – from 2,79- to 57,69.10^{-3} kg.m^{-3} (or in approximately 20-fold relationship). The relationship between the mass densities for well-established fluids is similar – about 4, which is of the same order. In the case of gases, the mass density depends on the pressure and it changes within very broad limits. For the atmospheric air, for instance, at an altitude of 10 km the density diminishes about 10^6 times. In view of this characteristic the aerosol systems in limited volume rather resemble fluids than gases, although in view of the absolute mass density value they come closer to gases.

4. REFERENCES

[1] N. Fuchs, N., Mechanics of Aerosols, Moscow, AS of USSR, Publishing House, 1955. /in Russian/.

[2] E. Regener, Z. Phys Chem., 1928.

[3] A. Petrova, Investigating Some Physical Properties of Aerosol Systems in Limited Volume, dissertation paper, Sofia, 1977. /in Bulgarian/.

[4] A. Antonov and L. Uskesselieva, About the Speed of Lessening Free Aerosol Limits in Aerosols Formed in Limited Volume, Papers of BAS, volume 34, №1, 1981. /in Russian/.

[5] A. Antonov and K. Damov, Method for Changing the Viscosity of Aerosol Systems, Odessa, XV AU-Union Conference, vol. 2, 1989, p.16. /in Russian/.

[6] K. Damov, and A. Antonov, Investigating the kinematic Viscosity of Aerosol Systems in quasi-liquid State, Comptes rendus de l’Academie bulgare des Sciences, Tome 48, №2, 1995, 29.

[7] K. Damov and A. Antonov, On the measurement of kinematic Viscosity of Aerosol Systems, 9th International Conference on Surface and Colloid Science, Sofia, 1997.

[8] K. Damov, Method and Structure for Determining, the Dynamic Viscosity of Aerosols, Miscellany of Investigations by Young Researchers, SWU Blagoevgrad, 1991, p.132. /in Bulgarian/.

[9] K. Damov, A. Antonov, Mathematics and Natural Sciences, South-West Univ. “Neofit Rilsky”, Blagoevgrad, Vol.1, 2005, 346. /in Bulgarian/.

[10] K. Damov, A. Antonov, Determining the Mass Density of Aerosol System in limited Volume via Laser Light Scattering, Journal of Applied Electromagnetism, Institute of Communication and Computer Systems, Athens-Greece. /in print/

ELECTRON SPIN INFLUENCE ON A LINEAR RESPONSE OF MAGNETIZED PLASMA

Ilia Giudjenov, Marek Tassev

South-West University ‘Neofit Rilski’, Blagoevgrad, Bulgaria

Peter Polyakov, Alexander Rusakov, Natalia Rusakova

Moscow State University, Moscow, Russia

***Abstract**: A spectrum of waves propagating in magnetoactive plasma along an external magnetic field taking into account electron spin is analyzed. A new branch of electromagnetic waves in magnetized plasma propagating along an external magnetic field is shown to appear due to the intrinsic magnetic moment of electrons.*

***Keywords:** Plasma, Hydrodynamics, Spin, Permittivity tensor, Electromagnetic waves.*

1. INTRODUCTION

In investigations of linear wave propagation in plasma, one usually neglects a value of a particles’ magnetic moment. Here we analyze the influence of the electron intrinsic magnetic moment on an eigenwave spectrum of homogeneous magnetoactive plasma for waves propagating along an external magnetic field on the basis of a hydrodynamic approach. As one will see below, this introduces some changes in the eigenwave spectrum in the case of dense plasma.

2. INITIAL EQUATIONS

In general, spin dynamics cannot be described on the basis of classical mechanics since it is an essentially quantum object. However, at certain conditions, an average value of the magnetic moment approximately satisfy an equation of classical precession [1]. We limit us with this approximation for the nonrelativistic theory:

(1) $$\frac{d}{dt}\vec{\zeta} = \left[\vec{\Omega}\vec{\zeta}\right],$$

where $\vec{\Omega} = \frac{g}{2}\frac{e\vec{B}}{mc}$, $\vec{\zeta} = \left\langle \vec{S} \right\rangle = \left\langle \frac{\hbar}{2}\vec{\sigma} \right\rangle$ is an average value of the spin operator by a classical wavepacket state, which moves along a classical trajectory, and g is the Landé factor.

Instead of an average spin value, it is convenient to use magnetization $\vec{I} = 2\mu n_e \vec{\zeta}/\hbar$ *and thus the following equation instead of (1):*

(2) $$\frac{\partial \vec{I}}{\partial t}+(\vec{v}\nabla)\vec{I}+\vec{I}\,\mathrm{div}\,\vec{v}=[\vec{\Omega}\vec{I}].$$

Particles with spin generate a so-called spin current:

(3) $$\vec{j}_S = c\,\mathrm{rot}\,\vec{I},$$

which appears as an addendum in Maxwell’s equations:

(4) $$\mathrm{rot}\,\vec{E}=-\frac{1}{c}\frac{\partial \vec{B}}{\partial t},\ \mathrm{div}\,\vec{B}=0,$$

(5) $$\mathrm{rot}\,\vec{B}=-\frac{1}{c}\frac{\partial \vec{E}}{\partial t}+\frac{4\pi}{c}\left(\vec{j}+\vec{j}_S\right),\ \mathrm{div}\,\vec{E}=4\pi\rho,$$

Furthermore, the presence of spin results in a change of Lorentz force due to an additional ponderomotive force that acts on magnetic moments in an inhomogeneous magnetic field:

(6) $$\vec{F}=\frac{1}{mn_e}\left((\vec{I}\nabla)\vec{B}+[\vec{I}\,\mathrm{rot}\,\vec{B}]\right)=\frac{1}{m_0 n}\nabla(\vec{I}_0\vec{B}).$$

Let us supplement the above with hydrodynamics equations: the continuity equation:

(7) $$\frac{\partial n}{\partial t}+\frac{\partial}{\partial \vec{r}}(n\vec{v})=0$$

and Euler’s equation:

(8) $$\frac{\partial \vec{v}}{\partial t}+(\vec{v}\nabla)\vec{v}=-\frac{e_0}{m_0 c}[\vec{v}\vec{H}]-\frac{e_0}{m_0}\vec{E}-\frac{1}{m_0 n}\left(\nabla P-\nabla(\vec{I}_0\vec{H})\right).$$

3. PERMITTIVITY TENSOR

After standard procedures of linearization and Fourier transformation, one yields the following expressions for permittivity tensor components in the case of wave propagation along the external magnetic field ($k_x = 0$):

(9) $$\varepsilon_{xx}=\varepsilon_{yy}=1-\frac{\omega_p^2}{\omega^2-\omega_B^2}-\frac{g^2}{4}\frac{k_z^2c^2}{\omega^2-\frac{1}{4}g^2\omega_B^2}\frac{\omega_\mu\omega_B}{\omega^2}.$$

(10) $$\varepsilon_{xy}=\varepsilon_{yx}^*=i\frac{\omega_B}{\omega}\frac{\omega_p^2}{\omega^2-\omega_B^2}+i\frac{g}{2}\frac{k_z^2c^2}{\omega^2-\frac{1}{4}g^2\omega_B^2}\frac{\omega_\mu}{\omega}.$$

(11) $$\varepsilon_{zz}=1-\frac{\omega_p^2}{\omega^2-k_z^2V^2}.$$

(12) $$\varepsilon_{xz}=\varepsilon_{zx}=\varepsilon_{yz}=\varepsilon_{zy}=0.$$

where $V^2 = \lambda\Theta/m$ *is the squared thermal velocity,* $\omega_p = \sqrt{4\pi e^2 n_0/m}$ *is the plasma frequency,* $\omega_B = eB_0/mc$ *is the electron cyclotron frequency and* $\omega_\mu = 4\pi e I_0/mc$ *is a characteristic frequency, which determines spin influence on plasma properties.*

The dispersion equations are the following:

(13) $$\frac{k_z^2 c^2}{\omega^2} = \varepsilon_{xx} \pm i\varepsilon_{xy} .$$

(14) $$\varepsilon_{zz} = 0 .$$

The second one describes Langmuir waves and the spin doesn't affect this equation. The first one is equivalent to the following:

(15) $$N^2 = \frac{\omega \pm \frac{g}{2}\omega_B}{\omega \pm \frac{g}{2}\left(\omega_B - \omega_\mu\right)}\left(1 - \frac{\omega_p^2}{\omega\left(\omega \pm \omega_B\right)}\right).$$

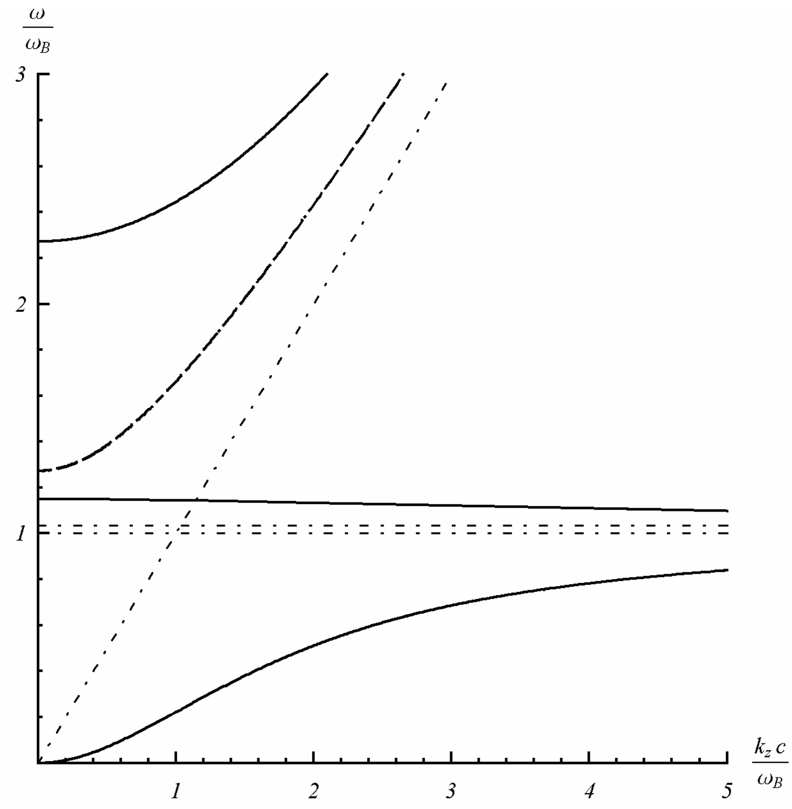

Fig. 1: Dispersion curves for transverse waves propagating along the external magnetic field for $\omega_p = 1{,}7\omega_B$, $\omega_\mu = 0{,}1\omega_B$, $g = 2{,}3$.

Fig. 1 demonstrates dispersion curves for equation (15). The dashed and solid lines correspond to the upper and lower signs, respectively; the dash-dotted lines are their asymptotes $\omega = \omega_B$ and $\omega = \frac{g}{2}\left(\omega_B - \omega_\mu\right)$. One can see that a new branch of electromagnetic waves appeared in the vicinity of cyclotron frequency due to the presence of electron spin. We note that the above parameter values are chosen for visual demonstration only (in particular, g is much closer to 2) to show a qualitative shape of the curves.

4. RESULTS, DISCUSSIONS, CONCLUSIONS

An analysis of dispersion relations for waves in magnetoactive plasma taking into account an electron spin shows a new eigenwave branch to appear in the vicinity of cyclotron frequency with a resonance at frequency $\omega = \frac{g}{2}\left(\omega_B - \omega_\mu\right)$ for transverse waves propagating along an external magnetic field. In dense plasma, the magnetization can be large enough for this frequency to significantly differ from the cyclotron one and thus qualitatively new effects in the resonance regions. We also note that the shape of this branch doesn’t depend on the thermal straggling in the hydrodynamic approach.

5. REFERENCES

[1] Krall, N., Trivelpiece, A. W. (1973) Principles of Plasma Physics, New York, McGraw-Hill.

[2] Polyakov, P. A. (1979) O gidrodinamicheskom opisanii voln v plasme s uchetom spina elektronov. Izvestiya vuzov SSSR, 3, 101-103 [in Russian].

[3] Kim, N. E., Polyakov, P. A., Rusakov, A. E. (2005) Kollektivniye spinoviye effekty v klassicheskikh plasmennykh sistemakh (Collective spin phenomena in classical plasma systems), Nelineiny mir (Nonlinear world), 3, 155–162 [in Russian].

[4] Kuzmenkov, L. S., Kharabadze, D. E. (2004) Volny v sistemakh chastits s sobstvennym magnitnym momentom (metod kvantovoy gidrodinamiki), Izvestiya vuzov. Fizika, 4, 87-93.

ESTABLISHMENT OF THE DEPARTMENT OF PHYSICS AT THE SOUTH-WEST UNIVERSITY N. RILSKI

Ivan Amov, PhD, Honourable Professor of the South-West University

South West University, Blagoevgrad

In 1976, in the town of Blagoevgrad, was established a affiliate faculty of the Sofia University “St. Kl. Ohridski”, specialized in education of Kindergarten and Elementary Teachers. In 1983, the Faculty has separated as an independent Higher Pedagogical Institute and become an important cultural and ideological centre in the Region of Southwest Bulgaria. For a first time in the history of Bulgarian Higher Education, a specialty of Entrepreneurial and Polytechnic Education has been offered through the faculty of Engineering-Pedagogy. Other specialties include Pedagogical Interaction with Children with Behaviour Problems, Bulgarian Language, and History.

During 1985, Prof. Dr. I. Amov and his Assistant Krasimir Damov began teaching physics at the Faculty of Engineering-Pedagogy. Their team grew in the following years when Prof. Dr. A. Antonov, from Bulgarian Academy of Science joined them in teaching courses in Lasers as well as Prof. Dr. L. Yukselieva teaching courses in field of Aerosol’s

Physics. Due to an increased interest and high number of applications, the entrance exams were marked by a large team of Professors from The Higher Institute of Architecture and Civil Engineering, among who were Prof. Dr. N. Ivanchev, Prof. Dr. R. Pirinchieva, and Prof. Y. Georgieva. Part of this committee was the Vice Dean , Prof. Dr. Vassil Metev (picture 1).

Pic. 1.

Pic. 2

In 1987, interviews and tests were conducted to hire more Associate Professors for teaching courses in Physics and Physics and Mathematics. Some of them were Eng. Plamen Gramatikov, D. Doshkova, V. Gaberov, K. Dimitrov, R. Popova, V. Vukova, R. Vasileva, and others. The first physicists with the faculty were D. Kaisheva and I. Rupelski; technicians T. Petrov and M. Manolev, and lab consultant is V. Kovachev, student.

The majority of the Lab Equipment used through the first year was borrowed from VIAS. Similar to engineering organization of VIAS, a manufacturing and educational complex employing students was created in VPI. Most of the students working in it were ones who failed courses and did an apprenticeship for a period of eight months. Production of Lab Equipments for Physics has been the main focus of the Student’s complex. Pioneered by prof. N. Bojkov, two course projects were included in the curriculum. The first one emphasising on the technical application of the physics while the second one on the methodology. An example of such a project was one of the student theses called: “Physics instruments, developed in entrepreneurial classes”. Project like this one helped us create unique lab basis. There were created physics instruments which parameters competed with international and well recognized companies such as Siemens and Texas Instruments. The Student Educational Manufacturing Complex received orders from Electroimpex for supplying lab equipment to some schools in Nigeria, Mozambique and other developing countries. At this time, prior to us being recognized as an Independent University, the equipment produced by us was labelled as being produced by the University in Blagoevgrad, Bulgaria (pic. 2). As a result of our cooperation with Electroimpex, they had provided us with labs in Mechanics, Optics, and Electricity and Magnetism, which were all produced in the Bument’s Aviation Institute (pic. 3).

In addition to the above labs, we had received high quality testing equipment, ampermeters and voltmeters class 0.2, generators, and oscilloscopes from Tesla and Metra companies in Czechoslovakia (pic 4).

Pic. 3

Pic. 4

At the National Physics Conference 1987 – Pazardjik, our team presented laser, video, and laboratory equipment. A group of twenty students from Blagoevgrad demonstrated the application of such lab equipment (pic 5). This lead to increasing the number of applicants for physics at Blagoevgrad University from Vidin, Montana, V. Turnovo, Burgas, Varna, Stara Zagora, and other towns.

Acad. M. Borisov has accepted an invitation to teach a series of lectures to the physics students (pic 6). He congratulated us for our achievements and encouraged us to further look at the curriculum for year four and the creation of scientific labs. Taking further his recommendations, we had created three streams in our program, Metrology, Physics & Biophysics, and Methodology of the Education in Physics and Technical Sciences. The Metrology had further transformed into the field of Alternative Energy under the project director Associate Professor P. Gramatikov, PhD. Under the scientific advising of Associate Professor St. Shtrakov, PhD , A. Stoilov defended successfully a PhD thesis in this brunch of science. He became the first of our students to receive PhD degree. An important part of the popularization of the Physics among the Blagoevrad’s community is the exhibition with topic “Chernobyl” and the lecture of prof. Chvetan Bonchev, past Dean of the Faculty of Physics with the Sofia University. More promotional lectures had been thought by other professors, among who is Prof. Dr. Sazdo Ivanov, the longest-serving president of Technical University - Sofia and vice president of the Institute of Physics with the Bulgarian Academy of Science.

Pic. 5

Pic. 6

In honour to the father of the Bulgarian Physics, Acad. G. Nadjakov, the main teaching hall was named after his name. The first year physic’s students established alumni called Academic G. Nadjakov, while the physics and mathematics alumni was named after

Professor Dr. Elisaveta Karamihailova. When commemorating her Ninetieth birthday, students brought wreath at her tombstone. Prof. Dr. Chvetan Bonchev, said: “Students from Blagoevgrad, who didn’t know her are here, but some of her followers didn’t come.”

Although we had created a general physics lab, we still had some problems conducting specific lab experiments. The newly established experimental lab at VIAS (with Directors Kr. Krustev and N. Mihailov) began the development of unique lab equipment. In cooperation between the Higher Pedagogical Institute and VIAS, there were created “Photo electronic emission” (pic. 7, [1],116-120), “The Hall’s effect” (pic. 8, [1],136-139). The Optics Lab has received new equipment “Polarization of the light” (pic. 9)

Some of the experiments conducted in the Nuclear Physics Laboratory were the “Plank’s Constant” and “Electron’s mass calculation” ([1], 83-95). These experiments were further adopted in most of the Technical Universities in Sofia, Gabrovo, Russe, the High Military Schools in Bulgaria and others.

The Engineering specialty in the Radio-physics was developed after the transfer of Dr. M. Dimitrova from the Medical Academy to the Higher Pedagogical Institute and the creation of the Engineering Physics Department (pic. 10). The first Associate professor there was T. Hrulev.

Pic. 7

Pic. 8

Parallel with the educational process, scientific research in the field of biophysics was conducted under the directions of Prof. Dr. A. Antonov. He had brought a lot of expertise moving from the Bulgarian Academy of Science to University N. Rilski. Under the leadership of Prof. Dr. J. Stamenov, director of INRNE – BAS, and PhD student Ivo Angelov (former student in Physics at the SW University), a muon telescope was constructed. The Department of Physics has been proud with the in-house constructed 1.5 кWp photo-voltaic converter, and the converter of solar energy to thermal one. They has been mounted on the North Roof of the University.

Pic. 9

Pic. 10

Under the leadership of Associate Professor L. Mihov, PhD and Prof. Dr. L. Pavlov, research in the area of lasers and new telecommunication technologies were conducted. Assistant D. Kerina had done her PhD. in the field of condensed matter under the supervision of Prof. Dr. M. Gospodinov from BAS. Associate Professor Kerina, PhD was the youngest scientists in the Department of Physics to become associate professor. Very successful in the field of Methodology of Physics are Associate Professor P. Bozarova, PhD , Assistants Dr. R. Vasileva, PhD , Assistant R. Popova, Assistant V. Kovatchev and others. Most of our graduates have successful careers in regional meteorological centres, manufacturing plants, private companies, BAS, Schools, and other sectors of the economy. Our physics team successfully participates in many international seminars and experiments in USA, England, Norway, Taiwan, Switzerland, France, Russia, Greece, Germany, Spain, and other countries.

The Department of Physics at the Faculty of Natural Science and Mathematics currently offers Bachelor, Master and PhD degree programs (PhD programs in cooperation with BAS) as well as specialized courses for further education.

The Bulgarian National Agency for Evaluation and Accreditation, a body of the Council of Ministers, granted an institutional accreditation to the South West University on March 9, 2006 with the highest degree – VERY GOOD, for the longest period of Durability – 6 years.

REFERENCES

[1]. Manev, Hr., Physics Lab Textbook, 1995

COMPARATIVE STUDY OF METHODS FOR POTENTIAL AND ACTUAL EVAPOTRANSPIRATION DETERMINATION

Boyko Kolev

South-West University, Blagoevgrad, Bulgaria

***Abstract**: Two types of methods for potential and actual evapotranspiration determining were compared. The first type includes neutron gauge, tensiometers, gypsum blocks and lysimeters. The actual and potential evapotranspiration were calculated by water balance equation. The second type of methods used a simulation model for all calculation. The aim of this study was not only to compare and estimate the methods using. It was mainly pointed on calculations of water use efficiency and transpiration coefficient in potential production situation. This makes possible to choose the best way for water consumption optimization for a given crop. The final results find with the best of the methods could be used for applying the principles of sustainable agriculture in random region of Bulgarian territory.*

***Keywords:** neutron gauge, tensiometers, gypsum blocks, lysimeters, actual and potential evapotranspiration, water balance equation, simulation model.*

1. INTRODUCTION

There is a stable tendentious in the world during the past several years for increasing the yield from serials (wheat, maize, etc.). This is not only because of results in genetic area, but also because of new perfect agricultural technology applying in plant science. Unfortunately there are not only successes in this field but some negative tendentious could be finding. Especially for Bulgaria the last tendentious take part because of a lot of factors, which concentrated the idea for sustainable agricultural. Bulgarian limited water resources and no sufficient water use are the main reasons of this. Determining the potential production and its main components - potential evapotranspiration (ETP), transpiration coefficient (TRC) and water use efficiency (WUE) is the right way to find the solution for improving the situation. Two types of methods potential and actual evapotranspiration determining are compared in the study. The first type includes neutron gauge, tensiometers, gypsum blocks and lysimeters. The actual and potential evapotranspiration were calculated by water balance equation. The second type of methods uses a simulation model for all calculation. The experiments were carried out in the experimental field of the Poushkarov Institute of Soil Science near Tzalapitza village – Plovdiv region in Southern Bulgaria.

The aim of this study is not only to compare and estimate the methods using. It is mainly pointed on calculations of water use efficiency and transpiration coefficient in potential production situation. This makes possible to choose the best way for water consumption optimization for a given crop. The results find with the best of the methods could be used for applying the principles of sustainable irrigation scheduling in random region of Bulgarian territory.

2. MATERIALS AND METHODS

The experimental field of the Poushkarov Institute of Soil Science near Tzalapitza village – Plovdiv region in Southern Bulgaria is situated on about 188 meters above sea level on left riverside of Maritza River. The mean air temperature is 11.7 º C and the annual rainfall is 548 mm with maximum during the spring and summer and minimum during the autumn and winter (Hershkovich, 1984 [2]). The soil type in the experimental field was determined as Fluvisol (Alluvial Meadow soil). The field experiment was carried out on an area of 4 daa with winter wheat (Pobeda variety) in two variants (irrigated and without irrigation) each of them in four repetitions. Gravimetric method (Kolev, 1994 [4]), neutron probe (Vichev et al. (1996) [7]), electrical resistance blocks (Vichev et al. (1996) [7]) and tensiometers (Kolev, 1994a [5]) were used for the soil water content and soil water dynamics determination. For irrigation scheduling in the experimental plots were used compensation lysimeters (Glogov et al. (1986) [1]).

With gravimetric methods water content is determined from the weight difference of wet and dry sample. Typically, with gravimetric method the soil sample is collected and weighted. The sample is then dried in an oven at about 105 ºC until constant weight is reached, and the dry sample weight is determined. The basic equation expressing soil water content on a dry mass basic is:

(1) $$\mathrm{W} = \mathrm{M}_{\mathrm{w}} / M_s$$

Where:

W is the soil water content (g/g);

M_w is the mass of water in the soil sample (g);

M_s is the mass of the oven dry soil in the sample (g).

On a bulk volume basis the volumetric moisture content, Θ, (cm^3/cm^3, or cm/cm) is expressed as:

(2) $$\Theta = V_w / V_b$$

Where:

V_w is the volume of water in a soil sample (cm^3), which is approximately numerically equal to the mass of water, since the density of water ρ_w is approximately 1.0 g/cm^3;

V_b is the bulk volume of the sample (cm^3).

When the bulk density of the dry soil mass ρ_b (g/cm^3) is known and with the density of water being approximately 1.0 (g/cm^3), a very useful relationship is:

(3) $$\Theta = \rho_b * W / \rho_w = \rho_b * W \quad \text{(numerically)}$$

In obtaining accurate field data, the samples must not lose water between the time of collection and weighting. The cans should be as airtight as possible and should be weighted as soon as possible. After the sample is oven dried, it is typically cooled before re-weighting in the dry atmosphere of a desiccator or with the container lid on. This method is very time and manpower consuming, but it is still the most useful method in experimental works and irrigation practice (Kolev, 1994 [4]).

Tensiometers are commonly used in situ to measure soil water capillary pressure up to approximately 80 centibars (80 kilopascal KPa). If there is a definite relationship between soil water content and capillary pressure for the given soil it might be possible to determine water deficit and irrigation requirements. This means, that tensiometers could be used in lysimeters and irrigated variants only. When the soil water capillary pressure became bigger than 80 KPa it is necessary other methods to be used (Kolev, 1994a [5]).

Electrical resistance blocks allow determining soil moisture content in wide interval because of the relation between resistance of the porous material (measured by resistance meter) and moisture content and capillary pressure of the soil. The limitation of these blocks is the sensitivity of the resistance measurements to the salinity levels in the soil water. Gypsum blocks tend to deteriorate in the soil, especially in a sodic soil, or where the soil remains at high moisture levels for much of the season (Vichev et al. (1996) [7]).

The neutron probe method is an indirect method that measured the degree to which high-energy neutrons are slowed down (or thermalized) in the soil by the hydrogen atoms in water. The high-energy neutrons, which are emitted from a radioactive source, collide with atomic nuclei that are nearby. Since the hydrogen atoms in water have about the same mass, they are very effective in slowing the neutrons down. The rate at which thermal neutrons are detected relative to high-energy neutrons emitted is proportional to number of hydrogen nuclei in the vicinity of the source. The volume of soil measured by the probe varies with the moisture content. The radius of primary influence may be only 8 cm in the moist soil and 30 cm in the dry soils. Because of this sphere of influence, measurements closer than 18 cm to the ground surface are usually not made. The proportionality constant between thermalized neutron count and moisture content varies from probe to probe and with different access tubes. The calibration curve supplied with the probe can be used if the recommended access tube is also used. Calibration can be accomplished through comparison with results of gravimetric or other methods. Calibration with one soil can hold for all soil types, except in the presence of a material affecting thermalization.

The important ting is that neutron probe method could be used in very large range of soil water content: from permanent wilting point up to field capacity. This method could be applied for soil water content in both irrigated and non-irrigated experimental plots (Vichev et al. (1996) [7]).

Lysimeters are devices for measuring evapotranspiration. The crop is planted in large tanks and either trough measurement of weight loss, inflow-outflow, or other means the water losses to evaporation and transpiration can be quantified. When lysimeters are properly constructed and set in the representative sites, they can provide the most accurate measurement of evapotranspiration. Initial and maintenance costs have limited their use primarily to research, except in a few large irrigation projects. Further discussion of lysimeters for research purposes is present in Glogov et al. (1986) [1].

For calculating the potential winter wheat production a simulation model was used according to van Keulen and Wolf, (1986) [3] in the version suggested by Kolev, 1994a [5]. The reference crop evapotranspiration (potential evapotranspiration) ETP, according to this model could be calculated after relevant simulation procedure. This procedure uses Penman-Monteith (1965) [6] equation for ETP computing:

$$LE = \frac{1}{((\Delta+\gamma)*(1/h_u + 1/Cs)/1/h_u)}(\Delta R_N + h_u(e_d - e_a)) \tag{4}$$

Where:

E is the evaporation rate from water surface (kg/m^{2}d);

L is latent heat of vaporization of water (2450*10^3 J/kg);

Rn is net radiation (J/m^{2}d);

hu is the sensible heat transfer coefficient (J/m^{2}d °C);

ea is the water pressure at standard screen height (mbar);

ed is the saturation vapour pressure at air temperature;

Δ is the slope of saturation vapour pressure curve between the average air temperature and dewpoint;

Cs is conductance for water vapour, expressed in the same units as h_u.

In the case of crop canopy Cs represents the conductance of a large number of leaves placed in parallel and is referred to as the surface conductance. For a well – watered crop, i.e. under conditions of potential transpiration Cs appears much larger than h_u. The influence of the correction factor in Equation 4 is therefore rather small. For practical purposes, therefore, the Penman equation in its original form appears to be a useful estimate of transpiration losses by crops. In the case of water storage, the closure of stomata is reflected in a decrease of the canopy conductance Cs.

However, the difference in albedo between a water surface and a green crop surface, which is 0.05 for the first and roughly 0.25 for the latter, has to be taken into account. The water loss that is calculated in this way is referred to as the potential evapotranspiration of a closed, short green crop surface well supplied with water. The prefix ‘evapo’ is used, because no distinction is made between water loss by transpiration from the leaves and that by evaporation from the wet soil surface under the crop.

The rate of change in soil moisture content of the root zone could be described with a water balance equation follow:

(5)
$$RMS = (IM + (CD - D) - T) / RD$$

Where:
RSM is the rate of change in moisture content of the root zone (cm^3/cm^3.day);
IM is the rate of net influx through the upper root zone boundary (cm/day);
(CR-D) is the rate of net influx through the lower root zone boundary (cm/day);
T is the rate of crop transpiration (cm/day);
RD is the depth of the root zone (cm).

The maximum transpiration rate under conditions of optimum water supply is a function of total surface area of all transpiring leaves and the potential transpiration rate T_0. The latter represents transpiration under the prevailing environmental conditions of a well watered, closed, short, green, standard crop as defined by Penman. Assuming proportionality between light interception by the leaf surface and transpiration, the maximum transpiration rate is approximated by:

(6)
$$T_m = (1 - e^{-0.4*LAI}) * T_0$$

Where:
T_m is the maximum transpiration rate (mm/day);
T_0 is the potential transpiration (mm/day);
LAI is leaf area index (m^2/m^2).

Assuming the leaf area index of a closed standard crop to be 5 to 6, the potential transpiration rate can be written as:

(7)
$$T_m = (1 - e^{-0.4*LAI}) * T_0$$

Where:
ETP is the potential evapotranspiration (mm/day);
E_0 is evaporation (mm/day).
The maximum transpiration rate becomes:

(7)
$$T_m = (1 - e^{-0.4*LAI}) * (ETP - 0.1 * E_0)$$

Plants experience water stress if matric suction (ψ) is either too low or too high.

The relation between water use and dry-matter production was recognized already by early investigators in agricultural science and many experiments were carried out to determine the extract dependencies between two variables.

In case of a fully closed crop canopy, where soil evaporation is negligible the potential evapotranspiration determined by Penman’s equation equals to potential transpiration. In the situation where a crop has non-regulating stomata, the Penman’s equation underestimates the potential transpiration. Correction factors for such conditions, which have been calculated by comparing Penman values to transpiration values, calculated with a detailed physiologically based model of crop growth. The results are tabulated in Tab. 1.

Tab. 1: Correction factors for multiplying the ET to obtain potential crop transpiration in the absence of stomatal regulation.

Species	Sky condition	
	Clear	Overcast
C_3	1.47	2.1
C_4	1.6	3.0

Under conditions of temporary water shortage in the soil, leading to partial stomatal closure, assimilation and transpiration are affected approximately to the same event; hence the value of the transpiration coefficient remains constant. This characteristic permits an evaluation of influence of moisture shortage on production. If the amount of moisture available for plant uptake is lower than potential transpiration, actual transpiration falls short of the potential.

Although the relation between transpiration and assimilation may not vary under different nutritional conditions, overall water-use efficiency (WUE), expressed as dry-matter production per unit of water applied, either because of rain or by irrigation, may well be affected. It is important therefore to distinguish between field water use efficiency, which may include all sorts of losses and the true transpiration coefficient, which expresses the amount of water actually transpired per unit of dry-matter produced. In the water balance calculations both processes are treated therefore separately.

The review of the methods for soil water content determination shows that only gravimetric and neutron probe methods could be used in all range of available water content (between wilting point and field capacity) and for estimation of the simulation model predictions. These two methods will be compared in present study.

3. DISCUSSION

The yields in the irrigated variant and in the lysimeter were obtained after 6 times irrigation as follow: between 05.04-05.05. – irrigated with 53.6 mm 2 times; between 06.05-12.06. – irrigated with 67.8 mm 3 times; between 13.06-05.07. – irrigated with 16.1 mm ones. The soil water dynamics over post-dormancy period determined by gravimetric and neutron probe methods and simulation model are shown on Tab. 2.

Tab. 2: Soil moisture dynamic over post-dormancy period of winter wheat development.

Variants	Methods	Day/Soil moisture content (cm^3/cm^3)				
		05.04	05.05	12.06	22.06	05.07
Non-irrigated	Gravimetric	0.234	0.218	0.119	0.163	0.170
	Neutron probe	0.235	0.216	0.115	0.161	0.160
	Simulation model	0.248	0.201	0.140	0.150	0.165
Irrigated	Gravimetric	0.264	0.274	0.211	0.215	0.146
	Neutron probe	0.260	0.268	0.209	0.210	0.140
	Simulation model	0.270	0.290	0.220	0.230	0.180

The average difference between gravimetric and neutron probe methods is 0.0034 cm^3/cm^3, with standard deviation of 0.0037 cm^3/cm^3 and confidence limit of 0.0032 cm^3/cm^3 ($\alpha=0.05$) for the non-irrigated variants. The same values for irrigated variants are average - 0.0046, standard deviation - 0.0015 cm^3/cm^3 and confidence limit ($\alpha=0.05$) -

0.0013 cm^3/cm^3. This means, that neutron probe method could be successfully used as independent and reliable method for soil moisture dynamics determination. The average difference between gravimetric method and simulation model is 0.000 cm^3/cm^3, with standard deviation of 0.015 cm^3/cm^3 and confidence limit of 0.013 cm^3/cm^3 (α=0.05) for the non-irrigated variants. The same values for irrigated variants are average - -0.016 cm^3/cm^3, standard deviation - 0.010 cm^3/cm^3 and confidence limit (α=0.05) - 0.008 cm^3/cm^3.

The soil moisture dynamics is in direct relation with evapotranspiration. The results find by using of neutron probe and simulation model methods are shown in Tab. 3.

Tab. 3: Actual evapotranspiration (mm/day) over post-dormancy period.

Variants	Method	Period/Actual ET(mm/day)				Total ET (mm)	Mean ET (mm/day)
		05.04-05.05.	06.05-12.06	13.06-22.06.	23.06-05.07		
Non-irrigated	Neutron probe	1.6	2.3	1.8	0.9	166.3	1.8
	Simulation model	2.0	3.0	0.4	0.6	185.4	2.0
Irrigated	Neutron probe	1.9	4.8	3.0	7.0	358.1	3.9
	Simulation model	1.6	3.2	2.2	5.6	260.2	2.8

The average difference between neutron probe method and simulation model is 0.25 mm/day, with standard deviation of 0.93 mm/day and confidence limit of 0.91 mm/day (α=0.05) for the non-irrigated variants. The difference between total evapotranspiration determined by two methods is 19.1 mm (11.5 %) for the total evapotranspiration with a mean value of 0.2 mm/day for the whole period. The same values for irrigated variants are average - 1.33 mm/day, standard deviation - 0.59 mm/day and confidence limit (α=0.05) - 0.58 mm/day. The difference between total evapotranspiration determined by two methods is 97.9 mm (27.3 %) for the total evapotranspiration with a mean value of 1.1 mm/day for the studied period.

For finding an idea about the role of the water in yield formation transpiration coefficient and water use efficiency are used. The yields and the two important water efficiency parameters are presented in table 4.

As could be seen the lowest water use efficiency is in the lysimeter where for 1 kg grain was used 214 kg of water and the TRC is 510 kg/kg. According to the simulation model maximum TRC were find in non-irrigated variant – 633 mm/day or more than 24 % bigger than this in lysimeter. There were no principal differences between WUE and TRC determined by neutron probe and simulation model in irrigated variant. The most effective variant is non-irrigated, where for yielding of 1 kg grain was used only 156 kg of water, which is about 15 % smaller than water used for the same production in irrigated variant and more than 37 % smaller than used water in lysimeters.

Tab. 4: Yields, water use efficiency (WUE) and coefficient of transpiration (TRC) for winter wheat.

Variants	Methods	Yields (kg/ha)	WUE (kg/kg)	TRC (kg/kg)
Non-irrigated	Neutron probe	6450	156	388
	Simulation model	3950	286	633
Irrigated	Neutron probe	8150	179	478
	Simulation model	7800	178	500
Lysimeter	Neutron probe	7640	214	510

4. CONCLUSIONS

Neutron probe and gravimetric methods could be used for soil water content determination and for estimation of the results finding by using of the simulation model. The important advantage of the neutron probe method is that it is no as time-consuming as gravimetric method.

Simulation model gives good estimations of grain yield, water use efficiency and transpiration coefficient for irrigated areas.

The simulation model and lysimeter could be successfully used for winter wheat irrigation management and scheduling in Tzalapitza region.

5. REFERENCES

[1] Glogov L. et al., 1986. Management of the irrigation process for maize crop by compensation lysimeters. International Symposium “Water management for agricultural development”. Athens, 7th-11th April 1986. 280-282.

[2] Hershkovich E., 1984. Agricultural and climatic resources of Bulgaria. Published by Bulgarian Academy of Science. Sofia.

[3] Keulen H. van & J. Wolf [Eds.], 1986. Modelling of agricultural production: Weather, Soils and Crops. Simulation Monographs. Pudoc. Wageningen. The Netherlands.

[4] Kolev B., 1994. Utilization of a simulation model of winter wheat productivity. J. Plant Science. 5-6, 14-16. (Bulgarian).

[5] Kolev B., 1994a. Universal model applications for evaporation from free water surface and potential evapotranspiration calculation. In: Proceedings of the Fifth national symposium with international participation “Physics – Agriculture”, 119-124. (Bulgarian).

[6] Monteith J. L., 1965. Evaporation and environment. In: Fogg G.E. (Ed.) The state and movement of water in living organisms. Cambridge University Press, London.

[7] Vichev B., Kostov K., Kolev N., Kirkova J., 1996. A field study of device for soil moisture measurement. J. Agricultural machinery, 1, 38-42 (Bulgarian).

NOVEL MATERIALS FOR NONLINEAR OPTICS

Němec I.[a], **Matulková I.**[a], **Macháčková Z.**[a], **Císařová I.**[a], **Němec P.**[b], **Mička Z.**[a]

[a]*Department of Inorganic Chemistry, Faculty of Science, Charles University in Prague, Czech Republic.*
[b]*Department of Chemical Physics and Optics, Faculty of Mathematics and Physics, Charles University in Prague, Czech Republic.*

Abstract: *Novel materials for nonlinear optics, which are based on salts of guanidine and its derivatives, e.g. aminoguanidine, diphenyl-guanidine, guanylguanidine (biguanide) and phenylbiguanide, with selected inorganic (i.e. nitric, phosphoric, phosphorous, sulphuric) and dicarboxylic organic acids (i.e. oxalic, L-tartaric) have been prepared. Crystal structures, vibrational spectra, thermal behaviour and efficiency of second harmonic generation are presented and discussed.*

Keywords: *crystal structure, vibrational spectra, hydrogen bonds, second harmonic generation*

1. INTRODUCTION

Selected highly polarizable organic molecules are, according to their physical properties (large second order molecular polarizibilities, higher resistance to optical damage, etc.), very promising substances in the field of nonlinear optics (NLO). Many strategies [1] for forming acentric structures exhibiting second harmonic generation (SHG) have been followed and hydrogen bonded networks appear to be the most exciting among all these approaches. The utility of hydrogen bonded motifs in the generation of new materials have been extensively reviewed [2-5]. The ability of the hydrogen bonds, in particular, to orient polarizable cations in hydrogen bonded networks of anions has paved the way for the synthesis of a large number of materials for nonlinear optics [6-10] as these networks lead to non-centrosymmetric crystals for second harmonic generation.

So, one branch of NLO materials science is dealing with hydrogen bonded salts of polarizable organic cations. Materials based on these salts display a number of favourable properties: they are colourless, transparent and soluble, and have, in general, good mechanical properties, including relatively high melting points. Such thermal stability is crucial if SHG-active materials are to be successfully incorporated into working optoelectronic devices. In addition, the simplicity of the synthetic route makes it easy to generate a range of materials with a variation in a specific property, e.g. refractive index.

In this contribution we are reporting on novel compounds prepared in our research group, which are based on salts of guanidine and its derivatives, e.g. aminoguanidine, diphenylguanidine, guanylguanidine (biguanide) and phenylbiguanide, with selected inorganic (i.e. nitric, phosphoric, phosphorous, sulphuric) and dicarboxylic organic acids (i.e. oxalic, L-tartaric). The attention focused on guanidine and its derivatives is based on fact that guanidine is a substructure of many biologically important molecules [11]. Guanidine and its cation are special cases of n-π conjugated heteroallylic systems with six π electrons [12,13] (so called “Y aromaticity”). Such electron delocalization leading to “Y aromaticity” was also observed in the case of guanidine phenylderivatives [14]. Moreover, the richness of intermolecular interactions in this group of compounds (hydrogen bonds, Coulomb and van der Waals interactions) has recently been used in crystal engineering to design materials with required properties and predictable structure [11].

Crystal structures, vibrational spectra, thermal behaviour and efficiency of second harmonic generation are presented and discussed.

2. EXPERIMENTAL

Crystals were prepared from corresponding mixtures of aqueous or methanolic solutions by slow spontaneous crystallization. Collection of X-ray data was performed on a Nonius Kappa CCD diffractometer (MoK_α radiation, graphite monochromator). The infrared and Raman spectra were recorded on a Nicolet Magna 760 FTIR spectrometer equipped with Nicolet Nexus FT Raman module. The measurements of SHG at 800 nm were performed using Ti:sapphire laser (Tsunami, Spectra Physics). For quantitative determination of the SHG efficiency, the intensity of the back-scattered laser light at 400 nm generated in the powdered sample was measured by a grating spectrograph with diode array (InstaSpec II, Oriel) and the signal was compared with that generated in KDP (i.e. KH_2PO_4).

3. RESULTS AND DISCUSSION

3.1. Crystal structures

Crystal structures of several novel salts were solved and namely aminoguanidinium(1+) dihydrogen phosphate, aminoguanidinium(1+) hydrogen L-tartrate monohydrate, diphenylguanidinium(1+) nitrate, biguanidium(2+) L-tartrate, phenylbiguanidium(1+) oxalate and phenyl-biguanidium(1+) sulphate will be discussed. The crystal structures are generally based on alternating isolated cations and anions or alternating layers of cations and anions or on encapsulation of cations into anions network (see Fig. 1).

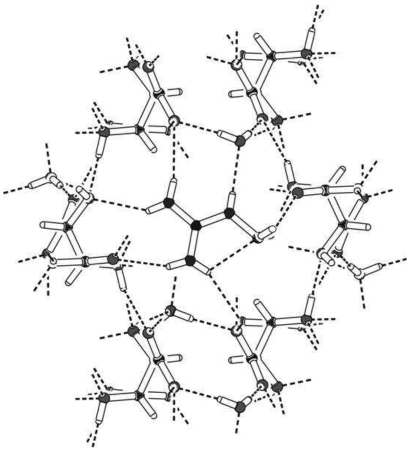

Fig. 1: Incorporation of aminoguanidinium cation in cavity formed by hydrogen L-tartrate anions and molecules of water.

In all these crystal arrangements hydrogen bonds of O-H...O, N-H...O and N-H...N type play role as the key bonding interactions.

3.2. Vibrational spectra

The FTIR and FT Raman spectra of prepared materials (see Fig. 2 as an example) were assigned employing quantum-chemical computational methods (*ab initio* and DFT methods). This assignment was performed not only for their identification but also with respect of their nonlinear optical properties (vibrational contributions to the first and second hyper-polarizabilities).

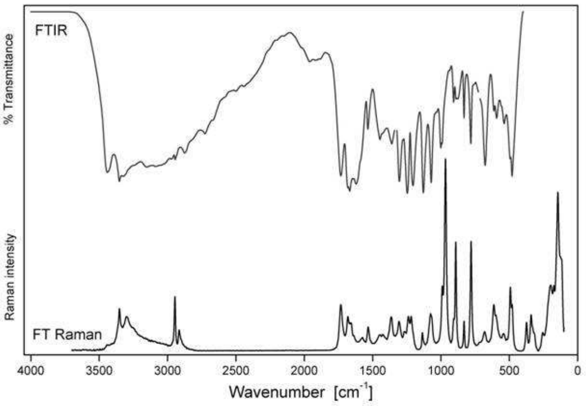

Fig. 2: Vibrational spectra of aminoguanidinium hydrogen L-tartrate monohydrate

3.3. Second harmonic generation

Quantitative measurements of SHG of powdered samples were performed at 800 nm relatively to KDP. Novel materials exhibit SHG efficiency ranging from 0.1 up to 5.6 (KDP = 1).

4. CONCLUSIONS

Several novel materials based on salts of guanidine and its derivatives with selected inorganic and organic acids were prepared. These materials were characterized by the methods of X-ray diffraction, vibrational spectroscopy and thermal analysis and also efficiency of second harmonic generation was determined. Combination of SHG-activity together with thermal stability and optical transparency is very promising for their prospective technical applications.

5. REFERENCES

[1] Guru Row T.N. (1999) Coord. Chem. Rev. 183, 81 and references therein.
[2] Etter M.C. (1991) J. Phys. Chem. 95, 4601.
[3] Aakeröy C.B., Seddon K.R. (1993) Chem. Soc. Rev. 22(6), 397.
[4] MacDonald J.C., Whitesides G.W. (1994) Chem. Rev. 94, 2383.
[5] Schuster P., Wolschann P. (1999) Monats. Chem. 130, 947.
[6] Aakeröy C.B., Nieuwenhuyzen M. (1994) J. Am. Chem. Soc. 116, 10983.
[7] Frankenbach G.M., Etter M.C. (1997) Chem. Matter. 4, 272.
[8] Aakeröy C. B., Hitchcock P. B., Moyle B. D., Seddon K. R. (1989) J. Chem. Soc. - Chem. Commun. (23), 1856 and references therein.
[9] Zyss J. (1991) Nonlinear Opt. 1, 3.

[10] Masse R., Durif A. (1990) Z. Kristallogr. 190,141.
[11] Raczynska E.D., Cyranski M.K., Gutowski M., Rak J., Gal J.F., Maria P.C., Darowska M., Duczmal K. (2003) J. Phys. Org. Chem. 16, 91.
[12] Magalhaes A.L., Gomes J.A.N.F. (1997) Int. J. Quantum Chem. 61, 725.
[13] Gobbi A., Frenking G. (1993) J. Am. Chem. Soc. 115, 2362.
[14] Binoy J., James C., Hubert Joe I., Jayakumar V.S. (2006) J. Mol. Struct. 784, 32.

MONITORING OF THE AEROSOLS RADIOACTIVITY AT BEO - "MOUSSALA"

I.Penev, M.Drenska, B.Damyanov, Tsc.Valova

Institute for nuclear research and nuclear energy, bulgarian academy of sciences, sofia, Bulgaria

N.Uzunov, N.Arhangelova

University of shumen "ep.konst. Preslavski", shumen, Bulgaria

Abstract: *The new monitoring system for aerosols radioactivity was realized at BEO-"Moussala", pick Moussala, 2971m. The system includes a sampler for big volume of air, ~ 1800m3 and H.P.Ge -spectrometer in the laboratory of INRNE-BAS. Method of sampling and measurements of the radioactivity and minimal detectable radioactivity are described. The firsts results of the natural radioactivity of 7Be are presented and discussed.*

Keywords: *aerosols, natural radioactivity, 7Be, minimal detectable radioactivity.*

1. INTRODUCTION

The presence of radioactivity in the air aerosols is caused mainly by natural process in the atmosphere and soil and by human activity. So called natural radioactivity in the air has two origin - from interaction of the high energy cosmic rays with elements in the lower stratosphere and upper troposphere and from penetration of the products of the decays of U235, U238 and Th232 to the air. The human activity, including nuclear accidents can give additional contribution of different isotopes. For example the nuclear fuel processing factories in the case of accident can spread some isotopes typical for spent fuel. The big electrical coal-fired power station can enrich the presence of uranium and thorium in the soil and in the air.

The natural radioactivity in the aerosols, mainly Be7 and Pb210 is attached to the aerosols with different aerodynamic diameter. Collecting the aerosols and analyzing the radioactivity could be very useful tool for understanding the physical processes in the atmosphere, including the washout, transport of the aerosols and the age of the aerosols in all kinds of atmospheric strata.

For more independent (without influence of local factors) measurements it is important to take samples as high as possible, or at different altitudes. All these considerations stimulated developing of the air-sampling device in the BEO-Moussala.

The heading „Introduction“ has to be written as „Introduction“ format, Arial 11 pt, single line spacing, 36 pt spacing before and 6 pt spacing after the capital letters.

2. METHOD OF SAMPLING AND MEASURING OF THE RADIACTIVITY OF THE AEROSOLS

In the Basic Ecological Observatory "Moussala" at pick Moussala, 2971m, have been build two sampling device with air turbine for high and low volume measurements. The bigger sampler has capacity ~ 1500-1800m^3/h, the smaller ~ 80-100 m^3/h, respectively. Both of them work with fiber type filters, the first one with size 50x50cm, second with 20cm on diameter. The area of the filters can be reduced, if necessary for smaller sampler. Usually the volume for each sample is ~ 15000m^3 for the big sampler and ~ 800m^3 for smaller one. In some cases this one could be reduced, depending on the weather conditions causing water crystals on the filter. It is used filter ФПП-15-1,5 with effectiveness ~ 95% for aerosols size 0.2 - 2.5mkm. Sampling's time is in the frame of 8-12h, depending of the weather conditions. The high humidity of the air it is not convenient for good sampling and after sampling the filter have to be dried on low temperature with dry air. The volume of the air passing through the filter measures every second and transforms to the standard conditions, at sea level and 0^{0}C temperature. The device for air debit shows volume for every second and integral volume. After sampling the filter is pressed with hydraulic press to the size of pill with diameter ~ 57mm and thickness ~ 15-17mm.

The gamma-spectrum of the filter sample with aerosols is measuring on H.P.Ge-spectrometer, with ~ 33% relative effectiveness and ~ 2.1keV energy resolution on 1.3Mev. Detector is surrounded by lead protection against environmental gamma-background.

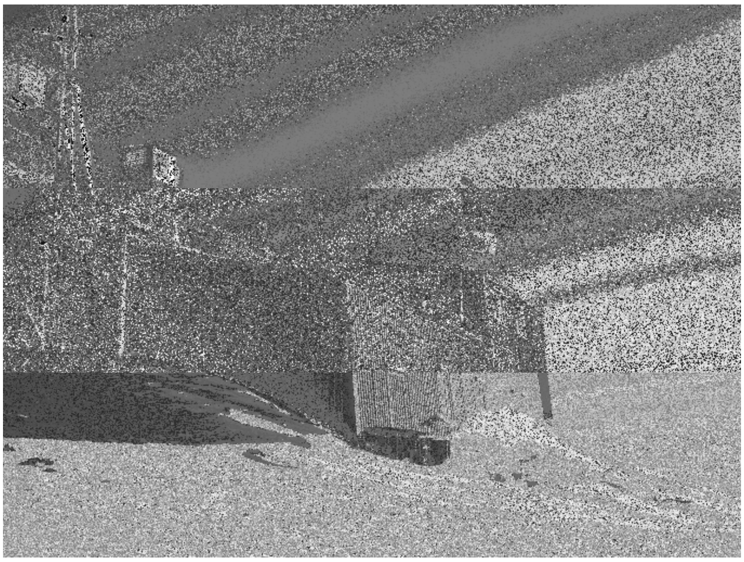

The aerosol sampler on BEO-"Moussala", turbine on the right corner of the building and the house for the filter on the roof.

The gamma spectra are processed by program "ANGES" /1/ developed in the INRNE-BAS.

The efficiency calibration of the detector system have been done with a standard source UTB/417 with volume and density same as the samples after pressing the filter. The standard source with several different isotopes, which covers the energy interval of measuring, has been prepared in the radiochemical laboratory of INRNE. In addition a comparison of the data for some samples was done in other laboratories, and good correspondence has been established.

3. SOME PROBLEMS OF THE AEROSOLS RADIOACTIVITY Format

Investigation of the aerosols radioactivity started in the 60-70th, but only in the last several years a better understanding of chemistry and physics of the processes in the different strata of atmosphere has been realized. This process has not been finished yet, and even became more important and more significant due to new problems with the global warming. Some new scientific groups started to measure the natural radioactivity and to compare and to try to draw a general conclusion from these data. Nevertheless the explanation of all atmospheric processes, including movement, transportation, condensation and residence time of aerosols is quite faraway to be complete. It was established, for example /2,4/ a ration between some of the isotopes and ozone concentration and residence time of the aerosols. Measurement of the activity of ^{210}Pb is more complecated, because of the very low energy of gamma-rays of this isotope. Our laboratory is being prepared to measure ^{210}Pb activity with appropriate sampler.

All quantity of ^{7}Be results from nuclear reactions between the high energy particles in the high atmospheric strata. mostly in the upper troposphere and in the lower stratosphere. The main mass of the ^{7}Be nuclei in this strata is attached to the aerosols with mean diameter ~ 0.3 - 0.4 µm. Then these aerosols are transported, depending on the weather conditions, to the other strata . The aerosols containing ^{7}Be become bigger with the time. But measuring the activity of the ^{7}Be we can receive information for the stratospheric intrusion. This one is important for better understanding of the behaviour of the ozone in the high altitude.

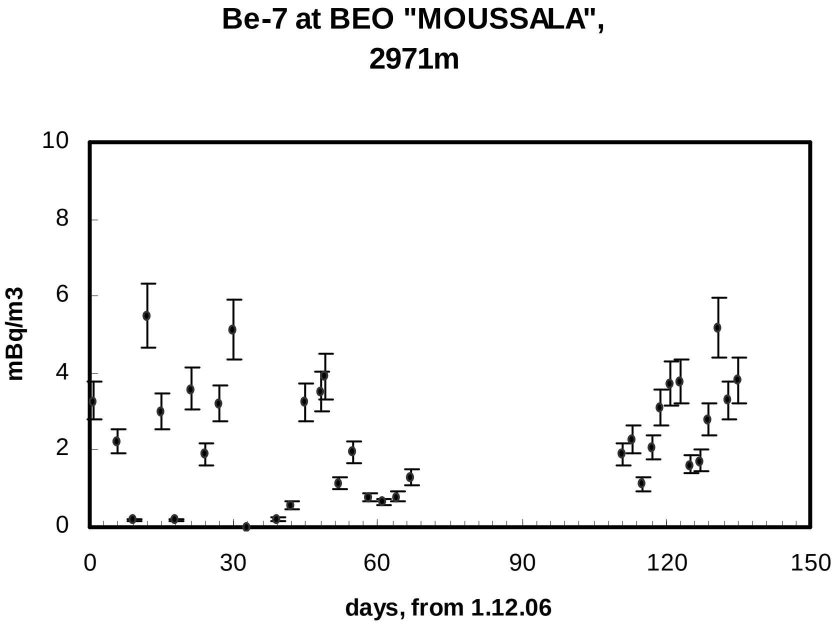

Tab.1 ^{7}Be in the aerosols at pick Moussala, in mBq per m^3 from beginning of December 2006 till the end of April2007.

Monitoring of the ^{7}Be at BEO - "Moussala" started on 1.12.2006 and with some interrupting is going on till now. Of coarse for more detail discussion and more determinate conclusions it is necessary to collect information for several years.

The first results for behavior of ^{7}Be at pick Moussala are presented in Tab.1

We observed during the December relatively big interval of the value of ^{7}Be.

This one could be initiated by the high intensity of cosmic rays during this time interval. From other side, if the similar behavior will be observed for a more long time, or more frequently this could be a sign for quite a strong exchange of the air mass with different altitude origin. In this case the specific place and altitude of the pick Moussala could be very useful for receiving a new information for processes in the atmosphere and for weather forecasting.

isotopes	$T_{1/2}$	energy of gamma-rays, KeV	% of decay	min. detect. concen-ration, micro Bq/m^3	der.air concentr. DAC/20 ITU-EU Bq/m^3	АЯР of R. of B. Bq/m^3	factor of sensibility R.B./min
^{134}Cs	2.06y	604	97.6	~ 7	20.8	6.0	0.8x10^6
^{137}Cs	30.0y	661	85.1	~ 4	10.7	3.2	0.80 x10^6
^{131}I	8.04d	364	81.7	~ 4	56.5	3.3	0.82 x10^6
^{133}I	20.8h	529	87.0	~ 5	760	29	5.8 x10^6
^{95}Nb	31.1d	765	99.8	~ 4	231	62	15 x10^6
^{95}Zr	64.0d	756	54.5	~ 6	70	19	3.1 x10^6
^{103}Ru	39.3d	497	91.0	~ 5	139	37	7 x10^6
^{60}Co	5.27y	1173	100	~ 3	13.5	4.0	1.3 x10^6
^{22}Na	2.6y	1274	100	~ 3	320	72	24 x10^6

Tab.2 The minimal detectable activity for some isotopes fission, or activation products

Monitoring of the aerosols radioactivity is significant in addition from other side. This is one of the way for controlling of the quality of the air in the case of transcontinental transportation of some human done radioactivity, for example after nuclear, or other accident. For such measurements, from environmental point a view it is necessary to know the detectable limit of the used device, i.e. the minimal radioactivity for some isotopes. Sore some isotopes, for fixed condition of sampling and measuring this has been investigated. These values are presented in Tab.2.

Factor of the sensibility is the ratio of mean activity per year for the public places for Republic of Bulgaria to the minimal detectable concentration gained with our system.

The same concentrations, proposed by Institute for Transuranium Elements, Karlsruhe, EU, are several times higher .

On reality this one means how many times the measured activity for some isotope is lower, than maximum permissible on the public places. For example for 137Cs, this is $0.8x10^6$, i.e. we can detect in the air almost one million times low activity, than it is permissible for public places. This is very low activity, which can be measured thanks to big volume of sampling
($\sim 15000m^3$) and long (10^5s) time of measuring on H.P.Ge
spectrometer.

4. CONCLUSIONS

Starting the monitoring of the aerosols radioactivity at BEO-"Moussala" INRNE-BAS has the unique possibility to receive a new data for physic of the atmosphere, global climate changes and environmental. In addition, the new device is in progress, for 210Pb which will improve the understanding of all data of radioactivity of aerosols.

5. ACKNOWLEDGEMENTS

We would like to thanks Prof. J.Stamenov, Director of INRNE-BAS, for permanent support and useful discussions and all staff of BEO-"Moussala" for incredible efforts for mounting of the device and taking samples during the very hard meteorological conditions.

6. REFERENCES

[1] Mishev, Pl., Vidolov, B., 1993, Research Contract 9493/RO Vienna, Austria, IAEA

[2] Baskaran, M., Show G.E., (2001), "Residence time of arctic haze aerosols using the concentrations and activity ratios of ^{210}Po, ^{210}Pb and ^{7}Be", J. Aerosol Sci. 32, 443-452

[3] Gaffney, J.S. and Marley, N.A., (2002) Measurements of beryllium-7 and ozone, Proceedings Volume, Fourth Conference on Atmospheric Chemistry Symposium: Urban, Regional and Globale-Scale Impacts of Air Pollutants, Amer. Meteor. Soc., 187-191

[4] Marley, N.A., Gaffney J.S., Cunningham, M.M.,., Orlandini, K.A., Paodle, R.,Drayton P.J., (2000) "Measurement of ^{210}Po, ^{210}Pb and ^{7}Be in size fractionated atmospheric aerosols: An estimation of fine aerosols residence times", Aerosols Sci.Technol. 32, 569-583

[5] Gaffney, J. S., Marley, N.A., Cunningham, M. M. and V. R. Kotamarthi, (2006). “^{7}Be Measurements in the Houston and Phoenix Urban areas: An Estimation of Upper Atmospheric Ozone Contributions.” *J. Air & Waste Management Association*, accepted for publication

A NOTE ON SOLAR CELL DIAGNOSTICS USING LBIC AND LBIV METHODS

Jan Salinger, Vitezslav Benda and Zdenek Machacek

CTU Prague, Faculty of Electrical Engineering, Department of Electrical Technologies, Czech Republic

Abstract: *As the solar cell market is one of the most quickly developing one between the renewable sources of energy, the demands on quantity and quality of these cells grows rapidly. For diagnostics of cell homogeneity, LBIC and LBIV methods are widely used. This paper deals with comparing two solar cell diagnostic methods via both the qualitative and quantitative analyses.*

Keywords: *Recombination, LBIC, LBIV, Solar Cell Homogeneity*

1. INTRODUCTION

Both LBIV and LBIC methods are based on measuring either short circuit current I_{SC} or open circuit voltage V_{OC} under conditions of local illumination by monochromatic light of a proper wavelength (usually realised by laser or LED diodes). Assuming the characteristic of a solar cell with series resistance R_s and parallel resistance R_p [1] under conditions of illuminated spot of area *A,* it is possible to find out for short circuit current (V = 0)

$$I_{SC} = AJ_{PV} - I_{01}\left[\exp\left(e\frac{R_s I}{kT}\right) - 1\right] - I_{02}\left[\exp\left(e\frac{R_s I}{2kT}\right) - 1\right] - \frac{R_s I}{R_p}, \qquad (1)$$

and for open circuit voltage it can be derived (supposing a high parallel resistance R_p)

$$(2) \qquad V_{0C} = \frac{2kT}{e}\ln\left(\frac{-I_{02} + \sqrt{I_{02}^{\;2} + 4I_{01}(I_{02} + I_{01} + AJ_{PV})}}{2I_{01}}\right).$$

I_{01} represents the diffusion component of the p-n junction reverse current, and I_{02} is the generation-recombination component of the p-n junction reverse current. J_{PV} is the density of current generated within the cell structure of thickness H by incident light. Non-uniformity in either the generation or the recombination rate over the area of the solar cell results in a non-uniform distribution of J_{PV} and consequently, in non-uniform distribution of both V_{OC} and I_{SC} under conditions of local illumination [2]. The use of different wavelengths of incident light allows obtaining different types of important information about non-uniformity in recombination rate in different depth below the solar cell surface [3].

2. EXPERIMENT

Matching the maps obtained by the LBIV method with those obtained by the LBIC method is subject of this paper. Even the LBIC method is relatively simple, its results are not always easy to interpret. The main reason arise from the position of measuring point on the I-V curve that can differ from short circuit conditions due to non-zero internal resistance of measuring device. As follows form (1), the short circuit current is very sensitive to the series resistance value that may depend on the distance between the light spot and the contact grid. On the other hand, this method can be used for detecting microscopic ruptures in the material, because these ruptures act as short circuit (reducing the shunt resistance value ~ 0), thus influencing the measured value of the short circuit current radically. From the equivalent circuit model of the solar cell follows, that the method LBIV operates in a well defined point of I-V characteristic, but it is insensitive to changes in shunt resistance value.

3. RESULTS AND DISCUSSION

Differences between maps obtained using LBIC and LBIV methods were studies experimentally. They were measured by both methods and with 6 different light wavelengths. Results obtained by using wavelength 670 nm laser diode are compared in Fig.1 (a residuum after wafer fabrication when the surface damaged layer after cutting the rod was probably not fully etched off).

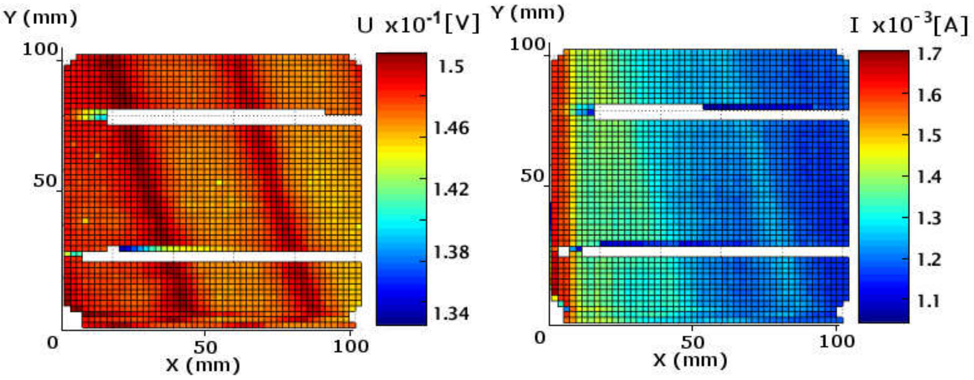

Next figures are showing differences between LBIV and LBIC method when diagnosing polycrystalline wafer

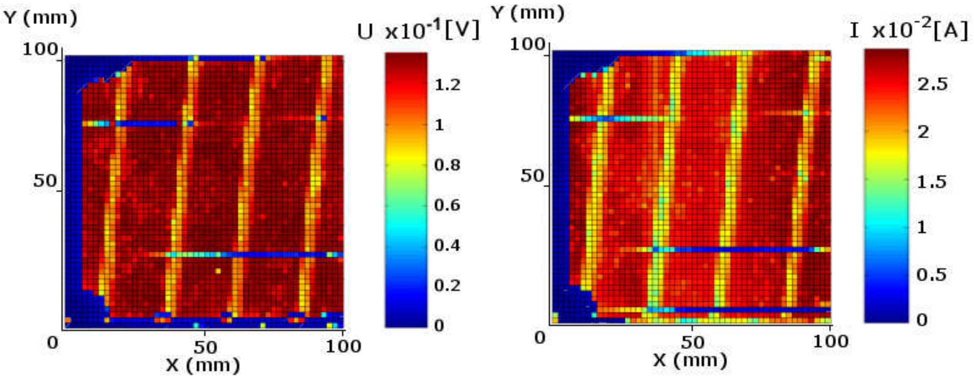

Other point of view is looking on the stability of the signal of both LBIC and LBIV method. From position of the working point on the I-V curve, one can expect, that the sensitivity of the LBIC signal is much bigger than of the LBIV method. This is because the position enables to shift the voltage from positive values to negative values with only very small current increase. Although, in this case, we are interested in current values (LBIC method), it is the voltage which is measured and which can dramatically change its value with varying current. This effect can be seen on the following pictures depicting the polycrystalline solar cell:

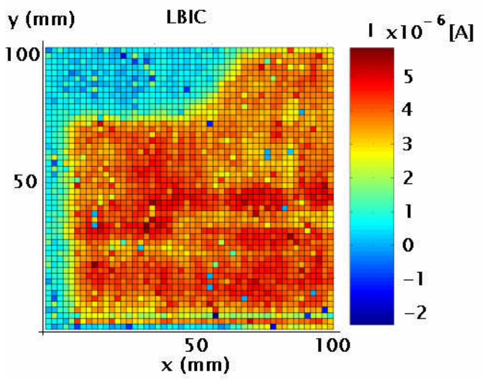

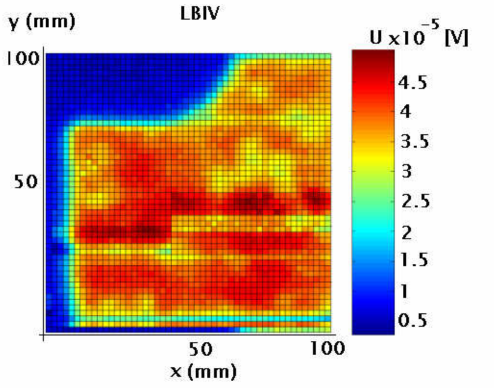

Here, the long wave light source was chosen (a semiconductor diode, 950 nm), so the signal coming from the measuring device is very low (see the scale on the LBIC map). From these maps, the LBIV method provides much better quality of the signal.

From studied wavelength range, this was the only one, where the LBIC signal stability was not found very useful. Thus, for gathering information about the crystalline solar cell structure deep under the surface, measurement with LBIV method should be conducted better than the LBIC one. When talking about structure deep under the surface, we are talking about crystalline structure of the raw material, from which the solar cell is manufactured – in case of studied mono- and polycrystalline solar cells, it is the P-type material structure.

5. REFERENCES

[1] Goetzberger A., Knobloch J. and Voss B.: Crystalline Silicon Solar Cells, J.Wiley & Sons, 1998

[2] Kress A., et al: LBIC measurements on low cost contact solar cells, Proc. 16th European Photovoltaic Conference on Solar Energy Conversion, Glasgow 2000, VA1.39

[3] Benda, V.: Diagnostics of Homogeneity of Recombination Rate in Individual Layers of Large-Area Silicon Solar Cells Using LBIV Metod, Proc. 20th European Photovoltaic Solar Energy Conference , Barcelona 2005, 670-673.

[4] Benda V., Macháček Z., A Note on Diagnostics of Homogeneity of Recombination Rate in Large-Area Silicon Solar Cells Using Local Irradiation, Pro. 21st European Photovoltaic Solar Energy Conference, 2006, 1508-1511.

[5] Benda, V. - Macháček, Z. - Salinger, J.: Diagnostic of the N^+ Layer Homogeneity in Large Area Silicon Solar Cells Using Local Irradiation. Proc. 21st European Photovoltaic Solar Energy Conference, 2006, 1512-1514.

INVESTIGATION ON THE THERMAL-ELECTROMOTIVE TENSION COEFFICIENT IN LOW INTENSITY MAGNETIC FIELD AND DETERMINATION OF THE KINETIC PARAMETERS OF Ag_4SSe

V. Vassilev[1], A. Amova[2], V. Vachkov[3]
[1] *UCTM-Sofia, Bulgaria, e-mail: venciv@uctm.edu*
[2] *UACEG-Sofia, Bulgaria*
[3] *SWU-Blagoevgrad, Bulgaria*

Abstract: *A determination method for the dispersion coefficient and the effective electron mass on the Fermi-surface and at the bottom of the conductivity gap, Fermi energy and the Kolodzaichak-Sosnovski parameter in the narrow gap semiconductor* Ag_4SSe *is developed using the experimental data from measurement of the thermo-electromotive tension coefficient in low intensity magnetic field, mobility and concentration of the electrons, and the thermo-electromotive tension coefficient in absence of magnetic field.*

Keywords: *narrow gap semiconductor, non-standard conductivity gap, kinetic parameters, thermal-electromotive tension coefficient.*

ВЪВЕДЕНИЕ

Изучаването на електричните свойства на полупроводниците е тясно свързано с познаването на зонната структура, т.е. каква е зависимостта на енергията на електрона (Е) от вълновия вектор (к) във валентната и проводимата зони. Параболичният закон на разпределение на електрони-те по енергии е валиден само в случаите, когато ширината на забранена-та зона (Eg) е много голяма. Само в този случай може да се пренебрегне взаимодействието между валентната и проводимата зони. В теснозонните полупроводници проводимата зона се отклонява от параболичния закон и това отклонение влияе съществено върху техните преносни характеристи-ки, а те от своя страна са свързани с концентрацията и поведението на носителите на заряд в реалната кристална решетка.

Носителите на заряд се намират в равновесно или в неравновесно състояние. Топлинните и магнитните свойства на твърдите тела са обус-ловени от свободни електрони и дупки, които се намират в състояние на статистическо (термодинамично) равновесие. Изучаването на поведение-то на носителите на заряд в неравновесно състояние, когато те се движат в кристала под действие на приложени външни полета (електрично, маг-нитно и топлинно), е от съществено значение за теорията и практиката.

Състоянието на електроните, намиращи се в термодинамично равно-весие, се описва от равновесната функция на разпределение на Ферми-Дирак $f_o(E)$. Ако електроните са в неравновесно състояние, то тогава се използва неравновесната функция на разпределение F(k,r), която пред-ставлява вероятността електронът с вълнов вектор **к** (квазиимпулс ħ.к) да се намира близо до точката r, намираща се в пространството вътре в без-крайния кристал.

Функцията на разпределение F(k,r) се получава от кинетичното у-ние, отчитайки следните физични съображения. Предполага се, че F(k,r) се променя под влиянието на две причини: а) под влияние на външни фак-тори – приложено поле, температурен или концентрационен градиенти; б) под влияние на стълкновението на електроните с колебанията на решет-ката (с фононите) или с дефектите на кристала.

Ако с $(\partial f/\partial t)_{\text{вф}}$ се означи изменението на функцията на разпределение под влияние на външни фактори, а с $(\partial f/\partial t)_{\text{ст}}$ – в резултата на стълкнове-ния, то в разглежданото стационарно състояние влиянието на тези факто-ри взаимно се компенсира:

(1) $(\partial f/\partial t)_{\text{вф}} + (\partial f/\partial t)_{\text{ст}} = 0$.

При наличието на външно електрично и магнитно полета, а също така и на температурен или концентрационен градиент, у-ние (1) има вида:

(2) $V.\nabla_r f - (e/\hbar).\{E_o - (1/c).[V.H]\}.\nabla_k.f = (\partial f/\partial t)_{\text{ст}}$.

Тук $V = (1/\hbar).E(k)$ е скоростта на електрона, (-е) - неговия заряд, ∇_r ∇_k градиент на пространствените координати и на вълновите вектори; E_o и H – напрегнатост на електричното и магнитното полета, с – скоростта на светлината, $\hbar = h/(2/\pi)$, а h – константата на Планк.

Главно два критерия определят приложимостта на това уравнение.

Единият от тях налага ограничения върху стълкновенията на носите-лите на заряд с топлинните колебания на решетката и с другите дефекти на решетката.Това ограничение се изразява с неравенството:

(3) $\hbar/\tau < к.T$,

където τ - време между две стълкновения. Тъй като подвижността на електроните $\mu = (e.\overline{\tau})/m$, то този критерий добива вида:

(3а) $\mu > (e.\hbar)/(m.k.T)$.

Критерий (3) може да се запише и по друг начин. Ако се умножат две-те страни със средната скорост $\overline{v}$ на електроните и се отчете, че $к.T/\overline{v} \approx \overline{p}$ (квазиимпулс), а $\hbar/\overline{p} \approx \lambda$ (дължина на вълната на носителя на заряд), то се получава:

(3б) $\overline{\lambda} > \lambda$,

където $\overline{\lambda} = \overline{v}.\overline{\tau}$ - средна дължина на свободния пробег.

В такъв случай, кинетичното уравнение е приложимо, ако средната дължина на свободния пробег на носителите на заряд е по-голяма от тяхната дължина на вълната на де Бройл.

Вторият критерий налага ограничение на стойността на напрегнатост-та на магнитното поле. По своята напрегнатост, магнитното поле се ква-лифицира като класическо и квантово. Класическата област е ограничена от такива стойности на магнитнотот поле, които не влияят на енергетич-ния спектър на носителите на заряд и на вероятността за преход от едно стационарно състояние в друго, иницииран от стълкновението между тях.

На свой ред, класическата област се дели на слаби и силни магнитни полета. Критерий за слабо магнитно поле е неравенството:

(4) $R >> \lambda$, или $\Omega.\tau << 1$, или $(\mu.H/c) << 1$.

В еднородно магнитно поле електроните се движат по винтова линия с ос, паралелна на магнитното поле и с радиу R: $R = m.c.V_{\perp}/\Omega$, където $V_{\perp}$ - проекция на скоростта върху плоскостта, перпендикулярна на магнитното поле, а $\Omega = e.H/(m.c)$ – кръгова честота на въртене на електрона в тази плоскост, известна още като циклотронна честота.

Магнитното поле е силно. ако неравенства (4) са в обратна посока.

В достатъчно силни магнитни полета и при ниски температури, когато $kT \leq \hbar\Omega$, дискретността на спектъра става съществена и магнитното поле, удовлетворяващо това условие, е квантуващо. Целта на настоящата ра-бота е да се разработи методика за определяне на някои кинетични пара-метри на полупроводници със сферична нестандартна зона (коефициент на разсейване и ефективна маса на носителите на заряд на повърхността на Ферми и на дъното на проводимата зона, енергията на Ферми и коефи-циента на Колодзайчак и Сосновски, характеризиращ степента на непара-боличност на проводимата зона), като се използват експерименталните данни от измерването на коефициента на термо-е.д.н. в слабо магнитно поле, подвижността и концентрацията на носителите на заряд и коефициента на термо-е.д.н. в отсъствие на магнитно поле.

Предимство на предлагания метод за определяне на кинетичните параметри на полупроводници със сферична нестандартна зона е, че се работи в слабо магнитно поле с произволна магнитна индукция, без да се изисква предварително познаване на някой от кинетичните коефициенти (най-често това е коефициентът на разсейване на носителите на заряд).

Експериментална част

За изроден полупроводник в слабо магнитно поле за Δα се използва изразът [1]:

$$(5)\quad \Delta\alpha = \alpha(H) - \alpha(0) = \frac{k}{e}\left(\frac{\mu H}{c}\right)^2 \frac{\pi^2}{3}\left(\frac{kT}{F^*}\right)\left(r - \frac{1}{2} - \gamma\right)$$

$$(6)\quad \alpha(0) = -\frac{k}{e}\frac{\pi^2}{3}\frac{2kTm(F)}{\eta^2(3\pi^2 n)^{\frac{2}{3}}}\left[(r+1) - \frac{2\eta^2(3\pi^2 n)^{\frac{2}{3}} m_n}{m^2(F)E_g}\right]$$

$$(7)\quad m(F) = m_n\left[1 + \frac{2\eta^2(3\pi^2 n)^{\frac{2}{3}}}{m_n E_g}\right]^{\frac{1}{2}}$$

$$(8)\quad F = \frac{E_g}{2}\left[\frac{m(F)}{m_n} - 1\right]$$

където: $\alpha(H)$ - коефициент на термо-е.д.н. в магнитно поле с интензитет H; $\alpha(0)$ - коефициент на термо-е.д.н. при отсъствие на магнитно поле; F – гранична енергия на Ферми; m_n - ефективна маса на електроните на дъ-ното на проводимата зона; m(F) - ефективна маса на електроните на Фер-ми-нивото; n - концентрация на електроните; T - температура на измерва-нето; r - коефициент, характеризиращ механизма на разсейване на носи-телите на заряд; μ - подвижност на носителите на заряд; F^* - параметър, определящ ефективната маса m(F) на повърхността на Ферми; γ - пара-метър на Колодзайчак и Сосновски, характеризиращ степента на непара-боличност на проводимата зона.

Параметрите F^* и γ. се задават със следните уравнения:

$$(9)\quad F^* = \frac{\left[\eta^2\left(3\pi^2 n\right)^{\frac{2}{3}}\right]}{\left[2m(F)\right]}$$

$$(10)\quad \gamma = \frac{\left[2\eta^2 m_n \left(3\pi^2 n\right)^{\frac{2}{3}}\right]}{\left[E_g m(F)\right]}$$

При решаване на системата уравнения (5)-(8) получаваме:

$$(11)\quad m(F) = \frac{\left[\alpha + \Delta\alpha\left(\frac{c}{\mu H}\right)^2\right]}{1{,}5B}$$

$$(12)\quad m_n = -\frac{A}{2} + \sqrt{\left(\frac{A}{2}\right)^2 + m^2(F)}$$

$$(13)\quad F = \left(\frac{E_g}{2}\right)\left[\frac{m(F)}{m_n} - 1\right]$$

$$(14)\quad r = \frac{\alpha}{Bm(F)} + \frac{Am_n}{m^2(F)} - 1;\ \gamma = \frac{Am_n}{m^2(F)},\ \text{където:}$$

$$(15)\quad A = \left(\frac{2\eta^2}{E_g}\right)\left(3\pi^2 n\right)^{\frac{2}{3}} = 0{,}213.10^{-66}.\frac{n^{\frac{2}{3}}}{E_g}$$

$$(16)\quad B = -\left(\frac{k^2}{3}\right)\left(\frac{\pi^2}{e}\right)\frac{2T}{\left[\eta^2\left(3\pi^2 n\right)^{\frac{2}{3}}\right]} = -0{,}735.10^{41}.\frac{T}{n^{\frac{2}{3}}}$$

Използвайки уравненията (11)-(16), стойностите за $\Delta\alpha(H)$ и данните за $\alpha(0)$, μ и n от работа [2], определихме коефициента на разсейване r и ефективната маса на електроните на повърхността на Ферми m(F) и на дъното на проводимата зона m_n, енергията на Ферми F и параметъра на Колодзайчак и Сосновски γ в Ag_4SSe, синтезиран по методика описана в работа [2].

При измерване на коефициента на термо-е.д.н. работихме в магнитно поле с интензитет $1{,}99.10^5\ \frac{A}{m}$. Получените стойности за $\Delta\alpha = \alpha(H) - \alpha(0)$ са представени на фиг. 1.

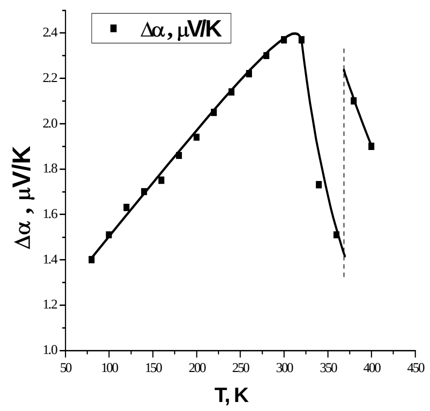

Фиг. 1 Температурна зависимост
на $\Delta\alpha$

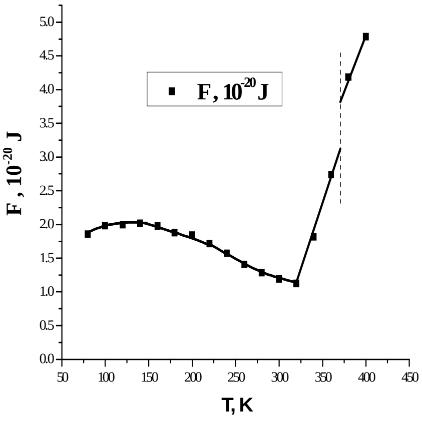

Фиг. 2 Температурна зависимост
на F

Екстремната точка в зависимостите m$_n$, m(F), F, $\gamma = $ f(T) при T ≈ 320 K се дължи на настъпването на собствена проводимост. Над тази темпера-тура Ферми-нивото рязко се отдалечава от дъното на проводимата зона. Такъв ход на зависимостта на F=f(T) – фиг. 2 се наблюдава, когато кон-центрацията на донорите е много голяма и областта на собствена прово-димост настъпва преди още напълно да са се йонизирали примесните атоми [5]. Този ход на F оказва определящо влияние на зависимостите m$_n$, m(F) = f(T) – фиг. 3.

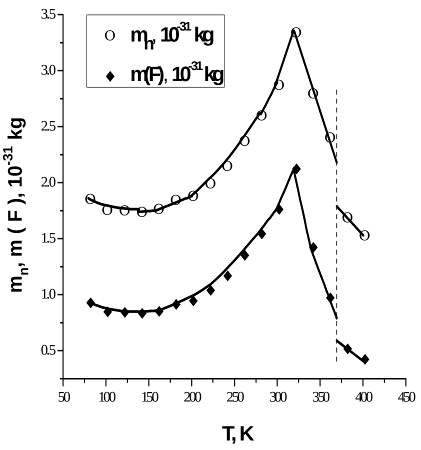

Фиг. 3 Температурна зависимост
на m$_n$ и m(F)

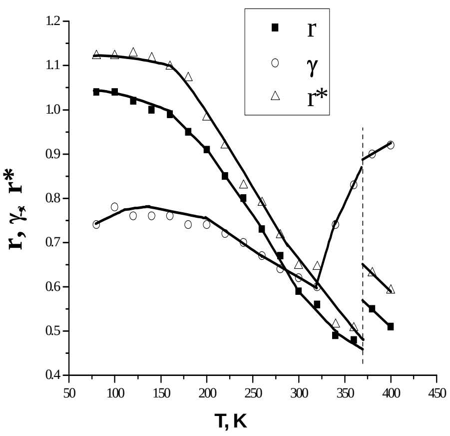

Фиг. 4 Температурна зависимост
на r и γ

При повишаване на температурата, коефициентът на разсейване на-малява – фиг. 4, т.е. нараства влиянието на механизма на разсейване на електроните от топлинните колебания на решетката.

Високите стойности на γ (γ>0,6), свидетелстват за значително откло-нение на проводимата зона от параболичния закон E ≈ k^2. (В случай на стандартна зона, когато ефективната маса не зависи от енергията и сле-дователно, от концентрацията на носителите на заряд, коефициента на
Колодзайчак и Сосновски γ =0).

При около (367±2) K се наблюдава скок в зависимостите m_n, γ, r, m(F) = f(T), което се дължи или на фазовия преход $\alpha \leftrightarrow \beta$. Аналогичен извод е направен и при изследването на други електрични свойства на Ag_4SSe [6]

Получените стойности за m_n и r, както и ходът на зависимостите m_n, r =f(T) са аналогични на същите, получени съответно от експерименталните данни за коефициента на термо-е.д.н. в отсъствие на магнитно поле [4] и в силно магнитно поле – r* [3] – фиг. 4.

3. ЗАКЛЮЧЕНИЕ

1. Определени са коефициентът на разсейване и ефективната маса на електроните на повърхността на Ферми и на дъното на проводимата зона, енергията на Ферми и коефициента на Колодзайчак и Сосновски в Ag_4SSe, като са използвани експерименталните данни от измерването на коефициента на термо-е.д.н. в слабо магнитно поле, подвижността и кон-центрацията на електроните и коефициента на термо-е.д.н. в отсъствие на магнитно поле.
2. Получени са следните стойности за основните кинетични коефи-циенти на Ag_4SSe при 300 K: F = $1{,}19.10^{-20}$J; $m_n = 0{,}19m_0$; m(F) = $0{,}31m_o$; r = 0,59; γ = 0,62.

4. ЛИТЕРАТУРА

[1] Аскеров, Б.М., (1970), Кинетические Эффекты в полупроводниках. Наука, Л.

[2] Василев, В., З. Бончева-Младенова, (1981), Електофизични свойства на Ag_4SSe, ВХТИ – С., **28** (1), 143-147.

[3] Василев, В., В. Въчков, К. Томова, А. Амова, (2006), Коефициент на разсейване на електроните в теснозонния полупроводник Ag_4SSe, Int. Sci. Conf. “UNITECH’ 06”, Gabrovo, 24-25 November 2006, Proc., vol. III, 458-462.

[4] Василев, В., А. Амова, К. Томова, В. Въчков, (2006), Определяне на ефективната маса на електроните в теснозонния полупроводник Ag_4SSe, J.TU – Plovdiv, **13** (10), 83-87.

[5] Молдованова, М., (1977), Физика на полупроводниците. Наука и изкуство, С.

[6] Vassilev V.S., Z.G. Ivanova, (2003), Reversible $\alpha \leftrightarrow \beta$ phase transition in the narrow-gap semiconducting Ag4SSe compound, Bull. Chem. Tech. Macedonia, 22 (1), 21-24

THE USE OF BIOMASS FOR SIMULTANEOUS PRODUCTION OF HEAT AND POWER IN THE RURAL REGION

MAJCHRZYCKA A., KOZAK T.

Szczecin University of Technology, The Faculty of Mechanical Engineering,
70-310 Szczecin, Piastów 19, Poland

Abstract: *The paper discusses combined production of heat and power (CHP) from biomass in a small-scale power plant placed in the rural region. Based on power and heat demands of the rural region and biomass supply, the CHP system was selected. Preliminary economic and ecological analysis were performed and discussed.*

Keywords: *biomass, cogeneration*

1.INTRODUCTION

Combined production of heat and power (CHP) is one of the methods leading to improvement of energy production cost-effectiveness. Compared do separated production of heat and energy, CHP enables better utilisation of the fuel chemical energy and finally to reduce fuel consumption and emission of pollutants. CHP systems are the most effective, when applied for energy production for a local region energy demands because energy transmission costs are relatively low. Recently, in Poland there is growing interest of biomass combustion technology, particularly regarding the solid biofuels combustion. Because of biomass great accessibility its utilisation systematically increases, particularly in the rural regions of Poland. Increasing interest in biomass utilisation and CHP systems follows from EU and the Polish energy policy that is aimed at increasing share of energy from renewable sources. The target is for energy produced from renewable sources to account for 7,5% of total energy consumption by 2010, and for 14% in 2020 .Therefore, Polish legislation and EU directives support all activities concerning application of renewable energy sources[3], particularly combined heat and power production [6]. In view of large biomass potential, one can expect that in the nearest future Poland will rapidly develop combined heat and power production based on biomass. Among the different renewable sources of energy, biomass is very valuable for combustion and gas production. Biomass is an organic matter deriving from plants, generated through the photosynthesis. Resources of biomass are renewable and easy accessible, however the most important factor deciding about its use for energy production is low pollutants emission. During biomass combustion, oxygen combines with the carbon contained in biomass to produce CO_2 and water, emission of SO_2 is very low. The process is therefore cyclic because of CO_2 assimilation to produce new biomass. This is the reason, why biomass combustion is potentially considered as CO_2 neutral, although some emissions occurs. Biomass used for bioenergy production comes from woods, orchards and industrial wood residues. Estimated potential of wood biomass in Poland is as follows: the total wood resources of 158 6 PJ and industrial wood residues potential of 53,9 PJ [1].Straw, grain and agricultural residues may be used as the other energy crops for bioenergy. Short rotation plantations e.g. willow, poplar or herbaceous crops are additional energy crops that will contribute to increase biomass potential in the rural regions. North-Western Poland is the region of the large estimated biomass potential 195 PJ[1]. Biomass can be used in combustion processes in the different forms as: firewood, sawdust wooden chips, wooden residues, wheat straw, grass and different biomass densified products: briquettes, pellets. There are some practical problems concerning the use of biomass, one of them is biomass high bulk volume, which results in high transportation costs and requires large storage capacities. Therefore, biomass used as the fuel is usually converted into densified products. Densified biofuel is of high quality and can be used in a fully automatic operation, in household appliances and combined heat and power (CHP) plants. The calorific value of a fuel, moisture content and chemical characteristics are the most important characteristics for biofuels. The calorific value of wood, containing 60% of moisture is of 6-8 GJ/t and for dry wood is of 19 GJ/t[1],[10].The other properties of the size reduced wood residues influencing: combustion, transportation, storage and environment are as follows: bulk density, ash content and composition, volatile matter, chemical composition (sulphur, nitrogen, hydrocarbons and chlorine content).

2.THE USE OF BIOMASS IN A SMALL HEAT AND POWER GENERATING PLANTS

Biomass can be applied for bioenergy in the following processes: combustion in the stoker fired or fluidised bed boilers , co-firing with the other fuels, gasification and pyrolysis. Combustion of biomass is the most popular technique for energy production. Special types of furnaces of the different constructions have been developed for combustion of solid biomass: the stoker fired, moving grate furnaces, conventional grate furnaces, cigar burners and stationary or circulating fluidised bed boilers. The devices used for combustion of solid biofuels range from small domestic stoves (1 -10 kW) to the large boilers used in power and CHP plants (>5 MW). Combustion of biomass in the stoker fired boilers or conventional grate boilers are the most popular applications for biomass combustion. In case of low biomass calorific value, the fluidised bed boilers are recommended. Gasification, pyrolysis and biomass co-firing with the fossil fuels are the other technologies for conversion of biomass. Combined heat and power production from biomass can be realised in the following processes:

- direct combustion of biomass in the stoker steam or fluidised bed boilers, connected with the low power steam turbine,
- generation of wood distillation gas and then gas combustion in steam boiler assembled with steam turbine, coupled with generator,
- generation of wood distillation gas and then gas combustion in Diesel engine (or gas turbine) with heat recovery system, coupled with generator.

The other technologies for combined heat and power generation: the Stirling engine system, the direct biomass combustion system with gas turbine and heat recovery system or biogas engine are still in research.

3. COMBINED HEAT AND POWER GENERATION SYSTEM WITH DIRECT COMBUSTION OF BIOMASS IN A STEAM BOILER

Combined heat and power generation can be realised not only in a larg CHP plants but also in a small and medium local CHP plants[2],[4],[1],[9]. Large biomass resources, new energy policy, regarding CHP and financial problems in a rural regions cause that the local authorities are looking for relatively not expensive but advanced technologies for combined heat and power generation. An example of the biomass use for combined heat and power generation will be presented here. It was assumed, that bioenergy will be produced to cover energy demands of the region of 18.060 ha, of 4.000 inhabitants scattered in 28 villages. The rural region is very attractive for tourism. The major part of the region is covered with woods of area 4 620 ha. At present, electric energy is delivered to the region from the power grid. Most of the buildings in the region are heat supplied from the small local boiler houses but mainly from an individual coal/coke/wood fired stoves. The region in question, is of very high natural value and the large biomass resources, estimated annual wood (wood chips, wood residues, etc.) supply is about 10.400 t, therefore biomass deployment for combined heat and power production will lead to positive environmental benefits, particularly reduction of pollutants emissions. The other advantages of the biomass use in the region are as follows: reduction of energy manufacturing costs, development of small scale commodity production and tourism, decreasing unemployment and finally, improvement of the living standard in the region.The total energy requirement and the characteristics of energy recipients and their demands are the main factors deciding about the choice of the suitable biomass combined heat and power technology. It was assumed, that power requirement in the region is N_e= 1,2 MW_e and heat demand N_t=6 MW_t. Combined heat and power system will be biomass (wood residues) fired. The total efficiency of heat and power generating plant is related to the biomass conversion technology, the kind of biofuel, conversion efficiency and costs-effectiveness indicators. Selected CHP system consists of: boiler, extraction turbine, generator, condenser, and reduction-cooling steam bleeder station. The scheme of cogeneration system is presented in Fig.1. The condensation turbine set with steam extraction, of the type P1.2-13/6, manufactured by Power Electric Co. Ltd[11] is characterised with:

- nominal power output– 1200 kW
- the nominal inflow steam parameters:
    - absolute pressure - 1,3 MPa, (operating range 1,1 ÷ 1,4 MPa),
    - the temperature - 235 ^{0}C, (operating 220 ÷ 250℃),
- the nominal parameters of extracted steam:
    - the total pressure - 0,6 MPa, (operating range 0,5 ÷ 0,7 MPa),
    - steam flow - 4,0 t/h (operating operating range 0 ÷ 9 t/h),
- the nominal pressure of steam extracted of the turbine – 10 kPa

The calculations were performed for the turbine nominal parameters. Heat produced by CHP plant is applied for heating and preparation of the warm water. It was assumed that 10% of heating power will be used for preparation of the warm water. Heat requirement depend upon the ambient temperature, that is usually given in a form of the systematic diagram. In order to simplify calculations, it was assumed that the heating system runs, through all the heating period, with thermal efficiency corresponding to the mean temperature of the heating period for that climatic zone i.e. t = 4 ^{0}C .Mean heating demand of N_T=3000 kW was calculated from the relationship given in [9]. In view of fact, that during heating season, extraction steam doesn't meet heating requirements, cogeneration system is equipped with reduction–cooling station, that plays role of peak load device. Fuel energy transformation efficiency is one of the basic indicators determining efficiency of heat and electric energy production. For cogeneration system in question, the total efficiency of combined heat and power production is of 76,4 %, watt-hour efficiency of 12,7 % and thermal efficiency of 63,7 %.

At assumption that biomass (wood residues) cost is of 63 €/t, annual amount of biomass that is to be burned in CHP plant is of 15 750 t, therefore annual exploitation costs, regarding biomass purchase average 992 250 €. Comparing combustion of biomass with combustion of hard coal of cost 125 €/t it can be concluded that the total annual exploitation costs increase to 1 260 250 €, it means that cost is about 20% higher compared to the use of biomass.

The kind of fuel burned in CHP system has an effect on the fuel costs and emission of pollutants[8].

Environmental charges are dependent upon air pollutants emission. In case of combined heat and power system fuelled with biomass, environmental charges are less than 7.500 €. In case of hard coal combustion in CHP system, environmental fee is of 58.000 €, that means that is 7 times higher, compared to combustion of biomass.

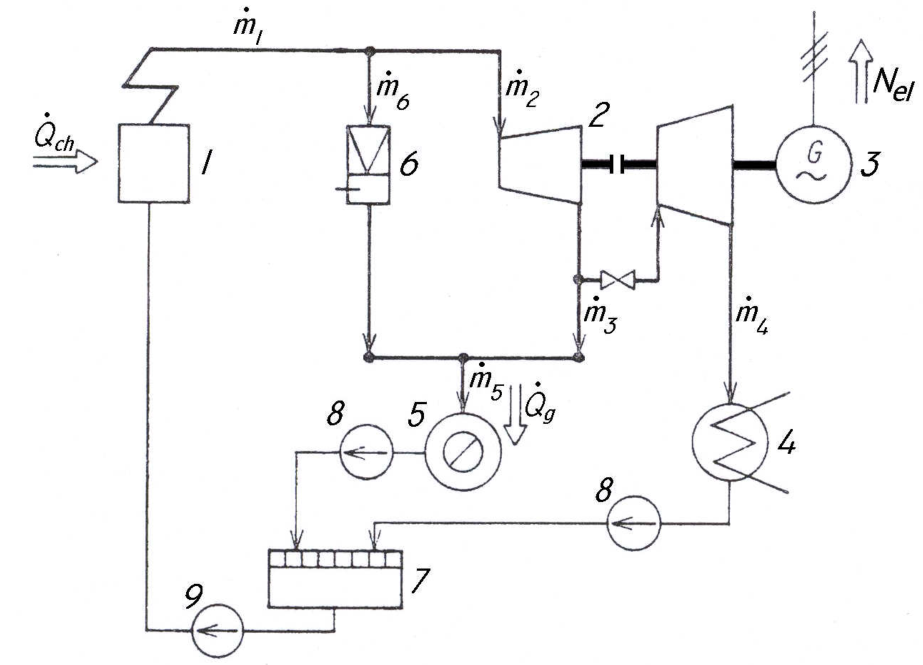

Fig.1:Scheme of thermal cycle:1-the boiler, 2-turbine, 3-electric generator,4 - condenser, 5-heat sink, 6-reduction–cooling station, 7–the condensate tank, 8-the condensate pumps, 9-feed water pump

4.CONCLUSIONS

As it follows from an analysed case, annual biomass (wood) supply in the region doesn’t meet fuel requirements for combined heat and power production. To provide heat and power covering energy requirements in the region, it is necessary to supply CHP plant with an additional amount of biofuel. As there is a large straw potential in the region, straw is considered as the best supplementary fuel for analysed CHP system. In the nearest future, short rotation plantations of energy crops, cultivated on waste lands can be additional biomass resource, supplying CHP system. Recently, one can observe increasing interest in combined heat and power generation based on biomass as the fuel. Decision regarding building of CHP plant in the region should be preceded with careful technical analysis of different CHP variants, particularly CHP systems of a small power. CHP system presented in the paper enables total reduction of CO_2 and nearly SO_2. Apart from evident benefits of the biomass use for combined heat and power generation, it is necessary to remember about some hazards that can occur: not stable biomass quality, regularity of biomass supply, functioning of the biomass feeding devices, corrosion of heat exchangers, NO_x emission. However, the CHP plant profitability is of the utmost importance. Cost effectiveness of investment is also very important problem as charge of energy sale should be maintained at the level ensuring repayment of investment costs. In spite of the above mentioned problems, one should expect dynamic development of biomass CHP systems as it is one of the ways to achieve assumed targets for energy produced from renewable sources to account for 14% in 2020. Production of energy in biomass CHP will contribute to meet the requirement of reducing carbon dioxide emission.

5. REFERENCES

[1] Kogeneracja z biomasy, Przewodnik inwestora, Europejskie Centrum Energii Odnawialnej w Instytucie Mechanizacji i Elektryfikacji Rolnictwa, (2002) Gdańsk, 1-43.

[2] Laudyn D., Pawlik M., Strzelczyk F.(2000) Elektrownie, Warszawa, , WNT.

[3] Ministerstwo Ochrony Środowiska, Strategia rozwoju energetyki odnawialnej w Polsce, 2001.

[4] Portacha, J.(2002) Badania energetyczne układów cieplnych elektrowni i elektrociepłowni, Warszawa, Oficyna Wydawnicza Politechniki Warszawskiej,

[5] Rozporządzenie Rady Ministrów z dnia 20 grudnia 2005 roku w sprawie opłat za korzystanie ze środowiska (Dz.U. Nr 260, poz. 2176).

[6] Rozporządzenie Ministra Gospodarki, Pracy i Polityki Społecznej z dnia 30.05.2003r.:W sprawie szczegółowego zakresu obowiązku zakupu energii elektrycznej i ciepła z odnawialnych źródeł energii oraz energii elektrycznej wytworzonej w skojarzeniu z wytworzeniem ciepła, 2003.

[7] Skorek J., Kalina, J.(2005) Gazowe układy kogeneracyjne, Warszawa, WNT,.

[8] Wskaźniki emisji substancji zanieczyszczających wprowadzanych do powietrza z procesów energetycznego spalania paliw., 1,96, , 1996, Warszawa, MOSZNiL.

[9] Ziębik A., Szargut J.(1995) Podstawy gospodarki energetycznej. Gliwice,. Wydawnictwo Politechniki Śląskiej,

[10] Zwierzchowski R.,(2005) Technologie energetycznego wykorzystania biomasy w aspekcie budowy elektrociepłowni małej lub średniej mocy, Ekologia-Energie Odnawialne-Ciepłownictwo w Polsce i na Świecie, (XII), 11-146.

[11] http://www.powerelectric.com.pl

COMPARATIVE ANALYSIS OF USING ALTERNATIVE FUELS FOR HEATING PURPOSES IN AN INDIVIDUAL HOUSE

MAJCHRZYCKA A., KOZAK T.

Szczecin University of Technology, The Faculty of Mechanical Engineering,
70-310 Szczecin, Piastów 19, Poland.

Abstract: *The paper reports cost analysis of energy production for heating, ventilation and preparation of hot water in a small house with the use of the different kinds of conventional fuels and biofuels and electric heating system. Keywords: heating costs, alternative fuels*

1.INTRODUCTION

The target is for energy produced in Poland from renewable sources to account for 7,5% of total energy consumption by 2010, and for 14% in 2020 therefore, there is growing interest in biofuels. Accessibility and competitive prices cause that biofuels are considered for energy production in individual houses. Presented paper is aimed at comparative analysis of the use of fossil and alternative fuels for heating purposes of an individual house. At the beginning energy demand for the real object - the one floor individual house with attic and garage annex will be determined. The ground floor (without cellar) consists of: vestibule, wc, kitchen, dining room, saloon, hall, 2 bathrooms, 3 bedrooms, store room and garage. Attic is not used as a living space. The house is covered with the gable roof of the slope 15°. The total house area of 225,5 m^2; the usable area of 146,0 m^2, the cubature of 496,1 m^3. The house is for n = 5 inhabitants oriented. The house heating demand was determined at the following assumptions: minimal 24-hour consumption of warm water t = 60 ^oC , V=60l /capita The total thermal power demand for the house heating and preparation of the warm water $\dot{Q}$= 11,44 kW. House heating demand Q_{co} = 68.149 MJ was determined taking into account the different heating periods during a year. The total annual heat demand for heating and preparation of the warm water Q_a = 88 795 MJ.

2.HEATING SYSTEMS

Selection of heating system should be preceded with economic analysis of the use of different kind of fuels and heating systems. It was assumed that energy demand for the house in question is the same for each case of energy production. The cost effectiveness analysis of the following heating systems will be carried out for the heating systems presented in Table 1.

Table 1. An analysed heating systems of an individual house.

The kind of fuel/ heating system	Net calorific value $\dot{Q}_i$ [MJ/kg]	Purchase price [€/t]	Type of the boiler	Gross boiler price [€]
Firewood (20% of moisture)	14,72	63	Ling COMBI LC 4S, [9]	2.364
Willow chips	12,00	40	Ling COMBI LC 4S, [9]	
Wheat straw	14,3	55	Biowat U245, [11]	2.348
Wood briquettes	17,8	125	Ling COMBI LC 4S, [9]	2.364
Pellets	18,5	100	Ling COMBI LC 4S, [9]	2.364
Pea-ecocoal	26	138	Ling COMBI LC 4S, [9]	2.364
Hard coal	23	125	Ling COMBI LC 4S[9]	2.364
Crushed stone sand	19,00	93	WARMET SDS, [9]	1.318
Natural gas GZ-50	48,00	509	ZW 23 1 KE ,[10]	912
Light fuel oil	42,6	755 .	Vitorond 100,VIESSMANN, [12]	3.008
Electric heating -G11 –twenty four hour tariff	0,1010[€/kWh]		2 Accumulative THERMOR unit heaters, [9]	1.245
Electric heating -G12 – the night tariff	0,0498 [€/kWh]		2 Accumulative THERMOR unit heaters, [11]	1.825

Characteristics and purchase prices of the fuels and the boilers were taken from actual price lists and literature [2],[3],[4],[9],[10],[11],[12]. For hard coal and biomass combustion, efficiency of the boilers was assumed to be $\eta = 0,80$ and $\eta = 0,90$ for combustion of natural gas or oil.

3. HEATING COSTS

To analyse profitability of the different heat sources, unitary heat production cost, annual investment outlays and the running costs are determined. Heat production cost consists of supply energy costs (fuels, electricity) and costs resulting form the investment outlays. Cost resulting from the investment outlays depends upon purchase and installation costs, annual heating consumption and the investment outlay service rate. The unit cost of heating produced by the different heat sources can be written as follows [7]

$$k_c = \frac{k_z}{\eta} + \frac{p\,I}{Q_a} \qquad (1)$$

k_z - unit cost of supply energy [€/GJ],
η - heat source efficiency,
p - annual investment outlays service rate,
I - heat source investment expenditures [€],
Q_a - annual heat demand [GJ/a].

Annual heating demand for the house in question is determined as follows:

$$Q_a = \frac{24\dot{Q}S_d}{t_i - t_e} \qquad (2)$$

where:
Q - heating power demand for the house, [kW],
S_d - degree-day number, $S_d = 3781$
t_i, - computational temperature inside the room, t; = 20 °C
t_e - computational temperature in space adjacent to the wall, $t_e = -16$ °C.

Annual service rate of the investment expenditures includes the rates of discount and depreciation. At calculation of profitability at the constant prices, usually the rate of discount is assumed to be 6 - 8 % [1] The real rate of discount was assumed to be 8 %, depreciation rate was assumed to be constant 5,6 %. Capital costs given in equation (1) refer only to heat source, costs of the pipelines, fittings and heaters are not included. Estimated annual operating costs determined from annual heating demand and heat production costs presented are in Table 2 enable to compare the heating unit costs, taking into consideration the fuel cost, fuel net calorific value and efficiency of the heat source and the heating costs including capital costs of the heat source and annual operating costs for the different heating systems.

4. DISCOUNTED HEATING COSTS

Economic effect covering the whole exploitation period of the heating system is usually described as Net Predicted Value, NPV. In fact, it is total predicted profit discounted to year zero, expressed in currency of this year . It is the objective function of the analysis in question [1],[8]:

$$NPV = \sum_{t=0}^{t=n} \frac{(CI_t - CO_t)}{(1+r)^t} \qquad (3)$$

where: CI_t – Cash inflow), €,
CO_t – (Cash outflow), €,
r - discount rate,
t - successive year of exploitation,
n - operating time for installation.

Tab.2: Production unit costs and annual operating costs for different heat sources

The kind of fuel, heating system	Supply energy unit costs [€/GJ]	Heat production unit costs [€/GJ]	Heat unit costs eq.(1) [€/GJ]	Operating (fuel)costs [€/a]
Firewood (20% of moisture)	4,25	5,31	8,93	471,2
Willow chips	3,33	4,17	7,79	370,0
Wheat straw	3,85	4,81	8,41	427,0
Wood briquettes	5,62	7,02	10,64	623,5
Pellets	6,76	8,45	12,07	749,8
Pea-ecocoal	5,29	6,61	10,23	587,0
Hard coal	5,435	6,79	10,41	603,2
Crushed stone sand	4,868	6,09	8,105	541,5
Natural gas GZ-50	10,56	11,78	13,18	1111,0
Light fuel oil	17,72	19,69	24,30	1748,5
Electric heating -G11 –twenty four hour tariff	0,1010 €/kWh	28,04	29,95	2490,0
Electric heating -G12 – the night tariff	0,0498 €/kWh	13,83	16,53	1228,2

Fig. 1 shows discounted expenditure for house heating at assumption of 10 years of exploitation.

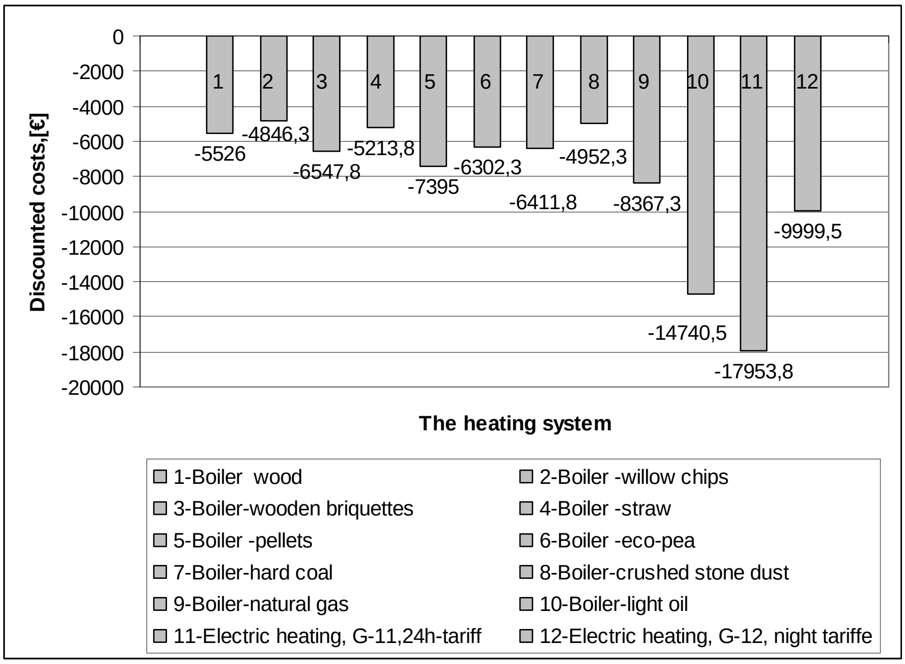

Fig.1: Discounted expenditures of heating system after 10 years of exploitation.

5. ECOLOGICAL ANALYSIS

Emissions of the pollutants into atmosphere were determined by means of the index method, presented in papers [4],[6],[13]. Estimates for emissions gaseous pollutants and dust released into the atmosphere during combustion of the analysed fuels are presented in Table 3.

Table 3. Emissions of gaseous substances and dust released into the atmosphere from burning of the different fuels.

No	Fuel	Emission [kg/a]				
		CO_2	CO	SO_2	NO_x	Dust
1	Wood	**0**	**13,3**	**0**	**17,8**	**10,3**
2	Briquetted wood	**0**	**4,4**	**0**	**3,8**	**3,5**
3	Pellets	**0**	**4,4**	**0**	**3,8**	**0,5**
4	Straw	**0**	**13,3**	**0**	**17,8**	**34,9**
5	Hard coal	**8013**	**399**	**66,6**	**13,3**	**141**
6	Network natural gas GZ-50	**4958**	**1,1**	**0**	**8,9**	**0**
7	Light fuel oil	**6869**	**1,6**	**17,3**	**16,0**	**0**

6. SUMMARY

Economical and ecological analysis of the conventional and alternative fuels use for heating purposes of an individual house was performed. Heat generation unit costs are influenced by the quality and unit price of the fuel and efficiency of the boiler. Implementation of the biofuel quality certification system is essential for the quality of combustion technology and emission. As it follows from analysis, biofuels and hard coal are the most cost – effective for energy production for domestic purposes. Only the price of hard coal is comparable to that of wooden briquette or pellets. The highest costs refer to electricity, oil and natural gas GZ-50 heating technology Discounted expenditures of heating system after 10 years of exploitation are the most advantageous for willow chips fuelled boiler. Energy production from biofuels can be considered as environmentally friendly, provided that the pollutants emissions are reduced by means of the choice a specific combustion system. To determine emission of pollutants and fees for introducing to the atmosphere each of the pollutants , emission indices are essential.

7. REFERENCES

[1] Górzyński J.(2000) Audyting energetyczny.Warszawa,NAPE S.A.

[2] Lewandowski W .(2003).: Proekologiczne źródła energii odnawialnej. Warszawa WNT.

[3] Odwieczne paliwo (2003), Rynek Instalacyjny (4) , 61-63.

[4] Praca zbiorowa (2002): Kogeneracja z biomasy. Europejskie Centrum Energii Odnawialnej,IBMER, Gdańsk, 2002, 1-43.

[5] Praca zbiorowa(2005): Ogrzewanie budynków za pomocą biopaliw stałych. Gdańsk., Bałtycka Agencja Poszanowania Energii S.A.,

[6] Racjonalizacja przetwarzania i użytkowania energii. Wskaźniki techniczno-ekonomiczne i środowiskowe. Holendersko- polski pogram współpracy poszanowania energii SCORE, Gdańsk, 1999.

[7] Rubik M.: Współpraca sprężarkowych pomp ciepła z instalacjami odbiorczymi. COW, 7, 1997, 25-29.

[8] Skorek J., Kruppa R.(2000): Analiza ekonomiczna zastosowania pompy ciepła w typowym budynku jednorodzinnym Gospodarka paliwami i energią (4), 9-17.
[9] www.ekoszok.szczecin.pl
[10] www.junkers.com/pl
[11] www.taniegrzanie.org.pl
[12] www.viessmann.pl
[13] Zawistowski J.(2004),(2005) Biomasa w ogrzewnictwie indywidualnym i komunalnym (p.1), Rynek Instalacyjny (11), 53-55. (p.2), Rynek Instalacyjny 1/2, 30-34

PREPARATION OF $MgFe_2O_4$ /SiO_2 NANOCOMPOSITES BY SOL-GEL METHOD

P.Holec [1,2], J. Plocek [1], D. Nižňanský [1,2], J.Vejpravová[3]

[1] Institute of Inorganic Chemistry, ASCR, 25068 Rez u Prahy, Czech Republic
[2] Department of Inorganic Chemistry, Faculty of Science, Charles University of Prague, Albertov 2030, 128 40 Prague 2, Czech Republic
[3] Charles University, Faculty of Mathematics and Physics, DES, 121 16 Prague 2, Czech Republic

1. INTRODUCTION

Nanocomposites have been the subject of many studies during past years beacause of the new properties they are expected to exhibit. One of the interesting groups consists in metal oxide compounds in a silica matrix. These materials can have interesting magnetic and magnetooptical properties.

This work presents the preparation of $MgFe_2O_4$/SiO_2 system and characterization of the phase relations of the system. The sample were prepared by the sol-gel method. Magnesium ferrite is one of the important magnetic oxide with spinel structure. Magnesium ferrite is used as catalyst [1], humidity sensor [2], for different biomedical application and etc.

Sol-gel method can produce desired materials without high initial costs. The particle size can be controlled by the parametres of the heat treatment. The advanatges of this method are the better homogeneity of materials and lower temperatures of treatment.

The resulting samples were then characterised using powder X-ray diffraction, Mössbauer spectroscopy, magnetic measurements, HRTEM and SEM.

2. SAMPLE PREPARATION

The samples were prepared using conventional sol-gel method. Magnesium and iron nitrates were used as spinel precursor. TEOS (tetraethylorthosilicate), nitric acid (as an acid catalyst), formamide (as a modifier), methanol (as a solvent). Iron nitrate and magnesium nitrate were first dissolved in methanol. The gelation time was approximately 24 h at 40ºC. The samples were left 24 h for ageing. Then they were progressively dried at 40ºC for 2 days in flowing N_2-atmosphere. After drying, they were preheated first at 300ºC and then at various temperatures (800, 900, 1000, 1100ºC) under normal atmosphere. The samples were heated for four hours at above mentioned heating temperatures [3,4,5].

3. X- RAY DIFFRACTION MEASUREMENT

X- ray diffraction all samples indicate the presence of quartz manifested by the characteristic very broad diffraction at 2θ (with the maximum about 22°). The diffraction patterns exhibit broad peaks that become sharper with the increasing temperature of the heat treatment. This corresponds well to crystal growth. In the $MgFe_2O/SiO_2$ system, mainly the diffraction of the spinel phase was observed for all annealing temperatures.

4. MÖSSBAUER SPECTRA

The Mössbauer spectra measurement was carried out at room temperature, 4 K, 4 K and magnetic field 5 T and 3 T. Table 1. represents the spectra measurement was carried out at room temperature. The samples treated at 800 and 900 consist of a dublet that representes the nanoparticles (lesser than criticial size) which are still in the superparamagnetic state. The samples treated at 1000 and 1100℃ show very large singlet and sextet, which is badly discriminability. Therefore we were carried out the next measurement at 4 K. All samples measurement at 4 K show two sextets of the spinel only the samples treated at 800℃ show one doublet and two sextets. In order to determine the cation distribution in the $MgFe_2O_4/SiO_2$ samples, Mössbauer measurements in an external magnetic field were necessary. Table 2. represents the spectra measurement was carried out at 4 K and magnetic field 5 T. All samples measurement at 4 K and magnetic field 5 T and 3 T show two sextets. These results correspond with magnetic measurements.

Tab. 1: The room temperature Mössbauer spectra of the $MgFe_2O_4$ samples treated at different temperatures at range of 800 - 1100℃.

Heating temperature (℃)	Isomer shift δ (mm/s)	Qaudrupole splitting ΔE_q (mm/s)	Hyperfine field BHF (T)	Relative area (%)
800				
Subsp.	0.3326 ± 0.003	1.0346 ± 0.001	–	100 ± 0.11
900				
Subsp. 1.	0.5971 ± 0.005	0.8769 ± 0.007	–	64.5 ± 1.60
Subsp. 2.	0.7138 ± 0.046	0.7886 ± 0.166	10.8822 ± 3.157	35.5 ± 3.16
1000				
Subsp. 1.	0.2954 ± 0.007	0.0253 ± 0.264	–	83.0 ± 0.30
Subsp. 2.	0.1801 ± 0.021	–0.3861 ± 0.023	26.8784 ± 0.494	17.0 ± 0.27
1100-R				
Subsp. 1.	0.3532 ± 0.020	0.0770 ± 0.048	9.2783 ± 2.641	89.1 ± 8.17
Subsp. 2.	0.2611 ± 0.026	0.0048 ± 0.045	44.2646 ± 0.243	10.9 ± 1.88
1100-P				
Subsp. 1.	0.4116 ± 0.022	0.1787 ± 0.051	11.0913 ± 0.740	85.9 ± 2.65
Subsp. 2.	0.3683 ± 0.018	0.0187 ± 0.036	44.2243 ± 0.166	14.1 ± 0.73

Tab. 2: Mössbauer spectra recorded at 4 K in an external magnetic field 5 T.

Heating temperature (℃)	Isomer shift δ (mm/s)	Qaudrupole splitting ΔE_q (mm/s)	Hyperfine field BHF (T)	Relative area (%)
800				
Subsp. 1.	0.4342 ± 0.004	0.0004 ± 0.010	48.3182 ± 0.061	54.5 ± 3.05
Subsp. 2.	0.4474 ± 0.006	–0.0385 ± 0.014	43.4375 ± 0.133	45.5 ± 3.19
1100-R				
Subsp. 1.	0.3539 ± 0.002	0.0100 ± 0.002	55.9771 ± 0.010	38.0 ± 0.27
Subsp. 2.	0.4792 ± 0.002	0.0016 ± 0.003	48.3545 ± 0.011	62.0 ± 0.40
1100-P				
Subsp. 1.	0.3480 ± 0.002	0.0067 ± 0.004	53.8833 ± 0.017	31.7 ± 0.72
Subsp. 2.	0.4663 ± 0.002	0.0058 ± 0.004	50.3040 ± 0.023	68.3 ± 0.99

5. MAGNETIC MEASUREMENTS

Magnetization curve of $MgFe_2O_4/SiO_2$ was determined for all amples at 300, 100 and 2 K. Coercivity are zero at 100 and 300 K, which indicates that the samples are superparamagnetic.

Below T_B, the magnetic particles are frozen and magnetic moment of the particles is fixed, and hysteresis appeares in the magnetization curves. We can see that the saturation magnetization values increase as the particle size increases with the annealing temperature.

We can see the convergence of the ZFC and FC curves at high temperatures and the separation at lower temperatures is typical of superparamagnetism. It is clear that the samples calcinated at lower temperatures are superparamagnetic, while those treated at higher tempertures have a ferrimagnetic character.

6. HRTEM AND SEM OBSERVATION

Direct parcticle size observation by means of HRTEM confirms the tendency by X-ray diffraction. The particle size rapidly increases with an increase in the heating temperature.

7. CONCLUSIONS

In order to determine the cation distribution in the $MgFe_2O_4/SiO_2$ samples, Mössbauer measurements in an external magnetic field were necessary. The spectra show asymmetric broadening of the [B]-sites lines indicating the presence of several subpatterns arising from the different possible nearest-neighbour (A)-site configurations via supertransfer mechanism. In contrast, the (A)-site lines do not show any structure that indicates the presence of narrow field distribution in agreement with the usually (A)-site supertransferred hyperfine field. Therefore, the data were analysed using a fitting procedure which takes into account hyperfine field distribution for the Fe^{3+}. The structural formula of $MgFe_2O_4$ is usually written as $(Mg_{1-x}Fe_x)[Mg_xFe_{2-x}]O_4$ where round and brackets denote sites of tetrahedral (A) and octahedral [B] coordination respectively, and where x represents the degree inversion. The degree of inversion, calculated from the subspectral area ratio. So the formula can be written as $(Fe_{0.37}Mg_{0.63})[Fe_{1.63}Mg_{0.37}]O_{4.}$

The Mössbauer spectra and the X-ray diffraction patterns confirmed the presence of the spinel phase. Magnetic measurements showed a superparamagnetic behaviour of the samples heated at lower temperature and ferrimagnetic character for the samples heated at higher temperature. The $MgFe_2O/SiO_2$ spinel phase, which is formed in the studied nanocomposite is stable up to 1100℃ annealed sampl e. This work aims to show the suitability of this way of the preparation of magnesium ferrite nanoparticles in the silica matrix.

Acknowledgement: The authors thanks for financial support of the Grant Agency of the Academy of Sciences of the Czech Republic 106/07/0949

8. REFERENCES

[1] Busta, G., Finocchio, E., Lorenzelli, V., Trombetta, M., and Rossini, S.A. (1996) J. Chem. Soc., Faraday Trans. 92, 4687.

[2] Shimizu, Y., Arai, H., and Seyima, T. (1985) Sens. Actuators 7, 11

[3] Nižňanský, D., Lančok, A., Hutlová, A., Rehspringer, J.L., and Buršík, J. (2001) Int. J. Inorg. Mater. 3/6, 479.

[4] Hutlová, A., Nižňanský, D., Plocek, J., Buršík, J., and Rehspringer, J.L. (2003) J. Sol-Gel Sci. Technol. 26, 473.

[5] Plocek, J., Hutlová, A., Nižňanský, D., Buršík, J., Mička, Z., and Rehspringer, J.L. (2003) J.Non-Cryst. Solids 70, 315.

ELECTRICAL PARAMETERS OF C-SI PHOTOVOLTAIC CELLS IN DEPENDENCE ON TEMPERATURE AND IRRADIANCE

Zdenek Machacek[1], Vitezslav Benda[1] and Radim Barinka[2]

[1] CTU Prague, Faculty of Electrical Engineering, Department of Electrical Technologies, Czech Republic
[2] Solartec,sro, Roznov p. Radh., Czech Republic

Abstract: *Presented paper describes the dependences of all important parameters of silicon photovoltaic cells on both temperature and irradiance obtained using cell tester Pasan IIc. The knowledge about system behaviour in real operating conditions is desirable for photovoltaic applications.*

Keywords: *photovoltaic cell efficiency, irradiance, temperature*

1. INTRODUCTION

Parameters of PV cells and modules are given by producers as data valid under Standard Testing Conditions (STC), i.e. spectrum AM 1,5 irradiation 1000 W/m^{2}and cell temperature 25℃. In real conditions, PV modules us ually operate at higher temperatures. The temperature change I-V characteristics of photovoltaic cells (PV cells, solar cells) takes effect mostly on the value of the open circuit voltage V_{OC} and in this way are usually discussed in literature (see e.g. [1], [2]). Less information is available about temperature dependence of other PV cells parameters under conditions different from Standard Testing Conditions (STC), i.e. irradiation 1000 W/m^2, spectrum AM 1,5 and cell temperature 25℃.

In practical applications, photovoltaic systems never operate under STC and knowledge about dependences of all main parameters of PV cells and modules on both irradiance and temperature is desirable. In this work we present results of measurements PV cell I-V characteristics in a broad range of temperature and irradiance using cell tester Pasan IIc.

2. PV CELL PARAMETERS

For our measurements, a 4-inch monocrystalline silicon Si PV cells (manufacturer Solartec, s.r.o.) were used. Parameters of PV cells measured under Standard Testing Conditions (STC), i.e. spectrum AM 1,5 irradiation 1000 W/m^{2}and cell temperature 25℃ using solar simulator Pasan IIc are shown in table 1.

Tab. 1: Parameters of the measured solar cell during STC.

Parameter	Notation	Units	Values
Short circuit current	I_{SC}	A	3,21
Open circuit voltage	V_{OC}	V	0,59
Conversion efficiency	η	%	13,64
Fill factor	FF	%	74,18
Power at MPP	P_M	W	1,405
Voltage at MPP	V_{MP}	V	0,483
Current at			

Concerning the crystalline silicon PV cells, the theoretical assumption gives the open circuit voltage drop approximately 0,4 % / ℃. The temperature dependence of cell parameters at different irradiance level is less known. Therefore, a set of measurements was conducted for authentication of the influence of temperature and irradiance on the PV cell parameters.

3. EXPERIMENT

For our experiments, PV cells were measured using cell tester Pasan IIc. The tester is based on flash-lamp techniques allowing fast I-V measurements and eliminating the risk of PV cell heating during the measurement.

The photovoltaic cell was attached using special contacting system that was adjusted for the ability to be heated. Whole contact system was placed on a heated desk with adjustable temperature. Irradiance was regulated by changing the distance between the flash lamp and the measured photovoltaic cell. Lower irradiance was achieved using a gray filter that was put in front of the lamp. This way, irradiance ranging from 100 W/m^2 to 1000 W/m^2 was obtained. The temperature ranged from 20 ℃ to 100 ℃.

4. RESULTS AND DISCUSSION

The dependences of measured voltage-current characteristics on the temperature at irradiation 1000 W/m^2 are illustrated on the figure 1. Similar sets of characteristics were measured also at irradiance 450 W/m^2, 300 W/m^2, 200 W/m^2 and 100 W/m^2. This way, dependences of all important cell parameters on both temperature and irradiance were obtained. Here with this cell, almost linear decline of V_{OC} on the average in 0,38 % / ℃ (see figure 2, radiance 1000 W/m^2) was measured. With the drop of the PV cell open circuit voltage, the maximum power output and thus the efficiency decrease as well.

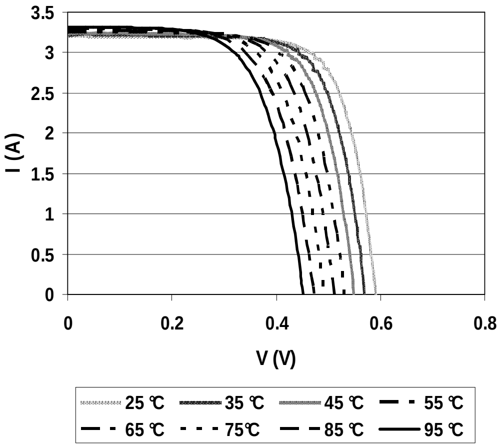

Fig. 1: The temperature influence on the current-voltage characteristics of the PV cell for irrradiance 1000 W/m^2

The measured decrease of the efficiency of the PV cell during the temperature increments as a function of the PV cell temperature and the irradiance is illustrated in figure 3 and figure 4. Here, the efficiency decreases with the temperature linearly, in average by 0,53 % / ℃ (for 1000 W/m^2). With decreasing irradiance, the rate of the efficiency decrease is lower.

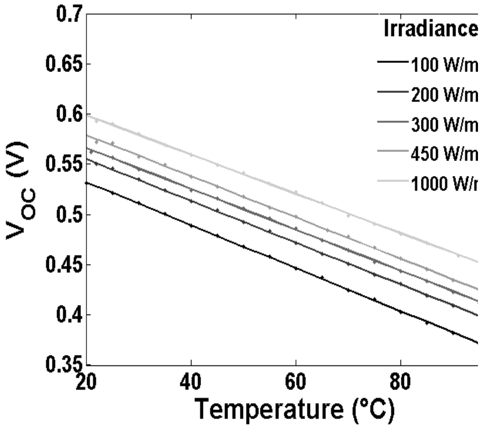

Fig. 2: Measured values of V_{OC} of the PV cell as a function of the cell temperature for different irradiance.

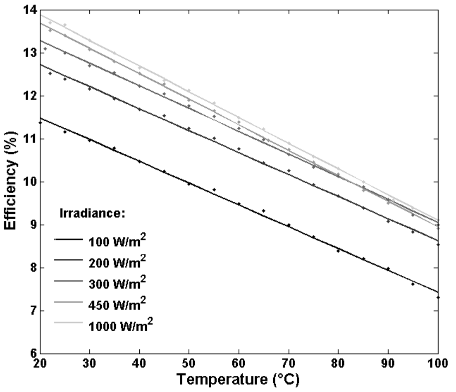

Fig. 3: Measured PV cell efficiency as a function of the cell temperature for different values of radiance.

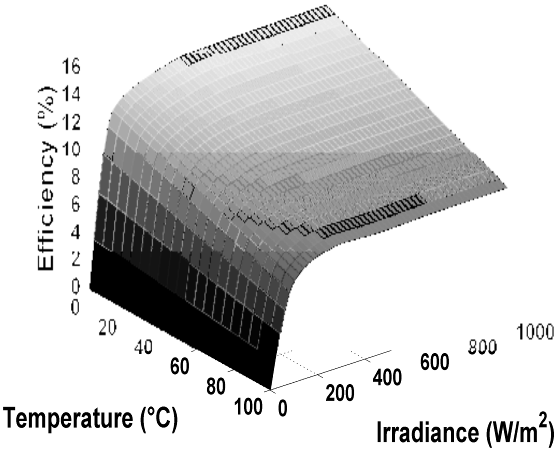

Fig. 4. : The progression of efficiency of the measured PV cell as a function of the cell temperature (range from 0 to 100 °C) and irradiance (range from 0 to 1000 W/m^2).

These basic trends can be observed in practical applications. PV system efficiency is much higher during the winter months, than in the summer and, as well, this efficiency changes during the day (during sunny summer day, the total PV cell temperature difference can rise up to 45 °C), (see [3]).

The rest of the PV cell parameters change with the temperature as well, but their influence is not as big as it is of the parameters mentioned above. The short circuit current I_{SC} grows slightly with linear dependence on the temperature, as it is shown in the figure 1. This increase is as low as 0,05 % / °C. The rest of the basic PV cell parameters are the fill factor FF, series resistance R_s and parallel resistance R_p. The value of the fill factor decreases with increasing temperature by approximately 0,2 % / °C, the value of series resistance increases with increasing temperature almost linearly by approximately 0,32 % / °C and the value of parallel resistance decreases with increasing temperature also almost linearly by approximately 0,7 % / °C. These values were measured on the PV cell with the radiance of 1000 W/m^2 and in temperature range from 20 °C to 100 °C. The measured dependences of R_s and R_p on temperature and irradiance are shown in Fig.5 and Fig.6.

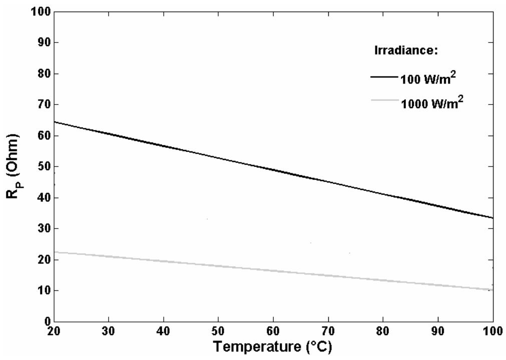

Fig.5. Measured dependence of R_p on temperature for different irradiation levels

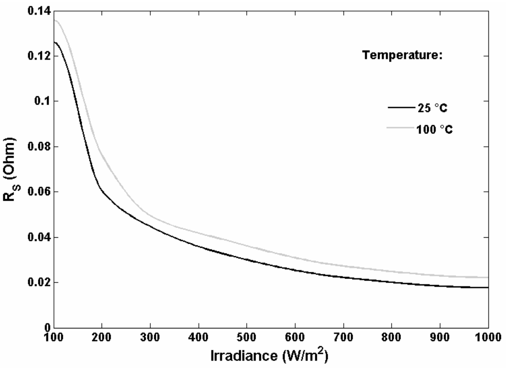

Fig.6. Measured dependence of R_S on irradiance at different temperatures

5. CONCLUSION

Because of heating of the PV cells during their utilization (heating by the solar radiation), cooling of these cells is needed. Thence it follows the requirement for as low cell temperature as possible. For each application, it is necessary to dispose of such as construction, which enables effective cooling (natural, if it possible), for example: by enabling of the surrounding air circulation that can lead to a dramatic increase of the PV system efficiency. Other possibility how to keep the PV cell temperature as low as possible is the hybrid solar cell system. Hybrid panels combine the functions of the PV panel and the photo-thermal collector for the water heating. The back surface of the solar cells is with the aid of electrically insulating but thermally conducting layer connected with a system of pipes with circulating cooling medium. This medium is instrumental for the heat transfer, which is subsequently stored in the reservoir as heated water. In this way, such a combined system for using the solar energy can operate.

6. REFERENCES

[1] Goetberg A., Knobloch, J. and Voss B.: Crystalline Silicon Solar Cells, J.Wiley & Sons., Chichester, 1998
[2] Markvart T., Castaner, L.: Solar Cells, Elsevier, Oxford, 2005
[3] Benda, V., Machacek, Z.: A Comparison of Operating Conditions for Facade and On-Roof Applications of Photovoltaic Systems in Prague. In The Integration of The Renewable Energy Systems into the Buildings Structures. Patras: TEI Patras, 2005, s. 35-39.

ROLE OF THE GEOSTROPHIC FLOW IN THE LIQUID CORE OF THE EARTH

A. Anufriev [1], M. Tassev [2]

[1]Geophysical Institute, ul.Acad.G.Bonchev, bl3, Sofia1113, Bulgaria,
[2] South-West University, Department of Mathematics, Blagoevgrad, Bulgaria,
e-mail: matassev@abv.bg

Abstract. *The momentum equation for the flow in the Earth's liquid core which depends on two small parameters (the Ekman, E, and the Rossby, R_o numbers), is transformed to a form which depends on other two parameters:* $\sqrt{E}$ *and* $\lambda = \sqrt{E}/R_o$*. The first of them is still small, but the other one exceeds* $\sqrt{E}$ *approximately with six orders of magnitude. The Ekman suction boundary conditions for the inviscid flow in the bulk of the Earth's core also depend on the first parameter only. Therefore we search for the solution of the hydrodynamic problem in the form of the decomposition in the small parameter* $\sqrt{E}$*. The equations obtained show that the flow of the leading approximation in* $\sqrt{E}$ *decomposition depends on the only parameter* λ*. This means that for fast rotating fluids* $\lambda = \sqrt{2\Omega\nu}/V_1$ *becomes the universal parameter (as e.g. the Reynolds number* $R = V_1 L_1/\nu$ *in the hydrodynamics) and all flows can be classified only by it. The whole flow is presented as a sum of the force and the geostrophic flows. The former satisfies the no-normal flow boundary condition and can be directly determined in terms of integrals of the force. The latter is directed along* ϕ *and satisfies the no-slip boundary condition. It obeys the equations which depend on time derivative of the geostrophic velocity.* ***So the geostrophic flow is the only part of the whole flow which has its own time behavior.*** *It evolves together with magnetic field and temperature distributions. In the opposite, the force flow fits instantly to the force and its time behavior is defined entirely by that of the force distribution.*

Key words: *geodynamo, Taylor state, inviscid limit*

INTRODUCTION

The flow in the liquid core of the Earth is driven by the Archimedean and the Lorentz forces. This area is situated between the inner core boundary (ICB) and the core mantle boundary (CMB). Determination of this flow is an important part of the whole geodynamo problem. The dimensionless momentum and continuity equations for it can be written in a form:

(1.1,2) $$R_o \bar{\rho}\left[\frac{\partial \mathbf{V}}{\partial t} + \mathbf{W}\times\mathbf{V}\right] = -\bar{\rho}\nabla P - \bar{\rho}\mathbf{1}_z \times \mathbf{V} + \mathbf{F} + \bar{\rho}\, E\,\Delta\mathbf{V}, \qquad \nabla\cdot\bar{\rho}(r)\mathbf{V} = 0,$$

where $\mathbf{W} = \nabla\times\mathbf{V}$, $\mathbf{F} = \mathbf{F}^a + \mathbf{F}^b$, $P = p/\bar{\rho} + \mathbf{V}^2/2$ and p is the pressure. Here $\mathbf{F}^a = r\,A\,(\bar{\rho}(r)\,\bar{g}(r)/r)\,C$ is the Archimedean and $\mathbf{F}^b = R_m \mathbf{J}\times\mathbf{B}$ is the Lorentz forces where $\mathbf{J} = \nabla\times\mathbf{B}$ and C and **B** are the super-adiabatic temperature and the magnetic field strength. (Generally C and be considered as co-density). The dimensionless parameters, the Ekman, the Rossby and the Reynolds magnetic numbers are defined respectively as

(1.3) $$E = \frac{\nu}{2\Omega L_1^2}, \quad R_o = \frac{V_1}{2\Omega L_1}, \quad R_m = \frac{V_1 L_1}{\eta}$$

where L_1, V_1, L_1/V_1, $\sqrt{2\Omega\eta\bar{\rho}_1\mu_o}$, ρ_1, $2\Omega\bar{\rho}_1 V_1$ and $2\Omega\bar{\rho}_1 V_1 L_1$ are the space, the flow velocity, the time, the magnetic field strength, the density, the force and the pressure scales. Note that the viscous force in compressible liquid, generally speaking, differs from this in (1.1). However this difference is essential only outside the thin layers where the viscous force is negligible.

The Ekman number in the Earth's core is extremely small: E ~10^{-15}. This leads to great difficulties in the computer resolution of the thin layers ($\delta = O(\sqrt{E})$) on the core's boundaries. That is why *E* in the existing computer simulations is typically accepted to be several orders of magnitude greater than its real value (see e.g. Glatzmaier and Roberts (1995, 1996a), Jones et al (1995) Fearn and Morrison (2001) who accept E to be in the range (10^{-3} to 10^{-5}).

The value of E above is obtained for the kinematic viscosity. The turbulent viscosity enhances the value of the Ekman number with several orders of magnitude. However, even the turbulent E hardly exceeds 10^{-10}. A question of principle arises here: whether the flow of the computer simulations carried out for the relatively large values of the Ekman number keep valid for its small values? And yet another question. Is it possible to reformulate the numerical flow problem in a way which could be free of the difficulties connected to the resolution of the thin boundary layers? Here we are trying to answer both questions.

When solving the momentum equation we can neglect the changes of the field in the bulk of the core, but we must take them into account in the thin layers. Thus we assume that during the flow fitting, the magnetic field remains unchanged only in the interior of the liquid core, but not in the thin boundary and space layers. The magnetic field in the layers fits together with the flow. Respectively, the boundary conditions (2.4) for the flow outside the boundary layer on its outer surface are obtained by solving the momentum and the induction equations into the layer.

EQUATION AND BOUNDARY CONDITIONS

The momentum equation (1.1) depends on two small parameters: the Ekman and the Rossby numbers. Let us transform this equation dividing it by $\sqrt{E}$:

(2.1,2) $$\frac{\bar{\rho}}{\lambda}\frac{\partial \mathbf{V}}{\partial t} = \frac{-\bar{\rho}\,\nabla P - \mathbf{1}_z \bar{\rho} \text{ x } \mathbf{V} + \mathbf{F}}{\sqrt{E}} - \frac{\bar{\rho}}{\lambda}\mathbf{W} \times \mathbf{V} + \sqrt{E}\Delta \mathbf{V} \;, \quad \nabla \cdot \bar{\rho}(r)\mathbf{V} = 0$$

Then new momentum equation depends on other two parameters:

(2.3) $$\sqrt{E} = 3.5 \times 10^{-5}\sqrt{\frac{\nu}{\eta}} \quad \text{and} \quad \lambda = \frac{\sqrt{E}}{R_o} = \frac{\sqrt{2\Omega\nu}}{V_1} = 3.3 \times 10^{1}\sqrt{\frac{\nu}{\eta}}$$

In these estimations we have used the following parameters from Roberts and Glatzmaier (2000): the typical value of the westward drift $V_1 = 5 \times 10^{-4}\,\mathrm{ms}^{-1}$ and the value of the magnetic diffusivity $\eta = 2\mathrm{m}^2\mathrm{s}^{-1}$. As a space scale, the radius of the liquid core of the Earth $L_1 = r_2 = 3.4 \times 10^6\,\mathrm{m}$, is used.

We assume that the turbulent viscosity is not smaller than $\nu_M = 10^{-6} m^2 s^{-1}$ and does not exceed $\eta = 2\,\mathrm{m}^2\,\mathrm{s}^{-1}$.

Then λ is situated in the interval: $2.3 \times 10^{-2} \le \lambda \le 3.3 \times 10^{1}$. For all possible values of the turbulent viscosity λ exceeds $\sqrt{E}$ with approximately six orders. Therefore, we will further assume that (2.1) depends on the only small parameter $\sqrt{E}$.

The smallness of this parameter allows us to treat the flows in the bulk of the Earth's core as inviscid ones and neglect the last (viscid) term in rhs of (2.1). The neglecting of this term reduces the order of the equation and the no-slip boundary condition for it must respectively be replaced by others.

The Ekman suction boundary conditions are obtained by solution of the momentum and the induction equations into the boundary layer. The suction into the layer is proportional to the jump of the normal component of the curl of the flow in it. Respectively the boundary conditions for the flow out of the layer in the North and the South hemispheres take the form:

(2.4)
$$\bar{\rho}(r_1)\,\mathbf{r}_{\pm 2}\cdot\mathbf{V}(\mathbf{r}_{\pm 2}) = m\sqrt{E}\,\gamma\,(\mathbf{r}_{\pm 2})\,\mathbf{r}_{\pm 2}\cdot\nabla\times\left[\mathbf{V}(\mathbf{r}_{\pm 2})-\mathbf{1}_\phi s\omega_2\right]$$
$$\bar{\rho}(r_1)\,\mathbf{r}_{\pm 1}\cdot\mathbf{V}(\mathbf{r}_{\pm 1}) = m\sqrt{E}\,\gamma\,(\mathbf{r}_{\pm 1})\,\mathbf{r}_{\pm 1}\cdot\nabla\times\left[\mathbf{V}(\mathbf{r}_{\pm 1})-\mathbf{1}_\phi s\omega_1\right]$$

where $\mathbf{r}_\pm = 1_s s \pm \mathbf{1}_z |z|, \omega_{1,2}$ is the angular velocity of the correspondent boundary and

(2.5)
$$\gamma\,(r_{1,2},\vartheta,\phi) = \bar{\rho}\,(r_{1,2})\sqrt{\frac{\sqrt{\cos^2\vartheta+B_r^4}-B_r^2}{2(\cos^2\vartheta+B_r^4}}$$

Equation (2.1) and the boundary conditions (2.4) depend on the small parameter $\sqrt{E}$ and they respectively hint that the flow can be searched in the form of expansion in this parameter:

(2.6) $\mathbf{V}(r) = \mathbf{V}^{(0)}(r)+\sqrt{E}\mathbf{V}^{(1)}(\mathbf{r})+\ldots \qquad P(\mathbf{r}) = P^{(0)}(r)+\sqrt{E}P^{(1)}(\mathbf{r})+\ldots$

The substitution of (2.6) into (2.4) yields to the boundary condition of the leading

(2.7,8) $\bar{\rho}(\mathbf{r}_1)\,\mathbf{r}_{\pm 1}\cdot\mathbf{V}^{(0)}(r_{\pm 1}) = 0\,,\quad \bar{\rho}(\mathbf{r}_2)\,\mathbf{r}_{\pm 2}\cdot\mathbf{V}^{(0)}(r_{\pm 2}) = 0\,,$

and the next

(2.9) $\bar{\rho}(r_1)\,\mathbf{r}_{\pm 1}\cdot\mathbf{V}^{(1)}(\mathbf{r}_{\pm 1}) = \pm\gamma(\mathbf{r}_{\pm 1})\,\mathbf{r}_{\pm 1}\cdot\nabla\times\mathbf{A}^{(0)}(\mathbf{r}_{\pm 1})$

(2.10) $\bar{\rho}(r_2)\,\mathbf{r}_{\pm 2}\cdot\mathbf{V}^{(1)}(\mathbf{r}_{\pm 2}) = \pm\gamma(\mathbf{r}_{\pm 2})\,\mathbf{r}_{\pm 2}\cdot\nabla\times\mathbf{A}^{(0)}(\mathbf{r}_{\pm 2})$

approximations, where

(2.11) $\mathbf{A}^{(0)}(\mathbf{r}_{\pm 1,2}) = \mathbf{V}^{(0)}(r_{\pm 1,2})-\mathbf{1}_\phi s\omega_{1,2}.$

Signs “+” and “–“ at $\mathbf{r}_\pm$ refer to the North and the South hemispheres in the core. Summarizing and subtracting “+” and “–“ components of (2.7) and (2.8) we obtain the boundary conditions for the quadruple flow and the dipole flow of the leading approximation.Proceeding analogically with (2.9) and (2.10) one can obtain the boundary conditions. Finally, we can obtain the boundary condition for a particular but important case of the axisymmetric flow. This flow for both approximations has a form:

(2.12) $$\bar{\mathbf{V}}(s,z) = -\frac{\mathbf{1}_\phi}{\bar{\rho}(r)s}\times\nabla\bar{\chi}(s,z) + \mathbf{1}_\phi\bar{V}_\phi$$

Combining (2.7,8) and (2.12) one can obtain: $\partial\bar{\chi}^{(0)}(r_{1,2},\vartheta)/\partial\vartheta = 0$ where (r,ϑ,ϕ) are the polar spherical coordinates. From here it follows that the streamline function $\bar{\chi}^{(0)}(r,\vartheta)$ is constant on the boundaries. Further we will accept this constant to be zero:

(2.13) $\bar{\chi}^{(0)}(r_{1,2,}\vartheta) = 0$

Eq. (2.12) also can be transformed to its quadruple-dipole form:

(2.12q,d) $$\bar{\mathbf{V}}_q(s,z) = -\frac{\mathbf{1}_\phi}{\bar{\rho}(r)s}\times\nabla\bar{\chi}_d+\mathbf{1}_\phi\bar{V}_{q\phi}\,,\qquad \bar{\mathbf{V}}_d(s,z) = -\frac{\mathbf{1}_\phi}{\bar{\rho}(r)s}\times\nabla\,\bar{\chi}_q + \mathbf{1}_\phi\bar{V}_{d\phi}\,;$$

Then averaging over ϕ we obtain the boundary conditions of the next approximation for the axisymmetric flow:

Let us assume that both problems of the leading and the next approximations are resolved and a solution in the form (2.6) is obtained. As (2.6) shows, the leading part of the flow does not depend on the Ekman number. Respectively, the flow depends on the only parameter λ.

Thus we can conclude that in the case of small $\sqrt{E}$ and R_o the flow doesn't depend separately on both these parameters, but only on their relation $\lambda = \sqrt{E}/R_o$. It means that λ at small values of $\sqrt{E}$ and R_o becomes the universal parameter for the fast rotating flow as e.g. the Reynolds number in the hydrodynamics. We noticed in the beginning of this section that the Rossby number and the square root of the Ekman number are both of order of 10^{-5}. However the problem with $E \sim 10^{-5}$ is out of up-to-date computer possibilities. Nevertheless, this problem can be relatively easily solved for the greater values $\sqrt{E}$ and R_o e.g. $\sqrt{E} = R_o = 10^{-2}$. Our discussion above shows that both flows (with the same λ) must be close to one another. Respectively, a very complicated from computer simulation point of view problem can be replaced with another, more resolvable, one.

By replacing (2.6) into (2.1), we can obtain the momentum equations of the leading and the next approximations. However, prior to this, let us consider the equations for the kinetic energy and the angular momentum.

THE LEADING APPROXIMATION PROBLEM

The substitution of (2.6) into (2.1) yields to the equations of the leading approximation:

(3.1,2) $$-\bar{\rho}\nabla P^{(0)} - \bar{\rho}\mathbf{1}_z \times \mathbf{V}^{(0)} + \mathbf{F} = 0, \qquad \nabla\cdot\bar{\rho}\mathbf{V}^{(0)} = 0$$

Equation (3.1) is obtained in supposition that the typical time scale t_1 of the processes is of order of L_1/V_1. This supposition fails for the very fast processes when $(V_1/L_1)t_1\lambda \sim \sqrt{E}$. The typical time for this fail is very small: $t_1 \sim (L_1/V_1)(\sqrt{E}/\lambda) = = (1/2\Omega)$. It follows from here that equation (3.1) is valid if the typical time of the correspondent processes is much larger than a few hours: t_1 » $(1/2\Omega)$.

The azimuthal component of the axisymmetric flow is not included into the boundary conditions (2.7,8). Respectively it cannot be determined from them. It satisfies the continuity equation identically: $\nabla\cdot\bar{\rho}(r)\mathbf{1}_\phi \overline{V}_\phi^{(0)}(s,z) \equiv 0$ and therefore cannot be determined by this equation either. Therefore the azimuthal axisymmetric flow of the leading approximation cannot be determined in its frame. The next approximation is needed to define it. But nevertheless an essential part of the axisymmetric azimuthal flow can be defined in this approximation.

Dividing (3.1) by $\bar{\rho}$ and applying the curl operator yields to

(3.3) $$\frac{\partial \mathbf{V}^{(0)}}{\partial z} = \mathbf{1}_z(\nabla\cdot\mathbf{V}^{(0)}) - \nabla\times\frac{\mathbf{F}}{\bar{\rho}}$$

It follows from here that the ϕ component of the axisymmetric azimuthal flow can presented as a sum of the force, $\overline{V}^F = s\overline{\omega}^F(s,z)$, and the geostrophic, $\overline{V}^g = s\overline{\omega}^g(s)$, flows: $\overline{V}_\phi^{(0)} = s\overline{\omega}^F + s\overline{\omega}^g$, where the equation for $\overline{\omega}^F$ takes a form:

(3.4) $$\frac{\partial\overline{\omega}^F}{\partial z} = -\frac{1_\phi}{s}\nabla\times\frac{\overline{\mathbf{F}}}{\bar{\rho}}; \quad \left(= \nabla\cdot\left[\frac{\mathbf{1}_\phi}{s}\times\frac{\overline{\mathbf{F}}}{\bar{\rho}}\right]\right)$$

The force in (3.4) consists of the Archimedean, $\overline{\mathbf{F}}^a = \mathbf{r}A(r)\bar{\rho}\overline{C}(s,z)$, and the Lorentz, $\mathbf{F}^b = R_m\mathbf{J}\times\mathbf{B}$, parts. In conclusion of this section let us emphasize again that all the components of the flow except its geostrophic part can be defined in the leading approximation. Respectively the flow of the leading approximation can be presented as a sum of the force flow $\mathbf{V}^F(s,\phi,z)$ which is defined in this approximation and the unknown geostrophic flow $\mathbf{1}_\phi V^g = \mathbf{1}_\phi s\overline{\omega}^g(t,s)$:

(3.7) $$\mathbf{V}^{(0)} = \mathbf{V}^F(s,\phi,z) + \mathbf{1}_\phi s\,\overline{\omega}^g(t,s)$$

The force flow $\mathbf{V}^F$ consists of the axisymmetric and the non-axisymmetric parts:

$$(3.8) \qquad \tilde{\mathbf{V}}^{(0)} = \tilde{\mathbf{V}}^{F}(s,\phi,z)\,; \qquad \overline{\mathbf{V}}^{F}(s,z) = -\frac{\mathbf{1}_\phi}{\overline{\rho}(r)s}\times\nabla\overline{\chi}^{F}(s,z) + \mathbf{1}_\phi\overline{V}_\phi^{F}(s,z)\,,$$

The force flow establishes instantly by means of pressure. Respectively, its time dependence is defined by the time dependence of the force. Thus it has no its own time dependence. To emphasize this, we do not include *t* in the list of its variables.

THE NEXT APPROXIMATION PROBLEM

In order to obtain the equations of the next approximation, we substitute (2.6) into (2.1,2) and take (3.1,2) into account. Then we get:

$$(4.1{,}2) \qquad \frac{\partial\mathbf{V}^{(0)}}{\partial t} - \mathbf{V}^{(0)}\times\nabla\times\mathbf{V}^{(0)} = -\lambda\left[\nabla P^{(1)} + \mathbf{1}_z\times\mathbf{V}^{(1)}\right]; \quad \nabla\cdot\overline{\rho}\mathbf{V}^{(1)} = 0\,.$$

Note that, since the force flow does not depend directly on time, the only non-vanishing time derivative in lhs of (4.1) is that of the geostrophic velocity.. This equation which is the ϕ component of (4.1), can be directly obtained from (4.5), taking (3.7) into account.

$$(4.3) \qquad \frac{\partial s\overline{\rho}\,\overline{V}_\phi^{g}(s,t)}{\partial t} = \nabla\cdot\left[\mathbf{1}_z\lambda\overline{\chi}^{(1)} - \overline{\mathbf{V}_m^{(0)}\overline{\rho}sV_\phi^{(0)}}\right]$$

In section 4 we have introduced the function M(s) describing the distribution of the angular momentum of the liquid core. The integration of (4.3) over the same volume as in section 4, gives the equations for $M_{q,d}(s)$:

$$(4.4) \qquad \frac{dM_{q,d}(s)}{dt} = \lambda\Upsilon_{q,d\delta}(s) + \Upsilon_{q,dF}(s)$$

Here the quadruple and dipole angular components of the angular momentum are defined by the expressions:

$$(4.5) \qquad M_{q,d}(s) = \int_0^s sds\, s^2\mathcal{R}(s)\,\overline{\omega}_{q,d}^{g}(s)\,dz\,, \quad \text{where} \quad \mathcal{R}(s) = \int_{z_b}^{z_2} dz\overline{\rho}(r)$$

Eq. (4.5) shows that the angular momentum of the whole body is presented as a sum of momentums of the liquid cylindrical shells rotating with the angular velocities $\overline{\omega}_{q,d}^{g}(s)$. The torques $\Upsilon_{q,d\delta}$ and $\Upsilon_{q,dF}$ in (4.4) has a form like (4.9) and (4.10)

$$(4.6) \qquad \Upsilon_{q,d\delta}(s) = \int_0^s s\,ds\,\Pi_{d,q}(s)$$

$$(4.7) \qquad \Upsilon_{q,dF}(s) = s^2\int_{z_b}^{z_2} dz\,\overline{\rho}\left[\overline{V_s^F\,V_\phi^F(s,z)}\right]_{q,d}$$

where $\Pi_{d,q}(s)$ is defined by (4.9a) and z_b is defined again by (4.8). Since the whole flux across the cylinder surface between the ridged boundaries vanishes, the integral

$$\int dz\,\overline{\rho}\,\overline{s}\,\overline{V}_s^{(0)}(s,z)\,V^g(s) = 0$$

vanishes as well. Respectively the geostrophic velocity is not included in rhs of (4.7).

By differentiating (4.4) in respect of *s* inside the tangent cylinder one can obtain equations for the geostrophic angular velocity:

$$(4.8) \qquad \frac{\partial\omega_q^g(s)}{\partial t} - \frac{\lambda}{s^2}\frac{\overline{\chi}_d^{(1)}(s,z_2) - \overline{\chi}_d^{(1)}(s,z_1)}{\mathcal{R}(s)} = \frac{\mathfrak{I}_q(s)}{\mathcal{R}(s)}\,; \qquad s < r_1\,,$$

$$(4.9)\qquad \frac{\partial\omega_d^g(s)}{\partial t}-\frac{\lambda}{s^2}\frac{\overline{\chi}_q^{(1)}(s,z_2)-\overline{\chi}_q^{(1)}(s,z_1)}{\mathfrak{R}(s)}=\frac{\mathfrak{I}_d(s)}{\mathfrak{R}(s)};\qquad s< r_1,$$

where

$$(4.10)\qquad \mathfrak{I}(s)=\frac{\overline{\rho}(r_1)\,\overline{V_s^F\,V_\phi^F}(s,z_1)}{z_1}-\frac{\overline{\rho}(r_2)\,\overline{V_s^F\,V_\phi^F}(s,z_2)}{z_2}+\frac{2}{s^2}\int_{z_1}^{z_2}dz\,\overline{\rho}\,\overline{V_s^F\,V_\phi^F}(s,z)\qquad s< r_1$$

Equations for the boundary fluxes $\overline{\chi}_{q,d}^{(1)}(s,r_{1,2})$ can be obtained from the boundary conditions

The angular momentum $M_{q,d}$ and respectively the geostrophic flow change due to the small fluxes of the angular momentum into the “cylinder” with radius *s*. That is why both values gradually change with time.

The solution of these equations has to obey some additional conditions. The first of them arises due to the requirement of limitation of the *z* component of the flux at the axis OZ: $V_z^{(1)}=(1/s)(\partial\overline{\chi}^{(1)}/\partial s)$. The second one is a sequence of oddness of $\overline{\chi}_d^{(1)}$ in respect of z. From here it follows that $\overline{\chi}_d^{(1)}$ has to vanish at the equator of ICB and CMB.

DISCUSSION

The momentum equation for the flow in the Earth's core (1.1,2) is commonly written in a form which depends on two small parameters, the Ekman, E, and the Rossby, R_o, numbers. We rewrite this equation in a form (2.1,2) which depends on other two parameters $\sqrt{E}$, and $\lambda=\sqrt{E}/R_o$. The first of them is small yet but the other one is not small and exceeds the first one with approximately six orders. Boundary conditions (2.4) depend only on the first parameter $\sqrt{E}$. Therefore we search for the solution of the problem in the form of decomposition (2.6) in this parameter. Then the flow of the leading approximation can be presented as a sum of the geostrophic and the force flows.

The force flow is defined directly by the force and satisfies the no-normal boundary conditions (2.7,8). The non-axisymmetric meridional flow has two, $\tilde{V}_s^F(s,\phi,z)$ and $\tilde{V}_z^F(s,\phi,z)$, components which can be defined by these conditions on the top and the bottom boundaries at any cylinder with radius *s*. Then the ϕ component of this flow, $\tilde{V}_\phi^F(s,\phi,z)$, can be obtained from the continuity equation (2.2). The axisymmetric meridional flow depends on only one function $\overline{\chi}^{(0)}(s,z)$, but it also has to satisfy this condition on the top and the bottom boundaries. These two conditions for the only function $\overline{\chi}^{(0)}(s,z)$ are over-constraint for the problem. That is why an additional condition (4.3) has to be satisfied in the liquid core. This condition is the *Taylor constraint*.

The force flow establishes instantly by means of pressure. Respectively, its time dependence is defined wholly by the time dependence of the force. Thus it does not have its own time dependence. To emphasize this we do not include *t* in the list of its variables.

The geostrophic flow is defined by two mechanisms: (4.8,9) concerned to fluxes of the angular momentum and related to the Ekman suction into the boundary layers. As (4.3) shows, the geostrophic flow is defined by two fluxes of the angular momentum. The first one, $1_z\lambda\overline{\chi}$, describes transport in *s* direction of the angular momentum connected to the angular velocity $1_z\Omega$ of the reference framework. The other flux $\overline{\rho}s\overline{\mathbf{V}_m V_\phi}$ of the angular momentum in (4.3) is related to the transfer of the angular momentum density $\overline{\rho}sV_\phi$ by the meridional flow $\mathbf{V}_m$ averaged over ϕ. The second mechanism defining the geostrophic flow is related to the Ekman suction into the boundary layers. Both the geostrophic and the force flows create the suction, but only the first one can fit together with the boundary mass flux, since the second one is already defined by the force. This flux is restricted by the mass conservation. So it establishes instantly (only in a few minutes) by means of pressure. That is why these equations do not depend on time, opposite to the “momentum” equations (4.8,9).

REFERENCES

[1].Glatzmaier, G. A., and P. H. Roberts (1995). A three-dimensional convective dynamo solution with rotating and finitely conducting inner core and mantle, *Phys. Earth Planet. Inter.,* **91**, 63-75.

[2].Glatzmaier, G. A., and P. H. Roberts (1996a). An anelastic evolutionary geodynamo simulation driven by compositional and thermal convection, *Physica*, *D***97**, 81-94.

[3].Glatzmaier, G.A., and P.H. Roberts (1996b). Rotation and magnetism of Earth's inner core, *Science*, **274**, 1887-1891.

[4].Roberts, P.H., and G.A. Glatzmaier (2000). Geodynamo theory and simulations, *Reviews of Modern Physics*, **72**, 1081-1123.

[5].Jones C.A., A.W. Longbotton, R. Hollerbach (1995). A self-consistent convection driven geodynamo model, *Phys. Earth Planet. Inter*., **92**, 119-141.

[6].Fearn, D.R. and G.Morrison (2001). The role of inertia in hydrodynamic models of the geodynamo, *Phys. Earth Planet. Inter.*, **128**, 75-92

CONSERVATION LAWS IN THE EARTH'S LIQUID CORE (II)

A. Anufriev [1], M. Tassev[2]

[1]Geophysical Institute, ul.Acad.G.Bonchev, bl3, Sofia1113, Bulgaria,
[2] South-West University, Department of Mathematics, ul.Iv.Mihailov 66, Blagoevgrad,2700,
Bulgaria, e-mail: matassev@abv.bg

Abstract. *In the previous talk we have shown that the momentum equation for the Earth's liquid core can be rewritten in terms two parameters:* $\sqrt{\mathrm{E}}$ *, where* $E = \nu / 2\Omega L_1^2$ *is the Ekman number . The whole flow is presented as a sum of the force and the geostrophic flows. The first one can be directly determined in terms of integrals of the force. The second one obeys the equations which depend on time derivative of the geostrophic velocity. So the geostrophic flow is the only part of the whole flow which has its own time behavior. It evolves together with magnetic field and temperature distributions. In the opposite, the force flow fits instantly to the force and its time behavior is defined entirely by that of the force distribution. There are two (the inviscid* $\lambda \to 0$ *and the viscous controlled* $\lambda \to \infty$*) limits in which the whole flow does not depend on* λ *and hence on E. Therefore the flow converts in Taylor state in these limits. Depending on the viscosity, the parameter* λ *for the Earth's core changes from* 2.3×10^{-2} *for the kinematic viscosity to* 3.3×10^{1} *for the greatest value of the turbulent viscosity* $\nu_T = \eta$ *where* η *is the magnetic diffusivity. So both types of the Taylor state flows can be realized in the Earth's core. From computer simulations point of view the viscous controlled case is especially important, because all the simulations use implicitly* λ *» 1. For example, Glatzmaier and Roberts (1995, 1996) in fact carried out their simulations for* λ *~* 10^3*. Thus their asymptotic (at* $\lambda \to \infty$*) solution is approximately suitable for the Earth's core conditions with the "turbulent"* $\lambda = 3.3\times10^{1}$*. It is not trivial, since if we adopt the same values of* $\nu(=\nu_T=\eta)$ *and* V_1 *for Venus where Ω is with two orders of magnitude smaller, then λ becomes of order of 1 and the viscous controlled numerical results become unapplicable to this planet. Moreover, being independent of* λ *(and respectively of E), the viscous controlled computer simulated flows convert into Taylor state and so describe adequately the flow in the Earth's core for the turbulent viscosity. This is also a non-trivial conclusion, taking into account that the typical values of the Ekman numbers in computer simulations typically exceed these in the Earth core with ten orders! Though the computer simulations describe satisfactory the flows with large* λ*, they are unapplicable to solve the problem with smaller values of* λ *and especially in the inviscid limit* $\lambda \to 0$*, due to the necessity of resolution of the thin boundary layers. We believe that this difficulty can be overcome by creating computer codes on the base of the equations presented here which are free of this necessity.*

Key words: *geodynamo, Taylor state, inviscid limit*

INTRODUCTION. DEFINITION OF THE PROBLEM

In the previous talk we have shown that the momentum equation for the Earth's liquid core can be rewritten in terms two parameters: $\sqrt{\mathrm{E}}$, where $E = \nu / 2\Omega L_1^2$ is the Ekman number and $\lambda = \sqrt{2\Omega\nu}/V_1$:

$$(1.1,2) \qquad \frac{\bar{\rho}}{\lambda}\frac{\partial \mathbf{V}}{\partial t} = \frac{-\bar{\rho}\,\nabla P - \mathbf{1}_z \bar{\rho}\ \mathrm{x}\ \mathbf{V} + \mathbf{F}}{\sqrt{\mathrm{E}}} - \frac{\bar{\rho}}{\lambda}\mathbf{W}\times\mathbf{V} + \sqrt{\mathrm{E}}\Delta\mathbf{V}\ , \quad \nabla\cdot\overline{\rho}(r)\mathbf{V} = 0$$

In these estimations we have used the following values of parameters taken from Roberts and Glatzmaier (2000): the typical value of the westward drift $V_1 = 5\times10^{-4}\,\mathrm{ms}^{-1}$ and the value of the magnetic diffusivity $\eta = 2\mathrm{m}^2\mathrm{s}^{-1}$. As a space scale, the radius of the liquid core of the Earth $L_1 = r_2 = 3.4\times10^{6}\,\mathrm{m},$. Then we can obtain an estimate for the new parameters:

(1.3) $$\sqrt{\mathrm{E}} = 3.5\times10^{-5}\sqrt{\frac{\nu}{\eta}} \quad \text{and} \quad \lambda = \frac{\sqrt{\mathrm{E}}}{\mathrm{R_o}} = \frac{\sqrt{2\Omega\nu}}{\mathrm{V_1}} = 3.3\times10^{1}\sqrt{\frac{\nu}{\eta}}$$

We assume that the turbulent viscosity is not smaller than $\nu_M = 10^{-6} m^2 s^{-1}$ and does not exceed $\eta = 2\mathrm{m^2 s^{-1}}$. Then λ is situated in the interval: $2.3\times10^{-2} \le \lambda \le 3.3\times10^{1}$. For all possible values of the turbulent viscosity λ exceeds $\sqrt{\mathrm{E}}$ with approximately six orders. Therefore, we will further assume that (1.1) depends on the only small parameter $\sqrt{\mathrm{E}}$ and they respectively hint that the flow can be searched in the form of expansion in this parameter:

(1.4) $$\mathbf{V}(r) = \mathbf{V}^{(0)}(r) + \sqrt{\mathrm{E}}\mathbf{V}^{(1)}(\mathbf{r}) + \ldots \qquad \mathrm{P}(\mathbf{r}) = \mathrm{P}^{(0)}(\mathrm{r}) + \sqrt{\mathrm{E}}\mathrm{P}^{(1)}(\mathbf{r}) + \ldots$$

As it has been shown in our talk 1 the flow of the leading approximation satisfies on the solid boundaries of the core the no-normal-flow boundary conditions:

(1.5q, 6q) $$\bar{\rho}(\mathrm{r}_1)\,\mathbf{r}_1\cdot\mathbf{V}_{\mathrm{q}}^{(0)}(\mathbf{r}_1) = 0, \qquad \bar{\rho}(\mathrm{r}_2)\,\mathbf{r}_2\cdot\mathbf{V}_{\mathrm{q}}^{(0)}(\mathbf{r}_2) = 0;$$

(1.5d, 6d) $$\bar{\rho}(\mathrm{r}_1)\,\mathbf{r}_1\cdot\mathbf{V}_{\mathrm{d}}^{(0)}(\mathbf{r}_1) = 0, \qquad \bar{\rho}(\mathrm{r}_2)\,\mathbf{r}_2\cdot\mathbf{V}_{\mathrm{d}}^{(0)}(\mathbf{r}_2) = 0.$$

whereas the flow of the next approximation satisfies (see e.g. Anufriev and Hejda 1998) the Ekman suction boundary conditions:

(1.8q) $$\bar{\rho}(\mathrm{r}_1)\,\mathbf{r}_1\cdot\mathbf{V}_{\mathrm{q}}^{(1)}(\mathbf{r}_1) = -\gamma_{\mathrm{q}}(\mathrm{r}_1)\,\mathbf{r}_1\cdot\nabla\times\mathbf{A}_{\mathrm{q}}^{(0)}(\mathbf{r}_1) - \gamma_{\mathrm{d}}(\mathbf{r}_1)\,\mathbf{r}_1\cdot\nabla\times\mathbf{A}_{\mathrm{d}}^{(0)}(\mathbf{r}_1);$$

(1.9q) $$\bar{\rho}(\mathrm{r}_2)\,\mathbf{r}_2\cdot\mathbf{V}_{\mathrm{q}}^{(1)}(\mathbf{r}_2) = \gamma_{\mathrm{q}}(\mathrm{r}_2)\,\mathbf{r}_2\cdot\nabla\times\mathbf{A}_{\mathrm{q}}^{(0)}(\mathbf{r}_2) + \gamma_{\mathrm{d}}(\mathbf{r}_2)\,\mathbf{r}_2\cdot\nabla\times\mathbf{A}_{\mathrm{d}}^{(0)}(\mathbf{r}_2);$$

(1.8d) $$\bar{\rho}(\mathrm{r}_1)\,\mathbf{r}_1\cdot\mathbf{V}_{\mathrm{d}}^{(1)}(\mathbf{r}_1) = -\gamma_{\mathrm{q}}(\mathrm{r}_1)\,\mathbf{r}_1\cdot\nabla\times\mathbf{A}_{\mathrm{d}}^{(0)}(\mathbf{r}_1) - \gamma_{\mathrm{d}}(\mathbf{r}_1)\,\mathbf{r}_1\cdot\nabla\times\mathbf{A}_{\mathrm{q}}^{(0)}(\mathbf{r}_1);$$

(1.9d) $$\bar{\rho}(\mathrm{r}_2)\,\mathbf{r}_2\cdot\mathbf{V}_{\mathrm{d}}^{(1)}(\mathbf{r}_2) = \gamma_{\mathrm{q}}(\mathrm{r}_2)\,\mathbf{r}_2\cdot\nabla\times\mathbf{A}_{\mathrm{d}}^{(0)}(\mathbf{r}_2) + \gamma_{\mathrm{d}}(\mathbf{r}_2)\,\mathbf{r}_2\cdot\nabla\times\mathbf{A}_{\mathrm{q}}^{(0)}(\mathbf{r}_2);$$

where

(1.10q, d) $$\mathbf{A}_{\mathrm{q}}^{(0)}(\mathbf{r}_{1,2}) = \mathbf{V}_{\mathrm{q}}^{(0)}(\mathbf{r}_{1,2}) - \mathbf{1}_{\phi}\mathrm{s}\omega_{1,2}; \qquad \cdot\,\mathbf{A}_{\mathrm{d}}^{(0)}(\mathrm{r}_{1,2}) = \mathbf{V}_{\mathrm{d}}^{(0)}(\mathbf{r}_{1,2})\,.$$

and

(1.11) $$\gamma(\mathrm{r}_{1,2},\vartheta,\phi) = \bar{\rho}(\mathrm{r}_{1,2})\sqrt{\frac{\sqrt{\cos^2\vartheta + \mathrm{B}_{\mathrm{r}}^4} - \mathrm{B}_{\mathrm{r}}^2}{2(\cos^2\vartheta + \mathrm{B}_{\mathrm{r}}^4}}$$

Here, instead of presentation of the flow separately in the North and the South hemispheres of the core, we search for a solution in terms of values of the dipole and the quadruple symmetries in the upper (the North) hemisphere only. We will call a scalar field the quadruple one, if it is even in respect of z. Respectively, the field of the dipole type is an odd one in respect of z. We can say that the vector field is of a dipole type, if its *z* component is an even function of *z* and its *s* and ϕ components are odd functions. The vector field of the opposite symmetry, whose *z* component is an odd function of *z* and *s* and ϕ components are even functions, will be called the field of the quadruple symmetry. Indexes “1” and “2” here and further refer respectively to the Inner Core Boundary (ICB) and the Core Mantle Boundary (CMB).

By replacing (1.6) into (1.1), in the talk 1 we have obtained the momentum equations of the leading and the next approximations. Here we will consider the equations for the kinetic energy and the angular momentum.

KINETIC ENERGY

Multiplying (1.1) by **V** we obtain the equation for the kinetic energy in the bulk of the core:

(2.1) $$\frac{1}{\lambda}\frac{\partial}{\partial t}\frac{\bar{\rho}\,\mathbf{V}^2}{2} = \frac{-\nabla\cdot P\,\overline{\rho}\,\mathbf{V} + \mathbf{V}\cdot\mathbf{F}}{\sqrt{\mathrm{E}}}$$

The replacement of (1.6) into (2.1) gives the equation for the kinetic energy of the leading approximation:

(2.2) $$-\nabla \cdot \mathrm{P}^{(0)}\, \overline{\rho}\, \mathbf{V}^{(0)} + \mathbf{V}^{(0)} \cdot \mathbf{F} = 0$$

Equation (2.2) shows that in order to avoid the enormous changes of the kinetic energy in (2.1) the pressure of the leading approximation adjusts in such a way that its work compensates the work of the force at any location. Then the whole (integrated over the whole core) force work of the leading approximation vanishes due to the boundary conditions (1.5,6):

(2.3) $$\iiint \mathbf{V}^{(0)} \cdot \mathbf{F}\, \mathrm{d}^3\mathbf{r} = \iint \mathrm{P}^{(0)}\, \overline{\rho}(\mathrm{r})\, \mathbf{n} \cdot \mathbf{V}^{(0)}\, \mathrm{dS} = 0 \cdot$$

It follows from (2.3) that the whole Archimedean work of the leading approximation converts into the work of the Lorentz force (and then into the Ohmic dissipation).

Subtracting (2.2) from (2.1) we obtain the equation for the kinetic energy in the next approximation:

(2.4) $$\frac{1}{\lambda}\,\frac{\partial}{\partial \mathrm{t}}\frac{\overline{\rho}\, \mathbf{V}^{(0)^2}}{2} = -\nabla \cdot \left[\mathrm{P}^{(0)}\overline{\rho}\, \mathbf{V}^{(1)} + \mathrm{P}^{(1)}\overline{\rho}\, \mathbf{V}^{(0)}\right] + \mathbf{V}^{(1)} \cdot \mathbf{F}$$

The small kinetic energy changes are defined by the terms of the next approximation. Though both (the leading and the next approximations) pressures are included into (2.4), the last one vanishes due to (1.7,8) from the equation for the whole kinetic energy:

(2.5) $$\frac{\partial}{\partial \mathrm{t}} \iiint \mathrm{d}^3\mathrm{r}\, \frac{\overline{\rho}\, \mathbf{V}^{(0)^2}}{2} = \lambda\left[\iiint \mathrm{d}^3\mathbf{r}\, \mathbf{V}^{(1)} \cdot \mathbf{F} - \iint \mathrm{dS}\, \mathrm{P}^{(0)}\overline{\rho}\, \mathbf{n} \cdot \mathbf{V}^{(1)}\right]$$

Eq. (2.5) shows that the kinetic energy of the leading approximation flow changes due to the work of the force and the pressure of the leading approximation over the flow of the next approximation. The pressure work is transformed into energy flux in the boundary layer. Its value is defined by the Ekman suction (1.9,10). This flux compensates the energy loss into the layer.

Let us imagine that the liquid in the Earth's core was not conductive. Then the magnetic field and respectively the Lorentz force would be absent. The equation (2.3) in this case takes a form:

(2.6) $$\iiint \mathbf{V}^{(0)} \cdot \mathbf{F}^{\mathrm{a}}\, \mathrm{d}^3\mathbf{r} = 0$$

This means that the flow of the leading approximation establishes in such a way that the work of the Archimedean force is balanced by the heating, due to the opposite process.

ANGULAR MOMENTUM

Averaging the ϕ component of the momentum equation (1.1) over ϕ we obtain the equation for the density of the angular momentum relative axis OZ:

(3.1) $$\frac{1}{\lambda}\frac{\partial \mathrm{s}\, \overline{\rho}\, \overline{V_\phi}}{\partial\, \mathrm{t}} = \nabla \cdot \overline{\mathbf{m}}, \qquad \text{where} \quad \overline{\mathbf{m}} = \frac{\mathrm{s}\, \overline{\mathbf{B}_{\mathrm{m}}\mathrm{B}_\phi} + \mathbf{1}_{\mathrm{z}}\, \overline{\chi}}{\sqrt{\mathrm{E}}} - \frac{\overline{\rho}}{\lambda}\mathrm{s}\, \overline{\mathbf{V}_{\mathrm{m}}\, \mathrm{V}_\phi} \quad (+\sqrt{\mathrm{E}}\, \nabla\, s\, \overline{\rho}\, \overline{V}_\phi)$$

Here index “m” refers to the meridional (s and z or *r* and ϑ) components of any vector and $\overline{\chi}(\mathrm{s},\mathrm{z})$ is the streamline function of the axisymmetric (1.12) part of the flow. Eq. (3.1) is, in fact, the law of conservation of the angular momentum relative axis OZ. This means that the changes of this momentum in any axisymmetric volume are defined only by the momentum flux $\overline{\mathbf{m}}$ across its boundaries. This flux, as (3.1) shows, consists of three parts. The first of them, $\mathrm{s}\, \overline{\mathbf{B}_{\mathrm{m}}\mathrm{B}_\phi}/\sqrt{\mathrm{E}}$, is related to the torque created by the Lorentz force. The second one, $\mathbf{1}_z \overline{\chi}/\sqrt{\mathrm{E}}$, describes the transportation in *s* direction of the angular momentum connected with the angular velocity $\mathbf{1}_z\Omega$ of the reference framework. And, finally the last term of the momentum flux $\overline{\mathbf{m}}$ in (3.1), $\lambda\,\overline{\rho}\,s\,\overline{\mathbf{V}_m V_\phi}$, is simply the flux of the angular mo-mentum density $\overline{\rho}\,s\,V_\phi$ in direction of the meridional flow $\mathbf{V}_m$ averaged over ϕ. Since Ω » V_ϕ / s, the relation between the third and the second terms is small ~ R_o. If neglecting this term, we obtain $\overline{\mathbf{m}}$ in the leading approximation: $\sqrt{E}\,\overline{\mathbf{m}}^{(0)}(s,z) = s\,\overline{\mathbf{B}_\mathbf{m} B_\phi} - \mathbf{1}_z \overline{\chi}^{(0)}$. Respectively, the leading approximation of (3.1) yields:

$$\sqrt{E}\,\nabla \cdot \overline{\mathbf{m}}^{(0)} = \frac{\partial \overline{\chi}^{(0)}(s,z)}{\partial z} + \nabla \cdot s\,\overline{\mathbf{B}_m B_\phi} = 0 \tag{3.2}$$

Equation (3.2) with boundary condition (1.12) defines the meridional flow of the leading approximation. Its streamline function can be easily expressed in terms of integrals in respect of *z*. Integration of (3.2) over *z* between two solid boundaries yields to Taylor constraint:

$$\int_{z_{botton}}^{z_{top}} \nabla . s\overline{\mathbf{B}_m B_\phi} = \left(= \int_{z_{botton}}^{z_{top}} \overline{F}_\phi \right) = \overline{\chi}^{(0)}(s, z_{botton}) - \overline{\chi}^{(0)}(s, z_{top}) = O(\sqrt{E}) \tag{3.3}$$

Thus Taylor constraint becomes the required condition for the existence of the axisymmetric meridional flow.

Let us integrate (3.2) over the whole volume of the liquid core. Since $\overline{\chi}^{(0)}(r_{1,2}) = 0$ we obtain:

$$\int_0^\pi \sin^2 \vartheta \left[r_1^3\,\overline{B_r B_\phi}(r_1, \vartheta) - r_2^3\,\overline{B_r B_\phi}(r_2, \vartheta) \right] d\vartheta = O(\sqrt{E}) \tag{3.4}$$

This estimation is interesting to compare to the note of Glatzmaier and Roberts in (1996b) who write: *“... That is, when we integrate the absolute value of the moment of the magnetic stress* $|B_r B_\phi| / \mu_o$ *(instead of* $B_r B_\phi / \mu$*) over the inner core boundary, we consistently obtain values three orders of magnitude greater than* Γ_B*“.* In this context it is fit to remind also the papers of Gubbins (1981) and Hollerbach and Jones (1993), who, considering the electromagnetic torque on the inner core, concluded that it must be very small, almost completely cancelling itself.

Combining (1.6) and (3.1) and (3.2) shows that the change of the angular momentum is defined by the momentum flux of the next approximation:

$$\frac{\partial s \overline{\rho}\,\overline{V_\phi}^{(0)}}{\partial t} = \nabla \cdot \left[\mathbf{1}_z \lambda\,\overline{\chi}^{(1)} - \overline{\mathbf{V}_m^{(0)} \overline{\rho}\,s\,V_\phi^{(0)}} \right]. \tag{3.5}$$

This equation allows studying the distribution of the angular momentum in the liquid core. Let us consider the part of the liquid core bounded by a cylinder with radius *s*. The angular momentum of this volume can be obtained by the integration of (3.5) over it. Taken the divergence theorem into account we obtain:

$$\frac{dM(s)}{dt} = \lambda \Upsilon_\delta(s) + \Upsilon_F(s) \tag{3.6}$$

where

$$M(s) = \int_0^s s\,ds \int_{z_b}^{z_2} \overline{\rho}\,s\,\overline{V}_{q\phi}^{(0)}(s,z)\,dz \tag{3.7}$$

is the angular momentum of the volume and

(3.8) $z_b = z_1 = \sqrt{r_1^2 - s^2}$ when $s \le r_1$ and $z_b = 0$ when $s \ge r_1$.

The torque Υ_δ acting on the boundaries and the torque Υ_F acting on the cylinder surface are defined by the expressions:

$$\Upsilon_\delta(s) = \int_0^s s\,ds\,\Pi_d(s), \tag{3.9}$$

(3.9a) $\Pi_{d,q}(s)=\overline{\chi}^{(1)}_{d,q}(s,z_2)-\overline{\chi}^{(1)}_{d,q}(s,z_1)$, if $s< r_1$ and $\Pi_{d,q}(s)=\overline{\chi}^{(1)}_{d,q}(s,z_2)$ if $s > r_1$

(3.10) $$\Upsilon_F(s)=s^2\int_{z_b}^{z_2}dz\,\overline{\rho}\left[\overline{V^{(0)}_{qs}\,V^{(0)}_{q\phi}}(s,z)+\overline{V^{(0)}_{ds}\,V^{(0)}_{d\phi}}(s,z)\right].$$

Thus the Earth's core angular momentum distribution *M(s)* is defined by two torques. The first of them $\Upsilon_\delta(s)$ is the torque connected to the boundary flux on both boundaries. This change of the momentum is related to the transport of the angular momentum connected to the rotation of the reference framework with the angular velocity $\mathbf{1}_z\Omega$. Function $\overline{\chi}^{(1)}(s,z)$ can be presented as a sum $\overline{\chi}^{(1)}(s,z)=\overline{\chi}^{(1)}_d(s,z)+\overline{\chi}^{(1)}_q(s,z)$ of its odd and even components in respect of *z*. The transfer carried out by the flux related to $\overline{\chi}^{(1)}_q$ is compensated in the North and the South hemispheres. Therefore, only the transport connected to the odd function $\overline{\chi}^{(1)}_d$, changes the angular momentum. For example $\overline{\chi}^{(1)}=\overline{\chi}^{(1)}(r)(2sz/r^2)$ is the flux that changes this momentum effectively.

The second torque $\Upsilon_F(s)$ defines the flow velocity which is determined in terms of the force into the liquid core. Therefore we call it the force torque. It is defined by the even component of $\overline{V^{(0)}_sV^{(0)}_\varphi}$ in respect of *z*. So the flows of the dipole and the quadruple types generate this torque effectively. The force torque works in the whole core but as (3.10) shows, it vanishes at $s=r_2$. So the equation for the angular momentum of the whole liquid core converts into

(3.11) $$\frac{dM_2}{dt}=\lambda\left[\frac{r_1^2}{2}\int_0^\pi d\vartheta\,\sin 2\vartheta\,\overline{\chi}^{(1)}_d(r_1,\vartheta)-\frac{r_2^2}{2}\int_0^\pi d\vartheta\sin 2\vartheta\,\overline{\chi}^{(1)}_d(r_2,\vartheta)\right]$$

where $M_2=M(r_2)$.

Taking (1.12) into account we can rewrite (3.11) also in the form:

(3.12) $$\frac{dM_2(t)}{dt}=\lambda\,\frac{r_2^4}{4}\int_0^\pi d\vartheta\,\sin\vartheta\,\cos 2\vartheta\left[\overline{\rho}(r_2)\overline{V}^{(1)}_r(r_2,\vartheta)-\frac{r_1^4}{r_2^4}\overline{\rho}(r_1)\,\overline{V}^{(1)}_r(r_1,\vartheta)\right]$$

Note that as (3.11) shows, the angular momentum of the liquid core is driven by two torques acting on ICB and CMB. Respectively, the same torqueses (with the opposite signs) act over the inner core and the mantle. This yields to equations for their angular momentum:

(3.13) $$\frac{d\omega_1}{dt}=-\frac{\lambda}{I_1}\frac{r_1^2}{2}\int_0^\pi d\vartheta\sin 2\vartheta\,\overline{\chi}^{(1)}_d(r_1,\vartheta)$$

(3.14) $$\frac{d\omega_2}{dt}=-\frac{\lambda}{I_3}\frac{r_2^2}{2}\int_0^\pi d\vartheta\sin 2\vartheta\,\overline{\chi}^{(1)}_d(r_2,\vartheta),$$

where I_1 and I_3 are the inertia momentum of the inner core and the mantle, respectively.

By assuming that the mass flux on both boundaries is of the same order, we obtain a crude estimation for the relation between the angular accelerations of the inner core and the mantle:

(3.15) $$\frac{d\omega_1}{dt}\bigg/\frac{d\omega_2}{dt}=\frac{\rho_3}{\rho_1}\left(\frac{r_3}{r_2}\right)^2\left(\frac{r_3}{r_1}\right)^3 7\times 10^1,$$

where ρ_1 and ρ_3 are densities of the inner core and the mantle and r_3 is the radius of the Earth.

DISCUSSION

Defining the force flow from the equations (1.1,2) (1.3) and (1.2) we obtain the functions which are included in equations for the geostrophic flow. Then the solution of these equation gives the whole flow.

The *Taylor state* is called an assumed solution which does not depend on the Ekman number in the inviscid limit $E \to 0$. The force flow obeying the no-normal-flow boundary condition does not depend on *E*. *So only the geostrophic flow, which depends on the Ekman number E by means of* λ*, disturbs the Taylor state conditions.* There are two limits, the inviscid one $\lambda \to 0$ and the “viscous controlled” limit $\lambda \to \infty$ when this disturbance is violated and the whole flow converts into Taylor state.

The inviscid flow is of a real geophysical interest since $\lambda = \sqrt{2\Omega\nu} / V_1$ for the kinematic values of viscosity is a small one, $\lambda \sim 10^{-2}$. In this discussion we fix the velocity scale, V_1, by the typical value of the westward drift. If we admit that the velocity scale can change, then we could call it a case of fast flow (or a case of slow rotation, supposing that Ω can change as well, which could be interesting in respect of Venus).

It is important to emphasize that the opposite (the viscous controlled) limit is also applicable in context of the Geodynamo shows, λ is relatively great for the turbulent viscosity. In the viscous controlled case the geostrophic flow loses its own time dependance and is defined inside and outside the tangent cylinder by the Ekman suction on the boundaries. How does this reflect on the flow? Let us consider e.g. the energy equation. The time derivative of the kinetic energy, as shows, is equal to the difference between the force work and the layer dissipation, multiplied by λ. In the case of large λ this difference tends to be zero. So in the computer simulations it is defined mainly by random computer errors. A large parameter λ enhances essentially ($\sim 10^3$) their influence. Therefore one can expect that the time derivative of the kinetic work must be very discontinuous. Fig 1 of Glatzmaier and Roberts (1995) confirms this conclusion.

As we noticed above, the computer simulated flows are at asymptotically large values of λ. For example, Glatzmaier and Roberts (1995,1996) in fact carried out their simulations for *E* $\sim 10^4$ and $R_o \sim 10^{-5}$, i.e. for $\lambda \sim 10^3$. In order to decrease this large value to the maximal real one ($\lambda \sim$ 30), these authors have to diminish *E* with three orders of magnitude, which is hardly possible for the existing computers. All the more it is impossible to obtain a computer solution with a small λ, implying the kinematic viscosity in *E*. That is why we propose to use another way which is based on decomposition of the flow .This implies the creation of a computer code for solving the equations presented here. This code would be free of the difficulties concerning the resolution of thin boundary layers.

The axisymmetric part of the meridional force flow can be obtained by the integration of under boundary conditions. Its azimuthal part is defined by the equation . The non-axisymmetric part of the force flow can be analytically obtained from the equations and the boundary conditions . This problem also can be solved numerically.

Having evaluated the force flow, we can search for the only component of the flow which is not defined by the leading approximation problem, the geostrophic one. Equations define it inside the tangent cylinder and do this outside the tangent cylinder.

The problem is simplified additionally in the inviscid limit $\lambda \to 0$. Then we obtain the only simple equations for the geostrophic velocity, which can be solved numerically.

The equations for the viscous controlled case of large λ can be used for comparing our results with the numerical solutions. Let us emphasize here that not only the whole geodynamo simulations, but also some simple models such as “2.5” can be used for the test.

REFERENCES

[1]. Glatzmaier, G.A., and P.H. Roberts, 1995. A three-dimensional convective dynamo solution with rotating and finitely conducting inner core and mantle, Phys. Earth Planet. Inter., **91**, 63-75.

[2]. Glatzmaier, G.A., and P.H. Roberts, 1996a. An anelastic evolutionary geodynamo simulation driven by compositional and thermal convection, Physica, D**97**, 81-94.

[3]. Glatzmaier, G.A., and P.H. Roberts, 1996b. Rotation and magnetism of Earth's inner core, Science, **274**, 1887-1891.

[4]. Roberts, P.H., and G.A. Glatzmaier, 2000. Geodynamo theory and simulations, Reviews of Modern Physics, **72**, 1081-1123.

[5]. Jones C.A., A.W. Longbotton, R. Hollerbach, 1995 A self-consistent convection driven geodynamo model, Phys. Earth Planet. Inter., **92**, 119-141.

[6]. Fearn, D.R. and G.Morrison, 2001. The role of inertia in hydrodynamic models of the geodynamo, *Phys. Earth Planet. Inter.*, **128**, 75-92

[7]. Anufriev A., M.Tassev (2007).Role of the geostrophic flow in the liquid core of the earth. *In “Mathematucs and natural scienses, FMNS.*

TAILOR STATE FLOW IN THE EARTH’S LIQUID CORE

A. Anufriev [1], M. Tassev[2]

[1]Geophysical Institute, ul.Acad.G.Bonchev, bl3, Sofia1113, Bulgaria,
e-mail: anufriev@abv.bg
[2] South-West University, Department of Mathematics, ul.Iv.Mihailov 66, Blagoevgrad,2700,
Bulgaria, e-mail: matassev@abv.bg

Abstract. *It is shown that the whole flow in the Earth's liquid core can be presented as a sum of the force and the geostrophic flow. The first of them does not depend on the Ekman number E and consequently satisfies the Taylor state condition. The second one depends on E through parameter* $\lambda \sim \sqrt{E}$*. Thus the geostrophic flow is the only part of the whole flow which can disturb the Taylor state condition. However there are two limits (the inviscid* $\lambda \to 0$ *and the viscous controlled* $\lambda \to \infty$*), in which the whole flow does not depend on* λ *and hence on E. Therefore, in these limits the flow converts in Taylor state. Depending on the viscosity, parameter* λ *for the Earth’s core changes from* 2.3×10^{-2} *for the kinematic viscosity to* 3.3×10^{1} *for the greatest value of the turbulent viscosity* $\nu_T = \eta$*, where* η *is the magnetic diffusivity. So, both types of the Taylor state flows can be realized in the Earth's core. From computer simulations point of view the viscous controlled case is especially important, because all the simulations use implicitly* λ *» 1. For example, Glatzmaier and Roberts (1995, 1996) in fact carried out their simulations for* $\lambda \sim 10^{3}$*. Thus their asymptotic solution (at* $\lambda \to \infty$*), is approximately suitable for the Earth's core conditions with the “turbulent”* $\lambda = 3.3\times10^{1}$*. This result is not trivial, since if we adopt the same values of* $\nu(=\nu_T=\eta)$ *and* V_1 *for Venus where Ω is with two orders of magnitude smaller, then λ becomes of order of 1 and the viscous controlled numerical results become unapplicable to this planet. Moreover, being independent of* λ *(and respectively of E), the viscous controlled computer simulated flows convert into Taylor state and thus describe adequately the flow in the Earth's core for the turbulent viscosity. This is also a non-trivial conclusion, taking into account that the typical values of the Ekman numbers in computer simulations normally exceed these in the Earth core with ten orders!*

Key words: *geodynamo, Taylor state, inviscid limit*

INTRODUCTION. EQUATIONS AND BOUNDARY CONDITIONS

The Ekman number $E = \nu / 2\Omega L_1^2$ in the Earth’s liquid core is extremely small (~ 10 $^{-15}$). Here we show that Taylor state flow does exist. The flow in the Earth’s liquid core was decomposed in the small parameter $\sqrt{\mathrm{E}}$:

(1.1) $$\mathbf{V}(r) = \mathbf{V}^{(0)}(r) + \sqrt{\mathrm{E}}\mathbf{V}^{(1)}(\mathbf{r}) + \ldots, \qquad \mathrm{P}(\mathbf{r}) = \mathrm{P}^{(0)}(\mathrm{r}) + \sqrt{\mathrm{E}}\mathrm{P}^{(1)}(\mathbf{r}) + \ldots,$$

where indexes “ $^{(0)}$ ”, and “ $^{(1)}$ ”, refer to the leading and the next approximations, respectively.

The momentum and the continuity equations of the leading approximation do not depend explicitly on time:

(1.2,3) $$-\bar{\rho}\nabla \mathrm{P}^{(0)} - \bar{\rho}\mathbf{1}_z \times \mathbf{V}^{(0)} + \mathbf{F} = 0, \qquad \nabla \cdot \bar{\rho}\mathbf{V}^{(0)} = 0$$

The flow of the leading approximation satisfies the no-normal-flow boundary conditions on the Inner core boundary (ICB) ($r = r_1$) and the Core mantle boundary (CMB) ($r = r_2$):

(1.4,5) $$\bar{\rho}(\mathbf{r}_1)\,\mathbf{r}_{\pm 1} \cdot \mathbf{V}^{(0)}(\mathrm{r}_{\pm 1}) = 0, \qquad \bar{\rho}(\mathbf{r}_2)\,\mathbf{r}_{\pm 2} \cdot \mathbf{V}^{(0)}(\mathrm{r}_{\pm 2}) = 0,$$

The force flow is completely defined by the boundary conditions (1.4,5). The geostrophic flow identically satisfies these conditions and therefore cannot be defined by them. So it is determined in the next approximation, where the Ekman suction into the boundary layers is taken into account. Respectively, one more variable, the boundary flux $\chi(r_{1,2}, s)$, has to be taken into account. The equations inside the tangent cylinder ($s \le r_1$) have the form:

(1.8) $$\frac{\partial \omega_q^g(\mathrm{s})}{\partial t} - \frac{\lambda}{\mathrm{s}^2}\frac{\bar{\chi}_d^{(1)}(\mathrm{s},\mathrm{z}_2) - \bar{\chi}_d^{(1)}(\mathrm{s},\mathrm{z}_1)}{\mathscr{R}(\mathrm{s})} = \frac{\Im_q(\mathrm{s})}{\mathscr{R}(\mathrm{s})}; \qquad \mathrm{s} < \mathrm{r}_1,$$

(1.9) $$\frac{\partial \omega_d^g(\mathrm{s})}{\partial t} - \frac{\lambda}{\mathrm{s}^2}\frac{\bar{\chi}_q^{(1)}(\mathrm{s},\mathrm{z}_2) - \bar{\chi}_q^{(1)}(\mathrm{s},\mathrm{z}_1)}{\mathscr{R}(\mathrm{s})} = \frac{\Im_d(\mathrm{s})}{\mathscr{R}(\mathrm{s})}; \qquad \mathrm{s} < \mathrm{r}_1,$$

(1.10) $$\frac{\partial \bar{\chi}_d^{(1)}(\mathrm{s},\mathrm{r}_1)}{\partial \mathrm{s}} + \bar{\gamma}_q(\mathbf{r}_1)\frac{\partial \mathrm{s}^2(\omega_q^g - \omega_1)}{\partial \mathrm{s}} + \bar{\gamma}_d(\mathbf{r}_1)\frac{\partial \mathrm{s}^2\omega_d^g}{\partial \mathrm{s}} = -W_d(\mathrm{s},\mathrm{r}_1), \quad \mathrm{s} < \mathrm{r}_1,$$

(1.11) $$\frac{\partial \bar{\chi}_d^{(1)}(\mathrm{s},r_2)}{\partial \mathrm{s}} - \bar{\gamma}_q(\mathbf{r}_2)\frac{\partial \mathrm{s}^2(\omega_q^g - \omega_2)}{\partial \mathrm{s}} - \bar{\gamma}_d(\mathbf{r}_2)\frac{\partial \mathrm{s}^2\omega_d^g}{\partial \mathrm{s}} = W_d(\mathrm{s},\mathrm{r}_2), \quad \mathrm{s} < \mathrm{r}_1,$$

(1.12) $$\frac{\partial \bar{\chi}_q^{(1)}(\mathrm{s},\mathrm{r}_1)}{\partial \mathrm{s}} + \bar{\gamma}_d(\mathbf{r}_1)\frac{\partial \mathrm{s}^2(\omega_q^g - \omega_1)}{\partial \mathrm{s}} + \bar{\gamma}_q(\mathbf{r}_1)\frac{\partial \mathrm{s}^2\omega_d^g}{\partial \mathrm{s}} = -W_q(\mathrm{s},\mathrm{r}_1), \quad \mathrm{s} < \mathrm{r}_1,$$

(1.13) $$\frac{\partial \bar{\chi}_q^{(1)}(\mathrm{s},\mathrm{r}_2)}{\partial \mathrm{s}} - \bar{\gamma}_d(\mathbf{r}_2)\frac{\partial \mathrm{s}^2(\omega_q^g - \omega_2)}{\partial \mathrm{s}} - \bar{\gamma}_q(\mathbf{r}_2)\frac{\partial \mathrm{s}^2\omega_d^g}{\partial \mathrm{s}} = W_q(\mathrm{s},\mathrm{r}_2), \quad \mathrm{s} < \mathrm{r}_1,$$

where $\lambda = \sqrt{\mathrm{E}}/\mathrm{R}_o$, ω_1 and ω_2 are the angular velocities of the inner core and the mantle, respectively, and

(1.13) $$\Im(\mathrm{s}) = \frac{\bar{\rho}(\mathrm{r}_1)\,\overline{\mathrm{V}_s^F\,\mathrm{V}_\phi^F}(\mathrm{s},\mathrm{z}_1)}{\mathrm{z}_1} - \frac{\bar{\rho}(\mathrm{r}_2)\,\overline{\mathrm{V}_s^F\,\mathrm{V}_\phi^F}(\mathrm{s},\mathrm{z}_2)}{\mathrm{z}_2} + \frac{2}{\mathrm{s}^2}\int_{\mathrm{z}_1}^{\mathrm{z}_2} \mathrm{dz}\,\bar{\rho}\,\overline{\mathrm{V}_s^F\,\mathrm{V}_\phi^F}(\mathrm{s},\mathrm{z}), \quad \mathrm{s} < \mathrm{r}_1$$

(1.14q) $$W_q(\mathrm{s},\mathrm{r}) = \frac{\mathrm{s}}{\mathrm{z}}\left[\overline{\gamma_q(\mathbf{r})\ \mathbf{r}\cdot\nabla\times\mathbf{V}_d^F(\mathbf{r})} + \overline{\gamma_d(\mathbf{r})\ \mathbf{r}\cdot\nabla\times\mathbf{V}_q^F(\mathbf{r})}\right],$$

(1.14d) $$W_d(s,r)=\frac{s}{z}\left[\overline{\gamma_q(\mathbf{r})\mathbf{r}\cdot\nabla\times\mathbf{V}_q^F(\mathbf{r})}+\overline{\gamma_d(\mathbf{r})\,\mathbf{r}\cdot\nabla\times\mathbf{V}_d^F(\mathbf{r})}\right],$$

(1.15,16) $$\gamma\,(r_{1,2},\vartheta,\phi)=\overline{\rho}(r_{1,2})\sqrt{\frac{\sqrt{\cos^2\vartheta+B_r^4}-B_r^2}{2(\cos^2\vartheta+B_r^4}}\quad \text{and}\quad \mathfrak{R}(s)=\int_{z_b}^{z_2}dz\overline{\rho}(r)$$

Six equations (1.8,9) and (1.10-13) form the system of equations for the six quantities $\omega^g_{q,d}(s)$ and $\overline{\chi}^{(1)}_{q,d}(s,r_{1,2})$ inside the tangent cylinder. Outside it, the dipole component of the geostrophic flow is absent. Therefore we need only one equation such as (1.8):

$$\frac{\partial\omega^g(s)}{\partial t}-\frac{\lambda}{s^2}\frac{\overline{\chi}^{(1)}_d(s,z_2)}{R(s)}=\frac{\mathfrak{I}_q(s)}{\mathfrak{R}(s)}\ ,\qquad s>r_1,\qquad (1.17)$$

where

$$\mathfrak{I}(s)=-\frac{\overline{V_s^F\ V_\phi^F(s,z_2)}}{z_2}+\frac{2}{s^2}\int_0^{z_2}dz\overline{\rho}\,\overline{V_s^F\ V_\phi^F(s,z)},\quad s>r_1.\qquad (1.18)$$

Eq, (1.17) includes the only boundary flux $\overline{\chi}_d^{(1)}(s,r_2)$. So in this region we need an equation only for this component of the flux:

$$\frac{\partial\overline{\chi}^{(1)}_d(s,r_2)}{\partial s}-\overline{\gamma}_q(\mathbf{r}_2)\frac{\partial s^2(\omega^g-\omega_2)}{\partial s}=W_d(s,r_2),\quad s>r_1\qquad (1.19)$$

Thus outside the tangent cylinder we need only two equations (1.17,19) instead of six equations in the region inside it.

INVISCID FLOW

Equations for the geostrophic flow (1.8,9) and (1.17) depend on parameter λ defined in talk 1:

$$\lambda=\frac{\sqrt{E}}{R_o}=\frac{\sqrt{2\Omega\nu}}{V_1}=3.3\times10^1\sqrt{\frac{\nu}{\eta}}\qquad (2.1)$$

The estimate (2.1) shows that for the molecular viscosity $\nu=\nu_M$, parameter λ is a relatively small one: $\lambda\sim10^{-2}$. That is why the consideration of the problem with a small λ is a problem of physical interest. Further we will call this problem the inviscid one.

As (1.8), (1.9) and (1.17) show, the geostrophic flow changes due to the difference of the meridional boundary fluxes on the top and the bottom boundaries and due to the angular momentum connected with the azimuthal force velocity, $s\overline{\rho}\overline{V}_\phi^F$, transferred by the meridional force flow, $\overline{V}_s^F$. It can be assumed, that in the inviscid limit, when $\lambda\to0$, the first of these mechanisms attenuates and respectively these equations transform into the following ones:

(2.2) $$\frac{\partial\omega_q^g(s)}{\partial t}=\frac{\mathfrak{I}_q(s)}{\mathfrak{R}(s)}\ ,\qquad s<r_1;$$

(2.3) $$\frac{\partial\omega_d^g(s)}{\partial t}=\frac{\mathfrak{I}_d(s)}{\mathfrak{R}(s)},\qquad s<r_1;$$

(2.4) $$\frac{\partial\omega^g(s)}{\partial t}=\frac{\mathfrak{I}_q(s)}{\mathfrak{R}(s)},\qquad s>r_1;$$

where $\mathfrak{I}(s)$ is defined by (1.18) in terms of the force flow. We declared in section 1 that the force flow is determined completely by the forces. The following scheme of solving the geodynamo problem on this base can be imagined. First, we can determine the temperature and the magnetic field distributions at a given time step. Then we obtain the force flow which establishes instantly by means of pressure. This flow defines rhs of (2.2,3). By integrating these equations we obtain new values of the geostrophic flow which have to be used in the next time step (together with the force flow, of course).

It is important to emphasize that equations (2.2-4) does not depend on λ and respectively on E. This means that the flow described by these equations present a Taylor state.

The approach (2.2-4) of solving the geostrophic part of the flow as a time-dependent problem while treating the ageostrophic part as a time-independent problem was developed by Jault (1995).

THE VISCOUS CONTROLLED APPROXIMATION

Turbulence effectively enhances the viscosity and respectively enhances λ as well. As (2.1) shows, the maximum possible values of λ at $\nu = \eta$ is of order of $3\mathrm{x}10^1$. Therefore this viscous controlled case, λ » 1, is also a problem of physical interest. It is additionally an interesting one, because all the computer simulations implicitly suppose that λ » 1. For example, Glatzmaier and Roberts (1995,1996) in fact carried out their simulations for E ~ 10^{-4} and $R_o \sim 10^{-5}$. To compare our estimation with the results of the computer simulations, we consider in this section the case of large viscosity ($\lambda \to \infty$).

If we adopt λ » 1 then the flux in the bulk of the core depends on *s* only: $\nabla \cdot \mathbf{1}_z \lambda \overline{\chi}^{(1)} = 0 \to \overline{\chi}^{(1)} = \overline{\chi}^{(1)}(\mathrm{s})$. It follows from here that the next approximation meridional flow has only a *z* component:

$$(3.1) \qquad \overline{\mathbf{V}}^{(1)} = -\frac{\mathbf{1}_\phi}{\overline{\rho}(\mathrm{r})\mathrm{s}} \mathrm{x} \nabla \overline{\chi}^{(1)}(\mathrm{s}) = \frac{\mathbf{1_z}}{\overline{\rho}(\mathrm{r})\mathrm{s}} \frac{\partial \overline{\chi}^{(1)}(\mathrm{s})}{\partial \mathrm{s}} = \mathbf{1}_z \overline{\mathrm{V}}_z^{(1)}(\mathrm{s}, \sqrt{\mathrm{s}^2 + \mathrm{z}^2}),$$

The space density of the mass flux $\overline{\rho}(\mathrm{r})\overline{\mathrm{V}}^{(1)} = (1_z / \mathrm{s})(\partial \overline{\chi}^{(1)}(\mathrm{s}) / \partial \mathrm{s})$ of this flow does not depend on *z*. Respectively the flux coming out from the Ekman layer on the bottom boundary of the liquid core enters without any changes into the layer on the top boundary at any *s*. The averaged over ϕ boundary condition of the next approximation can be rewritten in the form:

$$(3.2) \qquad \frac{\partial \overline{\chi}_\pm^{(1)}(\mathrm{s})}{\mathrm{sds}} = \pm 2\overline{\gamma}(\mathbf{r}_{\pm 1})\omega_1 - \frac{\overline{\gamma(\mathbf{r}_{\pm 1})\mathbf{r}_{\pm 1} \cdot \mathbf{W}^{(0)}(\mathbf{r}_{\pm 1})}}{\mathrm{z}_1}, \quad (= \overline{\rho}(\mathrm{r}_1)\overline{\mathrm{V}}_z^{(1)}(\mathrm{s}, \pm \mathrm{z}_1))$$

$$(3.3) \qquad \frac{\partial \overline{\chi}_\pm^{(1)}(\mathrm{s})}{\mathrm{sds}} = \pm 2\overline{\gamma}(\mathbf{r}_{\pm 2})\omega_1 - \frac{\overline{\gamma(\mathbf{r}_{\pm 2})\mathbf{r}_{\pm 2} \cdot \mathbf{W}^{(0)}(\mathbf{r}_{\pm 2})}}{\mathrm{z}_2}, \quad (= \overline{\rho}(\mathrm{r}_2)\overline{\mathrm{V}}_z^{(1)}(\mathrm{s}, \pm \mathrm{z}_2)),$$

where $\mathbf{W} = \nabla \times \mathbf{V}$.

Outside the tangent cylinder, (*s* > r_1), the bottom and the top boundaries are $-\mathrm{z}_2(\mathrm{s})$ and $z_2(s)$. Then by equalizing rhs of (3.3) at $-\mathrm{z}_2(\mathrm{s})$ and $\mathrm{z}_2(\mathrm{s})$ we obtain:

$$(3.4) \qquad \frac{\overline{\gamma(\mathbf{r}_2)\mathbf{r}_2 \cdot \mathbf{W}^{(0)}(\mathbf{r}_2)} - \overline{\gamma(\mathbf{r}_{-2})\mathbf{r}_{-2} \cdot \mathbf{W}^{(0)}(\mathbf{r}_{-2})}}{z_2} = 2\left[\overline{\gamma}(\mathbf{r}_2) + \overline{\gamma}(\mathbf{r}_{-2})\right]\omega_2 ;. \quad .r_1 < s < r_2.$$

Inside the tangent cylinder the bottom and the top boundaries are $z_1(s)$ and $z_2(s)$ in the upper hemisphere and $-z_2(s)$ and $-z_1(s)$ in the lower one. Then combining (3.2) and (3.3) we obtain the equations for $\mathbf{W}^{(0)}$ inside the tangent cylinder in the North and the South hemispheres:

$$(3.5) \quad 0 < \mathrm{s} < \mathrm{r}_1 \qquad \frac{\overline{\gamma(\mathbf{r}_{\pm 2})\mathbf{r}_{\pm 2} \cdot \mathbf{W}^{(0)}(\mathbf{r}_{\pm 2})}}{z_2} + \frac{\overline{\gamma(\mathbf{r}_{\pm 1})\mathbf{r}_{\pm 1} \cdot \mathbf{W}^{(0)}(\mathbf{r}_{\pm 1})}}{z_1} = \pm 2\left[\overline{\gamma}(\mathbf{r}_{\pm 1})\omega_1 + \overline{\gamma}(\mathbf{r}_{\pm 2})\omega_2\right],$$

Let us remind that the whole flow of the leading approximation has a form: $V^{(0)} = \mathbf{1}_\phi \overline{V}^g(s) + \mathbf{1}_\phi \overline{V}^F(s,z) - (\mathbf{1}_\phi / \overline{\rho}(r)s) \times \nabla \overline{\chi}^{(0)}(s,z) + \tilde{\mathbf{V}}_\phi^{(0)}(s,\phi,z)$. The only unknown quantity in this flow is the geostrophic velocity $\overline{V}^g = s\overline{\omega}^g(s)$. The normal component of the curl takes the form: $\mathbf{r}.\overline{\mathbf{W}}^{(0)} = \mathbf{r}.\overline{\mathbf{W}}^{g} + \mathbf{r}.\overline{\mathbf{W}}^{F} + \mathbf{r}.\tilde{\mathbf{W}}_\phi^{(0)}$ where

$$\mathbf{r}.\overline{\mathbf{W}}^g = \pm \frac{|z|}{s}\frac{\partial s^2 \overline{\omega}_\pm^g}{\partial s}; \qquad \mathbf{r}.\overline{\mathbf{W}}^F = \pm \frac{|z|}{s}\frac{\partial s^2 \overline{\omega}^F}{\partial s} + s\mathbf{1}_\phi.\nabla \times \frac{\overline{\mathbf{F}}}{\overline{\rho}}$$

in the North and the South hemispheres respectively.

Thus (3.4), (3.5) are in fact equations for the angular geostrophic velocity $\overline{\omega}^g(s)$. Taking (3.4) into account we obtain equations for this value outside the tangent cylinder

$$\frac{\partial s^2\left[\overline{\omega}^g(s) - \omega_2\right]}{sds} = \frac{\overline{\gamma}(\mathbf{r}_{-2})\mathbf{r}_{-2}\cdot\overline{\mathbf{W}}^F(\mathbf{r}_{-2}) - \overline{\gamma}(\mathbf{r}_2)\mathbf{r}_2\cdot\overline{\mathbf{W}}^F(r_2)}{z_2(\overline{\gamma}(\mathbf{r}_{-2}) + \overline{\gamma}(\mathbf{r}_2))} - \frac{\overline{\tilde{\gamma}(\mathbf{r}_2)\mathbf{r}_2\cdot\tilde{\mathbf{W}}_\phi^{(0)}(\mathbf{r}_2)} - \overline{\tilde{\gamma}(\mathbf{r}_{-2})r_{-2}\cdot\tilde{\mathbf{W}}_\phi^{(0)}(\mathbf{r}_{-2})}}{z_2(\overline{\gamma}(\mathbf{r}_{-2}) + \overline{\gamma}(\mathbf{r}_2))}, \qquad r_1 < s < r_2 \tag{3.6}$$

and inside it in the North and the South hemispheres

$$\frac{\partial s^2\left[\overline{\omega}_\pm^g(s) - \omega_2\right]}{sds} = 2\frac{\overline{\gamma}(\mathbf{r}_{\pm1})[\omega_1 - \omega_2]}{\overline{\gamma}(\mathbf{r}_{\pm1}) + \overline{\gamma}(\mathbf{r}_{\pm2})} \mp \frac{\overline{\gamma}(\mathbf{r}_{\pm1})r_{\pm1}\cdot\overline{\mathbf{W}}^F(\mathbf{r}_{\pm1})}{(\overline{\gamma}(\mathbf{r}_{\pm1}) + \overline{\gamma}(\mathbf{r}_{\pm2}))z_1} \mp \frac{\overline{\gamma}(\mathbf{r}_{\pm2})\mathbf{r}_{\pm2}\cdot\overline{\mathbf{W}}^F(\mathbf{r}_{\pm2})}{(\overline{\gamma}(\mathbf{r}_{\pm1}) + \overline{\gamma}(\mathbf{r}_{\pm2}))z_2} \mp \frac{\overline{\tilde{\gamma}(\mathbf{r}_{\pm1})\mathbf{r}_{\pm1}\cdot\tilde{\mathbf{W}}_\phi^{(0)}(\mathbf{r}_{\pm1})}}{(\overline{\gamma}(\mathbf{r}_{\pm1}) + \overline{\gamma}(\mathbf{r}_{\pm2}))z_1} \mp \frac{\overline{\tilde{\gamma}(\mathbf{r}_{\pm2})\mathbf{r}_{\pm2}\cdot\tilde{\mathbf{W}}_\phi^{(0)}(\mathbf{r}_{\pm2})}}{(\overline{\gamma}(\mathbf{r}_{\pm1}) + \overline{\gamma}(\mathbf{r}_{\pm2}))z_2} \qquad r_1 < s < r_2. \tag{3.7}$$

Equations (3.6), (3.7) allow to find $\overline{\omega}^g$ inside and outside the tangent cylinder and so to define the whole flow of the leading approximation.

In the last part of this section we will discuss the azimuthal flow near the axis OZ. Any continuous function $\Phi(s,\phi,z)$ near this axis does not depend on ϕ. Respectively, $\overline{\gamma}$ vanishes here and so $\overline{\gamma\mathbf{r}.\mathbf{W}^{(0)}}$ takes a simple form: $\overline{\gamma\mathbf{r}.\mathbf{W}^{(0)}} = \overline{\gamma}\mathbf{r}.\overline{\mathbf{W}}^{(0)}$ where

$$\mathbf{r}.\overline{\mathbf{W}}^{(0)} = \frac{z}{s}\frac{\partial s\overline{V}_\phi^{(0)}}{\partial s} - s\frac{\partial \overline{V}_\phi^{(0)}}{\partial z} = \frac{z}{s}\frac{\partial s^2\overline{\omega}^{(0)}}{\partial s} - s^2\frac{\partial \overline{\omega}^{(0)}}{\partial z} \sim 2z\overline{\omega}^{(0)}(z); \qquad \left(\overline{\omega}^{(0)} = \frac{\overline{V}_\phi^0}{s}\right)$$

As a result, (3.5) in the North and the South hemispheres near this axis can be written as:

$$\overline{\gamma}(\pm z_2)\overline{\omega}^{(0)}(\pm z_2) = -\overline{\gamma}(\pm z_1)\overline{\omega}^{(0)}(\pm z_1) + \overline{\gamma}(\pm z_1)\omega_1 + \overline{\gamma}(\pm z_2)\omega_2 \quad \text{at } s = 0. \tag{3.9}$$

Our scale for the magnetic field $\sqrt{2\Omega\eta\overline{\rho}_1\mu_o} = 1.9\,\mathrm{mT}$ is a rather big one. So one can assume that the dimensionless magnetic field is small: $B_r^2 << 1$ at the boundaries. Then it follows from (2.5) that $\overline{\gamma}(r_{1,2}) \approx \overline{\rho}(r_{1,2})/\sqrt{2}$. We neglect the small difference between $\overline{\rho}_1$ and $\overline{\rho}_2$ and ω_2 in comparison with ω_1 and reduce (3.9) to the form:

$$\overline{\omega}^{(0)}(\pm z_2) \approx -\overline{\omega}^{(0)}(\pm z_1) + \omega_1 \qquad \text{at } s = 0 \tag{3.10}$$

It follows from (5.4) that

$$(3.11)\quad \overline{\omega}^{(0)}(\pm z_2) - \overline{\omega}^{(0)}(\pm z_1) = \Delta\omega^F_\pm, \quad \Delta\omega^F_\pm = -\int_{z_1}^{z_2} dz \nabla . \left[\frac{\mathbf{1}_\phi}{s} \times \frac{\overline{\mathbf{F}}(0, \pm z)}{\overline{\rho}} \right] \qquad \text{at } s = 0$$

By combining (3.10) and (3.11) we can the estimate the values of the local angular velocity $\overline{\omega}(s,z)$ on the outer sides of the layers on CMB and ICB near the poles of the liquid and the solid core:

$$(3.12)\qquad \overline{\omega}^{(0)}(\pm z_2) \approx \frac{\Delta\omega^F_\pm + \omega_1}{2}\ ;\ \overline{\omega}^{(0)}(\pm z_1) \approx \frac{\Delta\omega^F_\pm + \omega_1}{2} \qquad \text{at } s = 0\ .$$

From (1.2,3) we can obtain not only the difference between values $\overline{\omega}^{(0)}$ on the poles of the inner and outer core, but the *z* dependence of $\overline{\omega}^{(0)}(z)$ on the axis OZ as well:

$$(3.13)\qquad \overline{\omega}^{(0)}(z) = \overline{\omega}^{(0)}(z_1) + \frac{\overline{F}_s(s, z_1) - \overline{F}_s(s, z)}{s\overline{\rho}} - \int_{z_1}^{z} dz \frac{1}{s} \frac{\partial}{\partial s} \frac{\overline{F}_z}{\overline{\rho}} \quad \text{at } s = 0.$$

The force in this formula is a sum of the Archimedean and the Lorentz forces. Respectively, the azimuthal flow strength $\overline{\omega}^{(0)}(z)$ can be presented as a sum of the components $\overline{\omega}^{a(0)}(z)$ and $\overline{\omega}^{m(0)}(z)$. Taking into account the buoyancy force $\overline{\mathbf{F}}^a = \mathbf{r}A(r)\overline{\rho}C(s,z)$ (see Anufriev *et al*. (2005)) one can obtain the Archimedean part of $\overline{\omega}^{(0)}(z)$ at the axis OZ:

$$(3.13a)\qquad \overline{\omega}^{a(0)}(z) = \overline{\omega}^{a(0)}(z_1) + \text{const}\left[\overline{C}(z_1) - \overline{C}(z) - \int_{z_1}^{z} dz \frac{z}{s} \frac{\partial}{\partial s} \overline{C}(s,z) \right] \qquad \text{at } s = 0 \quad .$$

If we assume that the temperature at the axis OZ depends only on *r*, then we obtain: $(z/s)(\partial\overline{C}(r)/\partial s) = (z/r)(\partial\overline{C}(r)\partial r) = \partial\overline{C}(r)/\partial z$. In this case $\overline{\omega}^{a(0)}(z)$ converts into a linear function of temperature:

$$(3.13b)\qquad \overline{\omega}^{a(0)}(z) = \overline{\omega}^{a(0)}(z_1) + \text{const}[\overline{C}(z_1) - \overline{C}(z)] \qquad \text{at } s = 0.$$

Since the temperature is a monotonous function of *z*, $\overline{\omega}^{a(0)}(z)$ has to be monotonous as well.

DISCUSSION

The momentum equation for the flow in the Earth's core is commonly written in a form, which depends on two small parameters the Ekman, E, and the Rossby, R_o, numbers. We rewrite this equation into a form which depends on other two parameters $\sqrt{E}$, and $\lambda = \sqrt{E}/R_o$. The first of them is still small but the other one is not small and exceeds the first one with approximately six orders. Boundary conditions depend only on the first parameter $\sqrt{E}$. Therefore, we search for the solution of the problem in the form of decomposition (1.1) in this parameter.

As a result we obtain the equations (1.2,3) and the boundary conditions (1.4,5), which do not depend on E. Respectively, the force flow satisfying this problem does not depend on E as well. Therefore, this part of the solution satisfies the Taylor state condition.

The residuary part of the leading approximation flow, the geostrophic one, satisfies identically the boundary conditions (1.4,5) and so cannot by determined from them. It has to be defined from the system of equations (1.8-13), depending on λ and respectively on E. So the geostrophic flow depends, generally speaking, on the Ekman number.

The *Taylor state* is called an assumed solution, which does not depend on the Ekman number in the inviscid limit $E \to 0$. The force flow, which obeys the no-normal-flow boundary condition, does not depend on *E*. *So only the geostrophic flow, which depends on the Ekman number E by means of* λ *in (6.8,9) and (1.17), disturbs the Taylor state conditions.* There are two limits, the inviscid one $\lambda \to 0$ and the "viscous controlled" limit $\lambda \to \infty$ when this disturbance is violated and the whole flow converts into Taylor state.

The inviscid flow is of a real geophysical interest since $\lambda = \sqrt{2\Omega\nu}/V_1$ for the kinematic values of viscosity is a small one, $\lambda \sim 10^{-2}$. In this discussion we fix the velocity scale, V_1, by the typical value of the westward drift. If we admit that the velocity scale can change, then we could call it a case of fast flow (or a case of slow rotation, supposing that Ω can change as well, which could be interesting in respect of Venus).

It is important to emphasize that the opposite (the viscous controlled) limit is also applicable in context of the Geodynamo, since as (2,3) shows, λ is relatively great for the turbulent viscosity. This means that the results of the computer simulations, which assume implicitly that λ » 1, have a physical meaning. This is not trivial, since if we adopt the same values of η and V_1 for Venus (where Ω is smaller with two orders of magnitude), then λ becomes of order of 1 and the viscous controlled numerical results could be unapplicable to this planet. But as mentioned above, these results are applicable for the Earth. Moreover, being independent of λ (and respectively of *E*) the computer simulated flows convert into Taylor state and thus describe adequately the flow in the Earth's core. This is also a non-trivial conclusion, taking into account that the typical values of the Ekman numbers in computer simulations exceed these in the Earth core, typically with ten orders of magnitude.

As we noticed above, the computer simulated flows are at asymptotically large values of λ. For example, Glatzmaier and Roberts (1995,1996) in fact carried out their simulations for *E* $\sim 10^4$ and $R_o \sim 10^{-5}$, i.e. for $\lambda \sim 10^3$. In order to decrease this large value to the maximal real one ($\lambda \sim$ 30), these authors have to diminish *E* with three orders of magnitude, which is hardly possible for the existing computers. All the more, it is impossible to obtain a computer solution with a small λ, implying the kinematic viscosity in *E*. That is why we propose to use another way, which is based on decomposition of the flow (1.1). This implies the creation of a computer code for solving the equations presented here. This code would be free of the difficulties concerning the resolution of thin boundary layers.

REFERENCES

[1]. Anufriev, A.P., Jones, C.A. and Soward, A.M. (2005).``The Boussinesq and anelastic liquid approximations for convection in the Earth's core*", Phys. Earth Planet. Inter*. **152**, 163-190

[2]. Glatzmaier, G.A., and P.H. Roberts (1995). A three-dimensional convective dynamo solution with rotating and finitely conducting inner core and mantle, *Phys. Earth Planet. Inter.,* **91**, 63-75.

[3]. Glatzmaier, G.A., and P.H. Roberts,(1996a). An anelastic evolutionary geodynamo simulation driven by compositional and thermal convection, *Physica*, *D***97**, 81-94.

[4]. Glatzmaier, G.A., and P.H. Roberts, (1996b). Rotation and magnetism of Earth's inner core, *Science*, **274**, 1887-1891.

[5] Roberts, P.H., and G.A. Glatzmaier, (2000). Geodynamo theory and simulations, *Reviews of Modern Physics*, **72**, 1081-1123.

[6]. Jones C.A., A.W. Longbotton, R. Hollerbach,(1995) A self-consistent convection driven geodynamo model, *Phys. Earth Planet. Inter*., **92**, 119-141.

[7]. Jault, D., (1995). `Model-Z by computation and Taylor's condition*", Geophys. Astrophys. Fluid Dynam*. **79**, 99-124,

[8]. Fearn, D.R. and G.Morrison (200). The role of inertia in hydrodynamic models of the geodynamo, *Phys. Earth Planet. Inter.*, **128**, 75-92

ABOUT THE REGIONAL CLASSIFICATION SCHEMES AND MODELS IN THE GEOMORPHOLOGY AND PHYSICAL GEOGRAPHY OF BULGARIA

Tzanko Tzankov,

Ivan Drenovski

South-West University "Neofit Rilski"
Faculty of Mathematics and Natural Sciences
Department of Geography, Ecology and Environmental protection
2700 Blagoevgrad, 3 Polk. Dimov Str., SWU Building 4

Summary. *The detached branches of physical geography and geomorphology operate with different regional classification schemes or models. Each of them is based on the specific principal criteria, which are valid only for the relevant type of scientific investigations. This approach is not always observed in the practice of Bulgarian Physical Geography and Geomorphology. The modeling of the contemporary regional classification schemes is permanently actual scientific task. The improvement of these schemes will give the unique possibility to make new scientific generalizations.*

Key words: *Geomorphology, Physical Geography, regional classification, scheme, criteria*

The contemporary development of the physical geography is leading to its non stop division in new branches and special directions on the base of suitable principles and criteria. These circumstances require parallel actualization of the existing classification schemes and models. This question is very important for the current state of the geomorphology and physical geography in Bulgaria.

The efforts for preparation of regional and national geomorphologic maps were the most common science task through the last century in the national geomorphology. One typical example is the lately widely discussed effort for the preparation of Geomorphologic Map of Bulgaria in a scale 1:100000. The elaboration and the printing of small- and middle-scale geomprphological maps of the country or some parts of it was imposed from the necessity of unification and systematization of the very heterogeneous field information. The lack of exact and correct definite principles and criteria for the information systematization and the preparing of unified general legend was the crucial difficulty trough the mentioned period. The same problems accompany the experiments for regional geomorphologic dividing of the country or some parts of it. Negative effect had had the unjustified aspirations of almost all investigators to bind the Neogene's-Quaternary relief building with the responded Late Alpine, Alpine (!) and even Pre Alpine (!!) geologic-tectonic evolution in all the country or same its part. They were looking for the obligatory "genetic uniformity" between different in its character, time of activities and genesis, distortions and other landcrust processes. This misconception has his long existence as a result of the decades long leaded in Bulgarian geomorphology Phanerozoic geosynclinals (later lineament-geosynclinals) geoevolution model. The modern globally adopted mobility concept of plate tectonics has found his reflection in the Bulgarian national and regional geotectonic models in the last quarter of the twentieth century. This gives new possibilities for the correct analysis of the Neogene-Quaternary geomorphologic process in the country.

The underestimation of the polycomponent character of the geomorphologic knowledge is the next very important problem of the former attempts for preparation of large- or middle-scale geomorphologic maps of Bulgaria. The contemporary geomorphology is constructing his scientific models on the base of conclusions and the definitive generalizations (models) of many other sciences (Hydrology, Climatology, Geotectonic, Quaternary Geology, Geophysics etc.). This heterogenic information must be assimilated trough the specialized branches of geomorphology (Regional Geomorphology, Morphostructural Analysis, Climatic Geomorphology, Hydro geomorphology etc.). The results obtained must be used in the preparation of specialized maps or classification models which have to maintain only certain branches of geomorphology. For example – the morphostructural map characterizes the relief morphology only. Prepared on this way all geomorphologic thematic maps (or classification models) will be the really true base for the preparation of one correct and actual general geomorphologic map of Bulgaria.

The situation with the regionalization in physical geography is almost the same.

The regionalization is the necessary final stage in each geographical investigation, especially in the complex ones. On this stage scholars have to create synthetic picture from particular component analyses, revealing main features and specific peculiarities on certain territory. Each attempt for regional differentiation is attended with clarifying series of theoretical and methodological treatments about approaches, principles, methods, and criteria, aiming obtaining of maximum objective results. Nevertheless unavoidable essential feature of each regionalization is its subjectivity (Armand, D., 1975).

The main principle, on which every regionalization is based, is one of spatial entirety, continuity. According it the territory can be divided to strongly individual unique and whole areas with their own appellations.

Almost all Bulgarian scholars assume relief as a leading factor for physical geographic regionalization (Galabov et. al., 1975; Ivanov et. al., 1968; Mishev et.al., 1989; Petrov, 1997). Naturally the number, position and borders of physical geographic regions and districts are near the same as the main morphostructural provinces – normally 4 up to 6. This is proof that all superior regional units are differentiated on the base of geological or tectonic principal, rarely on the geomorphologic ones. The crucial disadvantage of discussed regional schemes is that geological or geomorphologic borders, as tectonic ones, are raised in rank of complex geographic borders. As a result defined superior units are too heterogeneous from the point of physical geography and do not reflect accurately and adequately specific character of regional landscape pattern. Besides, it makes impression, that nevertheless of total number of divided superior regional units, they are proportionally distributed in North and South Bulgaria (2 to 2, or 3 to 3). This is too illogical, taking in account that leading factor – relief, is much more highly varied in southern part of the country, than in the northern. As Wilhelmy, quoted by Batakliev (1934), said that concerning landscapes Bulgaria is present by repeatedly change of low and high regions, like frozen wave, in different stages of which alternate lowlands to high mountains.

No one of regional schemes in the course of Physical geography in schoolbooks for 9-th and 10-th classes of Bulgarian secondary school do not fully agree with discussed above, putted forward as a scientific researches.

To overcome this lack of correspondence new scheme of geographical regionalization is proposed (Velev et.al, 2002).

In addition this will help to unify characterization of different units in the same rank – regions, but not provinces, regions or districts unlikely this is made currently.

The mechanical application of the classification and regional divisions of certain scientific branch for the purposes of any other branch (or science!?) is a common mistake.

It is very danger for the university teaching. The contemporary level of knowledge is demanding proper classification, regional division etc. for every correct limited branch of the geomorphology and physical geography. Its preparing or actualization is a very important scientific task.

REFERENCES

[1] Alexiev, G. 2002. - Geomorphologic regionalization - in: Geography of Bulgaria, Sofia, Bulgaria, ForCom, BAS, in Bulgarian.
[2] Armand, D., 1975. – Science of landscape – Moscow, Russia, Science publ, in Russian
[3] Batakliev, Iv., 1934. – Landscape differentiation of Bulgaria - Annuary of Sofia university, History-philological faculty, 30, 1934, №13, in Bulgarian.
[4] Vaptsarov, Iv., et .al. 1997 Geomorphologic regionalization in: Geography of Bulgaria, Sofia, Bulgaria, BAS, in Bulgarian.
[5] Galabov, Zh., et.al., 1975 – Complex physical geographic regionalization of Bulgaria – in Problems of geography in Bulgaria, Sofia, Bulgaria, Science and art publishing, v.4, in Bulgarian.
[6] Ivanov, I., et. al., 1968 – An attempt for Complex physical geographic regionalization of Bulgaria – in Problems of geography in Bulgaria, Sofia, Bulgaria, Science and art publishing, v.2, in Bulgarian.
[7] Mishev, K., et. al., 1989 – The system of taxonomic units and its base – in Geography of Bulgaria, v.3 Physical geographic and socio-economic regionalization, Sofia, Bulgaria, BAS, in Bulgarian.
[8] Velev, St., et.al., 2002 - Physical geographic regionalization of Bulgaria- in: Geography of Bulgaria, Sofia, Bulgaria, ForCom, BAS, in Bulgarian

---

WASTE MANAGEMENT – MAIN PRINCIPALS AND PROBLEMS

Stefka Tzekova

South-West University, Blagoevgrad, Bulgaria

Abstract: *The waste management is the part of the global strategy for sustainable development. It gives the maximum priority on prevention waste generation, decreasing raw materials and energy resources consumption and the emissions reducing.*

Taking into account the scope of them as a part of material balance of the planet, Republic of Bulgaria place the base of the low regulation of the waste ten years before accepting us with equitable interests into the European Union. The negatives accumulated from the last century and slow down the cardinal change into the human thinking and human response to the waste mater lead to extend the problem.

Keywords: *competent authorities, waste management hierarchy, pollutant – pay, household waste treating.*

1. INTRODUCTION

The European Committee expects to follow the accepted by the Community in 1989 Strategy for Waste Management [1] and institute the principal, aims of politics and actions. Taking into account that waste management is a complex problem with a lot of components the Strategy is based on the following principals:

“Prevention” – formation the waste where it is technical possible or their reduction;

"Manufacturer responsibility" and "the 'Pollutant' mast Pay";

"Prevention" – the potential problems should be expected and must be avoided at the earliest possible stage;

"Closeness" the waste could be destroyed in the place, that is as close as possible to the place of their formation;

These principal are confirmed in Strategy [2] actualization where the waste management hierarchy is developed completely and concreted. The prevention of the waste formation considers as the first priority, following by the waste utilization and the final waste defusing is placed at the last place.

2. OBJECT AND METHODS

According to the European low requirements the basic of low regulations to waste management in Bulgaria were put with the Low for Limitation of Damage Action of Waste on the Environment. This low was improved and modified in 2003 by the Waste Management Low. This low consists of frame regulations for management of the four main classes waste – household, constructions, manufacturers and dangerous. It regalements the general conditions for activities doing for their collection, transportation, preliminary treating, using and utilization and describe the priorities in the hierarchy [3]:

Priority One: waste formation prevention;

Priority Second: waste using by recycling, reuse and/or extraction secondary raw material and energy;

Priority Third: final waste making harmless by deferring or burning of these waste, which could be remake and or utilize.

After waste management hierarchy introducing it is regulated the obligations for using waste as an alternative raw-material and energy source, which is helpful for basic natural resources preservation.

The responsibility for ecological management of different types of waste is divided mainly between different government authorities – Tab. 1, and local municipalities.

Tab. 1.

OBLIGATIONS

Ministry of Environment and Water of Bulgaria

Executive Environment Agency, Regional Inspectorates of Environment and Water

- They develop The National legislation and National programmes for Waste treatment
- They issue permissions for trans-border waste transport and apply the engagements according to Basel Convention
- They issue complex licenses for waste treatments
- They prepare annual report for waste management activities in the country
- They carry on public register for licenses issued and documents registered
- They keep the subsystem "WASTE" that is in NACEM included
- They project realization financing
- They control the waste management legislation

Ministry of Health

National Centre of Public Health Protection (NCPHP),

Regional Inspectorates of Public Health Protection and Control (RIPHPC)

- They participate in normative base of waste management development
- They specify the requirements for dangerous hospital waste,

medicines with expire suitability limit and drugs defusing - They participate in procedures, standards and methods for dangerous waste regulations and laboratory systems building - They realize control on the activity for dangerous waste destructions - They co-ordinate the permissions from the Regional Inspectorates of Environment and Water issued
Ministry of Agriculture and Forestry
- it issue the permissions for waste using in agriculture
- it specify and control the requirements for waste management in meat and food processing industries, agriculture and specify veterinary and sanitary requirements in their collection and defusing
Ministry of Finance
- it monitor over the Government resources expending for waste management sites
- it participate in projects connected with the damages from old pollutions ratification and coordination and projects that are financed by the EC and other international financial institutions
Customs Agency
- it monitor over the observance of requirements for import, export and transit transport of waste
Ministry of Economy and Energy
- it monitor over the commercial activities with waste of black and non-ferrous metals, issue the permissions and public register keeping
Ministry of Regional Development and Public Works
- together with the Ministry of Environment and Water of Bulgaria, the Ministry of Agriculture and Forestry, the Ministry of Health it issue the normative determine the requirement documents for determine the requirements for elections, building and exploiting of the places for building of equipments and installations for waste treatment
- it participated in developing the documents including technical requirements to equipments for processing and defusing of waste
- it monitor regional development and equipments for waste utilization and defusing on regional and national levels
Ministry of Interior
- it participate in developing and applying of normative orders for Go Out of Using Motor Vehicles (GOUMV)
- it monitor the firms activities that doing business activities with waste of black and non-ferrous metals
Ministry of Transport
- it determine the roles and order for waste transport by entering in the country air, water and land transport vehicles
- it develop the requirements for dangerous cargo transportation including dangerous waste
- it collect information about ship waste gearing and send it to the Ministry of Environment and Water of Bulgaria
- it monitor the unregulation throwing out the waste from ships into the sea areas of Republic of Bulgaria
National Statistical Institute

- it collect and process the information for household, buildings and production waste in the country by them types, amounts, economical activities, regions and etc.
State Agency for Metrology and Technical Surveillance
- it monitor the conforming to the permit in the Bulgarian market products that essential requirements are specified according to the technical requirements to the products Low and after their using the large numbers of widespread waste are generated
Civil Protection National Service
- it participate in normative order developing and applying. This order is connected with accident situations and disastrous with waste

3. CONCLUSIONS

The express as stated above could be concluded that local authorities have very serious engagements for different types of waste management, but their main responsibilities are concentrated on activities that connected with household and building waste management. As for household waste the comparatively good accounting are carried on (thoroughly for depot that are equipped with weighing machines) at the other hand the information for the building waste are very inaccurate and scanty. This is because of fact that the large numbers of Bulgarian municipality do not have the depots in regulation for such kind of waste and they are placed together with the household waste.

During the period from 2001 to 2004 years the mean generated amount of waste is about 13 450 000 t. The household waste is about 25 % of this amount.

The reality for the chain of waste treating from 2001 to 2004 years is [4]:

- The organized household waste collection covers about 84.2 % of the country population at the end of 2004 year. This is with 5.6 % more than in 2000 year.

- The organized household waste collection in the towns covers close to the 100 % of the citizens, but for the village population the percents are a little bit low than 40 %.

- The quota for household waste accumulation of 472 t. for 2004 year low than the mean quota for the EC.

Tab. 2.

Indicator	Measure	2001	2002	2003
1	2	3	4	5
Total collected amount	t.*1000/year	3211	3199	3209
Part of population cover by the organize waste accumulation	%	80,2	81,1	82,0

- The separate packing waste collection began in the country during 2005 year. The generated packing waste divided between household and business sector as 59 % to 41 % approximately.

- the amount of household waste depot for the period from 2001 to 2004 year show decreasing, but the building waste increased – Tab. 3.

Tab. 3.

Indicator	Measure	2001 year	2002 year	2003 year
Household waste	Thousands of tons	3211	3199	3209
Building waste	Thousands of m^3	650	600	773

- The numbers of the municipalities' depot and dunghills in 2004 were 633 with the area more than 780 ha. They do not response to the contemporary normative requirements with the exception of these that were building after 1997.

- The preliminary waste treatment before consignation is weakly included.

- At the end of 2004 year 20 of the expected regional depots for household waste were built and start using and 12 were in the process of building.

- The numbers of non- regulation dunghills are so large by now. From 5135 numbers only 3554 are closed.

The responsibilities that should be following by the municipalities according to the engagements assumed by the government are:

- Up to the 2020 year the amount of the biounfenced waste that is directed to the consignation should slow down to 35 % of the total weight amount of the biounfenced waste that were in 1995 year generated.

- Up to the end of 2008 year the recycling of paper should be reach to 60 %, metals – 50 % and wooden waste – 15 %;

- Up to the end of 2014 year about 60 % of the waste should be utilized and between 55-80 % of packing waste should be recycled.

- Up to the end of 2013 year the amount of the recycled plastic should be 22.5 % and recycled glass waste should be 60 %.

The all things mentioned above show that there is a lot work to do not only by the municipality authorities but also by every one of us for living 'without rubbish heaparound us' and to execute the motto 'You must think on global scale – and should do all at local scale'.

4. REFERENCES

[1] Communication from the Commission on a Community Strategy for Waste Management (SEC (89) 934 final of 18.9.1989) Endorsed by the Council in its Resolution of 7 May 1990 (OJ C 122/2., 18.5. 1990).

[2] Communication from the Commission on the Review of the Community Strategy for waste Management (COM (96) final 30 July 1996).

[3] The waste management low. Закон за управление на отпадъците, 2003. (Bulgarian).

[4] Forum 'Energy waste utilization', March, 2007. Форум "Енергийно оползотворяване на отпадъците", март 2007 г. (Bulgarian).

THE AIR POLLUTION PROBLEM IN FIRES AND ACCIDENTS

Luben Elenkov

South-West University N. Rilski, Geography, Ecology and Environment Protection Department Blagoevgrad, Bulgaria

Abstract: *In this paper we turn our attention to air pollution as caused by fires and accidents, and especially to pollutants generated in the burning of combustible material and forest fires.*

Some of the combustion products are absorbed in the outer soil layer, whereas smaller particles float high in the atmosphere over long periods of time (up to several years) and under the influence of weather conditions are transported over great distances and undergo a chemical transformation into acid rains and other toxic substances.

Keywords: *fire, accident, combustion products, toxic substances.*

1. INTRODUCTION

Often air pollution is caused by fires and industrial accidents. Almost every accident and explosion result in fires, as in military conflicts, and our experience of wars in the past and recent military conflicts teaches us that fires occur in situations of violence, irresponsibility, terrorism, incompetence and lack of organisation.

This paper puts an emphasis on fires and accidents and their role as pollutants of the atmosphere and more generally the environment, without examining the causes of their occurrence, growth and containment. Examples are presented to support the idea that air pollution caused by fire is an extremely grave calamity.

Forest fires are wide-spread and frequent phenomena. I am not interested in a statistical overview here, but it is enough to mention that in March 2007 over 60 fires occurred in 4 days in Bulgaria. In September 2004, gas emissions due to fire persisted for a month in Moscow. Important forest fires are registered in USA, Canada, Australia, Greece etc.

On September 8, 9, 10 and 11 2005, 1400 tons of coal burned up in Russe, leaving the city submerged in gas fumes for days.

In April 2007 in Tzalapitsa village the waste deposit site ignited and gas fumes poisoned the air in several villages for a week.

A fire raged in a plastic production factory in Targovishte on March 20 2007, polluting the air in the city. One finds similar examples to be a daily occurrence all over the world.

2. PROBLEM ARTICULATION AND AIMS OF THE STUDY

Forest fires and industrial fires and their role in polluting the atmosphere and the environment are an important issue worldwide. Apart from damages, fires cause polluting emissions on local, regional and global levels.

Smoke produced by combustion on high temperature levels has lower density than the surrounding atmosphere and is lifted upwards; heavy particles are pulled to the earth by the gravity, and light particles float in the atmosphere. Air movements due to differences in pressure can cause angle shifts in the smoke stratification or cause smoke turbulence. Combustible products are released in a fire: various gas, liquid and solid substances, whose chemical composition depends on the physical and chemical properties and the ignition temperature of the fuel. Smoke is a mixture of the combustion by-products and air. Some of the by-products that are released in the smoke are toxic for men, flora and fauna, such as carbon oxide, carbon dioxide, sulphur dioxide, nitrogen oxides, cyanides etc. [1, 2]

Without a steady supply of oxygen the fire is incomplete (as in buildings and closed areas) and it releases by-products such as carbon oxide, ketone groups, alcohols, aldehydes, cyanides, acids and other organic compounds.

Fig. 1 and 2 show that high concentration of by-products reduces the percentage of oxygen in the area, which is very dangerous for men. Moreover, combustion emits nitrogen oxides, sulphur dioxide, hydrogen sulphide, phosgene, chlore, ammonia and other toxic substances.

Combustible material when ignited releases over 2000 toxic compounds. [5]

Their occurrence depends on the chemical composition of the fuel and conventionally researchers turn their attention to the most dangerous and most common substances.

The smoke has several characteristics that account for pollutants: the smell of garlic, sulphur, almonds, sweet and acrid smells mean that there are highly toxic substances in the smoke.

In the area of the smoke cloud, combustion products are the main reason for casualties during fires and their consequences are visible for years.

Chemical analyses show that volatile substances polluting the atmosphere with toxic substances can form out of one and the same fuel with a different percentage of poison; depending on conditions of their dissociation. [1, 4]

The big quantity of toxic emissions and their different qualitative composition make it difficult to evaluate their physiological impact on men.

New materials are introduced in industry, their composition changes and this leads to the occurrence of new combustion products, whose composition is not yet studied. Take into consideration the fact that different kinds of fuel ignite at different temperatures and emit different kinds of toxic substances. It is a fact that hard wood fuel releases bigger quantities of carbon oxide than soft wood fuel. [2]

Different distribution and intensity of heat influences the speed of combustion and hence the smoke emission. For example, if fuel is vertically located and is not impeded by walls or other objects, the velocity of combustion is greater. In open-air fires, as is the case with forest fires, the speed of combustion and the smoke emission are constant variables, only if the fire is constantly fuelled in uniformly humid environment. (Fig. 3, 4)

What is more, if the inferno occurs in a radioactive area or passes over settled particles in mines, factories etc, its elevating power lifts them high above the fire and adds them to the pollutant substances in the affected area. Industrial fires and especially forest fires ought to be studied with regard to two aspects:

1. *Pollution at the moment of occurrence of the accident*, its containment and extinguishing, and up to the moment when toxic substances indicator is returned to its normal values (the process could span over a week).
2. *The effects of pollution spread over a period of time*: small and light particles and gas are lifted in the troposphere where they can drift for several years. They can travel, carried by air currents, over great distances and atmospheric conditions could result in a transformation of their chemical and physical characteristics.

The particles emitted in smoke represent a large class of chemical substances that exist as solid or liquid aerosols, and often contain sulphur and nitrogen oxides, volatile organic compounds, polycyclic aromatic hydrocarbon. [3, 5] The size of the particles in dispersion ranges from 1 to10 microns. [3, 6] The bigger ones are deposited on the ground or water surface and are eventually absorbed by men through the respiratory and the digestive systems and the skin. In contact with moist currents high in the atmosphere, lighter aerosols undergo a chemical transformation and return to the ground as acid rains and other toxic substances.

Research proves that the concentration of chemical compounds in the atmosphere is very high after a forest fire. The toxic cloud of pollutants can travel over 500 to 1000 km and more at 4 meters/second wind speed for a few days. In 2002 after a forest fire in Quebec, Canada, particle emissions reached Baltimore travelling over 1500 km of distance, and the concentration of toxic substances is 8 times the allowed rate.

The aim of this paper is to conduct a study of pollutants emitted in fires, explore how combustion products react during and after the fire, see how pollutants are sustained in the atmosphere, their chemical transformation and conditions of stability; explore on what distances they can spread and draw conclusions about how to improve anti-fire security and contain the fire in a rapid manner.

3. CONCLUSIONS

1. Combustion products affect men, flora and fauna, depending on the rate of their concentration and the time of interaction with the dangerous area.
2. Almost every fire emits by-products such as carbon oxide, carbon dioxide, sulphuric and nitrogen oxides etc.
3. Preventive measures: improve organisation and technical equipment in forests and industrial facilities.
4. Implement fire alarms, protective sprinkler systems and space-operating monitoring of fire localisation.
5. Educate population and technical personnel to contain small fire pockets and evacuate quickly.
6. Fire-fighting mechanism: locate, contain and extinguish the fire.

4. REFERENCES

[1] Gradev T. (1983) Градев Т., Продукти на горенето в условия на пожар и въздействието върху човека. Научно-Технически сборник ПО бр. 3, София 1983.

[2] Grozev, G.(1985) Грозев Г., Процесът горене и съпровождащите го явления. Сборник материали ПО, София 1985.

[3] Dragoev V., Agnes Galabova (2007) Драгоев В., Агнес Гълъбова. Пожари – въздействие върху околната среда. Сборник доклади. София 15-16 март 2007.

[4] Dimitrov S.(1995) Димитров С. Евакуация на хора при пожар в помещения и сгради. София 1995.

[5] Dimitrov S. (2005) Димитров С. Токсични вещества при горене. Сп. Сигурност и безопасност, бр. 11, 2005.

[6] Jivkov I. (1985) Живков И. Горене. Сборник материали ПО София 1985.

[7] Kartov R. (1999) Кътров Р. Използване на вентилационните инсталации при пожар в затворени обекти. НТС. Пожарна и аварийна безопасност, бр.14, 1999.
[8] Kartov R., Petar Klisarski (2005) Кътров Р., Петър Клисарски. Комплексна система за противопожарна защита. Сп. Сигурност и безопасност, бр.11, 2005.
[9] Bloomberg J. Impact of 2002 Canadian Fires Felt 700 Miles Away in Baltimore, Maryland, Science Daily, School of Public Healt

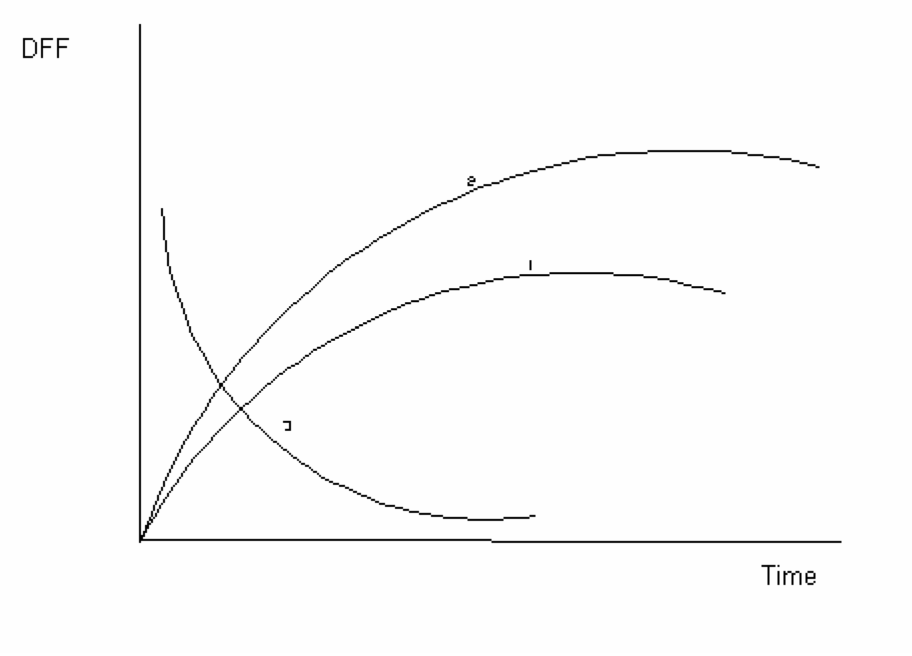

Fig. 1: Fire in a closed area – building.
1.Temperature
2. Combustion products
3. Oxygen level

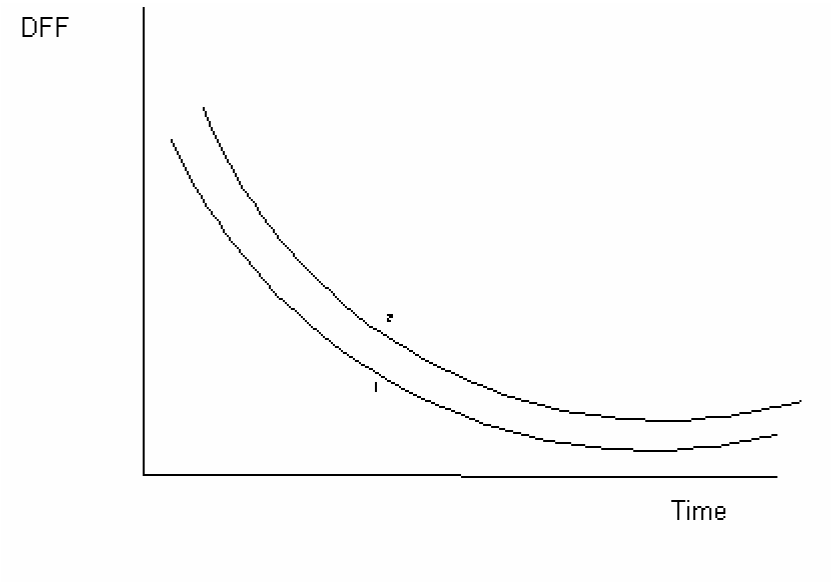

Fig. 2: Fire in a closed area.
1. Oxygen level decreases the longer the fire burns.
2. Critical temperature of combustion and inhaling of hot air.

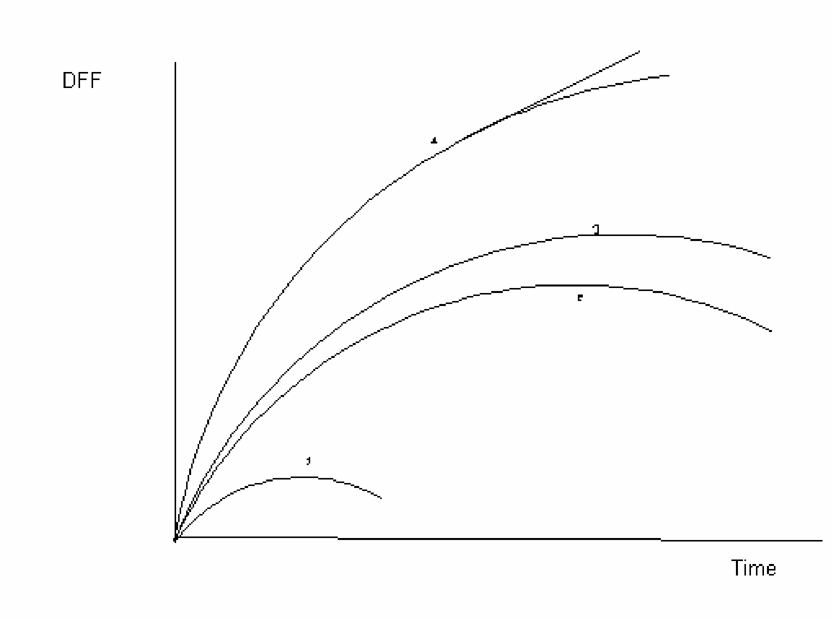

Fig. 3: Forest fires.
1. Temperature critical for men
2. Fire temperature
3. Flame height
4. Combustion products

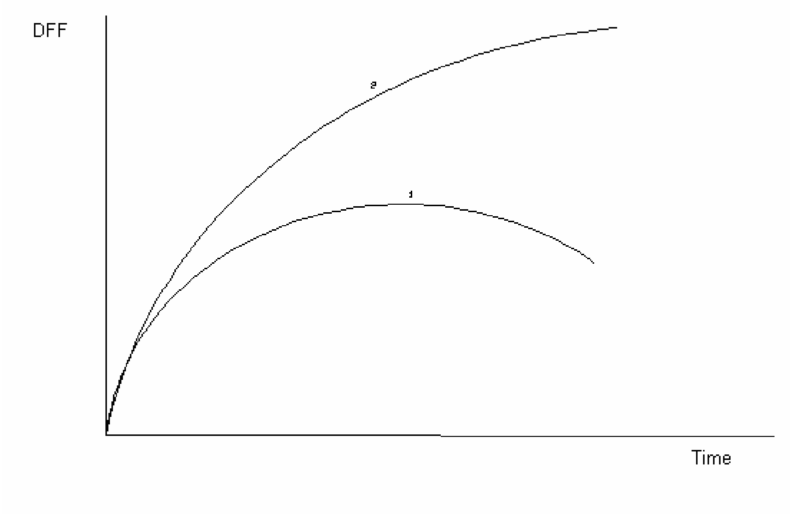

Fig. 4: Combustion products in the atmosphere.
1. Several days
2. Longer periods of time

POSSIBILITIES DERIVING FROM THE APPLICATION OF A COMBINATION APPROACH IN DEFINING THE REGIONS FOR SUPPORTIVE MEASURES

Maria Shishmanova

South-West University, Blagoevgrad, Bulgaria

Abstract*: this paper considers the possibilities for a fuller and thus more exact definition of the regions to receive special support by examining a longer (ten-year) period in the study of the socio-economic development they have attained by sub periods, this is then used in combination with the indicators used to qualify the regions of supportive measures in accordance with the Regional Development Act. This combination approach can be used as a means to correct certain cases, which have been classified into the wrong group of a certain region identified to be in need of supportive measures. This approach provides an opportunity for an even more detailed study.*

Keywords: *region of supportive measures, region of growth, attained socio-economic development*

1. INTRODUCTION

The Regional Development Act introduced the definition of the ’regions of supportive measures’. These are areas defined within the municipalities, which possess competitive advantages for economic development or are going through difficulties because of their geographic location and economic and labor specialization.

The economic growths regions are characterized by a relatively well built technical and business infrastructure, a developed educational network and demographic potential and have the potential for an accelerated economic development.

Planned investments in these regions primarily envisage the priority development of business infrastructure, including hi-tech parks and business incubators, the stimulation of innovations, technology transfer, development of related productions and investments in human resources. The expected result is to turn these regions into regional or local economic centers and spread their positive economic impact into neighbouring territories by means of cluster and subcontractor networks development, as well as by strengthening the agglomeration relations with the other city and town centers.

The purpose of the present study is to analyze the level of socio-economic development of the regions to receive special support and especially of the growth regions for a broader time span /1993 - 2004/ and compare this with the indicators used to determine the regions for supportive measures as per the Regional Development Act. The study also seeks to identify possibilities for an interaction between these two approaches for a more exact and perfected definition of these regions.

2. MATERIALS AND METHODS

To carry out the present study were used the *Regional Development Act*, published in the State Gazette's issue No14 / 20th February 2004, with the amendments as published in the State Gazette's issue No.32 / 12th April 2005; the Regional Development Plan of the Southwest Planning Region (2007 – 2013); research and studies of the socio-economic differences of municipalities in the Republic of Bulgaria for the years 1993, 1994-1996, 1997-1998, 1999-2000, 2001-2002., 2003-2004 (level of achieved socio-economic development).

The methodological approach employs SWOT analysis, a comparative analysis of the achieved level of socio-economic development of the municipalities, which are economic growth regions following the example of Blagoevgrad district, taking into consideration the actual situation and putting forward an approach that follows the actual socio-economic development in time-periods and subsequent application of the indicators used to determine the regions to receive special supportive measures.

3. RESULTS AND DISCUSSION

A general SWOT analysis must be made in order to come to a clear picture of the current situation at district level.

Tab. 1: Generalised SWOT Analysis of Blagoevgrad district

Blagoevgrad	Weaknesses
1. Geostrategic situation: borders with two countries, Greece and Macedonia. 2. The availability of a high-level administrative, economic and cultural centre. 3. The existence of an international transport corridor, a developed regional and local road network. 4. The availability of a wealthy historical and cultural heritage and traditions which are resources for a richly diversified tourist product. 5. Great tourism development potential: mountains and mineral springs.	1. Grave problems with agricultural production. 2. Monostructrured economy in the rural regions and in the regions in industrial decline. 3. Undeveloped potentials of the cross-border co-operation and development. 4. Relatively high unemployment level, especially in transborder regions. 5. Low quality of life and low living standard of population. 6. Non-sparing use of the natural potential for the development of tourism and economic activities.

6. Availability of ores and other mineral resources and forests 7. Environment favouring the development of ecological agriculture. 8. Rich water resources: the rivers Struma, Mesta and some others, incl. hydro-power resources. 9. High share of lands occupied by forests and availability of significant forest resources of economic importance	7. Strongly pronounced intraregional differences and availability of a great number of backward regions. 8. Mountainous relief, greatly impeding the development of the technical and social infrastructure 9. Feeble connections between research teams, universities and business
Opportunities	Threats
1. Development of various types of tourist products, such as winter sports, climatic and spa tourism, eco-tourism, hiking and knowledge tourism, rural tourism. 2. Development and intensification of cross-border co-operation with Macedonia and Greece. 3. Establishment of pre-conditions for new economic activities along the transport routes leading to existing and prospective border check-points with Macedonia and Greece. 4. Establishment of a logistic centre along the transport corridor. 5. Development of gas-supply infrastructure. 5. Establishment of pre-conditions for a recovery and upward development of agriculture. 6. Establishment of a regional information centre on the development of agriculture. 7. Access of local businesses to the common European market. 8. Diversification of the economy of rural and mountain regions and development of ecological productions. 9. Utilisation of significant resources from the EU Structural Funds. 10. Development of high-tech productions and improvement of the interaction between research institutes and business. 11. Enhancement of the investment attractiveness of the district and increase of foreign investments. 12. Development of cross-border and regional co-operation, shared use of educational, health and social infrastructures across the border.	1. Decrease of the economic activities after the introduction of European production standards at small- and medium-sized enterprises and a new surge in unemployment. 2. Emigration predominantly of the younger generation of high educational level and professional qualifications. 3. No concept for the development of ecological agriculture in this region. 4. Low professional qualification in the tourist industry, deteriorating the quality of the tourist product. 5. No availability of own funds in the local administration to formulate and implement a regional policy. 6. Deterioration of the market conditions for local SMEs as a result of the strong competitive thrust of European companies and a recession on the international markets. 7. Dependence of local administration on the state budget and inability to co-finance investment projects. 8. Slow-down of the implementation of important infrastructure projects.

As per Art. 7a (a new one, published in the State Gazette, issue 32 / 2005) (1) the territories of the **economic growth region** comprise municipalities with developed economy, transport, technical and social infrastructure, each of which complies with two thirds of the indicators below:

1. net incomes from sales per citizen to exceed 120 per cent of the country's average value for the three preceding years;
2. the average annual growth rate of net incomes from sales per citizen to exceed the country's average value for the three preceding years;
3. average salary level to exceed the country's average value for the three preceding years;
4. average annual salary growth rate to exceed the country's average value from the three preceding years;
5. average unemployment level to be less than 105 per cent from the country's average value from the three preceding years;
6. average annual unemployment growth rate to be less than 105 per cent of the country's average value of the three preceding years;
7. factor of age dependence to be less than 110 per cent from the country's average value for the three preceding years;
8. average annual population growth rate to exceed the country's average value for the three preceding years;
9. more than 50 per cent of the population reside in an area of developed transport infrastructure at a distance of up to 30 km from an expressway, class A motorway, railway station, civil airport or public port [1].

The economy of the **regions suffering from decline** is dominated by economic sectors in a process of restructuring or already restructured ones. It is marked by a decline in economic activities, decrease of employment and incomes, which result in more intensive migration processes.

The interventions in these regions target the diversification of the local economy by stimulating the economic initiative and attraction of business from outside the region, acquisition of new qualifications of human resources, construction of business infrastructure and rehabilitation of the existing production capacities.

The expected result is replacement of the production capacities that have been closed down by competitive SMEs, creation of new jobs and utilization of the existing economic development potential.

The economy of the **stagnant rural regions** is monostructured and dominated by the agricultural production sector, which however is not a market-driven one and is characterized by an extremely low technology level. These regions have a poorly developed technical and social infrastructure and access to public services is greatly impeded. More intensive migration processes can be observed, as well as village depopulation and ageing of the population.

Planned investments are intended to contribute to infrastructure development, improving access to public services and stimulating economic diversification by means of development of a subcontractor network and the tourist sector and preservation of the local natural, historical and cultural heritage.

The expected results are overcoming the demographic crisis in these regions by means of enhancing their attractiveness and achieving stable employment figures, improvements in the quality of infrastructure, development of the settlement network and strengthening the links to economic and consumer centers.

The **stagnant border regions in** are characterized by their border location, a closed-type underdeveloped infrastructure, underdeveloped local economy and pronounced migration processes.

Interventions are directed towards building transport and social infrastructures, enhancement of the human resource quality, stimulation of entrepreneurship and attraction of business from the outside.

A key instrument for the revival of these regions is cross-border co-operation, with the border location used as a way to heighten investment attractiveness of the stagnant border regions. Of importance is the shared use of social infrastructure, cultural exchange and joint initiatives against forest fires. The opportunities for socio-economic development of the **stagnant mountain regions** are heavily restricted by the mountainous relief, which makes more difficult the building of a technical, social and business infrastructure, limits the development possibilities for an up-to-date agri-farming and the food-processing industries.

Interventions aim to provide incentives to the set-up of new SMEs in the fields of ecological farming, tourism and various productions, based on specific local resources, the development of technical infrastructure and improved access to education, health care, social and administrative services.

The expected outcomes are diversification of the local economies, overcoming of the demographic crisis, development of the local settlement network and strengthening of the agglomeration links with the economic and consumer centers.

The municipalities, falling into the various categories of the regions identified for special support have been determined by enactment of the Regional Development Act after the latest amendments to it, as published in the State Gazette, issue 32/2005, by using official statistical information and data of the district administrations.

The defined regions are coordinated with the Regional Development Council to the Southwest Development Region, as is attested by a Protocol dated 17th June 2005 on the grounds of Order OA-19325.05.2005 [2].

Tab. 2: Scope of the regions for supportive measures in Blagoevgrad district.

District / Municipality	Stagnant rural region	Stagnant border regon	Stagnant mountain region	Economic growth region	Region in industrial decline
Blagoevgrad	**7**	**4**	**7**	**5**	**5**
Bansko				●	
Bellitza	●		●		
Blagoevgrad				●	
Gotse Deltchev				●	
Gurmen	●		●		
Kresna					●
Petrich				●	
Razlog				●	
Sandanski	●	●	●		●
Satovtcha	●	●	●		
Simitli					●
Stroumiani	●	●	●		●
Hadjidimovo	●	●	●		●
Yakorouda	●		●		
TOTAL FOR SWPR	***26***	***9***	***30***	***11***	***29***

Source: Development plan of the Southwest Planning Region 2007 – 2013.

The municipalities under consideration were defined as below, based on the *Regional Development Act* of 1999 and the subsequent Order on definition of the regions for special support measures: Blagoevgrad is to be an economic growth region, Bansko and Razlog failed allocation as regions for special measures of support, whereas G. Deltchev and Sandanski fell into the category of cross-border co-operation development region.

The socio-economic disparities among the municipalities in Bulgaria are subject of research using methodology based on the taxonomic method. The municipalities as multiple-value objects are subjected to comparison with a fictitious municipality, the latter being characterized by extreme (maximum or minimum) values of the individual indicators. The method employed has been developed on the basis of the cauterization principle and relates to the mathematically determined methods with quantitative evaluation of the similarity [3].

The socio-economic development estimate values, reached by municipalities, vary between 0 and 1. The nearer the value to 1, the worse the indication for the municipality concerned is.

Tab. 3: Rating of the growth regions in Blagoevgrad district".

Municipality	1993		1994-1996		1997-1998		1999-2000		2001-2002		2003-2004	
	Rating	Integr. appraisal	Rating	Average transf. integer. appraisal for the period	Average transf. integer. appraisal for the period	Average transf. integer. appraisal for the period	Rating	Average transf. integer. appraisal for the period	Rating	Average transf. integer. appraisal for the period	Rating	Average transf. integer. appraisal for the period
Bansko	112	0,8966	153	0,8590	102	0,8189	80	0,7835	95	0,6959	80	0,5655
Blagoevgrad	44	0,8614	30	0,7879	29	0,7298	26	0,6469	24	0,5583	29	0,4453
G. Deltchev	190	0,9202	123	0,8497	95	0,8137	99	0,7948	115	0,7110	68	0,5395
Petrich	140	0,9056	157	0,8610	130	0,8346	120	0,8071	75	0,6653	42	0,4710
Razlog	91	0,8878	107	0,8419	106	0,8200	124	0,8092	118	0,7180	79	0,5634
Average	49	0,8638	39	0,8053	46	0,7687	34	0,6985	41	0,6058	35	0,4612
Sandanski	121	0,8992	85	0,8067	85	0,8067	97	0,7941	89	0,6874	75	0,5558

Source: Studies of the Institute of Economics of the Bulgarian Academy of Sciences

When investigating the socio-economic development of the economic growth regions over a ten-year period it was found out that:

- The Municipality of Blagoevgrad is characterised by a positive development throughout: it rated 29th in the period 2003-2004, while it rated 44th in 1993. During the period it varied around the 29th position and upwards to 24th place. But it was always 5 to 6 steps above the country's average aggregate value for municipalities, and the difference between this average value and the municipal value for 1993 is 0,0024, whereas for the period 2003-2004 it goes up slightly and is 0,0159. The municipality of Blagoevgrad occupies the foremost position (29th) for the last period under consideration as compared with the other municipalities within the district, falling within the economic growth regions.
- The next municipality to come next after Blagoevgrad for the same period of 2003-2004 is the municipality of Petrich (it rates 42nd), which has an average transformed integral evaluation value of 0,4710, and thus falls below the country's average by 7 points. During the ten-year period, forming the object of our study, the municipal socio-economic development has been "steeply and progressively an upward one". While ranking 140th in 1993, it now occupies position 42nd.
- Gotse Deltchev municipality has gone on from occupying 190th position in 1993 to ranking 68th in the period 2003-2004. Within these ten years its socio-economic development during the first two time-spans was characterized as a "steeply upward one", the next two time-spans registered a "slight slump" (positions occupied were 99th and 115th) and during the last time-span it ranked 68th; or to summarise, it has climbed by 112 positions compared with the first time-span under consideration, with an average ranking for the country at place 49 for the first time-span and place 35 for the last time-span. The difference between the average arithmetical aggregate of the municipalities in the country and the average transformed integral estimate for Gotse Deltchev is 0,0564 for the first time-span, whereas for the last time-span it is 0,0783 from the average transferred integral evaluation value for the period, i.e. it has been driving slightly away from it, nevertheless it has been getting significantly onward in its development.
- The municipality of Razlog moved from 91st in 1993 to 79th, i.e. it has climbed only by 12 positions and thus its development is characterized as slow (it passed through positions 107, 106, 124, 118th position). It is indicative that after a downturn in its socio-economic development a period of extrication from the crisis is setting in, but still it is by 44 positions below the average arithmetical aggregate of the municipalities in Bulgaria. The difference between the average transformed integral estimate for the countray and the one for the municipality is 0,0240 for the first time-span and 0,0022 for the last one, i.e. Razlog comes very near to the degree of socio-economic development of the average arithmetical aggregate of the municipalities in Bulgaria.
- The municipality of Bansko occupies position 80 during 2003-2004 and was 112th in 1999. Its development went through a 'headstong' downturn in the period 1994-1996 (it ranked 153rd then), following which it consecutively occupied positions 102, 80, 95 and 80 for the studied periods, i.e. it displays "even fluctuations up and down" in its socio-economic development. The difference in the values of the average transferred integral estimate for the average arithmetical aggregate of municipalities in Bulgaria and the municipality stands at 0,1043, i.e. it is great enough and represents 45 positions below the average value, which occupies position 35.
- An intriguing and paradoxical case is presented by the municipality of Sandanski. The Southwest Region Development Plan defines this municipality as an industrial decline region and simultaneously as a stagnant rural and stagnant mountain region. The study on the socio-economic development of Bulgarian municipalities rates Sandanski 75th among a total of 264 ranking positions, i.e. ahead of Razlog and Bansko which are characterized as economic growth regions. It ranks below the average arithmetical value

of the aggregate of Bulgarian municipalities by 40 positions, but this means it possesses a certain potential to enhance its competitiveness and also that the municipality's economic climate improves with rapid paces. While following the positions it occupied during the ten-year period, it was revealed it had not gone back in its development. In this case a contradiction becomes apparent, as a region in a relatively good position has been defined as a rural and mountain region in stagnation and as a region in industrial decline.

4. CONCLUSIONS

Using the SWOT analysis of the district of Blagoevgrad as a basis and in comparison with the regions for special supportive measures in the district, and more especially the example of the economic growth regions, it becomes evident that a combination approach would contribute towards a more precise definition of these regions, both for formulation of the vision and strategic goals, as well as the measures for their development.

The socio-economic differences among the municipalities in Bulgaria are examined as multiple-value objects and compared with a fictitious municipality. This approach is conducive to the comparability between municipalities and comparability of the municipality or the region for special supportive measures with itself in respect of the status it had in time.

The indicators which correspond individually to two-thirds of the indicators used to define the regions for special support, result in a 'still-life'. The combination of this 'still-life' with a dynamic picture of processes enriches the possibilities for more accurate decision-making and a better process management in these regions.

5. REFERENCES

[1] Regional Development Act, published in the State Gazette, issue 14 of 20th February 2004; amendments and supplements published in the State Gazette, issue 32 / 2004; issue 8/2005; supplements in issue 24 / 2006 of the State Gazette.

[2] Plan za rasvitie na Yugozapaden raion za planirane za perioda 2007-2013 (2005) MRRB. (Development Plan of the Soiuthwest Planning Region for the period 2007-2013 /2005/, Ministry of Regional Development and Public Works).

[3] Jankova, N. (2005) Raslicia v rasvitieto I konkurentnosposobnost na obstinate v Bulgaria pres perioda 2000-2002g. Ikonomicheski institut, BAN, Ikonomicheski isledvania. br. 3, 3-35/ Differences in the development and competitiveness of the municipalities in Bulgaria in the period 2000-2002, Institute of Economics of the Bulgarian Academy of Sciences, Journal of Economic Research, issue 3, p.3-35.

POSSIBILITY FOR PREVENTION OF FIRES IN RURAL AREAS

Luben Elenkov, Maria Shishmanova

South West University "Neofit Rilski", Blagoevgrad, Bulgaria

***Abstract**: The present study targets an extremely important present-day issue: that of fire prevention in small-sized settlements of less than 1000 inhabitants. It is a problem that calls for a solution as these settlements represent 85% of all settlements in Bulgaria, their population is 1/6 of the country's total population and they have accumulated long-lived tangible assets of national importance. Order No.2 entitled 'Fire-prevention construction and technical regulations' does not envisage these settlements and this is an omission testifying to an unequal treatment of settlements and violation of human rights.*

***Keywords:** factors for fires, fire-prevention factors, measures, amendments to the regulatory framework.*

INTRODUCTION

As per Article 577, item 3 of Order No.2 *Fire-prevention construction and technical regulations* settlements of less than 1000 inhabitants are not treated at all.

Analyses reveal that in about 65% of fires the causes were not established or were unknown. In 72% of the cases with established causes forest fires originated because of failure to act in compliance with fire-prevention rules in forests or in their proximity [7].

The purpose of this study is to analyze some peculiarities of the settlements smaller than 1000 inhabitants and evaluate the potential possibility to solve this problem. These settlements need to be prepared and introduce technical and organizational arrangements for cases of fire, as well as to obtain an evaluation of their significance on a national scale.

1. Pre-conditions and factors for fires

The pre-conditions for origination and spread of fires relate to a number of factors:

- Climatic factors – droughts and extremely high temperatures relating to a global climate change;
- The afforested cultures are primarily conifers (white and black pines, spruce); a large part of them are located in the lower mountain belt of forests and vegetation or in the lower part of the medium belt. It is precisely among these species that the greater part of forest fires spread in recent years;
- Imperfect legal and regulatory framework, related to an inadequate state policy on forest preservation, fire prevention and fight with forest fires that have arisen;
- Non-existence of an early detection and fire alarm system;
- Lack of co-ordination in fire-fighting between various institutions and organizations, as well as a lack of a common work system;
- Low level of competence of the specialists working in the territory of the state forest fund and the appertaining areas;
- Lack of specialized technical equipment to fight forest fires;

Lack of a special-purpose fund was build to fight fires and strongly restricted budgetary resources [7].

Basic factors influencing a timely fire-prevention

Among the basic factors for a timely fire-prevention of settlements are their location, transport accessibility, characteristics of the environment such as type of a forestation, constant water-supply, type of structure of the buildings, demographic characteristics of the population and availability of fire-fighting equipment and respective arrangements.

Location and transport accessibility

Many of the villages and very small towns of population not exceeding 1000 are located at a distance and peripherally from the city centers. Furthermore there are areas in the mountain regions which are only accessible with difficulty where settlements are of the dispersed type, access to these is problematic and some of them can only be reached on foot. In their prevalence these settlements are situated in immediate proximity to huge forest areas and are mountainous settlements originated over an intricate terrain. Their accessibility to vehicles falls outside of the 30-minute isochrones of vehicle accessibility which is a complication in case of fire.

Characteristics of the environment and causes of fire

Of the total territory of the country agricultural land makes up 58.7 %, forests are 33.6%, and settlements and other urbanized areas occupy 5 % [2].

The forest fires in the last decade of the 20th century were 5719. The initial analyses of the reasons that led to them show that only about 1% of fires were caused by natural causes such as lightning, during the so called ‘dry thunderstorms’. The remaining 99% were to a lesser or greater extent related to human activity or failure to act [7].

Water supply

Despite the bad condition of the *Water-supply and Sewage Systems* and the great losses of water along it, the greater part of municipalities does not experience problems with the regular water supply to the population. The severest problems still remain in 26 administrative regional settlements where more than three fourths of the inhabitants were on a restricted water-supply regime. This gives rise to a considerable differentiation among municipalities and risks of various natures, incl. fires.

Almost one out of four municipalities experiences problems with the regular water supply to the population. When evaluating this fact, account needs to be taken of the unfavorable circumstances, caused by the extremely bad physical condition of the water supply and sewage system in the first place.

The Bulgarian municipalities range from 1 to 264 based on the share of the inhabitants in respect of water-supply regime (% of population with water supply 0), appearing in Table 1. The table lists the municipalities ranged first and last in respect of degree of water supply. Average indicators for the country are introduced such as individual ‘municipality’ and thus municipalities with a degree of regular or irregular use of water are differentiated and thus the clearest picture on the actual status of water supply of the municipalities is obtained.

In about 60% of municipalities the situation with the regular use of water is better than the country’s average, i.e. these municipalities apply water supply regime for less than 19% of their inhabitants (most often seasonally).

The gravest situation is observed in 35 municipalities, where about one third of the population is subjected to a water supply regime. The entire population of the municipalities, which appear below in Tab. 1, was affected by such a regime.

Tab. 1: Municipalities rated as per regularity of use of water in 2004.

Municipalities	Share of the population put on water use regime (% of population with water supply)	Ranking	Municipalities	Share of the population put on water use regime (% of population with water supply)	Ranking
Bansko	0	1	Chepelare	98,9	275
Ruzhintzi	0	2	Dobrich	100	258
Beloslav	0	3	Rackitovo	100	259
Panagyurishte	0	4	Zemmen	100	260
...and 60 other municipalities	0	64	Maddan	100	263
Average for the country	18,98	161	Neddelino	100	264
Koula	19,29	162	Chavdar	100	265

Source: Institute of Economics of the Bulgarian Academy of Sciences

The conclusion is that the differentiation among the municipalities in this respect is significant (the coefficient of variation is over 1.18) and is sue to the presence of (mostly seasonal) regime in a number of administrative territorial units during the analyzed year. The bad state of the water-carrying network also exerts an influence on this differentiation as it determines the quality and regularity of water supply. This is one of the reasons why a number of pre-accession programmes (SAPARD, PHARE) envisage possibilities for financing of municipal projects, intended to improve the water transportation network [6] and erection of installations for water-intake, especially in the settlements which are suffering from a water regime and in settlements where no sewerage system has yet been built.

Buildings per type of structure.

In this kind of distant villages and very small towns the basic economic occupations are agriculture and stock-breeding. Almost any residential building (a house) has various additional structures attached to it, such as a summer kitchen, animal premises, a barn, premise for the agricultural inventory, lean-tos and others, of non-solid timber structure. What must be underlined is that the roof structures of all buildings in the analyzed settlements are made of wood (Fig. 1). Apart from the small and very small settlements there are a number of dispersed recreation and tourist facilities such as resort and holiday villages, hotels, chalets, etc.

Almost in one half of the villages the buildings and auxiliary sheds are non-solid structures: timber framework [3]. This poses a great risk for a rapid spread of flames in a case of fire (see Tab. 2).

Tab. 2: Residential buildings as of 31st December 2005 as per type of structure (number).

Regions	Residential buildings - total		Type of structure of residential buildings					
			Ferro-concrete		Brickwork		Others	
	Number	%	Number	%	Number		Number	%
TOTAL	2127378	100	95 329	4,4	1578921	4,2	453 128	21,4
in towns	750992	100	60 344	2,8	606 531	0,8	84 117	16,4
in villages	1376386	100	34 985	2,5	972 390	8,9	369 011	48,6
Source: National Statistical Institute								

Fig. 1: Fire in a timberwork building.

Demographic characteristics of the population.

The population of almost all villages lowered in recent years and their age structure deteriorated, while others were depopulated. In these conditions, an occurrence of fire could have, depending on the circumstances, even a tragic outcome.

Tab. 3: Settlements of less than 1000 inhabitants – 2005.

Kinds of settlements	Settlements		Population	
	Number	%	Thou. inhabitants	%
Villages:				
Up to 100 inh.	1529	30,1	53,0	2,3
From 100 to 500 inh.	1915	37,7	503,9	21,9
From 500 to 1000 inh.	806	15,9	573,9	24,9
Total up to 1000 inh.	4250	83,7	1130,8	49,1
Towns				
Up to 1000 inh.	3	1,2	1,9	0,04

Source: National Statistical Institute.

Remark: % for the villages is from the rural population and the total number of villages, for the towns – from the urban population and the total number of towns.

The group of up to 100 inhabitants includes 140 villages without population as of 2005.

4250 villages have a population of up to 1000 inhabitants, which makes 83,7% total 5332 settlements in Bulgaria (2005). The towns of population up to 1000 inhabitants are only 3 of total 253, and of total population 1906 inhabitants [4]. It can be summarized that in 85% of settlements lives approximately one sixth of the entire population, but there are long-lived tangible assets which have not been financially evaluated, they also have a vitally important moral and to a certain extent, cultural and historical significance.

Availability of fire-prevention and fire-fighting equipment and the respective organizational arrangements

The introduction of a water supply regime in the summer months signifies that fire-prevention safety and personal safety of the population in the small settlements is not guaranteed. In this case also there is a lack of protection and preservation of forest and agricultural acreage (the wheat fields for instance in the Dobrudja and Ludogorie regions)

The equipped fire-fighting squads are predominantly domiciled in the towns. In practice this means that such regions are deprived of fire-prevention and -fighting in case of fire and disasters.

Each citizen is also a strict tax-payer to the state, against which the state is under the obligation to guarantee their fire safety.

Upon fire origination in a settlement in the mountain, a resort or holiday village or in a forest the situation may have become irreversible by the arrival of the special fire-fighting squads several hours later. No one is able to guarantee the prompt action of the fire-fighting squads. They may be called to duty elsewhere in the region at the same time, which will impede their timely intercession.

One of the needed measures that cannot be put off is the establishment of a local organization with the support of the municipality, the forestry, agricultural co-operatives or private farms, in which are to be included:

- Construction of water-supply support points;
- Provision of access to specialized water-intake equipment to the support water-supply points; where the possibility exists the existing wells are to be used;
- Examination of the available equipment (tractors, bulldozers, trucks and other suitable for transportation of people, water and excavation of protective land strips

with a view to limit the spread of fire; this equipment is to be registered so as to facilitate their use in case of need;

- Provision to the municipality of one heavy-duty passenger car, equipped with a water tank, motor pump and the respective other equipment;
- Development of a map of the risky sectors, specific and vulnerable sites, such as schools, kindergartens, administrative buildings and the entrance arteries to the forests;
- Campaigns against fire danger during the spring and summer seasons;
- Placement of information and warning boards at the road entrances to and exits out of the forests;
- Restriction of human access to forests in the hottest days and therefore of highest risk;
- Organization of anti-fire vigils over forests and fields and construction of watch-towers at suitable locations for this purpose.

The damages that will result from fires will be a thousand times higher than the costs of the proposed measures above, which are going to be used over a long period of time.

Conclusion

The small settlements, forests and agricultural fields, located at a distance from major settlements, as well as recreation facilities and other dispersed tangible or natural assets are peculiarly vulnerable and have not been provided against such types of risks. On principle, settlements have always originated by a spring or creek, i.e. a natural water source. This is the most secure water supply for fire-prevention and –fighting purposes. The erection of facilities provides safety and the security that one may rely on such a water source at all times. It has many advantages compared with the water mains, especially if the river flow is constant.

When drawing water for fire-fighting purpose from the water mains the disadvantages are that upon failure of only one hydrant or at breach of the mains a long sector or the entire mains will have to be stopped. There is frequently water regime, which means that at the riskiest moments of hot weather the water mains cannot be relied upon.

Fires can be easily extinguished if measures are undertaken to localize it within the initial 10 to 15 minutes, because the factor of time is decisive in a fire intensive development. When left to spread (which is the usual case until the arrival of the fire-fighting trucks coming from a distance of 40, 50 or more km), a fire becomes a disaster and be overcome only with difficulty, especially under unfavorable climatic conditions, such as high temperatures, winds and complex terrains.

Rural regions, small settlements and their peripheral zones adjoining forests are the most vulnerable in this respect.

This prompts the proposal and rapid introduction of the measures described above for the regions located at a distance from towns.

Resources from the special-purpose subsidies must be envisaged in the *Local Government and Administration Act,* to be intended for capital expenses for implementation of the programmes, related to the activities of prevention of the consequences from natural and industrial disasters [5].

On the grounds of the analysis above and the proposed measures a supplement to Order No.2 ‘*Fire-prevention construction and technical regulations*’ is put forward for settlements of less than 1000 inhabitants , or a new Order, which is to guarantee the safety of this type of settlements, too. Furthermore, the Order could regulate the use of available facilities and equipment and the organizational measures in floods and other natural calamities and disasters.

REFERENCES

[1] Order No. 2, Fire-prevention construction and technical regulations, State Gazette, issue 58, 1987, amendments and supplements in State Gazette, issue 33, 1994
[2] National Statistical Institute, Cadastre Agency, 2000
[3] National Statistical Institute, Fund of residential buildings, Residential buildings as of 31st Dec. 2005 in kinds of structure
[4] National Statistical Institute, Population 2005
[5] The municipalities are entitled to a special-purpose subsidies for prevention of natural and industrial disasters, 'Stroitelstvo i gradat', issue 17, (2007), p. 6
[6] Yankova, N.; G. Shopov, N. Chkorev, St. Ivanov et al. (2007),, Monitoring of the socio-economic and environmental differences between municipalities in the Republic of Bulgaria for the period 2003-2005, Institute of Economics to the Bulgarian Academy of sciences, p.45-53
[7] www.time-foundation.org.bg - Ecopolis, Municipality and the environment

SPECIAL FEATURES IN THE REGIME AND THE DISTRIBUTION OF THE RAINFALLS IN PART OF SOUTH-WESTERN BULGARIA

Krasimir Stoyanov, Stefka Ilieva

SWU "N.Rilski", Blagoevgrad, Bulgaria

***Abstract**: There are observed the special features in the territorial and local year distribution of the rainfalls in part of South-Western Bulgaria. It has been used data from 35 stations for a period of 30 years (1951-80). Some regularities in the regimen of the rainfalls has been reviled that are determined from the influence of the physics and geographical factors and differences in the atmosphere circulation.*

***Keywords:** rainfalls, South-West Bulgaria, annual regime, geographical distribution*

1. INTRODUCTION

The rainfalls are one of the basic climatic elements. Its amount and distribution is determined by the atmospheric circulation and the relief. The peculiarities in the geographic position of the South Western Bulgaria that is very close to Aegean Sea and to the path of the Mediterranean cyclones, as well as the diverse relief conditions determine significant horizontal differentiations in the rainfall distributions in this part of the country.

Major attention in the climatology is paid to the territorial distribution of the rainfalls. It is due to the complex time and space structure of the rainfalls, connected with the way of its measurement and its great territorial variability.

The aim of this paper is to analyse the regimen and the territorial distribution of the rainfalls in the mid stream of Struma River. A special attention is paid to the differences in the distribution of the rainfalls in the course of the year in territorial aspect. This attention results from the influence of the atmospheric circulation, and from the changes in the amounts of the rainfalls determined form the diverse relief features.

2. INFORMATION BASIS AND METHODS OF STUDY

Object of study is the year round distribution of the rainfalls in the tributary zone of mid Struma River- a part of South Western Bulgaria. Northern frontier of the explored area are the Kamenishka, Kyustendilska and Dupnishka kettles, and eastern frontier is the junction of Struma River with Iskar and Mesta rivers. On South and West the frontier coincides with the national border. 30 years period of observations is used for characterization of the rainfalls (1951-1980) [9]. In order that this is realized the data from 35 meteorological stations under the control of the Bulgarian Academy of Science -Sofia is processed.

Disadvantage of the data is the low density in the distribution of the stations in the western part of the tributary zone of Middle Struma River, as well as the lack of stations on the western slopes of Rila and Pirin mountains over 1400 m high. 13 of the stations have shorter period of observations, and six have some omissions in those observations. For all these stations an enlargement of the rows has been done by the mode of the proportions [13].

For the formation and the territorial distribution of the rainfalls an important role has the relief. The influence of the relief is mostly associated with the elevation above sea level. But along with this it must be also underlined the important role of the shape of the relief, the exposition and the inclination of the slopes, the position of the relief formations toward the atmosphere streams, etc.. The 35 stations that have been used are also grouped according to the local relief features (tab. 1). The predominant parts of them are situated in kettles and the valleys along the Struma river (14 stations), and also in the deep affluent valleys (8 stations). Only 5 stations are situated on the mountain slopes and ridges.

The rainfalls as a climatic element are explored in the works of [2], [4], [6], [7]. In more recent times the explored area is present in the works of [11], [12], [14]. Very actual are the studies of [1] and [14], about the climate changes and mainly of its two basic climatic elements - rainfalls and temperature. [4] works on the statistical structure of the monthly rainfall.

3. FACTORS THAT DETERMINE THE FORMATION THE AMOUNT AND THE REGIMEN OF THE RAINFALLS

3.1. Circulation of the atmosphere

A significant importance for the formation of rainfalls over Bulgaria has the Iceland cyclones, and especially those of them that are moving from South-East to east and from South to South-East. In the South-Eastern Bulgaria their influence is more limited. They cause the primary maximum of the rainfalls on late spring- May-June for the greatest part of the studied area (tab. 2). During the cold half of the year the Mediterranean cyclones have an important role for the forming of the rainfalls. They are the basic cause for the rainfalls in a part of the southern part of the studied area that is also confirmed by their monthly distribution (tab. 2). Their frequency is maximal during the late autumn and the winter.

Tab. 1: List of the stations used

№	Station	Date of opening	Altitude,m	Latitude	Longitude	Earth form
1*	Dolno selo**	01.01.1954	770	42°18′	22°28′	Kettle
2	Nikolichevtsi	01.07.1942	482	42°15′	22°44′	Kettle
3	Bobov dol	01.05.1920	640	42°22′	23°00′	Kettle
4	Gyueshevo	01.01.1930	944	42°14′		Near to North mountain slope
5	Garlyano	01.07.1947	998	42°15′	22°34′	Near to North mountain slope
6	Kyustendil	01.02.1894	518	42°17′	22°41′	Kettle
7	Tavalichevo**	01.02.1960	642	42°20′	22°54′	Kettle, near to south mountain slope
8	Nevestino**	19.11.1953	440	42°15′	22°50′	Kettle
9	Dupnitsa	01.02.1899	518	42°16′	23°07′	Kettle
10	Sapareva banya**	01.04.1952	712	42°17′	23°15′	Kettle
11	Osogovo Hut**	01.12.1930	1640	42°12′	22°37′	Southeast mountain slope
12	Rakovo**	01.01.1954	780	42°04′	22°43′	Deep valley
13	Vaksevo	01.05.1930	554	42°09′	22°50′	Deep valley
14	Boboshevo	10.01.1904	400	42°09′	23°00′	Deep valley
15	Rila	01.01.1925	470	42°06′	23°07′	Near to West mountain slope
16	Rila Monastery **	01.10.1892	1147	42°08′	23°21′	Deep valley
17	Kocherinovo	01.07.1904	405	42°05′	23°04′	Kettle
18	Logodazh**	13.01.1952	700	41°59′	22°55′	At the foot of East mountain slope
19	Blagoevgrad	01.07.1937	410	42°01′	23°06′	Kettle
20	Dobro pole**	08.10.1948	1209	42°06′	23°19′	Deep valley
21	Suhostrel**	16.01.1952	890	41°51′	23°01′	East mountain slope
22	Krupnik	01.08.1939	350	41°50′	23°08′	Kettle
23	Gradevo	01.04.1949	466	41°55′	23°12′	Kettle
24	Predel	01.11.1948	1142	41°54′	23°22′	Deep saddle
25	Breznitsa**	01.04.1954	400	41°44′	23°11′	Deep valley
26	Kresna**	01.05.1940	180	41°42′	23°13′	Kettle
27	Popina laka**	01.12.1939	1150	41°38′	23°27′	Deep valley
28	Sandanski	01.05.1918	191	41°34′	23°17′	Kettle
29	Dolene**	01.04.1953	720	41°26′	23°04′	Southwest mountain slope
30	Levunovo	16.07.1947	145	41°29′	23°19′	Kettle
31	Melnik	08.05.1930	382	41°31′	23°24′	Kettle
32	Pirin**	01.01.1953	680	41°33′	23°33′	Deep valley
33	Papazchair*	01.04.1950	1400	41°34′	23°39′	Mountain ridge-saddle
34	Klyuch**	01.02.1953	500	41°21′	22°59′	At the foot of North mountain slope
35	Goleshovo**	01.01.1952	760	41°25′	23°33′	At the foot of North mountain slope

*The numbers of the stations are like on fig. 1

**The stations are with shorter period of observations and with interruptions of the rows.

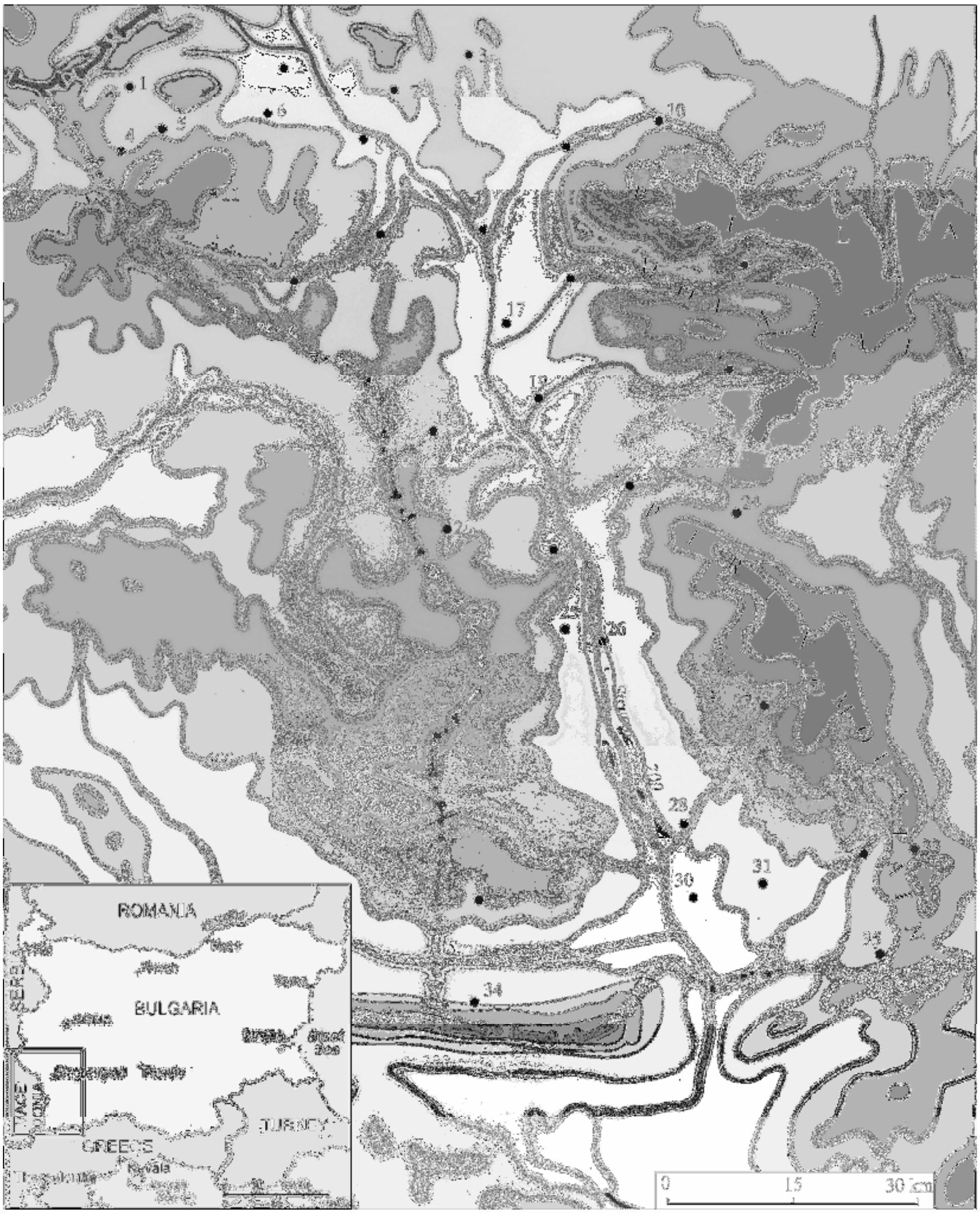

Fig. 1: Scheme of the position of the stations

3.2. Influence of the relief

The explored region is situated in the tributary zone of Struma River. This region is characterized with its mountain relief and big delevelling in the higher points. The highest point is Vihren peak in Pirin Mountain (2914 m)(fig.1). The Valley of Struma River limits the mountains from the Osogovo- Belasitsa mountain group on the East, and the mountains Rila, Pirin and Slavyanka on the West. The altitude of the river bed is lowering from 480m near Village Nikolichevtsi to 65 m near village Kulata. The influence of the orography has an effect in the big differences of the distribution of the rainfalls. The direction of the main mountains and the valley of the Struma River that is situated between them is interesting. According to [11], because of this reason, the air flows coming from the Western part of the horizon moisten the western slopes of the mountains, and the eastern slopes remain on rainfall shade and there the moisture is significantly lower. But this basic rule has significant changes on the region's territory. For example Berovo station (Macedonia) is situated in the upper Bregalnitsa River, on 824m altitude in the western end of the Maleshevska Mountain. Although its significant altitude it has annual falls of 647 mm, and Delchevo station (580 m altitude) has 541 mm rainfalls [8]. According to newer data 1971-2000 year, [3] the eastern regions of Macedonia has rainfalls as follows- Kriva palanka: 603mm, Berovo: 586.3mm. These values are comparable total annual falls on Logodazh station (700m altitude): 572.7mm, Kyustendil (518m): 616.5mm and Breznitsa (400m altitude): 841.3mm. The rainfall quantities in the deep valleys of the left inflows of Struma river from Rila and Pirin mountains are relatively small. Station Rilski Manastir (1147 m altitude) situated in the valley of the Rilska River has middle year round rainfalls of some 912.2mm, Dobro pole Station (1209 m) from the Blagoevgradska Bistritsa River has 800.4mm, and Popina laka station (1150 m) from Sandanska Bistritsa River has 803.5mm rainfalls. Because of lack of higher situated stations, as well as stations situated on the slopes, it is not possible to be given a quantity characteristic of the rainfalls in the higher parts of the mountains.

The local increase of the winter rainfalls on the northern slopes and in the foot of Belasitsa-Klyuch station (500 m alt.) is of interest. Such an increase of the winter rainfalls is observed also in the East Rodopa mountain- the northern foot of the Tsigansko Gradishte and Gyumyurdzhinski Snezhnik and in Strandzha Mountain [14]. The reason for that is in the paths of the Mediterranean cyclones - on the south of the country when combined with high pressure that is spreading over the country from north to north-west. On this situation the slopes with northern or northeastern exposition are a barrier for the cold air and the water vapor within it condense by orographic reasons. To the rainfalls of the hot front are also added orographic rainfalls in the cold air, so that the total sum is pretty high [14].

A great diversity in the distribution of the rainfalls is added from the fact that stations situated next to each other have significant differences in the annual amount of the rainfalls (for instance the stations Klyuch and Dolene, Kresna and Breznitsa (tab. 2), (tab. 3). Of great importance are also the features of the relief forms. The least amount of rain has in the kettles middle for the region of 588 mm, increasing to the mountain foots and in the river valleys. From north to south the sum of the rainfalls is almost unchanged, but when altitude is declining from 800-850 m to 150-200 m.

Tab. 2: Seasonal distribution of the rainfalls (in %)

№	Station	Altitude,m	**Cc***	Winter	Spring	Summer	Autumn	**Sum, mm**
1	Dolno selo	770	**1,22**	20,9	27,7	27,2	24,2	**613,6**
2	Nikolichevtsi	482	**1,12**	22,9	26,7	26,1	24,3	**597,5**
3	Bobov dol	640	**1,22**	20,4	28,8	26,1	24,6	**621,8**
4	Gyueshevo	944	**1,18**	22,7	28,3	25,7	23,3	**725,4**
5	Garlyano	998	**1,05**	25,3	28,5	22,7	23,5	**834,9**
6	Kyustendil	518	**1,11**	23,1	27,4	25,2	24,2	**616,5**
7	Tavalichevo	642	**1,18**	22,3	28,8	25,4	23,5	**610,6**
8	Nevestino	440	**1,07**	22,4	26,4	25,3	25,9	**553,5**
9	Dupnitsa	518	**1,23**	20,2	27,5	27,7	24,7	**604,8**
10	Sapareva banya	725	**1,42**	19,6	29,8	28,9	21,7	**715,3**
11	Osogovo hut	1640	**1,02**	24,9	26,9	23,7	24,5	**1016,7**
12	Rakovo	780	**1,02**	23,8	27,1	23,4	25,8	**725,4**
13	Vaksevo	554	**1,06**	24,1	28,0	23,4	24,5	**660,9**
14	Boboshevo	400	**1,12**	22,7	28,6	24,3	24,4	**577,7**
15	Rila	470	**1,07**	22,6	27,0	24,6	25,8	**598,2**
16	Рила monastery	1147	**1,16**	22,5	27,8	26,0	23,7	**912,2**
17	Kocherinovo	405	**1,03**	24,1	27,6	23,0	25,3	**543,2**
18	Logodazh	700	**1,11**	22,5	26,9	25,8	24,7	**572,7**
19	Blagoevgrad	410	**1,08**	22,8	27,0	24,8	25,4	**581,3**
20	Dobro pole	1209	**1,14**	22,0	26,8	26,5	24,7	**800,4**
21	Suhostrel	890	**1,07**	24,2	27,4	24,4	24,1	**779,1**
22	Krupnik	350	**0,90**	28,5	25,0	22,4	24,1	**651,8**
23	Gradevo	446	**0,95**	25,5	26,0	22,7	25,7	**755,7**
24	Predel	1142	**0,91**	26,8	25,9	21,7	25,6	**828,2**
25	Breznitsa	400	**0,78**	28,7	24,6	19,2	27,6	**841,3**
26	Kresna	180	**0,88**	26,8	25,8	20,9	26,5	**522,1**
27	Popina laka	1150	**0,94**	25,9	25,9	22,6	25,6	**803,5**
28	Sandanski	191	**0,88**	25,6	26,2	20,7	27,4	**531,1**
29	Dolene	720	**1,07**	22,4	29,9	21,8	25,9	**603,5**
30	Levunovo	145	**0,82**	26,3	26,2	18,9	28,5	**491,6**
31	Melnik	382	**0,93**	25,9	27,9	20,4	25,8	**549,1**
32	Pirin	753	**0,90**	26,9	25,8	21,7	25,7	**792,2**
33	Papazchair	1400	**0,93**	25,4	25,8	22,4	264	**946,7**
34	Klyuch	500	**0,62**	34,7	23,7	14,7	26,9	**1077,7**
35	Goleshovo	760	**0,88**	28,4	27,2	19,6	24,8	**811,2**

* Coefficient (index) of continent

Tab. 3: Middle month and year sum of the rainfalls

№	**Station**	I	II	III	IV	V	VI	VII	VIII	IX	X	XI	XII	**Sum**
1	Dolno selo*	45,5	*39,0***	42,7	46,2	**81,2****	76,7	49,8	40,5	40,7	50,8	56,9	43,6	**613,6**
2	Nikolichevtsi	45,4	40,3	44,0	45,2	**70,5**	66,0	51,6	*38,3*	39,3	49,0	56,8	51,1	**597,5**
3	Bobov dol	46,1	36,8	42,1	55,3	**81,9**	80,2	46,2	*35,8*	40,1	52,2	60,9	44,2	**621,8**
4	Gyueshevo	56,5	53,4	54,3	62,4	**88,8**	81,3	61,5	*43,6*	44,2	57,9	66,7	54,8	**725,4**
5	Garlyano	68,9	65,9	70,2	70,6	**96,8**	83,8	61,6	*44,2*	45,2	71,2	80,0	76,5	**834,9**
6	Kyustendil	47,8	45,9	47,7	49,0	**72,3**	65,8	54,2	*35,4*	38,9	50,4	60,2	48,9	**616,5**
7	Tavalichevo*	50,1	41,8	48,2	52,2	**75,6**	67,8	44,5	42,7	*32,5*	51,0	60,1	44,1	**610,6**
8	Nevestino*	42,9	37,4	38,2	44,6	**63,5**	60,1	44,2	35,9	*35,5*	49,1	58,5	43,6	**553,5**
9	Dupnitsa	41,0	38,3	*35,9*	57,0	73,2	**81,0**	46,8	39,7	39,0	48,9	61,4	42,6	**604,8**
10	Sapareva banya*	46,3	*44,0*	45,8	67,2	**99,9**	88,5	69,5	48,7	44,1	49,1	62,1	50,1	**715,3**
11	Osogovo *	93,0	77,2	76,2	83,2	**114,5**	107,8	75,9	*56,9*	58,0	87,6	103,9	82,5	**1016,7**
12	Rakovo*	55,6	55,7	52,9	58,9	**84,9**	75,4	52,4	*41,6*	41,8	67,0	78,0	61,2	**725,4**
13	Vaksevo	55,5	49,2	51,1	60,1	**73,6**	71,3	48,4	*34,9*	37,5	55,2	69,4	54,7	**660,9**
14	Boboshevo	43,6	41,6	41,9	57,5	66,0	**66,3**	41,2	*32,9*	33,9	45,5	61,6	45,7	**577,7**
15	Rila	43,4	40,4	42,4	52,9	66,1	**68,0**	40,3	*39,0*	40,2	50,5	63,4	51,6	**598,2**
16	Ril.manastir*	67,9	62,3	53,3	82,9	**117,0**	108,6	73,8	55,1	*52,8*	68,1	95,6	74,8	**912,2**
17	Kocherinovo	43,4	39,3	41,6	48,1	**60,4**	54,7	38,0	*32,2*	34,2	44,0	59,1	48,2	**543,2**
18	Logodazh*	44,0	40,3	42,3	44,7	**66,9**	62,8	50,3	*34,9*	35,6	49,5	56,6	44,8	**572,7**
19	Blagoevgrad	44,6	41,1	42,2	48,8	**66,2**	65,4	45,0	*33,7*	37,7	46,3	63,6	46,7	**581,3**
20	Dobro pole*	56,9	*51,0*	56,5	65,7	**92,4**	89,4	67,5	55,3	56,7	64,0	76,9	68,1	**800,4**
21	Suhostrel*	65,3	60,9	63,8	61,4	**88,2**	81,8	59,2	49,0	*47,6*	62,1	77,8	62,0	**779,1**
22	Krupnik	66,4	58,5	47,9	50,9	64,2	62,2	51,1	*32,4*	35,4	52,2	**69,8**	60,8	**651,8**
23	Gradevo	67,2	55,5	53,6	63,0	80,2	74,9	52,4	*44,2*	50,0	57,9	**86,5**	70,3	**755,7**
24	Predela	75,4	61,8	59,1	62,9	**92,7**	78,3	57,0	*44,2*	54,8	74,9	82,2	84,9	**828,2**
25	Breznitsa*	82,9	72,8	68,4	61,6	76,7	70,6	54,5	*36,1*	46,8	80,1	**105,0**	85,8	**841,3**
26	Kresna*	43,3	44,8	42,9	40,2	51,7	50,1	34,0	*25,0*	29,6	43,5	**65,0**	52,0	**522,1**
27	Popina laka*	76,3	61,4	63,3	64,2	80,7	80,0	59,6	*41,8*	47,5	67,0	**91,3**	70,4	**803,5**
28	Sandanski	47,1	40,8	43,4	42,0	53,7	49,1	32,7	*28,4*	31,3	49,6	**64,7**	48,3	**531,1**
29	Dolene*	41,8	45,9	46,6	53,0	**80,6**	57,7	40,7	*33,1*	39,9	54,0	62,7	47,5	**603,5**
30	Levunovo	43,1	39,6	38,4	39,1	51,5	43,5	26,4	*23,2*	30,9	48,3	**60,9**	46,7	**491,6**
31	Melnik	47,3	41,4	43,4	45,7	**64,0**	50,6	33,8	*27,8*	32,8	50,8	58,1	53,4	**549,1**
32	Pirin*	59,4	62,2	54,5	63,6	86,4	80,2	54,6	*36,9*	51,4	70,5	81,3	**91,2**	**792,2**
33	Papazchair*	84,9	72,3	60,4	80,3	**103,6**	90,0	67,4	*54,6*	54,7	93,8	101,0	83,7	**946,7**
34	Klyuch*	**138,0**	109,3	88,6	78,2	88,9	75,2	52,6	*30,8*	61,1	94,7	133,6	126,7	**1077,7**
35	Goleshovo*	80,7	63,0	68,9	67,4	84,1	72,9	50,6	*35,1*	46,5	73,4	81,6	**87,0**	**811,2**

* The stations are with shorter period of observation;

** The months with minimal and maximal rainfalls are marked

In the Kamenishka and Bobovdolska kettles the rainfalls are 600-650 mm, in the Kyustendilska kettle, along the Dzherman river, Boboshevsko-Kocherinovsko and Blagoevgradsko distensions the sum of the rainfalls is 550-600 mm. In the Simitliiska kettle the rainfalls are about 650 mm, and in the region of Sandanski and Petrich-500-550 mm. In the barrier like parts of the mountains the rainfalls are increasing and reach some

800-1000 mm. An interest represents the local increasing of the rainfalls in the northern foot of the Belasitsa Mountain.

4. DISTRIBUTION OF THE RAINFALLS

In the studied region is concluded that with the increasing of the altitude above the sea level is also increased the amount of the rainfalls. But this is irregular increasing on the different slopes and in the different kettles. If we separate the stations according to the shape of the ground that they are located on, then it is concluded that the stations situated in the kettles has middle year rainfalls of 588 mm. Follow the stations situated near the mountain slopes, mostly on the periphery of the kettles (743 mm), stations situated in the deep river valleys- 762 mm, and the mountain slopes and ridges have over 800 mm. Only in two stations-Osogovo and Klyuch the annual sum of the rainfalls passes 1000 mm. But while the first one is situated on a mountain slope on 1640 m altitude, the second station is from the small number of stations in the country with rainfall quantity over 1000 mm when the altitude is 500 m.

4.1. Seasonal distribution of the rainfalls

The seasonal distribution of the rainfalls is determined mainly by the peculiarities of the atmospheric circulation (tab. 2).

The winter rainfalls are less in the northern part of the area-20-23%, and there that is the driest season. On south the quantity of these rainfalls increases (25-29%) and for several stations winter is the most humid season. The reason for that is that the passing Mediterranean cyclones affect mostly the southern parts of the area. The rainfalls are occurring mostly on hot air fronts. They are moving over the country mostly from south-west to north-east. In that movement on the north the rainfalls and the total winter sum reduce its values. Klyuch station is typical with its great values of winter rainfalls.

For the greatest part of the region (25 stations) the spring is the most humid season. The participation of the spring rainfalls in the total annual rainfall balance shows relative uniform distribution in territorial aspect. In the northern part it is between 26 and 30% and on the south it reduces significantly – 24-25 %.

On the north the main rainfalls come with winds from north-west, when the passing of Atlantic cyclones increase its frequency, and along with it is also increasing the anticyclonic circulation from north-west. As a result the sum of the rainfalls is high and it is increased with over 50 mm in comparison with the winter on certain places.

During the summer the rainfalls reduce, especially noticeable in the southern half of the region, where that is the driest season. In the most northeastern and north-eastern regions the relative participation of the summer rainfalls is 27-29 % and on the south 19-23 %. Exception again is the Klyuch station with some 15 %. In the beginning of the summer the rushing of humid and cold ocean air to the temperate latitudes continues. That is mainly happening because of the faster moving cold fronts from west and north-west in the beginning part of the Azores maximum. The rains are short but intense.

To the end of the summer the cyclonic circulation reduces in difference of the anticyclonic that is realized by the moving to south-east anticyclones, and also by distribution of Azores anticyclones to east.

In the beginning of the autumn the atmosphere circulation is low, and as a result the rushes from the Atlantic Ocean are rare. Significance for the rainfall balance have the Mediterranean cyclones, especially during late autumn. For the major part of the region the rainfalls are relatively low – 22-25 % from the annual sum. On the south they are more significant and for the stations Levunovo, Sandanski, and Papazchair the fall is the most humid season.

By the indication coefficient (index) of continent (Cc) (tab. 2) it is possible to determine what influence is predominant – the Mediterranean or the temperate-continental. This index is indicating the proportion between the rainfalls during the spring-summer months (March-September) and the fall-winter months (October February) [14].

On the north Cc has values of 1.05 – 1.20 and the increasing is not only to the northern but also to the eastern direction.

In the middle part of the region between the Skrinski defile and Kresnenski defile Cc is either the 0.90 – 1.12, that corresponds clearly to the transition character of the regime of the rainfalls.

Southward from the Kresnensko defile this coefficient lowers, it drops under the value of one and with little exceptions (Breznitsa and Klyuch) it stays with values over 0.78. Even more, such a southern situated station like Dolene (1.07) has a value over one and significantly equal seasonal rainfalls. The data received for Cc even for the most southern areas show that a typical Mediterranean humid regimen is not observed (for instance Malko Tarnovo station – Cc 0.53). The data received for Klyuch (0.62) must be accepted with a little reserves, because of the short period of observation and also because of possible errors in the reports.

4.2. Monthly distribution of the rainfalls

In the monthly distribution of the rainfalls it is observed some peculiarities (tab. 3).

May is the month with maximal rainfalls for the major part of the territory of the region. The rains autumn mainly when there is coming cold ocean air coming mostly (some 65 %) from west north-west. Under the influence of the orography and the strong warming of the earth air, is formed a large amount of rain clouds (Cb). On the front are occurring wave distributions the speed is slowing, and in the area of the gusts the rainfalls are especially abundant. Great importances for the total amount of rainfalls have the internal mass showers, formed in unsteady air layers, following the cold fronts. The value of the rainfall sum is 50-90 mm, and in the mountain stations is over 100 mm. In the northern parts of the area June has close values and in the stations Boboshevo, Dupnitsa and Rila it is the most humid month.

For the most southern areas of the studied region the maximum of the rainfalls is during November, and sometimes also in December (Pirin and Goleshovo), coinciding with the maximum in the frequency of the Mediterranean cyclones. Some stations make an exception having maximum during the May, including Klyuch station which rainfall maximum comes during January, but the difference with November is hardly 6 mm. Although that the rainfalls during November are greater than those during May the differences are not very great – on the average of 12 mm.

The middle values of the rainfalls in November are 60 – 100 mm.

A month with a minimal rainfall is August. The exceptions are mainly for the month of February (in Dupnitsa – during March) – in the northern part of the region, or September but with small differences with August. The minimum during August and September is explained with the setting on that time minimum in the distribution of the Mediterranean cyclones, and also with the insignificant for the season influence of the cold fronts of the Atlantics cyclones. But basically the rainfall sums of February and September against August are with close values _ on the stations with the minimum during February the difference is 1.5-5 mm, and on those with minimum during September 0.1-5 mm. This shows that in general for the area August is the driest month. The middle values of the rainfalls are in the average of 25 – 45 mm.

February is the month with relatively low values of the rainfalls. During this month it is observed a secondary minimum of the rainfalls. On the south stations this minimum is almost not manifested. Basically the values of the rainfalls are between 40 and 65 mm.

5. CONCLUSIONS

The total sum of the rainfalls and its territorial distribution is influenced in a great degree from the complex morphological relief of the territory. But the relief does not influence on their distribution through the year. This distribution is determined from the specialties of the atmosphere circulation.

With the increasing of the high the rainfalls are also increasing, without having any major changes in the months with maximal and minimal sums of the rainfalls. It is also observed a local increasing of the rainfalls on the northern foots of Belasitsa Mountain, that also confirmed by the data from the Klyuch station.

In the distribution of the rainfalls through the year the territorial differences are also considered. The stations situated on the north of Blagoevgrad have transitional humid regime, and in the most north-eastern parts of the Kyustendil region also have temperate continental regime. Here the maximum of the rainfalls comes in May and rarely in June, and the minimum – in August. The stations on south from the Kresnesko defile are characterized with a Mediterranean humid regime – the maximum in November and less in December and the minimum again in August.

The coefficient of the continental characteristics lowers from north (Sapareva banya station – 1.42; Dolno selo – 1.22) on south (Klyuch station – 0.62), and between the stations Boboshevo and Krupnik it is about 1 (1.1-0.9), that shows some transitional character in the regime of the rainfalls.

In proportion in the annual sums, the winter rainfalls are increasing from north to south, and the summer rainfalls are reducing in the same direction.

Basically the values of the minimal rainfalls is not showing big differences in the territory of the region -25-30mm in the lowlands, and up to 50-60mm in the mountain parts. The values of the maximal rainfalls are in wider range – from 60 to 140 mm.

6. REFERENCES

[1] Chang, H.,Knight, G., Staneva, M., Kostov, D. (2002). Water resource impacts of climate change in southwestern Bulgaria, GeoJournal57, 159-168.

[2] Dimitrov, D. and oth. (1977) Blagoevgradski okrag,Geografska harakteristika, “Narodna prosveta”, Sofia, (in Bulg.).

[3] Drenovski,I., Stamenkova, V. (2005) Opit za sravnitelna klimatichna harakteristika na Yugozapadna Bulgaria. In: Zbornik ot III kongres na geografite, Skopje, (in Bulg.).

[4] Klimata na Bulgaria (1991) Publishing House of the Bulgarian Academy of Sciences. Sofia, (in Bulg.).

[5] Iankov, V. (1982) Varhu statisticheskata struktura na poleto na mesechnia valezh v Balgarskata chast ot vodosbora na reka Struma , “Hydrology & Meteorology”, XXXII, 4, (35-40), (in Bulg.).

[6] Koleva, E. (1984) Razpredelenie na mesechnite sumi na valezhite, “Hidrology and meteorology”,2, Sofia, (in Bulg.)

[7] Koleva, E., Peneva, R. (1990). Klimatichen spravochnik. Valezhi v Bulgaria, BAN, Sofia, (in Bulg.)

[8] Mavrodiev, J. (1980), In: Malesh I Piyanets, II, Skopje,71-92, (in Maced.)

[9] Meteorologichni godishnitsi (1951-1980), (in Bulg.).
[10] Stefanov, St. (1961) Varhu nyakoi osobenosti na mesechniite I sezonni sumi na valezhite, “Hydrology & meteorology”, 2, Sofia, (in Bulg.)
[11] Tishkov, H., Kalajdzhiev, G. (1999) Rekreatsionni turisticheski resursi, “SWU N. Rilski”, Blagoevgrad, (in Bulg.).
[12] Toplijski, D. (2006) Klimat na Bulgaria, Sofia, (in Bulg.).
[13] Vekilska, B. (1992) Rakovodstvo po klimatologia, SU”Kl. Ohridski”, Sofia, (in Bulg.).
[14] Velev, St. (1990) Klimata na Bulgaria, “Narodna prosveta”, Sofia, (in Bulg.).
[15] Velev, St. (2006) Global climatic change and Bulgarian climate, Geography’21, 1(XLIX), 2, 4-9. (in Bulg.)

COMPARATIVE ANALYSIS OF RESULTS FROM PRELIMINARY CANDIDATE-STUDENT’S EXAMS IN GEOGRAPHY OF BULGARIA BY TEST IN SWU “NEOFIT RILSKI” – BLAGOEVGRAD IN 2006-2007

Ivan Drenovski, Nadezhda Nikolova,
Krasimir Stoyanov, Emiliya Patarchanova

SWU “Neofit Rilski” – Blagoevgrad, Bulgaria

Abstract*: An attempt for comparison between the results of preliminary candidate-student’s exams in Geography of Bulgaria by test, hold in SWU “Neofit Rilski” – Blagoevgrad in 2006 and 2007 is made in the paper. A possible influence of some little changes in structure of the quiz, number and composition of questions is pointed out. Almost identical average results are obtained by candidate-students. Insufficient training and poor spatial orientation are established.*

Keywords: *preliminary candidate-student’s exams, marks, grades, test, quiz*

INTRODUCTION

For the second time after 2006, in May 2007 preliminary candidate-student’s exam in Geography of Bulgaria by test was hold in SWU “Neofit Rilski” – Blagoevgrad. In comparison with the previous year, a little bit easier quiz as a random combination of questions was drawn. In addition the total number of questions was reduced from 35 to 33. One open type and one cartographic question were removed. The structure of the quiz (28 closed, 3 open type and 2 cartographic questions) was slightly modified. The proportion of weights between different groups of questions was saved. The maximum amount of points is 42, as 1/3 of them – 14 points are obtained for the right answers to open type and cartographic questions [Drenovski, et al., 2006].

ANALYSIS OF The RESULTS

These changes were reflected weakly on the average results of the candidate-students, successfully passed exam. This year an average grade is Good 3.87, but last year it was Good 3.80. Normally the percentage of weak marks this year is lower – 28.7% (39,6% - last year). Very likely this may be explained with the fact that the candidate-students are familiar with the form and the structure of the test, due to the model quizzes putted during the campaign on the web-site of the SWU.

These percentages between 29 and 39 % are absolutely real and normal for the preliminary candidate-student's exams. Specific success and proportion between grades is shown below in Tab. 1. and in Fig. 1.

Tab. 1. Comparison between results from preliminary candidate-student's exams by test - 2006 and 2007 year

Marks:		2,00	3,00-3,49	3,50-3,99	4,00-4,49	4,50 - 4,99	5,00-5,49	5,50-6,00	Total:
2006	number	282	181	112	73	39	21	5	713
	percentage	39,6%	25,4%	15,7%	10,2%	5,5%	2,9%	0,7%	100,0%
2007	number	212	212	117	103	60	22	12	738
	percentage	28,7%	28,7%	15,8%	13,9%	8,1%	3,0%	1,6%	100,0%

The analysis of results shows, that the satisfactory and good marks are most common in the both years, as their sum is more than a half of the all grades - 51,9% in 2006 and 58,4% in 2007. The satisfactory marks (3,00-3,49) are 25,4% (2006) and 28,7% (2007), and the good ones (3,50-4,49) respectively 25,9% и 29,7%. The very good marks (4,50-5,49) are accordingly 8,4 % and 11,1%, but the excellent ones – only just 0,7% and 1,6%. All this proves that the form and content of test guarantee real selection and classifying of candidates, depending on their knowledge, but not on the grades from school-leaving certificate.

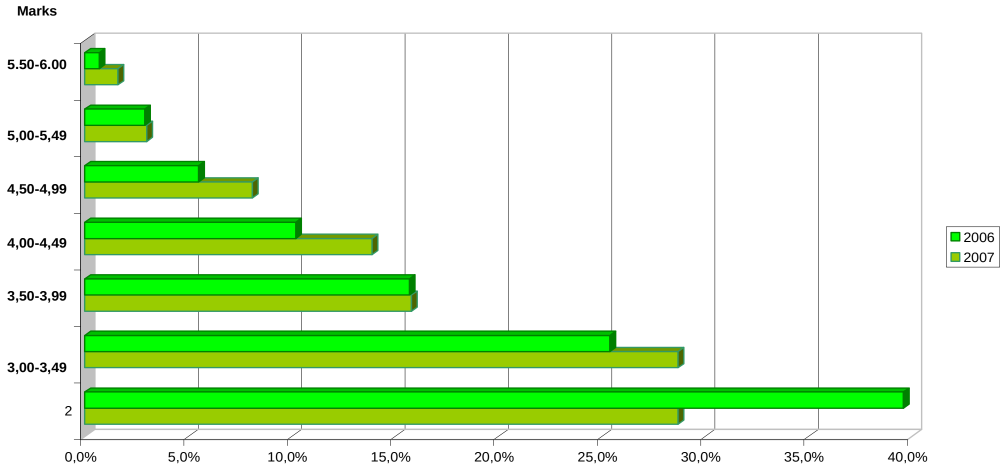

Fig. 1. Comparison between achieved examination marks (in percentage) from preliminary candidate-student exams by test - 2006 and 2007 year

The significant number of poor marks probably is due to the fact, that a large part of candidate-students sit for exam without any training in advance and rely only on their general knowledge to pass quiz. Obviously, in a number of cases, they try to guess the right answers of closed type questions. Mostly poor marks have candidates, answered only these questions. In addition in answers to the test in 2007 some common mistakes are met. For instance, a good half of candidate-students are point that the part of installed capacity in energetics is the biggest in nuclear, but not in steam-power plants, as it really is. Most likely this is due to the media fuss about nuclear power in Bulgarian society and politics. To many candidate-students don't know on which river particular reservoir is situated, for example, that dam lake “Ivailovgrad” is on Arda, but not on Maritsa river. They find it difficult to point where some reserves are located. Amazingly a lot of them don’t remember that the first Bulgarian reserve – “Silkosia” is in Strandzha. A very few of candidates know, that leading branch of national economy till 1944 was agriculture.

The biggest embarrassment candidate-students feel on answers of open type questions, where brief written answer is required. They should demonstrate intellectual capacities for generalization, reasoning and ratiocination. Most of them didn’t write at all, but the others didn’t get in questions, as a whole. For instance on a question for characterization of relief as a climate generating factor predominant part of answers are relating to general characterization of relief and particular hypsometric belts, or of climate and different climatic regions.

Owing to cartographic questions a great gaps in candidate-student’s spatial orientation are revealed. Most of them cannot get through the question about location and the type of ores and minerals, marked with the respective symbol. With regard of administrative division of the country the situation is much better, but nevertheless the mean level of orientation on the map is unsatisfactory.

CONCLUSIONS

New moment in composition of quizzes in 2007 is the choice of partially overlapping with the closed, cartographic and open type questions. The goal is to check up the level of concentration of candidates and their ability to make connection answering the questions. Unfortunately most of candidates didn’t make it.

REFERENCES

[1] Bizhkov, G. (1992) Theory and methodic of didactical quizzes, Sofia
[2] Drenovski, Iv., Patarchanova, Em., Stoyanov, K., Nikolova, N. (2006), Test On Geography Of Bulgaria As Preliminary Candidate-Student Exam In South-West University In Blagoevgrad. GEOGRAPHY' 21 - scientific-methodological magazine ISSN - 1312-6628, v.5, pp. 18-25, http://www.geography.iit.bas.bg/
[3] Radev, P., Alexandrova, Al., (2003) Didactical testology, Plovdiv

USING GIS OF SOIL RESOURCES IN DEVELOPING THE SIMULATION MODEL FOR ENVIRONMENT CONDITIONS MONITORING AND AGRICULTURAL PRODUCTION MANAGEMENT

Boyko Kolev, Penka Kastreva

*Associated Professor Boyko Kolev, Ph.D., South-West University of Blagoevgrad,
Geography, Ecology and Environment Protection Department, 66 "Ivan Mihailov" Str.,
2700 Blagoevgrad, Bulgaria
Associated Professor Penka Kastreva,, Ph.D., South-West University of Blagoevgrad,
Geography, Ecology and Environment Protection Department, 66 "Ivan Mihailov" Str.,
2700 Blagoevgrad, Bulgaria*

Abstract: *The maximum yield from different agricultural crops is determined by climatic conditions, soil cultivations and type of agricultural land use, crops species and effective soil water content variations.*

The simulation procedure for soil hydro-physical properties determination was realized by using soil particle size distribution data only. This is a good start position for develop a calculation algorithm for soil water content dynamic monitoring. Kolev, 1994 [2] realized this for the first time for Bulgarian soils, with developed in his Ph.D. thesis universal model.

The meteorological conditions could be modeling by using a simulation model, which was also suggested by Kolev, 1994 [2} in his Ph.D. thesis.

For better using of these models it is necessary in GIS of soil resources soil physical and water properties should be included into the attributive table - Kolev et al., 2006 [4].

The main aims of the study are:

To demonstrate a simulation procedure for soil hydro-physical properties determination by using the created soil particle size distribution database only.

To demonstrate how useful is the developed model for monitoring environment conditions and agricultural production management.

Keywords: *environment conditions, simulation model, soil classification scheme, effective soil water content, particle size distribution, soil physical properties.*

1. INTRODUCTION

Soil management means to create rules and mechanisms, which are created from last reaching of soil science and information about soil cover for effective use of productive resources of agricultural lands and protect their ecological functions.

For operative of legal information about soil resources the Soil Resources Agency developed Geographic Information System (GIS) that is based of soil survey in scale 1:10000 and together with constant land use and separation.

In GIS input an information as follow: soil cover, soil type, particle size distribution, depth of hard roc, salt and carbonate content, mean soil bonitet and soil category for non irrigated areas and bonited for 22 agricultural crops, slope and exposition of the areas, type and quantity of pollution est. This information make possible for optimal use of soil resources for crop production and to find technology for protection of their ecological functions (erosion, acidification, contamination, salinity, bogginess est.). GIS of Soil Resources (GISoSR) is open systems that allow including additional parameters by meaning of more detail agricultural lands description and make their management more effective during all cycle of agricultural production (Michalev et al., 2002 [5]).

The aim of this article is to estimate a method suggested by Kolev, 1994 [2]. The using of this method gives some possibilities for calculating of some physical and hydro-physical properties of given soil (Keulen & Wolf, 1986 [1]). When this soil parameters will be included in GIS of Soil Resources (GISoSR) we have better possibilities monitoring and management of crop production and realization of sustainable development in agriculture.

The following research considers the described physical and hydrophysical properties for two different soil types- Leached cinnamonic forest, heavy loamy to slightly clayey and Deluvial and deluvial-meadow, sandy and loamy, mainly stony for the region of the Razlog valley, as well as two different soil types- Alluvial and Alluvial-Meadow soils and Deluvial and Deluvial-meadow, sandy and loamy, mainly stony for the region of the Samokov valley. At the same time are estimated the possibilities offered by GISoSR for achieving a modern level of education for the “Soil Science”, **“** Soil cover in Bulgaria” and “ Pollution Aspects and Soil protection” students.

2. OBJECTS AND METHODS

The Razlog Valley is situated in the Region of Blagoevgrad around 60 km from Blagoevgrad. It is surrounded by the three largest mountains in the country - Rila, Pirin and Rodopi Mountain and has an elevation of 800m. The ground water table is near soil surface. The soils are cinnamonic forest and brown forest soils and are not fertile. In the valley of the Mesta river and its feeders can be described some regions with the more generous alluvial and alluvial meadow soils. This paper makes a study of only two of the typical for the region soil types - Leached cinnamonic forest, heavy loamy to slightly clayey and Deluvial and deluvial-meadow, sandy and loamy, mainly stony soils.

The Samokov area is situated around 60 km from Sofia. It is surrounded by the three mountains - Rila, Plana and Sredna Gora Mountains and has an elevation from 630 to 1400 m. The soils are cinnamonic forest and brown forest soils and are not fertile. At the foot of the mountain Deluvial and Deluvial-Meadow soils are presented. In the valley of the Iskar river and its feeders can be described some regions with the more generous Alluvial and Alluvial-Meadow soils. This paper is concentrated on two of the typical for the region soil types - Alluvial and Alluvial-Meadow and Deluvial and Deluvial-Meadow soils.

The climate is moderate continental. The mean annual air temperature is between 7-8 ºC and it going down to about 6 ºC for the places with evaluation above 1000 m. The sum of air temperature is about 2300 ºC with very high fluctuation. The temperature conditions are suitable for potato, flax, meadow and pastures.

The mean agronomic soil bonitet is about 43, which associated these soils with bonited group medium lands. It is varying form bonitet 3 for Soya bean (uselessness lands) to bonitet 65-69 for potato (useful lands) and bonitet 48 for winter wheat (medium lands).

The method offered by Kolev converts the Russian classification of the soils by their particle size distribution, which was used in Bulgaria, into their USDA classification. Here is used the integral curved line of the particle size distribution and the approximation is calculated after the regression model. This is shown in Kolev et al, 1996 [4] where also is calculated the hydrophysical properties of the soils. The same approach is also used for the determination of the hydraulic conductivity (*k*).

The effective soil water content $\boldsymbol{T_{pwc}}$ (m^3/ha^3), which have an important meaning for the regulation of the water amount in the soils, is determined by:

$$T_{pwc} = 100 * h * \alpha * (\mathrm{SM}_{\mathrm{fc}} - SM_w) \tag{1}$$

where:
α is the soil bulk density (g/cm^3)
h is the soil depth (m)
$\boldsymbol{SM_{fc}}$ **-** water content at field capacity (%)
$\boldsymbol{SM_w}$ - water content at permanent wilting point (%)

3. RESULTS AND DISCUSSION

The General view of the objects is shown on Fig. 1 and Fig. 2. Different soils are presented on Fig. 3. Fig. 4 show the water and hydro-physical properties, which here are already included in the attribute table of Samokov soils in GIS. The effective water resources Tpwc (m^3/ha^3) by (1) is calculated with GIS software ArcView 3.3 (function Calculate) - Fig. 5.

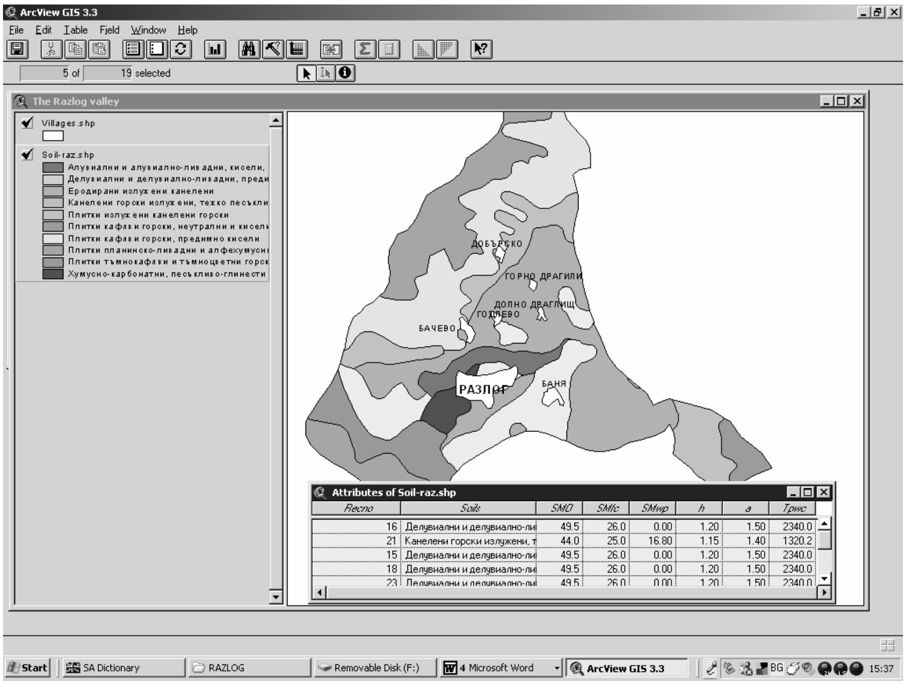

Recno	Soils	SMO	SMfc	SMwp	h	a	Tpwc
16	Делувиални и делувиално-ли	49.5	26.0	0.00	1.20	1.50	2340.0
21	Канелени горски излужени, т	44.0	25.0	16.80	1.15	1.40	1320.2
15	Делувиални и делувиално-ли	49.5	26.0	0.00	1.20	1.50	2340.0
18	Делувиални и делувиално-ли	49.5	26.0	0.00	1.20	1.50	2340.0
23	Делувиални и делувиално-ли	49.5	26.0	0.00	1.20	1.50	2340.0

Fig. 1: General view of the object Razlog.

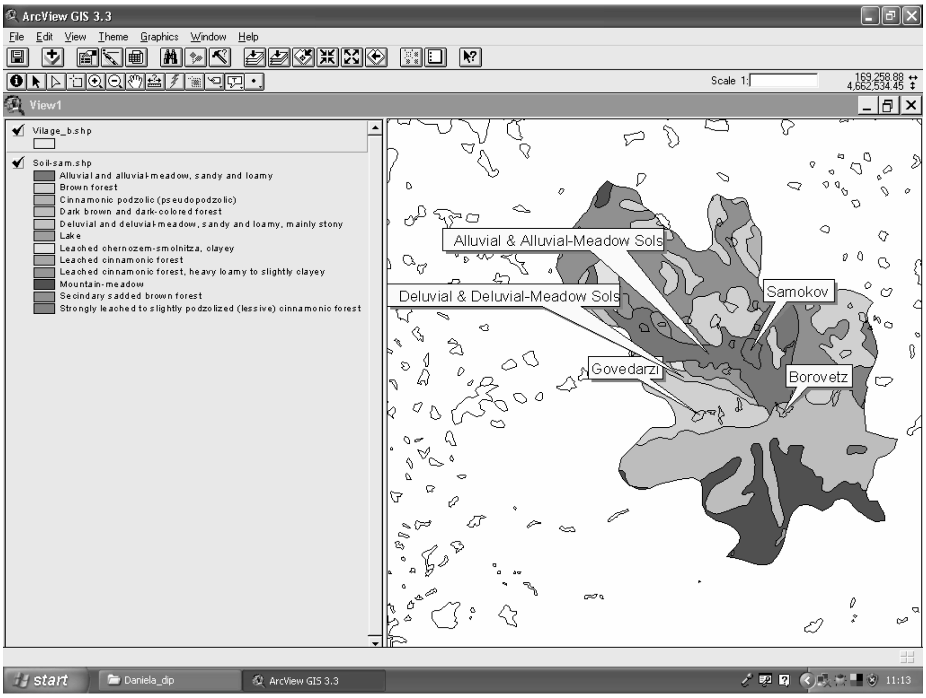

☑ Vilage_b.shp

☑ Soil-sam.shp

- Alluvial and alluvial-meadow, sandy and loamy
- Brown forest
- Cinnamonic podzolic (pseudopodzolic)
- Dark brown and dark-colored forest
- Deluvial and deluvial-meadow, sandy and loamy, mainly stony
- Lake
- Leached chernozem-smolnitza, clayey
- Leached cinnamonic forest
- Leached cinnamonic forest, heavy loamy to slightly clayey
- Mountain-meadow
- Secindary sadded brown forest
- Strongly leached to slightly podzolized (lessive) cinnamonic forest

Fig. 2: General view of the object Samokov.

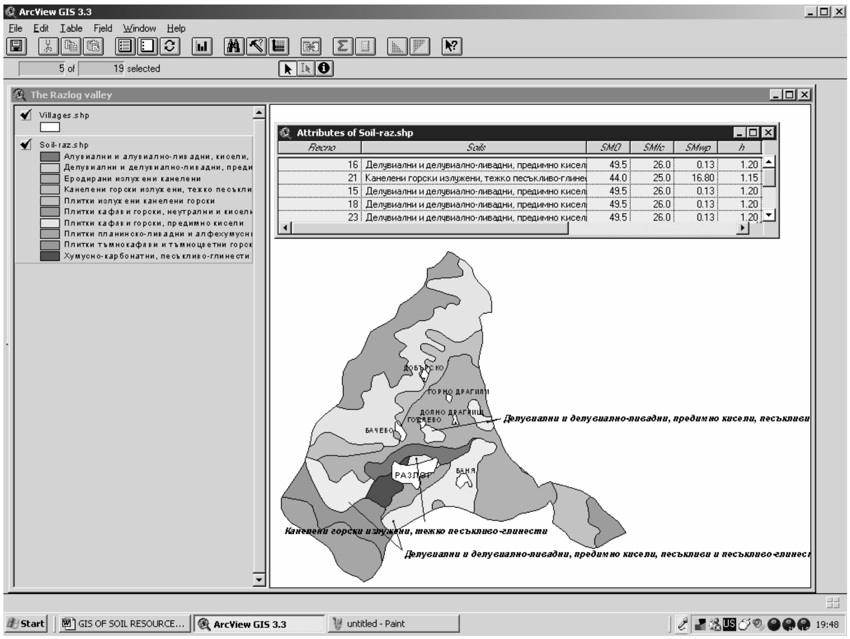

5 of 19 selected

☑ Villages.shp

☑ Soil-raz.shp

- Алувиални и алувиално-ливадни, кисели,
- Делувиални и делувиално-ливадни, преди
- Еродирани излужени канелени
- Канелени горски излужени, тежко песъкли
- Плитки излужени канелени горски
- Плитки кафяви горски, неутрални и кисел
- Плитки кафяви горски, предимно кисели
- Плитки планинско-ливадни и алфехумусн
- Плитки тъмнокафяви и тъмноцветни горск
- Хумусно-карбонатни, песъкливо-глинести

Attributes of Soil-raz.shp

Recno	Soils	SMO	SMfc	SMwp	h
16	Делувиални и делувиално-ливадни, предимно кисел	49.5	26.0	0.13	1.20
21	Канелени горски излужени, тежко песъкливо-глине	44.0	25.0	16.80	1.15
15	Делувиални и делувиално-ливадни, предимно кисел	49.5	26.0	0.13	1.20
18	Делувиални и делувиално-ливадни, предимно кисел	49.5	26.0	0.13	1.20
23	Делувиални и делувиално-ливадни, предимно кисел	49.5	26.0	0.13	1.20

Fig. 3: The Razlog soils.

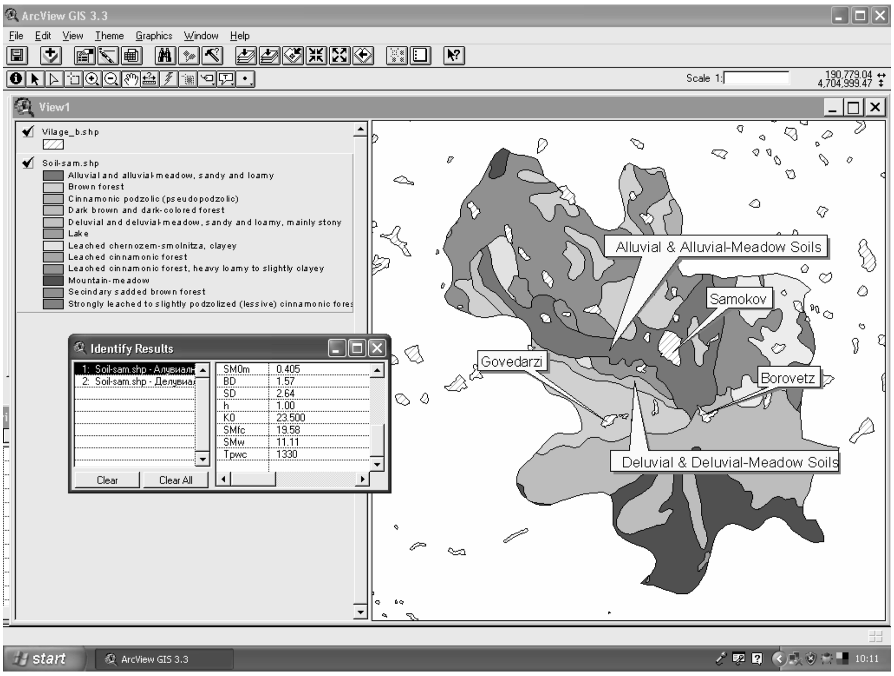

☑ Vilage_b.shp

☑ Soil-sam.shp
- Alluvial and alluvial-meadow, sandy and loamy
- Brown forest
- Cinnamonic podzolic (pseudopodzolic)
- Dark brown and dark-colored forest
- Deluvial and deluvial-meadow, sandy and loamy, mainly stony
- Lake
- Leached chernozem-smolnitza, clayey
- Leached cinnamonic forest
- Leached cinnamonic forest, heavy loamy to slightly clayey
- Mountain-meadow
- Secindary sadded brown forest
- Strongly leached to slightly podzolized (lessive) cinnamonic fores

1: Soil-sam.shp - Алувиалн
2: Soil-sam.shp - Делувиал

SM0m	0.405
BD	1.57
SD	2.64
h	1.00
K0	23.500
SMfc	19.58
SMw	11.11
Tpwc	1330

Fig. 4: Adding of SMO, SMfc, SMwp, KO, BD, SD and Tpwc into the attrubute table for the two Samokov soils.

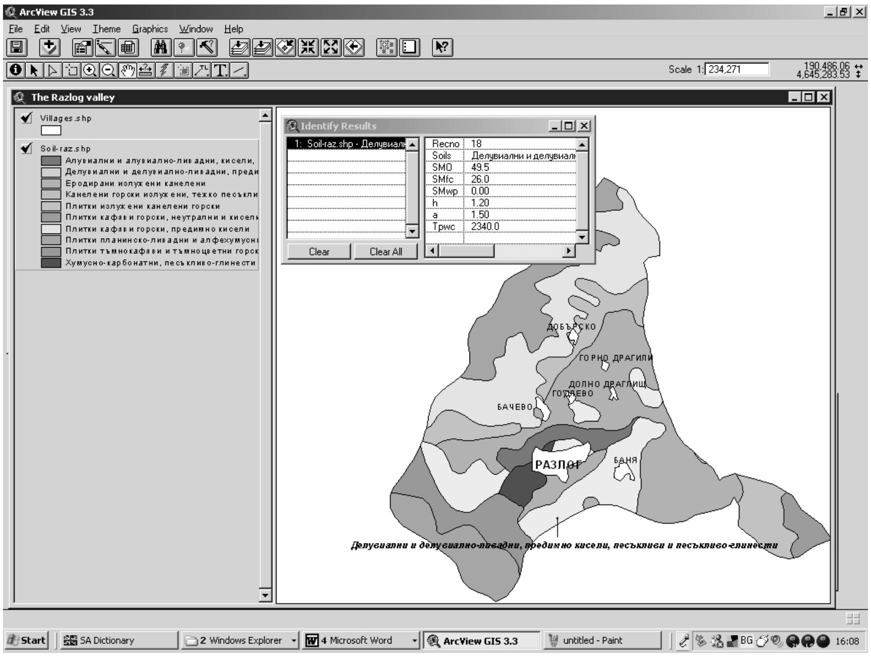

☑ Villages.shp

☑ Soil-raz.shp
- Алувиални и алувиално-ливадни, кисели,
- Делувиални и делувиално-ливадни, преди
- Еродирани излужени канелени
- Канелени горски излужени, тежко песъкли
- Плитки излужени канелени горски
- Плитки кафяви горски, неутрални и кисели
- Плитки кафяви горски, предимно кисели
- Плитки планинско-ливадни и алфехумусни
- Плитки тъмнокафяви и тъмноцветни горск
- Хумусно-карбонатни, песъкливо-глинести

1: Soil-raz.shp - Делувиалн

Recno	18
Soils	Делувиални и делувиалн
SMO	49.5
SMfc	26.0
SMwp	0.00
h	1.20
a	1.50
Tpwc	2340.0

Делувиални и делувиално-ливадни, предимно кисели, песъкливи и песъкливо-глинести

Fig. 5: Final results for Razlog soils.

4. CONCLUSIONS

The approach suggested by Kolev, 1994 [1] for calculating SM_{fc}, SM_{wp} and T_{pwc} and the values of total porosity (*SM0*), gives more quality and quantity information of the studied soil.

It is obvious that GISoSR with that information will improve there information using.

Of course such kind of study should continue with other Bulgarian soil types.

5. ACKNOWLEDGEMENTS

The authors thank to Damjan Mihalev, Dimitar Jivkov and Nevena Miteva from SRA – Sofia for their cooperation in realization of this scientific study.

6. REFERENCES

[1] Keulen, H., Wolf J., (Eds.), 1986, Modelling of Agricultural Production: Weather, Soils and Crops, Simulation Monographs, Wageningen, pp. 80-86.

[2] Kolev B. 1994 Dissertation for scientific degree Sofia(p. 10-35).

[3] Kolev, B. et al., 2006. The Geographic Information System of Soil Resource Using for Sustainable Agriculture Realization In: International Conference on Cartography and GIS, January 25-28, 2006, Borovets, BULGARIA.

[4] Kolev, B., et al., 1996, Derivation of Soil Water Capacity Parameters from Standard Soil Texture Parameters for Bulgarian Soils, Ecological Modelling (84), N<u>o</u> 1-3, Elsevier, Amsterdam, Holland, pp. 315-319.

[5] Michalev D. et al., 2002, Purposes and Possibilities of the Soil Resources Geographic Information System in Bulgaria, In: Proceedings of International Workshop September 30 – October 3, 2001, Sofia, Bulgaria, GorexPress, pp. 140-142.

HOUSEHOLD WATER CONSERVATION ATTITUDES IN BLAGOEVGRAD

William Clark

Abstract: *Residential water conservation programs can play an important role in water management planning; yet, in spite of water shortages, such programs have rarely been implemented in Bulgaria. This paper examines the obstacles and opportunities for household water conservation in Blagoevgrad, Bulgaria. Key informant interviews, focus groups, and a questionnaire were employed in collecting data regarding attitudes toward water management and conservation in Blagoevgrad. Results indicate a general lack of knowledge among residents regarding water saving devices and practices. The local water company has not placed a high value on water conservation education. Nevertheless, most residents show positive attitudes toward water conservation and a readiness to adopt water saving practices.*

1. INTRODUCTION

When facing a water shortage, a community must either develop new water sources or reduce demand. Due to the political, economic and environmental barriers to developing new water sources, water suppliers are increasingly looking to conservation to reduce demand (EPA 1994; Alitchkov and Kostova 1996; Platt and Delforge 2001).

In spite of chronic water shortages, domestic water conservation programs have not been widely promoted or implemented in Bulgaria. A comprehensive water conservation program could help communities avoid restrictive water regimes and postpone or eliminate the need to construct more dams (e.g., Featherstone 1996; Platt and Delforge 2001). A successful water conservation program depends on educating and convincing water users to reduce the amount of water they use. Unfortunately, most citizens in Bulgaria have had little exposure to information concerning the need, benefits, and means of water conservation. This article investigates the opinions, knowledge, and attitudes of residents of Blagoevgrad, Bulgaria regarding local water resources and household water conservation.

Most of the city’s water supply comes from the upper reaches of the Bistritsa River and its tributaries. The city does not have a drinking water reservoir and only minimal storage capacity in the form of cisterns which help regulate water flow. As in much of the country, the snow pack is the primary determinant of river runoff (Vassilev 1996; Knight and Steneva 1996). A reduction in snow accumulation during the winter can lead to shortages during the summer and fall. Climatic factors have a large influence on the city’s water supply. Recent climate change research points to the likelihood of decreased winter snowfall and earlier spring melting of the snow pack in the mountains of southwestern Bulgaria in the coming decades (Chang et al. 2002). Water diversions, high losses from the water supply network, and lack of water conservation also contribute to shortages.

2. BACKGROUND AND CONTEXT

There is a dearth of research on public attitudes and perceptions of water resource management in Bulgaria. In the United States and other industrialized nations there have been numerous studies on water conservation attitudes and behaviors. “Public education about the benefits of water conservation is critical for raising customer awareness and generating community support for conservation” (EPA 1994, 2-1; c.f. Platt and Delforge 2001). Corral-Verdugo (2002) demonstrated that water conservation know-how among domestic water users in Mexico was an important factor in successful water conservation efforts. Numerous studies have examined the water savings potential of low-flow toilets, showerheads and faucet aerators. The European Environmental Agency (EEA 2002) indicates that water reductions of up to 50 percent might be achieved by adopting such water-saving devices.

Study Approach

We employed a three-phase, mixed-method approach (e.g., Tashakkori and Teddie 1998), including both qualitative and quantitative methods. The initial phase involved semi-structured interviews with 21 key-informants in Blagoevgrad. This was followed by five focus groups composed of Blagoevgrad residents. Interviews and focus groups were conducted during the last three months of 2003. Finally, a questionnaire was delivered to a random sample of 750 of the city's residents between 10 and 30 June 2004.

Findings

Interview and focus group participants were eager to talk about water issues. Major concerns included water quality, water availability, the poor condition of the water supply infrastructure, the city's need for a reservoir, and the management of local water resources. When asked, "How concerned are you that Blagoevgrad will face water shortages within the next five years?" (five-point scale from not at all concerned to very concerned), 80.8 percent indicated they were very concerned, and 12.1 percent indicated moderate concern. When presented with a list of factors potentially contributing to shortages of drinking water, participants indicated the most important was lack of a reservoir, followed by climatic factors (Tab. 1).

Tab. 1. Factors contributing to drinking water shortages in Blagoevgrad.

Survey question: Which of the following items do you feel is most important in contributing to water shortages in Blagoevgrad. (N = 698).

Factor	**most important**	
	%	**N**
Lack of a reservoir to store up the springtime water	30.0	209
Climatic factors (lack of rain and snow, high temperatures)	22.2	155
Leaks from the old pipes in the water supply system	14.9	104
Water being diverted from the local watershed to Sofia	14.0	98
Lack of information about how citizens can save water at home	9.0	63
Industries using drinking water instead of their own sources	5.3	37
Citizen's using drinking water to irrigate gardens	4.6	32

There is overwhelming support for construction of a drinking water reservoir for Blagoevgrad. Plans for the Rakochevica Dam have existed for many years, but no construction date has been set. The estimated cost of the project is 25 million Euro (World Bank 2005). In the 21 interviews and five focus groups, only two individuals voiced opposition to reservoir construction. On the questionnaire, 68.8 percent strongly agreed and another 15.6 percent mildly agreed that "Blagoevgrad needs a reservoir in order to avoid future water shortages." Overall, residents of Blagoevgrad recognize the potential for serious water shortages and the general response has been to focus on developing new sources rather than reducing demand. This is the position of both the general populace and the local water supplier. One water company official stated that it is the water company's job to sell water, not to discourage its use.

The water company in Blagoevgrad has made little effort to educate its subscribers regarding water conservation. On the questionnaire, 79.8 percent strongly agreed and another 13.6 percent mildly agreed with the statement, "The ViK should provide customers with more information about ways of reducing water consumption".

The vast majority of study participants had a positive attitude toward water conservation. For example, 87.6 percent strongly agreed with the questionnaire statement, "I believe it is important to conserve water" with another 9.4 mildly agreeing. Motivations for water conservation can serve as important predictors of adoption of water saving behaviors (Corral-Vergugo et al. 2003). When asked about motivations for reducing water consumption, 52.8 percent of those surveyed cited avoiding a water regime as most important; 20.9 percent indicated concern for the environment, 16.3 percent stated civic responsibility, and 10 percent indicated saving money. Corral-Verdugo (2002) cites protecting the resource, cooperating with conservation campaigns, and keeping water prices low as being key motivations for reducing water usage in his survey of water users in two northern Mexican towns.

Although study participants appear motivated to reduce water consumption, they communicated a degree of powerlessness in being able to do so. Self-efficacy is a measure of a person's belief that he or she is able to perform a given action. People with higher levels of self-efficacy are more likely to follow through on a task and achieve positive results (Bandura 1994). The questionnaire indicated relatively low levels of self-efficacy in Blagoevgrad in connection with reducing household water consumption. For example, 27.7 percent strongly agreed, and 12.4 percent mildly agreed with the statement, "There is nothing ordinary citizens can do to avoid a water shortage in the city". When asked to react to the statement, "It would be very difficult for my household to reduce the amount of water we use," 29.2 percent strongly agreed, and 22.7 percent mildly agreed.

Slightly over 43 percent of questionnaire respondents indicated they had never heard of low-flow showerheads or toilets, and some communicated doubt that such devices even existed. Only 6.6 percent of respondents indicated they used water-saving toilets and 13.1 percent said they used water-saving showerheads.

When asked why more people do not use water saving fixtures in their homes, lack of finances was the main reason. During interviews and focus groups there was much discussion and interest in water saving devices, but most people considered them a luxury beyond their means. Over 85 percent of questionnaire respondents indicated lack of affordability as a very important factor in explaining the rarity of low-flow fixture adoption in Blagoevgrad.

Water pricing is often used to help reduce consumption. From the water company's perspective, setting prices is a balance between keeping water affordable and generating sufficient revenue for maintaining and improving the distribution system. Ideally, a pricing system should be economically efficient, be equitable and fair, and promote conservation (Boland 1993). A report from the Organisation for Economic Co-operation and Development (OECD) lists the following as important considerations in setting water prices: allocative (economic) efficiency, equity, financial requirements, public health, environmental efficiency, consumer acceptability and understanding, and administrative costs (OECD 1999, 17).

Most water economic studies indicate a large portion of residential water demand is rather price inelastic. However, recent, more sophisticated studies have shown that the elasticity of water demand is more complex and may vary considerably based on a variety of variables (Arbues et al. 2003; Martinez-Espineira and Nauges 2004). These studies indicate careful manipulation of price can be an important contributor to water conservation.

On the questionnaire, 69 percent considered the price of water in Blagoevgrad normal, while 25.6 percent considered it high, and 5.4 percent considered it low. When asked how the current water price affects water use, 48.1 percent indicated it has no impact, 44.6 percent said it encourages people to conserve, and 7.3 percent said it encourages people to waste water. Most studies show a strong positive correlation between household income and water consumption, with higher income households consuming significantly more water (e.g., Wang, et al. 1998). Increasing the price of water often leads to an overall reduction in consumption; however, much of the reduction is likely to be accounted for by poorer families, while higher income households show little change in water use patterns (Abu Qdais and Al Nassay 2001).

Interviews and focus group participants often had difficulty listing specific water conservation practices employed in their households. Water conservation was generally viewed passively (not using more water than necessary), rather than actively (engaging in specific behaviors with the purpose of reducing consumption). The questionnaire asked respondents to indicate the likelihood of their households adopting certain water saving practices (Tab. 2). Any method (such as limiting toilet flushes) which impinges on hygiene is likely to be rejected. Gilg and Barr (2006) found a similar hierarchy of willingness to adopt various water conservation measures in their study of households in Devon, UK.

Tab. 2. Adoption of household water conservation practices.

Survey question: How likely is your household to adopt the following methods in the coming year? (five-point scale from very unlikely to very likely)

	very likely	
	%	**N**
Replacing dripping faucets and repairing plumbing leaks in my home.	80.9	576
Replacing existing showers and toilets with modern fixtures specifically designed to use less water.	50.9	356
Using the washing machine more efficiently. Only running the machine when there is a full load.	48.5.	339
Turning off the tap while brushing teeth.	45.6	320
Sweeping terraces and steps instead of washing them with water.	39.2	275
Taking shorter showers.	37.3	263
Not flushing the toilet after every use.	5.9	41

On the questionnaire, 82.6 percent strongly agreed, and 11.0 percent mildly agreed with the statement, “It irritates me when I see drinking water used wastefully.” When discussing wasteful use of water, the majority of focus group and interview participants referred to network losses rather than in-home water usage. Non-revenue water (water loss due to leaks and water that is not metered due to faulty water meters or theft) is a major concern of the local company. Modernization of the water supply system in

Blagoevgrad has been on going and water losses have been significantly reduced, but it has been estimated as much as fifty percent of the water entering the system is unaccounted for.

The idea of wasteful or inappropriate water use by consumers, in most people's minds, applies only to times of drought or water shortage. Respondents were asked whether they considered certain water uses as appropriate during times of normal water supply and during times of water shortage (Tab. 3). Interestingly, cleaning steps and terraces had the highest percent of yes responses in both categories, perhaps reflecting the value placed on water for maintaining cleanliness.

Tab. 3. Perceptions of appropriate use of drinking water

Survey question: Do you feel the following uses of drinking water are appropriate? Please answer for times of normal water supply and for times of water shortage.

	normal water supply		**water shortage**	
	Percent Yes	**Total N**	**Percent Yes**	**Total N**
Cleaning steps and terraces	76.4	665	7.4	652
Washing carpets	55.3	655	4.7	659
Washing cars	45.4	668	3.4	668
Watering gardens	38.6	663	6.3	656
Cleaning sidewalks	36.2	657	5.6	658
Filling private swimming pools	27.5	662	2.9	664

4. DISCUSSION AND CONCLUSION

There are few comprehensive residential water conservation programs in Bulgaria and most people lack a clear understanding of how or why they should conserve water. Historically, Bulgarian water suppliers have looked to increasing the water supply rather than seeking to reduce demand. Without the active participation and support of the local ViK, a water conservation program is unlikely to succeed.

Currently the price of water in Blagoevgrad is not an effective deterrent to wasteful use. Alternative pricing schemes may serve to both ease the financial burden on the poor and restrain profligate use by the more affluent. Providing more information on water bills could increase water conservation awareness. Gaudin (2006) determined that providing marginal price information on water bills can contribute significantly to water conservation efforts.

Providing information about practical ways of reducing water consumption, and providing opportunities for public input in water management decision making are likely to increase self-efficacy and motivate greater willingness to adopt water conservation measures.

During years with normal precipitation, people give little thought to water availability and do not develop water conservation habits. An effective, on-going water conservation program should help water users develop sustainable conservation habits and is more likely to achieve success than emergency programs instituted only during droughts. Such programs should enable consumers to lower their water bills and also yield environmental benefits.

Residential water users in Blagoevgrad have indicated a desire for more information on water conservation. This study indicates water users have a positive attitude toward conservation and are open to the adoption of low flow fixtures, especially if provided an economic incentive or rebate. The installation of low flow fixtures in government buildings could serve as a model and showcase the technology. At the very least, the local water company could conduct residential water audits and provide information on the potential savings available by adopting low flow fixtures and other water conservation measures. Further research should seek to measure the effectiveness and quantify the water savings potential of various programs in the Bulgarian context.

5. LITERATURE CITED

[1] Abu Qdais, H., Al Nassay, H. (2001) Effect of pricing policy on water conservation: A case study. Water Policy 3(3):207-214.

[2] Alitchkov, D., Kostova, I. (1996) Possibilities for water conservation in Bulgaria. GeoJournal 40(4):421-429.

[3] Arbues, F., Garcia-Valinas, M., Martınez-Espineira, R. (2003) Estimation of residential water demand: a state of the art review. Journal of Socio-Economics 32(1): 81–102.

[4] Bandura, A. (1994) Self-efficacy. In V.S. Ramachaudran (ed.), Encyclopeida of human behavior (Vol. 4, pp. 71-81). New York: Academic Press.

[5] Boland, J. (1993) Pricing Urban Water: principles and Compromises. Water Resources Update 92: 7-10.

[6] Chang, H., Knight, C.G., Staneva, M., Kostov, D. (2002) Water resource impacts of climate change in southwestern Bulgaria. GeoJournal 57:159-168.

[7] Corral-Verdugo, V. (2002) A structural model of pro-environmental competency. Environment and Behavior **34(4)**: 531–549.

[8] Corral-Verdugo, V., Bechtel, R., Fraijo-Sing, B. (2003) Environmental beliefs and water conservation: An empirical study. Journal of Environmental Psychology 23(3):247-257.

[9] EEA (European Environmental Agency) (2002) Environmental Signals 2002. Benchmarking the millennium; environmental assessment report #9, European Environmental Agency. Available at: http://reports.eea.eu.int/environmental_assessment_report_2002_9 (accessed Sep 2004).

[10] EPA (Environmental Protection Agency). (1994) A guide to customer incentives for water conservation. Washington, D.C.: U.S. EPA Office of Water.

[11] Featherstone, J. (1996) Conservation in the Delaware River Basin. Journal of the American Water Works Association 88(1):42-51.

[12] Gaudin, S. (2006) Effect of price information on residential water demand. Applied Economics 38: 383–393.

[13] Gilg, A., Barr, S. (2006) Behavioural attitudes towards water saving? Evidence from a study of environmental actions. Ecological Economics 57(3):400-414.

[14] Knight, C. G., Steneva, M. (1996) The water resources of Bulgaria: an overview. GeoJournal 40(4):347-362.

[15] Martınez-Espineira, R., Nauges, C. (2004) Is all domestic water consumption sensitive to price control? Applied Economics 36: 1697–1703.

[16] OECD. (1999) Household Water Pricing in OECD Countries. Paris: OECD. Available at: http://www.olis.oecd.org/olis/1998doc.nsf/LinkTo/env-epoc-geei(98)12-final (accessed June 2006).

[17] Tashakkori, A., Teddlie, C. (1998) Mixed methodology: combining qualitative and quantitative approaches. Thousand Oaks, CA: Sage Publications.

[18] Vassilev, I. (1996) River runoff changes and recent climatic fluctuations in Bulgaria. GeoJournal 40(4):379-385.

[19] Wang, Y.,Byrne,J., Song, J., Chen, Y. (1998) The 1992-97 panel study of residential water conservation impact: Persistence of conservation performances of demand-side management programs. Newark, DE: Center for Energy and Environmental Policy, University of Delaware.
[20] World Bank. (2005) Bulgaria: Financing the water and wastewater sector. Available at:
[21] http://siteresources.worldbank.org/intbulgaria/Resources/Finaldocbulgariareport.pdf (accessed Jun 2006)

BIOLOGICAL WATER QUALITY ASSESSMENT OF THE BLAGOEVGRADSKA BISTRITSA RIVER BASED ON BENTHIC MACROINVERTEBRATE COMMUNITIES

Lidia Sakelarieva[1], Ivanka Janeva[2]

[1]South-West University, Faculty of Mathematics and Natural Sciences, Department of Geography, Ecology and Environmental Protection, 66 Ivan Mihailov Str., 2700 Blagoevgrad, Bulgaria
[2]University of Sofia, “St. Kliment Ohridski”, Faculty of Biology, Department of Hydrobiology and Ihtiology, 8,Dragan Tzankov Blvd., 1164 Sofia, Bulgaria

Abstract: *The Blagoevgradska Bistritsa River was researched in 2002 and 2003. The purpose of the study was to determine the contemporary ecological state of the river as the basic water source of the city of Blagoevgrad.*

The river water quality assessment on the basis of saprobiological and biotic indices by using benthic macroinvertebrate communities is presented and discussed in this paper.

The organic pollution of the river did not create significant environmental problems in 2002 and 2003. An improvement in the saprobic conditions in the river section after the city of Blagoewgrad was registered in comparison with the period 1978 – 1980.

Kewords: *water quality assessment, saprobiological indices, biotic indices, river ecosystems.*

1. INTRODUCTION

The biological analysis for determining the water bodies’ condition in respect to their quality has several advantages over the physical-chemical one. First of all it gives an account of the enduring state and its influence upon the water species populations and their communities. Moreover the biological parameters give the opportunity for water quality prognosis and management.

A great number of the hydrobiological researches of the Blagoevgradska Bistritsa River carried out in the period 1970 – 1981 studied the impact of the city of Blagoevgrad on the saprobic condition of the river [10], as well as the relation of this condition to the city waste water quantity [4], the river flow quantity [5] or the seasons [6]. According to the saprobiological index values in the period 1978 – 1980 [10] the Blagoevgradska Bistritsa River was xeno- and oligosaprobic in the section down to the city of Blagoevgrad with a tendency to β-mesosaproby in the section just before the city in summer and autumn. After Blagoevgrad the river section was more often polysaprobic during the summer – autumn low water and α-mesosaprobic during the spring high water.

Some theoretical methodical aspects of using various biological parameters in the saprobiological assessment of the river are also discussed in some of the publications [2, 3].

The Blagoevgradska Bistritsa River was researched in 2002 and 2003 in order to determine its contemporary ecological state [1, 12,13,14]. The river water quality bioassessment on the basis of benthic macroinvertebrate communities is presented and discussed in this paper.

2. MATERIAL AND METHODS

Relatively-quantitative hydrobiological samples (benthic macroinvertebrate animals) according to ISO 7828-1985(E) standard were gathered at 7 river stations (Parangalitsa, before Bodrost, Dobro pole, Slavovo, Bistritsa, before the city of Blagoevgrad, after Blagoevgrad – river mouth). The conditions at the last station were strongly influenced by the waste water (including industrial) of the city of Blagoevgrad.

The samples were gathered monthly in the vegetation period (from May to October) in 2002 and seasonally (May, August, October) in 2003.

The water quality assessment was made on the basis of two parameters – the Saprobiological index (S_R) of Zelinka & Marvan [9], and Rothschein [7], and the Bulgarian biotic index (BgBI) after Uzunov et al. [8]. The saprobic indices assess precisely the organic pollution quantity on the basis of the indicatory potential of the macrozoobenthic community. The pollution impact on the community is determined very well by means of the biotic indices which give an account of the community indicatory potential as well as of its taxonomic diversity. The complex use of both parameters provides a possibility of identifying of some other type of pollution, different from the organic one – toxic, inert, etc.

The categorization of the stations was made according to the Regulation № 7 (1986) of the MEW about the parameters and norms for quality assessment of the running surface waters.

3. Results and Discussion

3.1. Saprobiological index (S_R)

In 2002, excluding the last station, the index values were most stable in October and June (Fig. 1). The highest value was determined in May – 83,14 (xenosaproby) (st. 2), and the lowest one – in July – 24,25 (α-mesosaproby) (st. 7).

The index values for the first two stations showed stable xeno-oligosaproby (Fig. 2). Oligosaproby was determined only in May at station 1. That condition could be explained with the station location in the region of the rich of organic substances dark coloured mountain forest soils and dark brown forest soils [11] as well as with the possibilities of detention of a part of the coarse particulate organic matter during the spring heavy rainfalls and snow melting.

The values of the Saprobiological index characterized the conditions at stations 3 and 4 rather as xeno-oligosaprobic, and at stations 5 and 6 – as oligosaprobic. The numerical dominance of *Cryptochironomus* gr. *defectus* in the community at station 4 in September was the reason for the index lower value. According to the Saprobiological index the water quality at the first 6 stations was I category. Logically the index values were lower at the river mouth in the presence of saprobic pollution - α-mesosproby in summer (III category). That station was β-mesosaprobic in spring and autumn (II category). An improvement in the saprobic conditions of that river section was registered in comparison with previous studies [1].

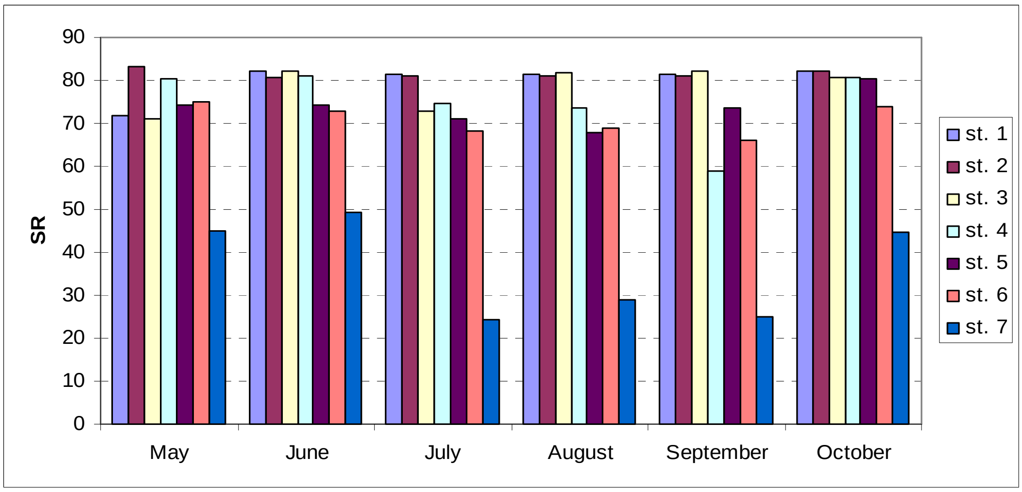

Fig. 1: Values of the Saprobiological index (S_R) in different months of 2002.

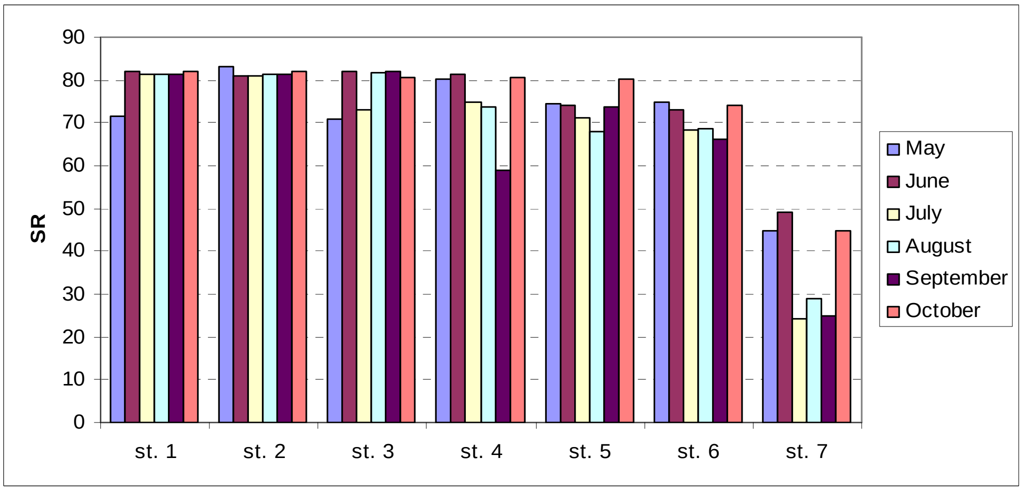

Fig. 2: Values of the Saprobiological Index (S_R) at the 7 stations in 2002.

In 2003 the Saprobiological index values along the length of the river, without the section after the city of Blagoevgrad, were comparatively most stable in summer (Fig. 3). The maximum value corresponding to xenosaproby was determined, as in 2002, in May – 84,72 (st. 2), and the minimum one – in August - 31,85 (α-mesosaproby) (st. 7).

The index values determined the conditions at the first 6 river stations (Fig. 4) as xeno-oligosaprobic (water quality I category), and at the last station – as β-mesosaprobic (II category) in spring and α-mesosaprobic (III category) in summer and autumn. In comparison with the autumn of the previous year the index had lower values at stations 4, 5, 6 and 7. That could be explained with the decreased river flow in the summer and autumn of 2003.

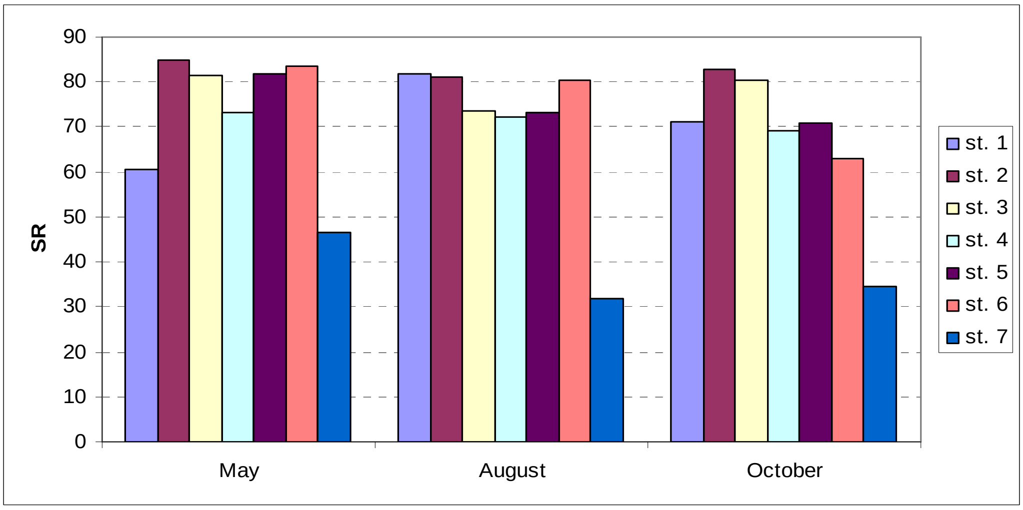

Fig. 3: Values of the Saprobiological index (S_R) in different months of 2003.

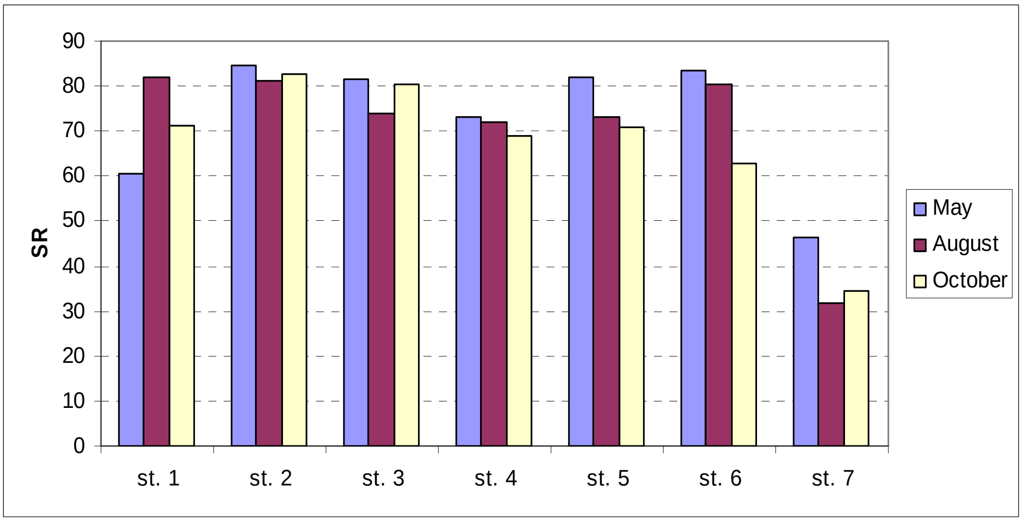

Fig. 4: Values of the Saprobiological index (S_R) at the 7 stations in 2003.

3.2. Bulgarian biotic index (BgBI)

The Bulgarian biotic index had its maximum value (BgBI = 10) for the first 6 river stations in 2002 except for station 3 in May, station 5 in October and Station 6 in June (BgBI = 9) - I category (Fig. 5). Its values were lower at the last station, which was III category (BgBI = 5) in July, and II category (BgBI = 6 or 7) in the other months.

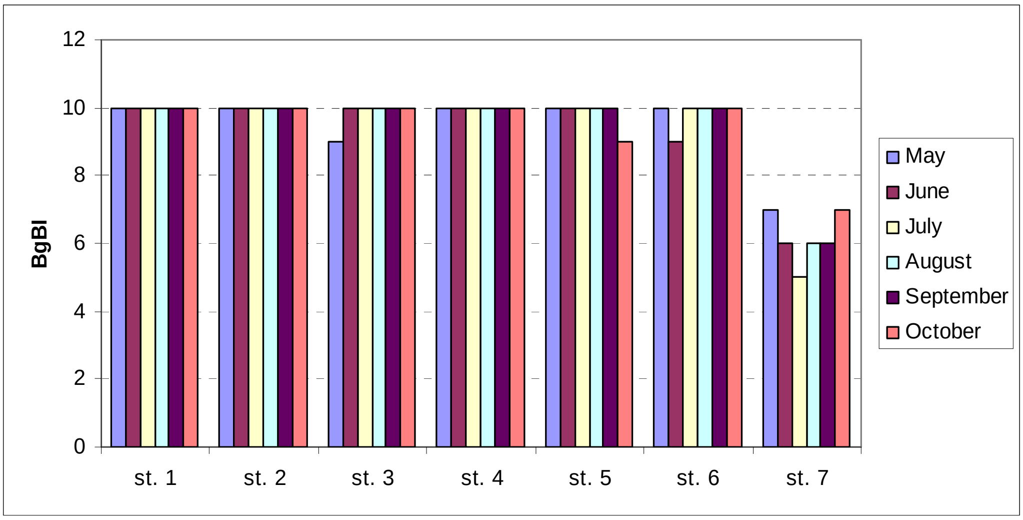

Fig. 5: Values of the Bulgarian biotic index (BgBI) at the 7 stations in 2002.

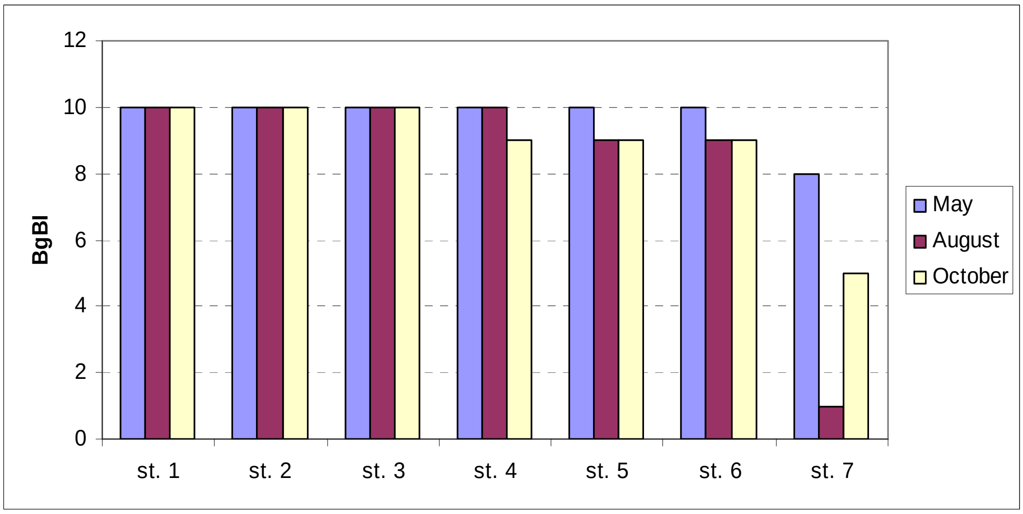

Fig. 6: Values of the Bulgarian biotic index (BgBI) at the 7 stations in 2003.

In different seasons of 2003 the Bulgarian biotic index (Fig. 6) also had maximum value (10) for the stations 1 – 6, except for station 4 in autumn and stations 5 and 6 in summer and autumn (BgBI = 9). The very high index value (8) at the last river station in spring of 2003 can be explained with the considerably improved river bottom conditions as a result of the high water for more than a year. However, in spring, the index had extremely low value (1) which corresponded to intensely polluted water out of admissible norms. At that time the river flow at the mouth consisted almost only of returned waste water, polluted probably not only with biodegradable organic matter but also with toxic substances.

4. CONCLUSIONS

- The saprobilogical condition of the Blagoevgradska Bistritsa river in the section down to the city of Blagoevgrad (stations 1 – 6) was xeno-oligosaproby or oligosaproby and corresponded to I category.
- The river section after the city of Blagoevgrad (st. 7) was β-mesosaprobic during high water, and α-mesosaprobic during low water (summer – autumn 2003) and the summer months of 2002.
- The organic pollution of the river did not create significant environmental problems in 2002 and 2003. An improvement in the river section after the city of Blagoewgrad is observed in comparison with the period 1978 – 1980.
- According to the Bulgarian biotic index values the general ecological condition of the river section down to Blagoevgrad (stations 1 – 6) corresponded to I category.
- The river mouth (st. 7) was II category during high water with only one exception - in July 2002, when it was III category. During low water – October and August 2003, this river section was III category or out of the admissible norms respectively.
- The inconformity of the Saprobiological index value (α-mesosaproby - III category) to the Bulgarian biotic index value (out of the admissible norms) for the condition of the river mouth in August 2003 presumed toxic pollution. This inconformity showed the necessity of using various parameters in water quality assessment.

5. REFERENCES

[1] Michailov, M., Sakelarieva L. (2006) An Assessment of the Stream Conditions in the Blagoevgradska Bistritsa River Watershed. In: Mathematics and Natural Sciences Proceedings of the International scientific conference, 8 – 11. 06. 2005, SWU “Neofit Rilsky”, Blagoevgrad, Vol. 2, 251-255.

[2] Natchev, N. (1985) Interrelation between Non-Specific Categories of Benthic Macrofauna as Criterion for Saprobic Zone Determination of Blagoevgradska Bistritza River, Hydrobiology 24, 23-31.

[3] Natchev, N. (1987) Normally distributed S_R data from Blagoevgradska Bistritza river, Hydrobiology 30, 81- 93.

[4] Natchev, N. (1988) Correlation and regression analysis of dependence between saprobic state of Blagoevgradska Bistritza River and sewage quantity of Blagoevgrad. Hydrobiology 33, 34-44.

[5] Natchev, N. (1989) Quantity of outflow and saprobity state along the lower reaches of Blagoevgradska Bistritza River, Hydrobiology 34, 30-38.

[6] Natchev, N. (1994) Seasons and saprobity state along the lower stretch of the Blagoevgradska Bistritza River, Hydrobiology 39, 102-112.

[7] Rothschein, J. (1962) Graficke znanornenie vysledkiv biologickeho hodnotenia cistoty vod, Veda a vyskum praxi VUVH, Bratislava, 9, 1-64.

[8] Uzunov, Y., Penev, L., Kovachev, S. & Baev, P. (1998) Bulgarian Biotic Index (BGBI) – an Express Method for Bioassessment of the Quality of Running Waters. Compt. Rend. Acad. Bulg. Sci. 37, 130-137.

[9] Zelinka, M., P. Marvan. (1961) Zur Präzisierung der biologischen Klassifikation der Reinheit fliessender Gewässer, Arch. Hydrobiol., 57, 389-407.

[10] Начев, Н. (1982) Влиянието на Благоевград върху сапробното състояние на Благоевградска Бистрица и Струма, Хидробиология 16, 32-42.

[11] Николов, Б., Минковска, Р. (1984) Картографиране на почвите във водосборния басейн на река Благоевградска Бистрица за целите на общонаучната ландшафтна карта, Горскостопанска наука 2, 15-21.

[12] Сакелариева, Л., Янева И. (2005) Динамика на състава и структурата на макрозообентосните ценози в река Благоевградска Бистрица. Биоразнообразиие Екосистеми Глобални промени. I Национална Научна Конференция по Екология, ПЕТЕКСТОН, София, 323-330.
[13] Сакелариева, Л. (2006) Процесът на урбанизация и влиянието му върху река Благоевградска Бистрица (еколого-исторически аспект). В: Mathematics and Natural Sciences Proceedings of the International scientific conference, 8 – 11. 06. 2005, SWU “Neofit Rilsky”, Blagoevgrad, Vol. 2, 433-440.
[14] Сакелариева, Л., Янева И. (2006) Оценка на качеството на река Благоевградска Бистрица въз основа на физико-химични параметри. Екология и индустрия, том 8 № 1-2, 249-251.

SOME QUESTIONS TOWARD THE RELATIONS AND THE WATER QUALITY CLASSIFICATION FOR THE RIVERS IN BULGARIA

Assoc.prof. eng. Michail As. Michailov, PhD

South-West University „Neophit Rilsky“ - Blagoevgrad, Bulgaria

The total length of the river network in Bulgaria is 19 761 km. About 3700 km (first of all in main rivers and in more anthropogenic endangered regions) are covering with stations of the National environmental monitoring system (NEMS) – subsystem “Water” [11]. In these stations is developed traditional monitoring for water quality parameters. Usually collected data are using for the rivers state assessment. As a classification system are used requirements in Regulation No.7 for surface water quality (SG No.96/1986). According to them there are three categories for surface waters in dependence of different uses.

The state(1999-2000) of the surface watercourses in Bulgaria is shown in the table1.

Table 1
Relative share of different water quality categories for surface watercourses in Bulgaria

Category	**I**	**II**	**III**	**Outside of category III**
Percentage %	4	38	34	24

Source: http://www.moew.government.bg

It is easy to see there are many questions about surface water quality in Bulgaria. A quarter of monitoring river lengths is outside of permissible category III. About 30 % in lower part of main watercourses are with water quality for irrigation and other not precise industrial needs. On the average of the country the water losses are more than 57 % and not small parts of them are related to bad management of the water systems [11].

Bulgaria has a good tradition in organised water management and law [6] so it is easy to apply new European regulations, especially Directive, establishing a framework for action in the field of water policy [3]. There is no doubt about necessity of new paradigm, first of all for rivers water quality classification**.

As it was note, in recent years in Bulgaria, there are three categories for the river water quality, according to the different use: domestic, industrial, irrigation, etc. - Regulation No.7 for surface water quality (SG No.96/1986). The main requirement is: *for a minimal mean monthly water quantity in the river (in year with a 95% probability) – lower concentration of pollutants then the permitted norms for the category of the river.* Additionally, there is a specific administrative approach in Ministry of environment and water (MOEW) to use the value of the 10% of the average flow as a norm (by written order from 2003 year).

There are many methodological questions about these requirements.

** A basic parts of these questions and of the article was presented on World Association of the Water and Soil Conservation (WAWSC) meeting in Sofia – 2003 [7].

The river discharge is an important parameter, but not enough for the specific conditions in the watercourses in Bulgaria representative explanation. Usually with this parameter depend on the emission and the permissible concentration of pollutants in streams and rivers, but as an environmental criterion it is not enough alone. So it is very difficult to find direct relationship between the river water quality parameters and the discharge, like $BOD_5 = f(Q)$, etc. For comparison, in table 2, are shown results of the coefficient of determination (R^2) for some main rivers in Bulgaria [14]. The relations are not representative enough (usually $R^2 < 0,3 – 0,4$).

Table 2

The water quantity and quality parameters relation - for some main rivers in Bulgaria

($BOD_5 = f(Q)$)*

№	River	*Coefficient of determination (R^2)*		
		Dissolved oxygen	BOD_5	COD (Manganese)
1.	Iantra	0.279 – 0,398	0.253 – 0,391	0.268 – 0,509
2.	Kamchia	0.296 – 0,443	0.262 – 0,311	0.296 – 0,349
3.	Maritca	0,259 – 0,522	0,267 – 0,372	0,256 – 0,322
4.	Arda	0,273 – 0,339	0,311 – 0,356	0,257 – 0,302
5.	Mesta	0.296 – 0,334	0.264 – 0,337	0.266 – 0,329
6.	Struma	0,285 – 0,336	0,292 – 0,350	0,270 – 0,335

* Respectively: $O_2 = f(Q)$ and $COD_{Mn} = f(Q)$

Source: www.bluelink.net/water

These results are not useful enough, because of the wrong methodological approach. It is difficult, even impossible, to receive a good results with this kind of interpretation the water monitoring network data. There is necessity of additional information, which is better to be asked of new water quality regulations.

Currently there are no regulations for the rivers and streams environmental flow managing. A number of scientific methods are available to determine the rivers and streams discharge. But it is insufficient to know the water quantity only (maximum, average, minimum, etc.). There are a lot of other parameters and factors which must to be include in the investigations.

The effects of discharge for the stream and river environmental conditions are direct and indirect. Direct influence has the amounts of sewage, industrial and other wastewater discharges, which must to be permit. But for lower parts of watercourses this influence become indirect with other meaning as aquatic environment.

First of all it is necessary to understand the main difference between rivers (streams) and other water objects (lakes, dams, pools, etc.), which depend on continuous movement of the water from upper till lower part of the watershed. In that case parameters like rivers depth, width and velocity are also important, except discharge. It is clear as the discharge increases or decreases so are happened to the river depth, width, and velocity. As a result this is a change of the physical conditions in rivers and streams, a change of the wetted part of watercourses and, finally, a change in the habitats of the aquatic species.

The protection of the biological diversity and the natural habitats of species in Bulgaria is a subject of special requirement, according to the Environmental Protection Act [4]. But for aquatic species these requirements are not defined enough, also as the duty for minimal ecological flow in watercourses [4,10].

The discharge changes are affected by different processes within the watersheds. As a natural physiographic or hydrologic unit each watershed is an area with a number of distinct recourses (geological, soils, forests, land, water, etc.) which use is important to receive economical benefits without ecological problems and harmful impact of human activities. In comparison with the middle and the end of XX century at the beginning of the XXI century it means - European living standards, modern industrial and agricultural practices, healthy environment, etc.

As an illustration for impact of human activities it is shown the analysis of the water quality monitoring data for Topolnitca river (tributary on Maritca river in South Bulgaria) about the dynamic of pH during long (1951-2001) period of time (fig.1).

Figure 1

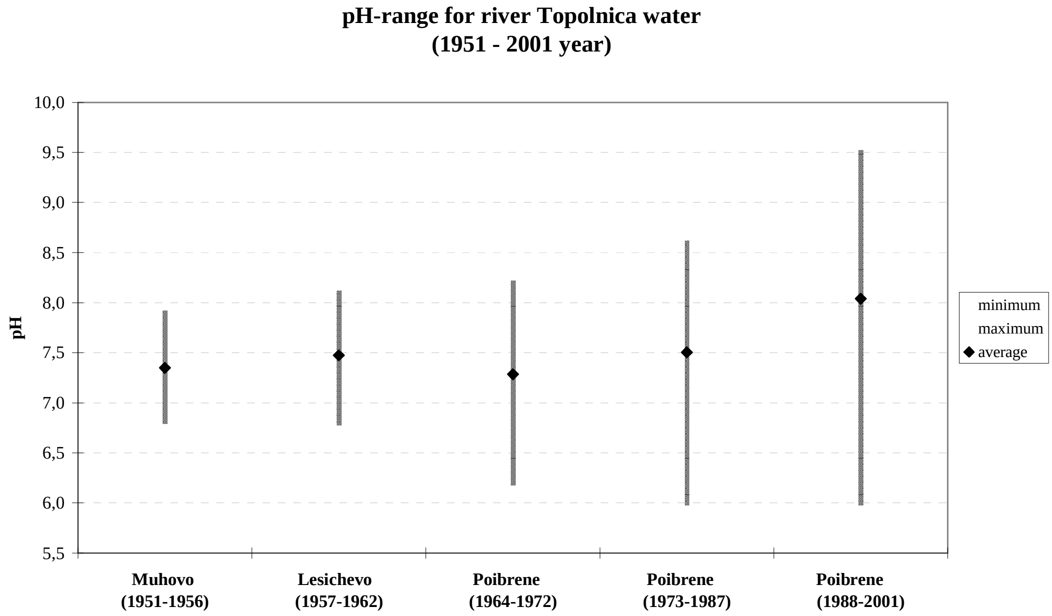

It is easy to see the big difference between pH range before 1965 and after 1970, unfortunately depend on the human impact in this period. These are important reasons for more critical analysis on current rules and possibility to take them into consideration of the new river water quality classifications.

It is clear the current regulations about river water quality classification in Bulgaria are not adequate enough to the new European requirements as the achievement a good water status till 2015 year [3] or the coordinated development and management of the different watershed resources in order to receive maximum results without compromising the sustainability of vital ecosystems, according to the Global Water Partnership (GWP) [13], for example.

For the improvement of the aquatic environment in the rivers a „good water status“ is defined as a state when „both their ecological status and their chemical status are at least good“ [3]. The importance of this requirement is the specific interpretation of rivers ecological and chemical status. It is not enough the chemical parameters to be only in permissible borders. This is the different pollutant sources obligation. The main purpose for rivers and watersheds is their ecological status and the striving for development „without compromising the sustainability of vital ecosystems“[13]. The data in fig. 1 are good example for the consequences and the ecological changes in the Topolnitca river watershed as a result of industrial development and with necessity of new regulations for the regimes of use and conservation of environmental components.

Table 3

Relation between flows in different parts of some main rivers in Bulgaria

River	**Correlation coefficients for different watercourses**				
Iskar	Iskar dam – Novi Iskar	Novi Iskar - Kunino	Kunino – Orehovitca		
	0,581	**0,921**			
Jantra	Gabrovo - Vetrentci	Vetrentci – Cholakovtci	Cholakovtci – Karantci		
	0,583	**0,862**			
Maritca	Belovo - Pazardjik	Pazardjik - Plovdiv	Plovdiv - Parvomai	Parvomai – Harmanli	Harmanli – Svilengrad
	0,816	**0,818**	**0,825**	**0,898**	
Mesta	Jakoruda – Momina kula	Momina kula - HadjiDimovo			
	0,942				
Struma	Rajdavitca-Boboshevo	Boboshevo - Krupnik	Krupnik – Marino pole		
	0,377	**0,168**			

Sources: Hydrological reference books for rivers in Bulgaria, hydrological yearbooks (1950-1983) (in bulg.), etc.

The establishment of permissible emission levels is only the first part of new environmental regulations. The more important part is the investigation on the specific parameters and conditions for the rivers and the watersheds in Bulgaria and their inclusion in the water quality regulations.

According to the EU Water Framework Directive [3] Bulgaria is in two eco regions – Eastern Balkan and Pontic Province. So it is important to find manners and tools to assess the differences between them. Unfortunately the rivers discharge only as a parameter is not quite enough. For example in Table 3 are shown the correlation coefficients as a relation results between discharges in separate part of main rivers in Bulgaria.

It is easy to see the different influence of the local conditions in the particular parts of the watersheds, especially for Iskar, Jantra and Struma rivers, which is necessary to take into consideration as a tool for the river conditions environmental assessment.

A lot of methods are used to define the ecological conditions in the rivers and the streams [2,8,9,12]. Each method makes different assumptions about what is most important for the surface water environment. It is possible to separate these methods in two basic groups according to their function:

- to establish a rivers or streams discharge to accept domestic and industrial effluents without any adverse impacts on permissible concentration of many chemical parameters as indicators for the environmental state,

- to establish a rivers or streams capacity to support a healthy aquatic community as a human impact assessment and an important strategic management tool.

Each group is important but good results are accessible after their combined operations and use only. In reality, the first group methods is assumed to roughly describe the rivers conditions. For example the „*Tennant*" method offer „poor" habitat conditions at 10%, „fair" at 30% and „good" at 40% or more of the mean river annual flow [2,8]. But it is not enough.

The second group of methods has two main sub-groups also, according to their structure, range, information base and including first of all:

- rivers (streams) hydrologic and hydraulic parameters, or
- biological indicators (macroinvertebrates, fish, etc.).

At first sub-group a combination of wetted perimeter, depth, width and water velocity is used to describe the minimum flow necessary to maintain acceptable habitat for fish and macroinvertebrates in watercourses (*Wetted Perimeter* , *R2Cross* or others methods [2,8]). For example the wetted perimeter in riffles is used as an index of fish food vailability [2].

The second sub-group (*Instream Flow Incremental Methodology (IFIM), Meso Habitat Simulator (MesoHABSIM), USEPA Rapid Bioassessment Protocols (HABSCORE), Australian River Assessment System (AUSRIVAS)* or other methods [2,8,12]) are developed for representing structural, functional and process elements of the biotic community and other „aspects of the habitat that are related to aquatic life use and which are a potential source of limitation to the aquatic biota"[8]. The basis assumption for this sub-group is that the physical and chemical factors in rivers are directly related to the macroinvertebrates and other aquatic biota. This is important position which is used as connection between different methods but it is difficult to apply in real practice.

Many of these difficulties are possible to eliminate with the new water quality classification for the rivers and the streams in Bulgaria. The examples above indicate the necessity of change to the recent regulations including the most useful parts of these methods for the natural conditions in Bulgaria and the European perspective: areas in upper parts of many watersheds (especially in the tributaries on the main rivers) with excellent for water quality conditions, changes in land use, industrial and communities development, environmental requirements, etc.

Any correction toward the representativeness of the water quality parameters would be useful for the new river classification scheme. An idea for the BOD_5 level is discussed below.

As it was published [5], Hynes (1960) have had stated that in 1898 the British Royal Commission on Sewage Disposal investigated a large number of British rivers and classified rivers according to the BOD_5 - (table 4). EEA concluded that river reaches slightly affected by human activities generally have a BOD below 2 mg O_2/l, whereas a BOD exceeding 5 mg O_2/l generally indicates pollution [5].

Table 4

River classification based on BOD_5

No.	**River class**	**BOD_5 (mg O_2/l)**
1.	Very clean	1
2.	Clean	2
3.	Fairly clean	3
4.	Doubtful	5
5.	Bad	10

Figure 2

Present concentration of BOD_5 or BOD_7 (mg O_2/l) in rivers in European countries

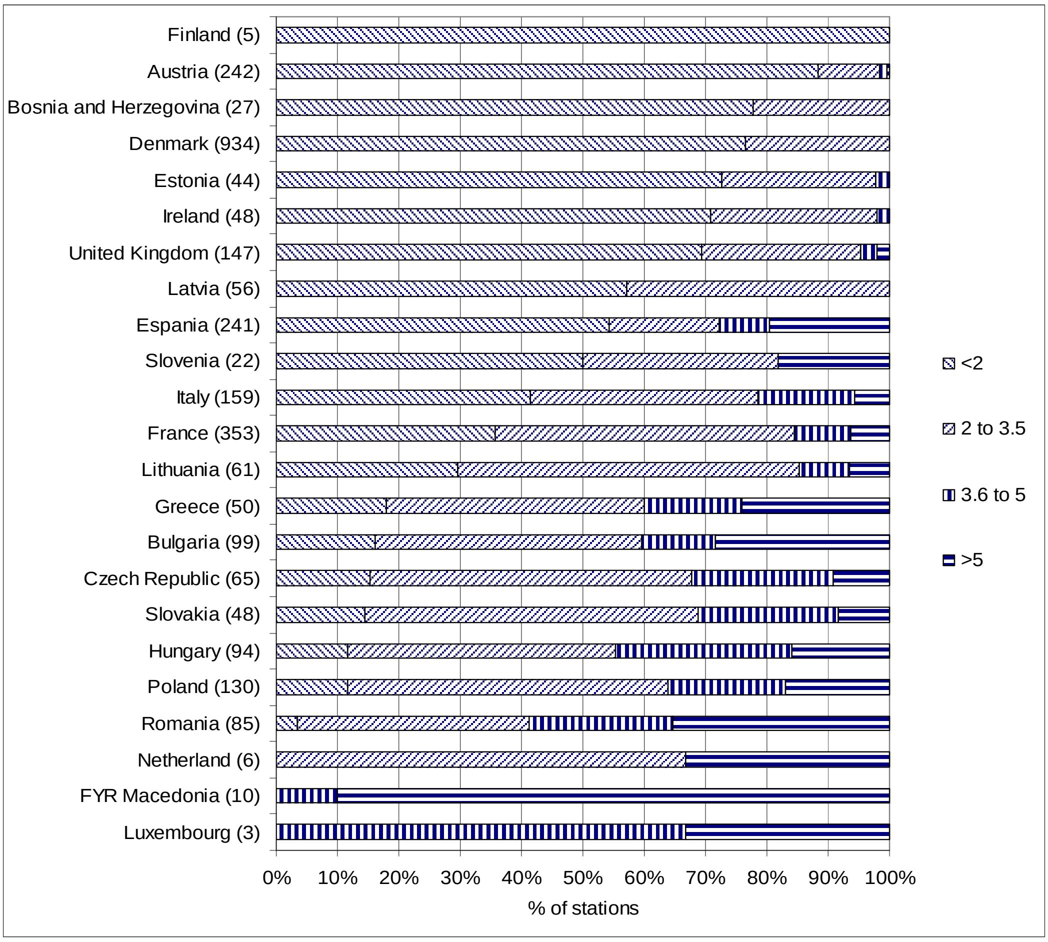

Source: http://themes.eea.europa.eu/IMS/ISpecs/ISpecification20041007131940/IAssessment1116505271445/view_content

The present statement and concentration of BOD_5 (or BOD_7) in rivers in European countries are shown at fig. 2.

It is interesting information, which would be useful as fundamental position in cases for comparisons of the results in the progress of the human activities regulations and the tools for the impact assessment.

It is easy to see the big differences between the conceptions about the water contamination level at the beginning and at the end of the XX century. An example, in comparison with the Water Quality Index (WQI) [1], is shown at fig. 3.

Figure 3
Water quality index (WQI)
Quality-value vs. BOD_5

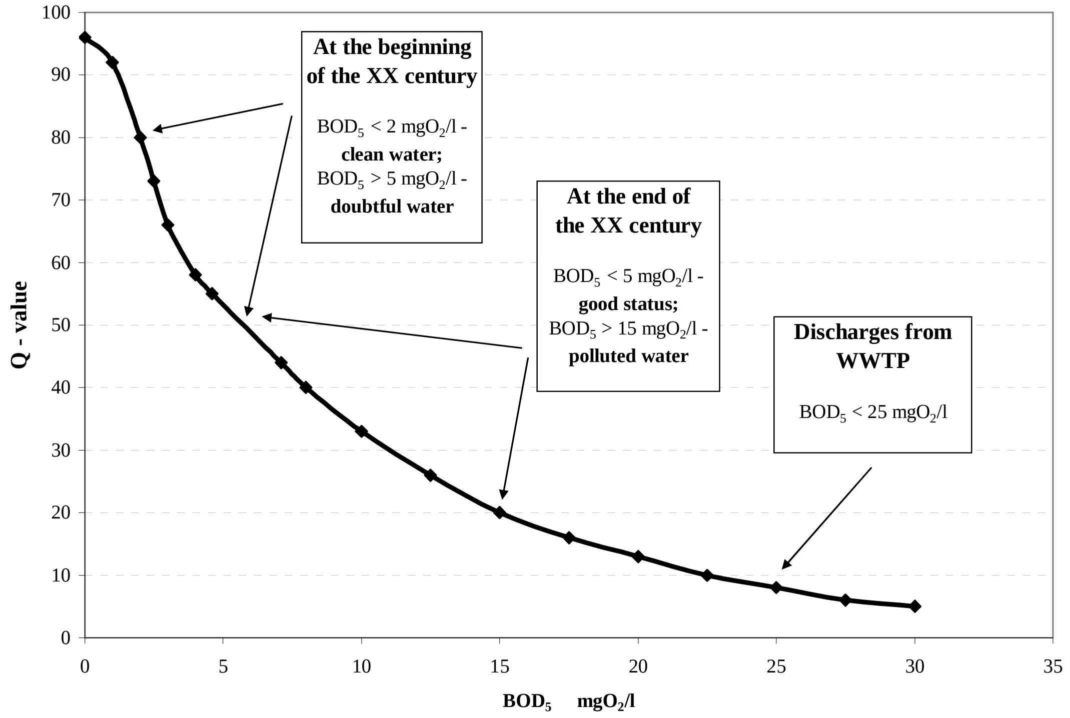

So, it is not enough to analyze and discuss these data (Table 4, Fig. 2 and 3) only. It is clear there are a lot of questions toward the water quality parameters and indicators. But the questions, mentioned above, are more complex.

The river quality classification is not only a part of the obligatory implementation of the national or international regulations. It is important to understand the main goals of the river water quality classification scheme as a ground for environmental friendly water usage at the beginning of the XXI century.

A lot of methodological questions (which were discussed here) are need special improvement. The BOD level as 15 - 20 mg O_2/l has had been acceptable for the last 20 – 30 years, but for the new century it is not the environmental friendly thinking.

As conclusion, it is time to note the necessity of changes: on the one hand – about the significance of the river water quality classification procedure and on the other hand – about rules, regulations and basic principles for their implementations.

The development of new principles for the river water quality classification procedure and the tools for their application shall be a very useful base for complex assessment of the water usage, the watercourses state and the environmental friendly perspective for the rivers and the streams in Bulgaria.

LITERATURE

[1] Adopt-A-River. Volunteer Stream Monitoring Training Manual. Hoosier Riverwatch. IDNR. Division of Fish and Wildlife. Fifth Edition. 2004.
[2] Armstrong, D.S., and Parker, G.W. - Assessment of Habitat and Streamflow Requirements For Habitat Protection, Usquepaug–Queen River, Rhode Island, 1999–2000. U.S. Geological Survey Open-File Report 02-438, 2003.
[3] Directive 2000/60/EC – Framework for ... water policy. OJ L 327, 22.12.2000.
[4] Environmental Protection Act - SG No.91/2002, Corrected, SG No.96/2002, …, SG No.77/2005, …, SG No.105/2006. Sofia.
[5] Indicators and methods for the ecological status assessment under the Water Framework Directive. (Linkages between chemical and biological quality of surface waters). Edited by A. Solimini, A. Cardoso, An. Heiskanen. Institute for Environment and Sustainability. EUR 22314EN. ISBN 92-79-02646-1. Luxembourg. 2006.
[6] Michailov. M.As. - About the surface water quality normative base in Bulgaria.„Ecology and industry“ 5, No.1-3, Sofia, 2003. (in bulg.).
[7] Michailov M. As. - Some methodological questions about rivers water quality classification in Bulgaria. WAWSC. Sofia – meeting. 2003.
[8] Parsons, M., Thoms, M. and Norris, R., - Australian River Assessment System: Review of Physical River Assessment Methods — A Biological Perspective, Monitoring River Heath Initiative. Technical Report no 21, Commonwealth of Australia and University of Canberra, Canberra. 2002.
[9] Snelder T., B.Biggs, M.Weatherhead, K.Niven - A brief overview of New Zealand’s River Environment Classification. National Institute of Water and Atmospheric Research, Riccarton, Christchurch, New Zealand.
[10] Water Act - SG No.67/1999, Corrected, SG No.81/2000, …, SG No.34/2001, …, SG No.108/2001, …, SG No.69/2003, …, SG No.77/2005, …, SG No.65/2006. Sofia.
[11] http://www.moew.government.bg
[12] http://www.niwa.cri.nz/ncwr/tools
[13] http://www.gwpforum.org
[14] http://www.bluelink.net/water

POSSIBILITIES FOR MANAGEMENT OF OLD POLLUTION FROM HOUSEHOLDS WASTE

Stefka Tzekova, Boyko Kolev

South-West University, Blagoevgrad, Bulgaria

Abstract: *The old pollution of the environment caused by households waste is one of the most serious environmental problems that must be solved because of their widespread on the territory of our country.*

A considerable part of already existing household wastes landfills and all unregulated refuse sites do not respond to the requirements of The National and European legislation. They are classified as old pollution as well.

The wide range and complexity of the problem require the application of an integrated approach that includes an initial evaluation, a detailed survey on the site with old pollution, an evaluation of the risk, a program for reducing the damages and their estimation, considered as steps in this article.

Keywords: *old pollution, process of evaluating of the old pollution, insulation.*

1. INTRODUCTION

The only practice used in Bulgaria for making harmless the household waste has been their dumping up to now. Considerable parts of the existing landfills do not respond to the requirements of the National and European Legislation - directive 1999/31/EU, exhibited in decree N$^{\underline{o}}$ 7 [1] and decree N$^{\underline{o}}$ 8 [2] for the following reasons:

-they were constructed before accepting the first specialized legislation for the waste ZOBBOOS [3] and decree N$^{\underline{o}}$ 13 [4] (substituted by decree No8/2004) and don’t respond to contemporary requirement for construction and operation;

-the sites of the old landfills constructed before 1997 were chosen extremely inadequate - along the river slopes, close to water bodies or in valleys of previous pits for inert materials with constant or seasonal water flows which caused washing away of the thrown waste light fractions and polluting of the surrounding territories and water ecosystems.

2. OBJECT AND METHODS

According to investigations of BANSIK, 2001 [5], 578631 ha of the total area of the country are lands with polluted or damaged soils (Tab. 1).

Tab. 1: Percentage share of the landfills from the damaged and polluted lands.

Regions of planning	Total area occupied by landfills ha	Share of the depots to the damaged and polluted lands (%)
North-West	1090,8	1,72
North-Central	2331,4	2,25
North-East	1636,2	1,88
South-West	1999,9	1,77
South-Central	13203,9	9,45
South-East	2087,9	2,91

The percentage share of the landfills from the areas with damaged and polluted soils is highest in the South-Central region of planning – 9,4%, followed by the South-East one – 2,9%. Occupied areas with landfills is about 3, 9 % in the country of all anthropological lands. In view of the fact that most of the landfills and refuse sites are defined as “old pollution” according to the Register established, National program for decrease of their number and danger were made. In order to realize the program, Methods and Guide defining the steps that should be followed in the old total pollution management were prepared [6].

The methods [7] include a step by step evaluation of the object on the basis of the extending of the gathered information content [8]: inventory of the hypothetical cases, history of the pollution, comprehensive survey, survey for insulation and accomplishment and control of the results from that insulation.

The methods used for evaluating of the landfills are adapted for the Bulgarian reality, and is a version of the Saxon methods for evaluating and treating of the old pollution.

The steps in the process of evaluation of the old pollution are specified as “levels of evidence” and after each one, the competent organization makes a decision if and in what form a necessity for further actions exists.

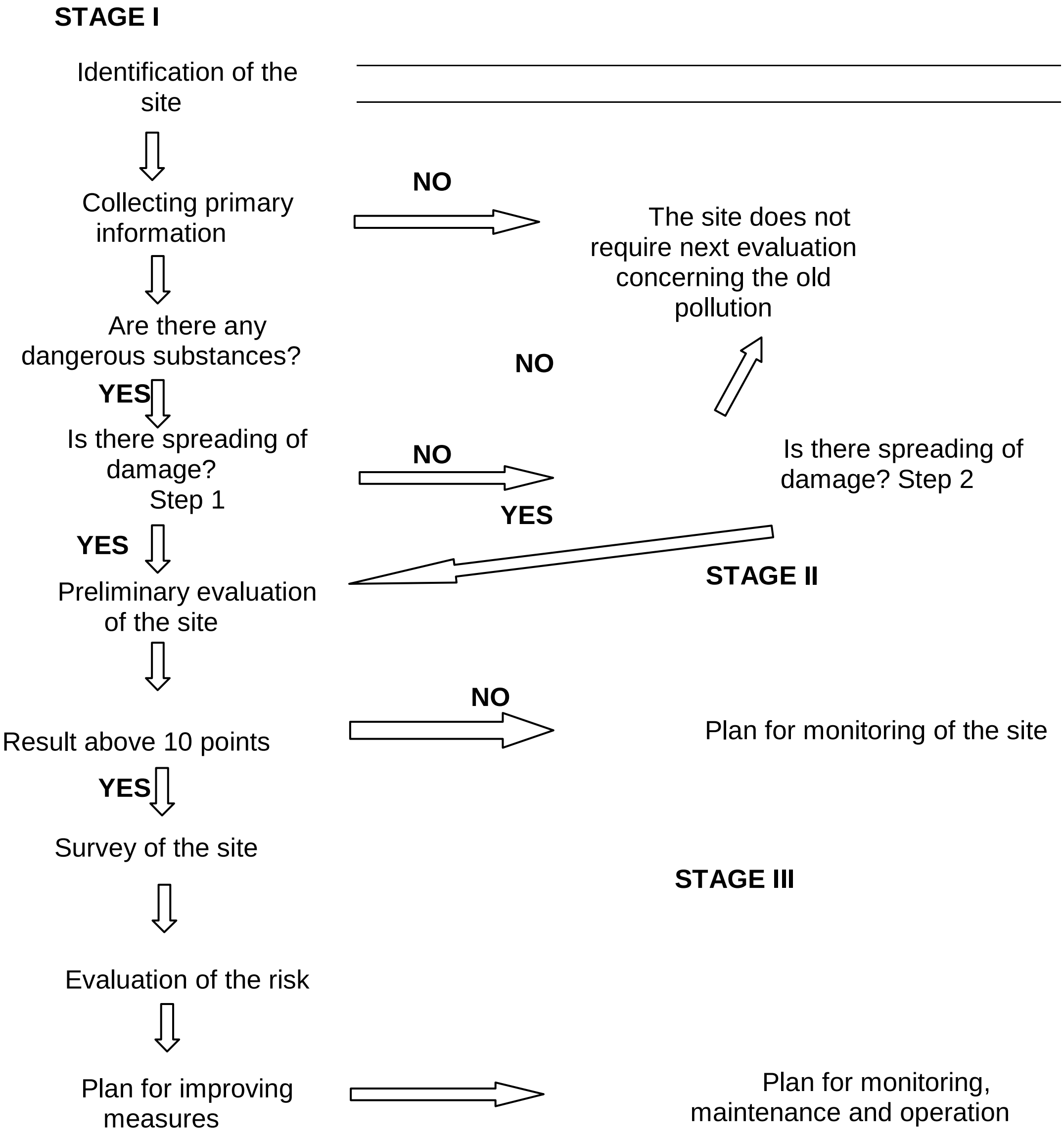

Fig.1. Evaluation of old pollution / POVVIK.

The aims and methods which are pursued into different stages in the management of old pollution are shown in Tab. 2.

Tab. 2: Stages, aims and methods.

Stages	Aims and Methods
1	2
Registering of hypothetical cases of old pollution and formal primary evaluation	The location of the depot, the amount and sorts of waste including dangerous one in documents, hydrology and geology of the area.
History of the pollution	Survey in historical plan to establish the main reasons for the possible pollution especially if household and industrial waste is thrown together, industrial archives, construction documents, National cadastre of lands, going round the place, expert evaluation
Orientating survey	Evaluation of the risk by comparison of concentration of the harmful substances of the depot with relevant controlling values; making controlling evaluation of the risk-program GEFA
Comprehensive survey	Taking probes, analysis and preparing the conclusive evaluation of the danger of the possible pollution and prognosis, and working out criteria for the following actions
Survey for insulation	Choice of optimum in ecological and economical aspect version for insulating by option of version: removal of old pollution and/or making safe
Insulation	Constant removal the danger by applying the stages: planning, accomplishment and monitoring
Control of results	Long-lasting effect, evaluation of the results from the insulation with long-term monitoring system.

Methods for evaluating and treating of old pollution are used for researching, inventory, evaluation and classification of 59 landfills for households waste from settlements with population above 20000 residents. Inventory landfills are classified into 4 groups according to the extent of the environmental risk as follow:

I-st group - very big risk -12 landfills
II-nd group - big risk -17 landfills
III-rd group - medium risk - 28 landfills
IV-th group - minimum risk

The landfill of the city of Blagoevgrad is classified as III-rd group.

3. CONCLUSIONS

In conclusion, it must be said that the Operation Program “Environment 2007-2013”, which has passed the first procedure for sanction from the European Commission will be supported by the cohesion fund and European fund for regional development. One of the priorities for financing is closely connected with reversing lands and soils and it is defined ‘Abolition of existing depots, unregulated refuses sites with waste and recovery of polluted areas’.

It must be a motive for putting into practice the research connected with “old pollution’. Moreover that planned budget for the program is about 1.8 billion Euros-1.4666 billion Euros came from the cohesion fund and European fund for regional development and 334 million Euros are from national finance. Twenty one percents of this means is allocated to the management of wastes.

4. REFERENCES

[1] Decree N^o 7 for the requirements which must be responded the sites for setting the equipment for treating waste.
[2] Decree N^o 8 for the conditions and requirements for building and operation of depots and other equipment and installation for using and making harmless the waste.
[3] Legislation for limiting the harmful influence of waste in the environment.
[4] Decree N^0 13 for conditions and requirements for making and operation waste depots- DV/isue153/1988/abolished/.
[5] BANSIK, 2001 final results for the occupation and use in the territory of Republic Bulgaria in 2001-MZG N020-2001.
[6] Tabakov B. Discussion report of project 00043507-“Making capacity for steady management of the lands in Bulgaria.
[7] National program for reducing the number and danger of depots and old pollution with waste “C&E Consulting and engineering Gm bH, IAOS, BT ”Engineering” ET”POVIK-OOS”, 2002.
[8] Guide for evaluating and treating the old pollution in Bulgaria, MOSV, 2001.

СЪДЪРЖАНИЕ – ТОМ I

INFORMATICS AND COMPUTER SYSTEMS, MATHEMATICS

METHODOLOGY IN EDUCATION

СЪДЪРЖАНИЕ – ТОМ II

CHEMISTRY

PHYSICS AND WORKSHOP “SOLAR SYSTEMS

GEOGRAPHIC ENVIRONMENT AND RESOURCES; ECOLOGY AND ENVIRONMENT PROTECTION